

University of Nottingham
UK | CHINA | MALAYSIA

Control of the Collateral Formation of Cardiovascular Disease by SRPK1

Sohni Ria Bhalla

A thesis submitted to the University of Nottingham for the degree of Doctor of Philosophy (PhD)

Supervisors: Prof. David O Bates &

Dr. Alan McIntyre

May 2021

Abstract

Vascular insufficiency in peripheral arterial disease (PAD) results in tissue ischemia. In response, circulating monocytes produce vascular endothelial growth factor (VEGF-A), a key regulator of angiogenesis. Patients with PAD and mouse models of ischemic disease have reduced soluble frizzled related protein (Sfrp5) resulting in increased wingless-type MMTV integration site family 5a (Wnt5a) activity. Monocytes from both humans and mice overexpress the anti-angiogenic VEGF-A isoform, VEGF-A_{165}b. VEGF splicing is regulated by the phosphorylation of serine/arginine splicing factors (SRSFs) by splicing factor kinases such as serine-arginine protein kinase 1 (SRPK1). The role of SRPK1 has been shown in multiple cell types, but the role in monocytes is unknown. Therefore, this thesis investigated the effect of SRPK1 on revascularisation using experimental hind limb ischemia (HLI) in a transgenic mouse model with monocyte specific Wnt5a overexpression (LysM-$Wnt5a^{Gain\ of\ Function}$) administered with an SRPK1 inhibitor. To determine the role of SRPK1 specifically in the monocytes, a novel double transgenic mouse model was generated with Wnt5a hyperactivity and SRPK1 knockout.

Monocyte specific $Wnt5a^{GOF}$ mice had a significantly slower blood flow recovery compared to wild type (WT) mice. This was associated with a reduced capillary and arteriolar density after ischemia in the gastrocnemius muscle. This impaired revascularisation was rescued with an SRPK1 inhibitor, SPHINX31 (post-surgery) and resulted in an increase in the capillary and arteriolar density. The impairment was due to monocyte derived SRPK1 as the revascularisation in LysM-$Wnt5a^{GOF}$ mice was rescued in a monocyte specific SRPK1 knockout mice ($SRPK1^{MoKO}$), which matched WT mice. This was also true in a model of obesity, when mice fed on a high fat/ high sucrose (HF/HS) also showed improved blood flow recovery in monocyte specific SRPK1 knockout compared with WT mice.

These results indicate that revascularisation in ischemic mouse models are dependent on monocytic SRPK1 through an unknown mechanism. Thus,

SRPK1 inhibition could be used as a potential novel therapeutic strategy for PAD.

Publications, Abstracts and Awards

Publications

D.H. Wilson, E.J. Jarman, P.R Mellin, L.M. Wilson, S.H. Waddell, P. Tsokkou, N.T. Younger, A. Raven, **S.R. Bhalla**, A. Noll, S.W. Olde Damink, F.G Schaap, P. Chen, D.O. Bates, J.M. Banales, C.H. Dean, D.J. Henderson, O. J. Sansom, T.J. Kendall, L. Boulter. (2020). *Non-canonical Wnt signalling regulated scarring in biliary disease via the planar cell polarity receptors.* Nature Communication.

K. Harrison, V. Ajruwon, S. Ali, N. Ashra, C. Banas, S. Barasa, **S.R. Bhalla,** A. Chakrabarty, N. Elelu, K.P. Ha, N. Ihekwaba, N. Mirza, S. Said, S. Sarmin, N. Sarveswaran, A. Simon, S. Vallath. (2019). *Workforce Diversity: Let's talk about race.* ELifesciences.

Abstracts

British Microcirculation Society 71st Annual Meeting - Poster presentation: Impaired Revascularisation After Ischemia Is Dependent On Monocytic SRPK1 In Diet-Induced Obese Mice.

7th UK RNA Splicing Workshop, UK, 2021 - Poster presentation: Impaired Revascularisation After Ischemia In Monocytic Wnt5a Is Dependent On Monocytic SRPK1.

3rd International Caparica Conference in Splicing, Portugal, 2020 - Poster presentation: The Role Of SRPK1 After Ischemia In Two Wnt5a Hyperactive Mouse Models.

Mini British Microcirculation Society, UK, 2020 - Oral presentation: Impaired Revascularisation After Ischemia In Monocytic-Wnt5a Is SRPK1 Dependent.

Vasculata, Milwaukee, USA, 2019 - Poster presentation: The SRPK1 Inhibitor SPHINX31 Reverses Impaired Revascularisation In Two Wnt5a Hyperactive Mouse Models.

Cancer and Stem Cells Divisional Meeting, University of Nottingham, 2019 - Poster presentation: The SRPK1 inhibitor SPHINX31 Reverses Impaired Revascularisation In Monocytes Overexpressing Wnt5a.

The Physiology Society, Aberdeen, 2019 - Poster presentation: Monocytic - Wnt5a Dependent Impaired Revascularisation Is SRPK1 Dependent.

3rd ESM-EVBO Conference, Maastricht, The Netherlands, 2019 - Poster presentation: Wnt5a Dependent Revascularisation After Ischemia Is SRPK1 Dependent

British Microcirculation Society 69th Annual Meeting, Exeter, 2019 - Poster presentation: The SRPK1 Inhibitor SPHINX31 Reverses Impaired Revascularisation In Monocytes Overexpressing Wnt5a.

UK RNA Splicing Workshop, UK, 2019 - Poster presentation: The SRPK1 Inhibitor SPHINX31 Reverses Impaired Revascularisation In Monocytes Overexpressing Wnt5a.

Awards

Splicing Travel Award, 2020.

Poster Presentation Prize At The 3rd International Caparica Conference, 2020.

British Microcirculation Society Student Assistance Scheme (SAS), 2020.

Terence Ryan Travel Award, 2020.

MRC Flexible Funding Award (Sum of £2,400), 2019.

Moors Instruments Travel Award, 2019.

The Physiology Society Travel Grant, 2019.

Vasculata Scholarship, 2019.

Poster Presentation Award At Vasculata, 2019.

MRC Flexible Funding Award (Sum of £950), 2019.

Poster presentation Award At The 3rd ESM-EVBO Conference, 2019.

British Microcirculation Society Student Assistance Scheme (SAS), 2019.

MRC Flexible Funding Award (Sum of £23,000), 2018.

Acknowledgements

Firstly, I would like to thank my supervisors, Professor David Bates and Dr. Alan McIntyre for giving me the opportunity to work on this project. Dave- Thank you for pushing me, believing in my abilities (especially at times when I doubted myself) and for giving me the confidence to present at multiple conferences all over the world. I would also like to thank the MRC for funding me and this research (plus the flexible funding grants that allowed me to pursue my *in vivo* studies!)

Dr. Claire Allen, thank you for taking me under your wing and teaching me everything you know in the GTTU! I wouldn't have known where to start without you. I consider myself very lucky to have you as a friend and mentor. I would like to thank Susan Ecob and Naomi Hunter for their patience and support from the moment I walked into the GTTU. Thank you for teaching me the basics and building my confidence with animal handling.

Thank you to our collaborator, Dr. Lydia Teboul at MRC Harwell for generating the SRPK1^{LoxP} mouse strain.

I was fortunate to work with brilliant people from the Tumour and Vascular Biology Labs, BioDiscovery Institute and Bio-Support Unit (BSU). Thank you for creating a fun, friendly and collaborative working environment.

Most importantly, I would like to thank my family for their unconditional love and never-ending support! My grandparents, Surinder and Sudershan, for their constant encouragement and kind words. My parents, Sunjeeb and Monica, thank you for your reassurance and patience and for allowing me to rant to you both on my good, bad and stressful days. Finally, my brother, Rishi, for constantly believing in me. I honestly couldn't have got through the past few years without you all by my side. These words do little to portray my gratitude- I am forever grateful to you all.

Declarations

I, Sohni Ria Bhalla, confirm that the work presented in this thesis was carried out in accordance with the requirements of the University's Regulations and Codes of Practice for Research Degree Programs and that is has not been submitted for any other academic award. I confirm that the work demonstrated in this thesis are my own. Where information has been derived from other sources, I confirm this has been indicated in the thesis.

SIGNED……

DATE…….....

List of Abbreviations

ANOVA	Analysis of Variance
αSMA	Alpha-Smooth Muscle Actin
bp	base pairs
BSA	Bovine Serum Albumin
BM	Bone Marrow
CAD	Coronary Artery Disease
CAG	CMV enhancer, chicken beta-Actin-promoter and rabbit beta-Globin splice acceptor site
cDNA	Complementary DNA
CLK	Cdc2-Like Kinase
Cre	Cre recombinase
CLI	Critical Limb Ischemia
C_t	Cycle threshold
CVD	Cardiovascular Disease
DAPI	4',6-diamidino-2-phenylindole
dH_2O	Distilled water
DMEM	Dulbecco's Modified Eagle Medium
DMSO	Dimethyl Sulfoxide
ELISA	Enzyme-Linked Immunosorbent Assay
eNOS	Endothelial Nitric Oxide Synthase
FBS	Foetal Bovine Serum
FIJI	Fiji is Just ImageJ
GOF	Gain of Function
GAPDH	Glyceraldehyde 3-phosphate dehydrogenase
Hetero	Heterozygous
HF/HS	High Fat/ High Sucrose
HIF-1	Hypoxia Inducible Factor 1
HLI	Hind Limb Ischemia
Homo	Homozygous
HRE	Hypoxia response element
Hx	Hypoxia
i.p.	Intraperitoneal

IB_4	Isolectin B_4
ICAM-1	Intracellular adhesion molecule-1
JNK	c-Jun N-terminal kinase
kDa	Kilodaltons
LDL	Low density lipoproteins
LoxP	Locus of X-over P1
LSI	Laser Speckle Imaging System
LysM	Lysozyme M
MCP-1	Monocyte chemoattractant protein-1
MMPs	Matrix metalloproteinases
MoKO	Monocyte KnockOut
MVD	Microvascular Disease
Na_3VO_4	Sodium Orthovanadate
NaF	Sodium Fluoride
NCBI	National Centre for Biotechnology
NP40	Non-ionic Polyoxyethylene 40
NRP-1	Neuropilin-1
ns	Non-significant
Nx	Normoxia
Ox-LDL	Oxidative low-density lipoproteins
PAD	Peripheral Arterial Disease
PVD	Peripheral Vascular Disease
pJNK	Phospho- c-Jun N-terminal kinase
PBMC	Peripheral Blood Mononuclear Cells
PBS	Phosphate Buffered Saline
PCR	Polymerase Chain Reaction
PFA	Paraformaldehyde
PHDs	Prolyl- hydroxylases
PMSF	Phenylmethylsulfonylfluoride
Pre-op	Pre-operative
Post-op	Post-operative
PVDF	Polyvinylidene Fluoride
qPCR	Quantitative Polymerase Chain Reaction
RBC	Red Blood Cells

RBP	RNA binding protein
RCF	Relative Centrifugal Force
rhVEGF	recombinant human Vascular Endothelial Growth Factor
RNA	Ribonucleic Acid
ROI	Region of Interest
ROS	Reactive Oxygen Species
ROSA26	ROSAβgeo26
rpm	Revolutions per minute
RPMI	Roswell Park Memorial Institute
RRM	RNA recognition motifs
RS	Arginine and Serine alternating residues
RT	Room Temperature
RT-PCR	Reverse Transcription Polymerase Chain Reaction
s.c.	Subcutaneous
SDS-PAGE	Sodium Dodecyl Sulphate-Polyacrylamide Gel Electrophoresis
SDF-1	Stromal derived factor-1
SEM	Standard Error of the Mean
Sfrp5	Secreted frizzled-related protein 5
Spl	Spleen
SR	Serine-rich
SRPK	Serine/Arginine Protein Kinase
SRSF	Serine/Arginine Rich Splicing Factor
TBS-T	Tris-Buffered Saline containing Tween
TG	Transgenic
TGFβ	Transforming growth factor beta
tm	Target mutation
VCAM-1	Vascular cell adhesion molecule-1
VEGF	Vascular Endothelial Growth Factor
VEGFR	Vascular Endothelial Growth Factor Receptor
VPF	Vascular permeability factor

Wnt5a	Wingless-type MMTV integration site family member 5a
WT	Wild type
x g	Times gravity

Table of Contents

Abstract 1

Publications, Abstracts and Awards 3

Acknowledgements 6

Declarations 7

List of Abbreviations 8

List of Figures 16

List of Tables 21

Chapter 1 22

1.1. Cardiovascular disease 23
1.1.1. Risk factors 24
1.1.2. Current treatments 25

1.2. Atherosclerosis 29
1.2.1. Plaque formation 29
1.2.2. Monocyte migration in response to hypoxia 31

1.3. Collaterals in CVD 32
1.3.1. Angiogenesis 32
1.3.2. Arteriolargenesis and arteriogenesis 32

1.4. VEGF-A 34
1.4.1. VEGF-A isoforms 34
1.4.2. VEGFR receptors and their downstream mechanisms 36
1.4.3. VEGF-A effects in ischemic diseases 37

1.5. SRPK1 39
1.5.1. SR proteins: Assembly of the spliceosome complex 39
1.5.2. The role of SRPK1 in alternative splicing 40
1.5.3. VEGF-A splice site selection in angiogenesis 41
1.5.4. SPHINX31 43

1.6. Hypothesis and Aims 45

Chapter 2 47

2.1. Cell culture 48
2.1.1. Suspension cell lines 48
2.1.2. Adherent cell line 48
2.1.3. Sub-culture and routine passage 48
2.1.4. Cell counting 49
2.1.5. Cryopreservation of cells 49
2.1.6. Reviving cryopreserved cells 49

2.2. Cell treatments 50
2.2.1. Wnt5a 50
2.2.2. SRPK1 inhibitor: SPHINX31 50
2.2.3. Hypoxia 50
2.3.4. Hyperglycaemia 50

2.3. Isolation of primary cells 50
2.3.1. Splenocytes 50
2.3.2. Bone marrow immune cells 51
2.4. CD11b selection 51
2.5. RNA extraction 52
2.6. cDNA synthesis 52
2.7. PCR 53
2.8. Protein extraction 55
2.8.1. Cell lysis 55
2.8.2. Tissue lysis 55
2.8.3. Protein quantification 56
2.9. Western blot 56
2.9.1. Sodium dodecyl sulfate-polyacryamide gel electrophoresis (SDS-PAGE) 56
2.10. Enzyme linked immunosorbent assay (ELISA) 58
2.10.1. Pan-VEGF and $VEGF_{165}b$ 58
2.11. Hind limb ischemia model 59
2.11.1. Surgery 59
2.11.2. SPHINX31 Treatments 61
2.11.3. HF/HS Diet 62
2.11.4. Measurement of blood flow recovery *in vivo* 62
2.11.5. Adverse effects 63
2.12. Immunofluorescence on gastrocnemius muscle 64
2.13. Statistical analysis 65
Chapter 3 67
3.1. Introduction 68
3.2. Methodology 70
3.2.1. Statistical analysis 71
3.3. Results 72
3.3.1. The LysM-$Wnt5a^{GOF}$ mouse model 72
3.3.2. LysM-$Wnt5a^{GOF}$ have impaired blood flow recovery 76
3.3.3. Capillary and arteriolar density 78
3.3.4. Expression of VEGF-A isoforms in the gastrocnemius muscle .. 82
3.4. Discussion 86
3.4.1. Generating the LysM-$Wnt5a^{GOF}$ mouse model 86
3.4.2. Wnt5a hyperactivity in monocytes impairs blood flow recovery following ischemic injury 87
3.4.3. Monocytic Wnt5a decreases the capillary and arteriolar density in the gastrocnemius muscle 88
3.4.4. The effect of VEGF-A protein in the gastrocnemius muscle of LysM-$Wnt5a^{GOF}$ mice post-ischemia 91
3.5. Concluding remarks 94

Chapter 4 ..... **95**

4.1. Introduction **96**

4.2. Methodology **98**

4.2.1. Statistical analysis 99

4.3. Results **100**

4.3.1. Impaired blood flow recovery in LysM-Wnt5a^{GOF} mice is reversed with SPHINX31 100

4.3.2. Capillary and arteriolar density 103

4.3.3. 3-day HLI study showed no difference in blood flow recovery 107

4.3.4. Expression of VEGF-A isoforms in the gastrocnemius at a protein level 109

4.3.5. Expression of *Flt1 (VEGFR1)* and *sFlt1* in the gastrocnemius muscle 112

4.4. Discussion **115**

4.4.1. SRPK1 inhibition reverses the impaired blood recovery in LysM-Wnt5a^{GOF} mice 115

4.4.2. SPHINX31 improves the capillary and arteriolar density in the gastrocnemius of LysM-Wnt5a^{GOF} mice post-ischemia 117

4.4.3. The effect of VEGF-A isoforms at a protein level in the gastrocnemius post-ischemia 119

4.4.4. The effect of Flt1/sFlt1 at an RNA level 121

4.5. Concluding remarks **124**

Chapter 5 ..... **125**

5.1. Introduction **126**

5.2. Methodology **128**

5.2.1. Statistical analysis 129

5.3. Results **130**

5.3.1. Developing the SRPK1^{LoxP} transgenic mice 130

5.3.2. The SRPK1 knockout mouse model 132

5.3.4. Generating a transgenic mouse model with monocyte specific Wnt5a hyperactive and SRPK1 knockout 136

5.3.5. SRPK1 knockout in monocytes reverses impaired blood flow recovery in LysM-Wnt5a^{GOF} mice 137

5.3.6. Capillary and arteriolar density 141

5.3.7. SRPK1 knockout reverses the impaired blood flow due to obesity 146

5.4. Discussion **148**

5.4.1. Generating and validating the SRPK1 knockout mouse model 148

5.4.2. Monocytic SRPK1 knockout alone did not significantly impair blood flow recovery 150

5.4.3. SRPK1 knockout in Wnt5a hyperactive mouse models reverses the impaired blood flow recovery in LysM-Wnt5a^{GOF} mice 151

5.4.4. Monocytic SRPK1 restores the arteriolar density, but not the capillary density of LysM-Wnt5a^{GOF} mice post-ischemia 154

5.4.5. No difference in the *Srpk1* expression in bone marrow immune cells of day 3 post-ischemic mice 156

5.5. Concluding remarks 160

Chapter 6 161

6.1. Introduction 162

6.2. Methodology 164

6.3. Results 165

6.3.1. Effect of serum starvation on cell growth and VEGF-A protein content 165

6.3.2. Non-canonical Wnt5a signalling in monocytic cell lines 167

6.3.3. Hypoxia 170

6.3.4. Hyperglycaemia 172

6.3.5. SPHINX31 173

6.4. Discussion 175

6.4.1. No effect with serum starvation 175

6.4.2. The non-canonical signalling pathway is not activated in monocytic cell lines 176

6.4.3. No effect on VEGF-A splicing in hypoxic conditions 178

6.4.4. No effect on VEGF-A splicing in hyperglycaemic conditions ... 179

6.4.5. SPHINX31 did not alter the VEGF-A splicing in monocytic cell lines 180

6.5. Concluding remarks 182

Chapter 7 183

7.1. COVID-19 Impact Statement 184

7.2. The Wnt5a-SRPK1 mechanism of action in ischemic mouse models 185

7.3. The HLI mouse model vs PAD: limitations 191

7.4. Clinical perspective: the bigger picture 192

7.4. Summary 195

REFERENCES 197

List of Figures

Figure 1.1.	Schematic diagram displaying the main steps that result in the formation of an atherosclerotic plaque.	30
Figure 1.2.	The structure of the human VEGF-A gene and its two families of isoforms.	36
Figure 1.3.	Structure of SR proteins.	40
Figure 1.4.	Factors that promote VEGF-A splicing.	42
Figure 1.5.	The mechanism of action of SPHINX31.	44
Figure 2.1.	Step by step guide to induce hind limb ischemia in mice (A-F).	61
Figure 2.2.	Measuring the speckle intensity using the Laser Speckle Imaging System.	63
Figure 2.3.	Side effects that occurred due to the incorrect ligation site of the left femoral artery.	64
Figure 3.1.	Developing mice with monocyte specific Wnt5a overexpression by Cre/LoxP strategy.	72
Figure 3.2.	Genotyping the LysM-Wnt5a^{GOF} transgenic mice.	74
Figure 3.3.	Validating the expression of *Wnt5a* in splenocytes of WT and LysM-Wnt5a^{GOF} mice.	75
Figure 3.4.	No significant difference in the blood flow recovery of WT and STOP-Wnt5a mice.	76
Figure 3.5.	LysM-Wnt5a^{GOF} have significantly impaired blood flow recovery compared to WT mice.	78

Figure 3.6.	LysM-Wnt5a^{GOF} mice have impaired angiogenesis compared to WT mice on post-operative day 21.	79
Figure 3.7.	LysM-Wnt5a^{GOF} mice have impaired arteriogenesis compared to WT mice on post-operative day 21.	81
Figure 3.8.	WT and LysM-Wnt5a^{GOF} mice did not alter the VEGF isoform expression at a protein level in the gastrocnemius muscle after HLI was induced on post-operative day 3	82
Figure 3.9.	WT and LysM-Wnt5a^{GOF} mice did not alter the VEGF isoform expression at a protein level in the gastrocnemius muscle HLI was induced for 3 days as determined by an ELISA.	84
Figure 4.1.	Impaired blood flow recovery in LysM-Wnt5a^{GOF} mice is reversed with SPHINX31.	101
Figure 4.2.	No difference in impaired revascularisation in LysM-Wnt5a^{GOF} mice treated with or without 0.32% DMSO.	102
Figure 4.3.	Impaired angiogenesis in LysM-Wnt5a^{GOF} mice is reversed with SPHINX31 on post-operative day 21.	104
Figure 4.4.	Impaired arteriogenesis in LysM-Wnt5a^{GOF} mice is reversed with SPHINX31 on post-operative day 21.	106
Figure 4.5.	Investigating a possible early effect of SPHINX31 in LysM-Wnt5a^{GOF} mice.	108
Figure 4.6.	WT and LysM-Wnt5a^{GOF} mice treated with and without SPHINX31 did not alter the VEGF isoform expression in the gastrocnemius muscle after HLI was induced on post-operative day 3.	109

Figure 4.7.	WT and LysM-Wnt5a^{GOF} mice treated with and without SPHINX31 did not alter the VEGF isoform expression in the gastrocnemius muscle on post-operative day 3.	111
Figure 4.8.	The effect of *Flt1* expression in the gastrocnemius muscle.	113
Figure 4.9.	The effect of *sFLT1* expression in the gastrocnemius muscle.	114
Figure 5.1.	Development and genotyping of the SRPK1^{LoxP} transgenic mouse performed by Transnetyx Inc.	131
Figure 5.2.	Schematic diagram displaying the homozygous SRPK1^{LoxP} mouse model without (essentially WT) and with Cre present (SRPK1^{MoKO})	132
Figure 5.3.	Determining the expression of *Srpk1* in selected CD11b^{+} monocytes of WT and SRPK1^{MoKO} mice using primers that span exon 1 and 3.	133
Figure 5.4.	Determining the expression of *Srpk1* in selected CD11b^{+} monocytes of WT and SRPK1^{MoKO} mice using primers that span exon 1 and exon 7/8.	134
Figure 5.5.	No difference in the blood flow recovery in WT and SRPK1^{MoKO} mice after inducing ischemia in the left femoral artery.	135
Figure 5.6.	Generating the monocytic specific Wnt5a overexpression and SRPK1 knockout mouse model.	137
Figure 5.7.	Schematic diagram displaying the transgenic mouse groups included in the 21-day HLI study.	138

Figure 5.8.	LysM-Wnt5a^{GOF} induced impairment of revascularisation is controlled by monocytic specific SPRK1 activity *in vivo*.	140
Figure 5.9.	LysM-Wnt5a^{GOF}: SRPK1^{MoKO} mice have an unaltered capillary density on post-operative day 21.	142
Figure 5.10.	LysM-Wnt5a^{GOF} mice have impaired arteriogenesis, which is reversed in LysM-Wnt5a^{GOF}: SRPK1^{MoKO} mice on post-operative day 21.	144
Figure 5.11.	The *Srpk1* expression in bone marrow immune cells on day 3 post-ischemia.	145
Figure 5.12.	Blood flow recovery is reversed in SRPK1^{MoKO} mice fed on a HF/HS diet.	147
Figure 6.1.	The effect of FBS concentration on cell density of THP-1 and U937 cells after 24 hours.	165
Figure 6.2.	The expression of pan-VEGF and VEGF-A_{165}b in THP-1 and U937 cells in 0, 0.5, 1, 2, 5 and 10% FBS.	166
Figure 6.3.	The expression of pan-VEGF and VEGF-A_{165}b in THP-1, U937 and RAW264.7 cells treated with Wnt5a.	168
Figure 6.4.	The expression of JNK and pJNK in THP-1 and U937 and RAW264.7 cells treated with Wnt5a.	169
Figure 6.5.	The protein expression of pan-VEGF and VEGF-A_{165}b treated with 0.5% or 10% FBS in Nx or Hx conditions in THP-1 cells.	170
Figure 6.6.	The protein expression of pan-VEGF and VEGF-A_{165}b treated with 0.5% or 10% FBS in Nx or Hx conditions in U937 cells.	171

Figure 6.7.	The expression of pan-VEGF and VEGF-A_{165}b in THP-1 and U937 cells cultured in 11, 20, 30 and 40mM glucose.	172
Figure 6.8.	The expression of pan-VEGF and VEGF-A_{165}b in THP-1 and U937 cells treated with SPHINX31.	174
Figure 7.1.	Schematic of the proposed mechanism that could be occurring in the LysM-Wnt5a^{GOF} mice with SRPK1 inhibition or SRPK1 knockout in the monocytes.	190
Figure 7.2.	A graphical abstract summarising the key findings of this thesis.	196

List of Tables

Table 1.	PCR primer sequences, annealing temperatures and product sizes.	54
Table 2.	List of primary antibodies.	57
Table 3.	List of secondary antibodies.	58
Table 4.	Simplified mouse names used and respective nomenclature (Chapter 3).	70
Table 5.	Simplified mouse names used and respective nomenclature (Chapter 5).	128

Chapter 1

Introduction

1.1. Cardiovascular disease

Cardiovascular disease (CVD) is a leading public health problem in the UK. Although death rates are declining, the number of patients diagnosed and living with the disease continue to rise (Bhatnagar *et al*., 2016). It has a severe impact on the patient's day-to-day activities, functional capacity and reduces their overall quality of life. This places a large financial burden on the NHS and the economy. In fact, CVD account for 60% of total health care costs (Luengo-Fernández *et al*., 2006). Globally, it accounts for one third of deaths (Wong, 2014).

The umbrella term, CVD, is used for a number of linked pathologies, including coronary artery disease (CAD), cerebral ischemia, peripheral arterial disease (PAD) and microvascular disease (MVD). These diseases often occur due to atherosclerosis, which is a slow progressive build-up of a plaque on the wall of the artery, which narrows the lumen diameter and reduces the blood supply to the associating tissue. An atheroma in the coronary artery reduces the blood supply to the myocardium resulting in CAD. Frequently patients experience symptoms including angina or myocardial infarction (if blood flow is severely restricted) (Sanchis-Gomar *et al*., 2016). Cerebral ischemia affects the carotid artery in the brain. This can result in a stroke (Zhao *et al*., 2013). PAD (also known as peripheral vascular disease, PVD) affects the femoral or iliac artery in the lower limbs. In the majority of cases, patients remain asymptomatic. In mild cases, patients experience intermittent claudication, which includes cramp, pain and aches in the calves and lower limbs. Critical limb ischemia (CLI) is a severe manifestation of PAD which occurs from a complete blockage of the artery resulting in ulcers, gangrene or necrosis (Gornik and Beckman, 2005, Gardner and Afaq, 2008). MVD is an independent disease associated with small 100μm vessels (including capillaries), which regulate vascular tone and blood delivery to the muscles and tissues throughout the body. Although it is commonly associated with retinopathy (eyes), nephropathy (kidneys) and neuropathy (feet) (Beckman and Creager, 2016). It can amplify the onset of large vessel atherosclerotic diseases. In fact, it is

strongly associated with amputations with 1 in 6 patients at risk. This is further amplified with PAD (Beckman *et al*., 2019, Behroozian and Beckman, 2020).

Atherosclerosis is the most common cause of PAD. However, it can less frequently arise in the absence of a plaque. This is known as non-atherosclerotic PAD which includes a collection of heterogenous diseases that result in the same clinical symptoms such as intermittent claudication. One example is fibromuscular dysplasia, which is associated with the thickening of the femoral or popliteal arterial wall. This results in ischemia of the lower limbs due to narrowing or complete blockage of the lumen (Okazaki *et al*., 2011, Sharma *et al*., 2014). Another example is popliteal arterial entrapment syndrome, which occurs if the artery or muscle is abnormally positioned causing compression of the popliteal artery behind the knee. This can result in stenosis, deterioration or complete occlusion of the artery (Levien and Veller, 1999, Weinberg and Jaff, 2012). Adventitial cystic disease is another example. It is a rare condition, which occurs by a the formation of a mucinous cyst on the inner lining of the adventitia (Weinberg and Jaff, 2012). A final example is Buerger's disease which results in inflammation of the vessel walls. When compared to atherosclerotic PAD, it was shown to have a similar impact by reducing the quality of life. However, the symptoms of CLI are present in majority of Buerger's disease patients compared to only half of the atherosclerotic PAD patients (Karakoyun *et al*., 2014). In addition to this, this group of patients are more at risk of amputations and vascular complications (including limb infections, ulcers and necrosis) (Le Joncour *et al*., 2018).

1.1.1. Risk factors

The formation of collateral vessels is an essential adaptive mechanism that occurs after obstruction of an artery or loss of arterioles. It is necessary to compensate for the deficient blood supply to protect and preserve the tissue jeopardised by ischemia. Metabolic diseases (including high blood pressure, obesity, diabetes and dyslipidaemia) inversely correlate with the

collateral flow grade, where a low grade correlates with fewer collaterals (Mouquet *et al*., 2009). Similarly, patients with a high metabolic syndrome score had a lower Rentrop collateral grade, where 0 to 1 indicates little to no collateral blood flow (Sasmaz and Yilmaz, 2009). The main contributing factor to poor collateral vessel development is diabetes (Abaci *et al*., 1999). This group of patients are 62% more likely to have poor collateral vessel development compared to non-diabetics (Hsu *et al*., 2014). In fact, this risk group are ten times more likely to require an amputation (White and Gray, 2007). Similarly, obesity (BMI >30kg/m^2) is another risk factor which results in a poor collateral circulation in ischemic heart disease (Yilmaz *et al*., 2003). Of the patients that are diabetic, 90% are obese suggesting a direct link between the two risk factors are contributing to CVD (Bramante *et al*., 2017). Importantly, the content of vascular endothelial growth factor (VEGF-A) in the serum of diabetic patients is elevated. However, the monocyte function and migration potential is impaired in this group of patients, even when stimulated with VEGF-A (Waltenberger *et al*., 2000). Similarly, in another study, diabetic CAD patients had an increase in VEGF-A production in the monocytes compared to the control group (Panutsopulos *et al*., 2003). Therefore, understanding why these patients are at a greater risk, but do not form collateral vessels, by overcoming this, could underpin the development of a radical and effective therapeutics to induce revascularisation.

1.1.2. Current treatments

After the assessment of blood flow via a diagnostic angiography, there are two main treatments to induce revascularisation via an endovascular and open surgical approach. A less invasive endovascular procedure is an angioplasty. This is where a balloon is attached to a catheter and inserted into the blocked artery. Inflation of the balloon (this can be coated with or without a drug) flattens the atherosclerotic plaque. To prevent future build-up, a stent can be implanted into the targeted artery. This is the first treatment of choice for symptomatic patients, which is shown to have high durability. However, there is a risk of a haemorrhage and recurrent

thrombosis within 30 days of the procedure (Fischer *et al*., 2006, Branco *et al*., 2015, Thukkani and Kinlay, 2015). Therefore, the likelihood that the treatment will need to be repeated is relatively high. In fact, this is shown to dramatically decrease the patients' survival rates (Nasseryan *et al*., 2016).

An alternative approach to induce revascularisation is a surgical bypass. This procedure involves an artificial or synthetic graft, which is inserted to circumvent the blockage. However, it does not remove the plaque or cure the disease itself. The highly invasive procedure is associated with significant post-operative complications and there is a risk of repeat blockage suggesting it is only a temporary solution (Slovut and Lipsitz, 2012). The above treatments are not a viable option for 20-30% of CLI patients. As a last resort, patients will require an amputation (Dua and Lee, 2016). The costs associated with the procedure and post-amputation care (including prosthetic services and physiotherapy) places a large financial burden on the public and healthcare costs (Graz *et al*., 2018). The downfalls of the invasive procedures highlight that there is a need to develop an alternative treatment to promote the regeneration of blood vessels which is non-invasive.

Novel stem cell-based therapies have been considered a promising approach given their ability self-renew and differentiate into various cell types (Botti *et al*., 2012). In 1997, Ashara *et al* identified the potential of $CD34^+$ haemopoietic stem cells from peripheral blood. They presented an endothelial phenotype *in vitro* and contributed to angiogenesis in ischemic tissues *in vivo* (Asahara *et al*., 1997). A non-randomised clinical trial showed that endothelial progenitor cells improved tissue perfusion (Lara-Hernandez *et al*., 2010), whereas a later study only enrolled five patients despite showing positive results with no major adverse effects. However, ABPI levels did not change 3 months post-treatment and recurrent foot ulcers appeared one year later (Tanaka *et al*., 2014). In both studies, there was no control group to compare against. Adipose derived mesenchymal stem cells have been proposed to have a strong angiogenic potential, and

a six-month early phase clinical trial on CLI patient led to an increase in collateral formation, improved walking distance and rest pain. It is important to note that this study had a small sample size (Lee *et al*., 2012). Although similar findings were presented in a phase I clinical trial in 2014, a small group of patients had to undergo an amputation on post-injection day 30, 90 and 150 (Bura *et al*., 2014). In 2017, a phase II double-blind clinical trial on chronic myocardial ischemia patients reduced hospitalisation and symptoms. However, it did not improve the function of the left ventricle (Henry *et al*., 2017). In an *in vivo* experimental study in mice, administration of adipose tissue derived stem cells after ischemia was induced resulted in impaired functional outcomes on post-operative day 7 and had no effect on muscle regeneration or capillary density for the duration of the study (Nammian *et al*., 2021).

Induced pluripotent stem cells (iPS) have unlimited self-renewal potential, and can be differentiated into vascular cell types. Co-administration of iPS differentiated into endothelial and smooth muscle cells improved blood perfusion, prevented necrosis and induced capillary and arteriole formation in animal models of PAD (Park *et al*., 2021, Rufaihah *et al*., 2011). However, there are major concerns with generating iPS. Reprogramming of cells requires a transcription factor such as the protooncogene cytoplasmic Myc (c-Myc) which is delivered by a retrovirus. If c-Myc is overexpressed, it may result in tumorigenesis. This is a major concern for clinical use (Okita *et al*., 2007, Chang *et al*., 2019). Positive effects were seen in patients given bone marrow transplantation (Arai *et al*., 2006) and animal models of cardiac reperfusion (Jackson *et al*., 2001). However, they have been shown to have limited therapeutic potential due to their poor survival rate (Müller-Ehmsen *et al*., 2006). Despite the significant amount of research and development in this area, to date there are no approved therapies for CVD that use stem cell-based therapies.

Alternative growth factor-based treatments have been considered a possible angiogenic therapeutic for CVD. Administration of VEGF-A via an intramuscular route in rabbits resulted in a large and extensive collateral

network (Takeshita *et al*., 1997). In mice, it stimulated an increase in revascularisation and blood flow recovery (Jazwa *et al*., 2013). Similarly, intramuscular administration of VEGF in diabetic mice improved blood reperfusion and capillary density compared to the control group and untreated C57/BLJ mice (Rivard *et al*., 1999). This was also seen in treated diabetic mice treated on post-ischemia day 10 (Li *et al*., 2007). The positive effects were also shown in early open label trials in patients with marked improvements in mobility, pain and limb salvage (Baumgartner *et al*., 1998, Kim *et al*., 2004). However, a double-blind placebo-controlled study confirmed that VEGF-A gene transfer did not reduce the risk of amputations despite showing improved healing of ulcers, reduced pain and some limited efficacy (Mäkinen *et al*., 2002, Kusumanto *et al*., 2006). Administration of a $VEGF_{121}$ adenovirus had little effect on mobility and quality of life. In fact, there was little difference to the placebo group (Rajagopalan *et al*., 2003). Although VEGF treatments induce angiogenesis, studies fail to demonstrate long term benefits thereby limiting its overall potential. There appears to be variabilities and inconsistences with the VEGF-A based treatments used in ischemic patients and animals.

Other growth factor approaches have also been investigated. Despite findings showing that administration of a low dose of fibroblast growth factor (FGF) on a weekly basis for 6 weeks resulted in severe proteinuria (Cooper *et al*., 2001), a phase I clinical trial using FGF treatment was attempted and this significantly improved the blood flow to the calf compared to the placebo group and did not induce proteinuria (Lazarous *et al*., 2000). Gene therapy using hypoxia-inducible factor-1a (HIF-1α) has also been considered a potential therapeutic. However, in a double blind-clinical trial the treatment failed to show differences between the placebo and treated groups (Creager *et al*., 2011). The unexpected side effects from existing treatments suggests that a greater understanding of potential mechanisms that are essential for collateral vessel formation will aid in the development of a new therapeutics. Thus, current collateralisation therapeutic approaches have so far failed to provide a clinical benefit, potentially due to a lack of

understanding of the details about why patients fail revascularise in the first place.

1.2. Atherosclerosis

1.2.1. Plaque formation

Endothelial dysfunction is associated with reduced endothelial nitric oxide synthase (eNOS) and superoxide dismutase (SOD) resulting in an accumulation of reactive oxygen species (ROS). Thus, low-density lipoproteins (LDLs) are retained in atherosclerotic regions and are spontaneously oxidised to generate oxidative LDLs (ox-LDLs) in the arterial intima. This drives the early stages of plaque formation (Linton *et al*., 2000, Rafieian-Kopaei *et al*., 2014). Inhibition of nitric oxide and production of ox-LDLs results in the activation of the nuclear factor kappa B (NF-κB) pathway. This induces the expression of vascular cell adhesion molecule (VCAM-1), intracellular adhesion molecule (ICAM-1) and monocyte chemoattractant protein (MCP-1) on the endothelial and smooth muscle cell surface (Linton *et al*., 2000, Bentzon *et al*., 2014, Cominacini *et al*., 1999). The expression of proinflammatory mediators (IL-1β and TNFα) is enhanced by Wnt5a resulting in a greater migration and infiltration of monocytes to this site (Rauner *et al*., 2012, Nakamura *et al*., 2016). Following transmigration and differentiation of monocytes into the intima, macrophages engulf ox-LDLs by phagocytosis to form foam cells. In fact, ox-LDLs have been shown to induce the transcription of Wnt5a in macrophages (Bhatt *et al*., 2012). Similar findings were presented in THP-1 derived macrophages resulting in phosphorylation of JNK at a protein level (Ackers *et al*., 2020). Further accumulation of foam cells creates 'fatty streaks' (Rafieian-Kopaei *et al*., 2014). The production of chemoattractants including transforming growth factor beta (TGFβ), FGF and the release of matrix metalloproteinases (MMPs) initiates the migration, proliferation and infiltration of smooth muscle cells from the tunica media to the surface on the intima. The cell volume of the intima increases to form an atherosclerotic plaque, which partially blocks the lumen and reduce the blood supply to the associating tissue (Linton *et al*., 2000). The type of plaque that forms affects

the severity and symptoms long term. A stabilised plaque has a thick fibrous cap due to the presence of smooth muscle cells resulting in a preserved lumen and therefore is unlikely to rupture. However, unstable plaques have a thin fibrous cap and is more likely to rupture resulting in the formation of a blood clot in the artery known as a thrombus, which can partially or completely block the lumen (Libby, 2012, Bentzon *et al*., 2014). The steps are summarised in Figure 1.1.

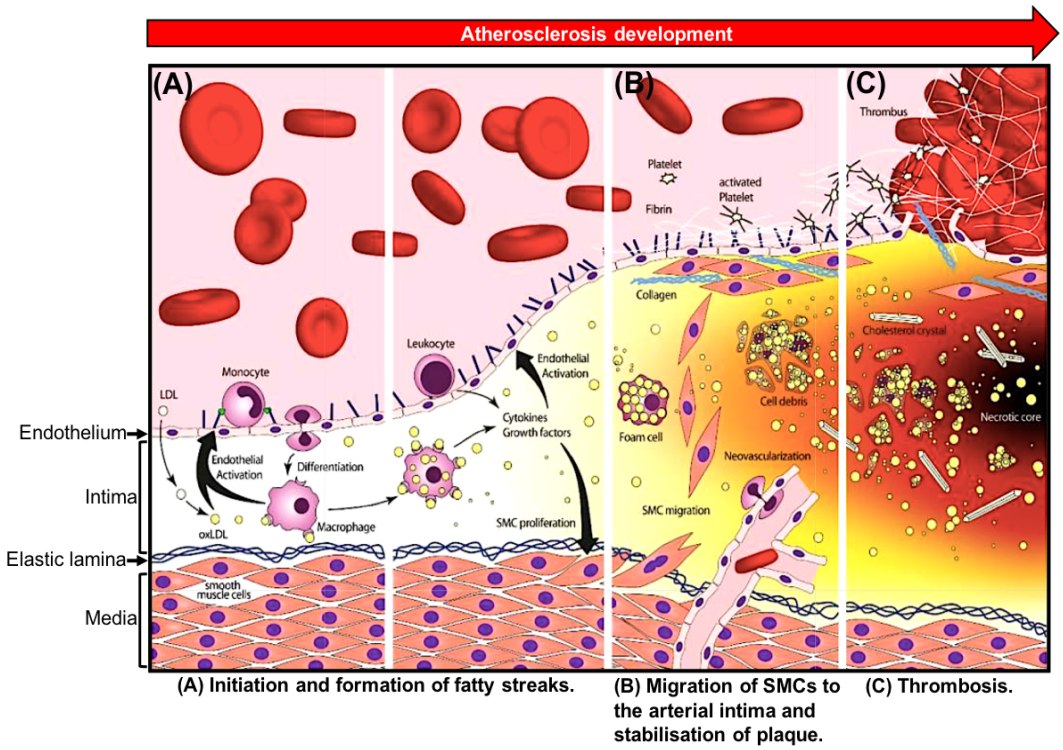


Figure 1.1. Schematic diagram displaying the main steps that result in the formation of an atherosclerotic plaque. (A) *Initiation and formation of fatty streaks: This occurs when LDL's are oxidised to oxLDLs, which stimulates the expression of adhesion molecules (including ICAM-1 and VCAM-1) on the endothelial cells and the secretion of chemokines (including MCP-1 and IL-8). Subsequently, monocytes are recruited, transmigrate and differentiate into macrophages, which play a role in the formation of foam cells by engulfing oxLDLs. Together leading to intimal thickening. Additionally, secretion of TNF*α and IL-6 *results in leukocyte recruitment.* ***(B)*** *Stabilisation of plaque: proliferating smooth muscle cells migrate from the media to the intima and stabilise the fibrous plaque.* ***(C)*** *Apoptosis of foam cells results in a necrotic core. Unstable plaques are more vulnerable, which can rupture and result in thrombotic events and complete blockage of the vessel. Image taken and adapted from (Steinl and Kaufmann, 2015).*

1.2.2. Monocyte migration in response to hypoxia

The production of precursor monocytes occurs in the bone marrow and gives rise to monocytes by haematopoiesis, which are then released into the bloodstream or reside in the spleen (Swirski *et al*., 2009). In normoxic conditions, hypoxia inducible factor alpha (HIF-1α) is degraded due to hydroxylation by prolyl-hydroxylase (PHDs) and polyubiquition (Strehl *et al*., 2014) Upon ischemic injury, monocytes adapt to the impact of reduced oxygen levels, increase their motility and alter their differentiation state. The inactivation of PHDs results in an upregulation and accumulation of HIF-1α, which dimerises to HIF-1β. This complex translocates to the nucleus and binds to the hypoxia response element (HRE) in the promoter region to mediate the transcription and stability of CXC-chemokine receptor 4 (CXCR4) along with other genes and gene receptors on the cell surface (Schioppa *et al*., 2003, Strehl *et al*., 2014). Exposure to chemokines, specifically stromal derived growth factor (SDF-1, also known as CXCL12) creates a gradient which is inversely proportional to the oxygen levels (Schioppa *et al*., 2003, Wei *et al*., 2012). This plays an important role in attracting monocytes to the site of ischemia.

Another chemokine receptor monocytes rely on is C-C chemokine receptor type 2 (CCR2) which aids the migration in the presence of MCP-1 (also known as CCL2) in ischemic animal models and inflamed atherosclerotic plaques (Boring *et al*., 1998, Dewald *et al*., 2005, Nahrendorf and Swirski, 2017). This response is further enhanced in the presence of Wnt5a (Rauner *et al*., 2012). Inhibition of CCR2 reduced the inflammatory response in myocardial infarction and migration of monocytes towards MCP-1 (Leuschner *et al*., 2011). Whereas administration of MCP-1 resulted in activation and accumulation of monocytes at the site of occlusion (Ito *et al*., 1997b). Surprisingly, MCP-1 has also been shown to have a role in collateral conductance (Pipp *et al*., 2003). Monocytes/macrophages appear to be major secretors of VEGF-A in hypoxic conditions (Wu *et al*., 2010). Therefore, understanding why some patients are unable to stimulate the

known angiogenic response and understanding the molecular mechanism is likely to be key in developing new therapies for cardiovascular disease.

1.3. Collaterals in CVD

1.3.1. Angiogenesis

The formation of narrow capillary microvessels from pre-existing vasculature is known as angiogenesis, which plays a significant role in pathological and physiological conditions (Folkman and Klagsbrun, 1987, Risau, 1997). There are two types of angiogenesis: non-sprouting (intussusceptive) and sprouting. Non-sprouting angiogenesis is the modification of pre-existing vessels by forming an intravascular pillar. This divides the vessel, which subsequently branches to become two independent capillaries (Burri and Djonov, 2002). In comparison, sprouting angiogenesis occurs when existing capillaries acquire a tip cell phenotype resulting in the formation of a sprout on an existing vessel (Risau, 1997). This is directed towards the concentration gradient of angiogenic factors such as VEGF-A (Connolly *et al*., 1989) and angiopoietin-1 (Ang-1) (Koblizek *et al*., 1998). These processes are driven by hypoxia and mediated by the activation of the transcription factor, HIF-1α, which subsequently activates the gene expression of VEGF-A (Ahn *et al*., 2014, Marti *et al*., 2000). Recent evidence has identified that the non-canonical Wnt5a signalling pathway is involved in the impaired angiogenic response in retinal myeloid cells (Stefater *et al*., 2011), adipose tissue (Karki *et al*., 2017) and PAD patients (Kikuchi *et al*., 2014). This will be addressed further in section 1.4 (below).

1.3.2. Arteriolargenesis and arteriogenesis

The vascular network consists of arterioles which connect to capillaries and are linked to the main arteries. However, the capillaries can develop into arterioles by a process called arteriolargenesis (also referred to as capillary arterialization). This is essential to regulate blood perfusion. It occurs when smooth muscle cells are recruited to the pre-existing, expanding capillary wall to develop into functional arterioles. This process was captured in the

mesentery by Benest *et al* in 2008 (Benest *et al*., 2008). Using this model, it has been shown that a combination of Ang-1, VEGF-A and vasodilators (e.g. eNOS to produce nitric oxide or prazosin) induce smooth muscle cell recruitment and coverage to develop functional vessels (Benest *et al*., 2008). It was later discovered that inhibition of VEGF-A (with sFLT1) and/or Ang-1 (with sTie2) in the presence of eNOS alone inhibited recruitment of smooth muscle cells and arteriolargenesis (Stone *et al*., 2017). This indicates that the three components are necessary to stimulate the process.

In comparison, arteriogenesis is an efficient adaptive mechanism. It is the remodelling and expansion of pre-existing collateral vessels to compensate for blood flow via other routes (Ito *et al*., 1997a, Scholz *et al*., 2001). This mechanism is not driven by hypoxia. The key stimulus in initiating arteriogenesis is the physical mechanical force. After an arterial occlusion, there is a change in blood flow which increases the blood pressure and fluid shear stress in the lumen of pre-existing collateral vessels (Tuttle *et al*., 2001, Pipp *et al*., 2004). The force acts on the endothelial cells on the vessel wall and activates the calcium dependent enzyme, eNOS, which converts l-arginine to l-citrulline and produces nitric oxide (Marletta, 1994). It diffuses into the smooth muscle cells, binds and stimulates the heme protein soluble guanylyl cyclase, which catalyses the dephosphorylation of GTP to cyclic GMP (Denninger and Marletta, 1999, Arnold *et al*., 1977). Thus, the synthesis of nitric oxide by eNOS is necessary to increase the lumen diameter and blood flow recovery resulting in a vasodilatory effect (Dai and Faber, 2010). This can then result in longer term remodelling of the arteriole to form a larger vessel. In fact, arteriogenesis increases the blood flow by 10-20-fold and increases the vascular reserve to the associating tissue (Schaper and Scholz, 2003). In rat models of cerebral ischemia, an increase in fluid shear correlated with collateral growth and monocyte accumulation compared with the control group (Schierling *et al*., 2009). In rabbits, administration of eNOS inhibitors, called L-NAME blocked the positive effects of high shear stress, reduced collateral conductance and resulted in the uncoupling of eNOS (Eitenmüller *et al*., 2006). Similarly, blood flow recovery was impaired and arteriogenesis was reduced in an eNOS

knockout mouse model post-ischemia and intramuscular administration of eNOS reversed these effects (Yu *et al*., 2005). This indicates the important of nitric oxide production for arteriogenesis.

Recent literature has shown a link between Wnt5a and eNOS resulting in nitric oxide production. In 2016, Brenton-Romero *et al* identified that endothelial activation was impaired in diabetic patients due to enhanced Wnt5a expression, and JNK phosphorylation downstream. This was shown to negatively correlate with flow-mediated dilation, as a result of impaired eNOS activation (Breton-Romero *et al*., 2016). Similar findings were presented by Cho *et al*, however this mechanism was reversed by treatment with recombinant Sfrp5, which inhibits the action of Wnt5a. (Cho *et al*., 2018). The results were consistent in the adipose tissue of severely obese patients. Farb *et al* confirmed that the vasodilatory response of the arterioles was impaired due to Wnt5a/JNK signalling and eNOS phosphorylation (Farb *et al*., 2016). The non-canonical Wnt5a signalling pathway will be explored throughout this thesis.

1.4. VEGF-A

1.4.1. VEGF-A isoforms

The protein now known as VEGF-A, was initially named vascular permeability (VPF) factor in 1983 (Senger *et al*., 1983). A further study in 1989, purified and cloned this protein for the first time. It was shown to induce its mitogenic effects specifically on endothelial cells and was given the name vascular endothelial growth factor (VEGF) (Ferrara and Henzel, 1989). In the same year, two independent cloning studies on VPF and VEGF confirmed that both proteins were the same (Leung *et al*., 1989, Keck *et al*., 1989). VEGF-A is important in 'normal' vascular development. This was shown in heterozygous *Vegf* knockout mouse model, which resulted in embryonic lethality (Carmeliet *et al*., 1996). VEGF-A has been shown to have a key role in vascular remodelling and vasodilatation (Hood *et al*., 1998, Connolly *et al*., 1989). In addition, VEGF-A has been shown to have a distinct role in a number of pathological processes including female

reproduction (Fraser *et al*., 2000), pre-eclampsia (Cooper *et al*., 1996), atherosclerosis (Couffinhal *et al*., 1997), and wound healing (Nissen *et al*., 1998).

The VEGF-A gene is organised into eight exons and seven introns. Following alternative splicing, multiple isoforms are produced of varying lengths. This includes VEGF-A_{121}, VEGF-A_{145}, VEGF-A_{148}, VEGF-A_{165}, VEGF-A_{183}, VEGF-A_{189} and VEGF-A_{206} in humans (Ferrara *et al*., 2003). Each isoform has exon 1 to exon 5, but differ in inclusion of the exon 6 (6a and 6b) and 7. The most widely studied and understood isoform of the VEGF-A family is VEGF-A_{165} (known as VEGF-A_{164} in rodents). In 2002, an additional isoform of VEGF-A_{165} was identified with anti-angiogenic properties (Bates *et al*., 2002). Therefore, the family of VEGF-A isoforms were differentiated into two distinct groups named VEGF-A_{xxx}a and VEGF-A_{xxx}b (where $_{xxx}$ denotes the number of amino acids), as indicated in Figure 1.2 and have opposing functions. They differ by 18 nucleotides, which encode for 6 different amino acids at the 5' end of exon 8a and 8b. Pro-angiogenic VEGF-A_{xxx}a is a result of proximal splice site selection at exon 8a (coding for Cys-Asp-Lys-Pro-Arg-Arg (CDKPRR)). Anti-angiogenic VEGF-A_{xxx}b is a result of distal splice site selection at exon 8b (coding for Ser-Leu-Thr-Arg-Lys-Asp (SLTRKD)) (Bates *et al*., 2002, Woolard *et al*., 2004). The key differences to note between the two families of isoforms is the loss of cysteine and positive charged arginine's in the VEGF-A_{xxx}a family with serine, lysine and negatively charged aspartic acid in VEGF-A_{xxx}b (Harper and Bates, 2008). This has significant implications, affecting their overall protein structure and biological function, which alters the downstream effects when bound to its receptors on the endothelial cell surface. It is important to note that exon 8b is well conserved across mammals with 86% similarity between humans and mice, where exon 8b encodes for seven amino acids Pro-Leu-Thr-Gly-Lys-Thr-Asp (PLTGKTD) in mice, resulting in a 165 amino acid isoform (VEGF-A_{165}b) rather than the 6 amino acids in exon 8a resulting in 164 amino acid isoform (VEGF-A_{164}a) (Bates *et al*., 2002).

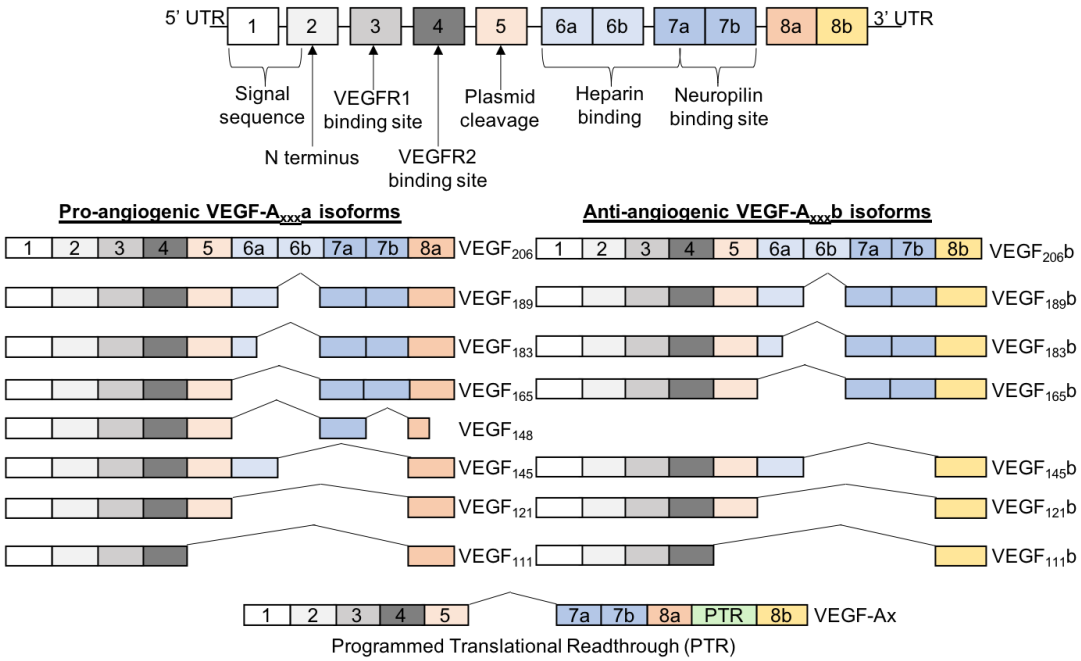


Figure 1.2. The structure of the human VEGF-A gene and its two families of isoforms. *Alternative splicing of VEGF-A at exon 8 (proximal or distal splice site) generates two families of VEGF-A isoforms, pro-angiogenic VEGF-A$_{xxx}$a and anti-angiogenic VEGF-A$_{xxx}$b. The function is associated with the alternative C terminus. Also, an additional isoform called VEGF-Ax arises from programmed translational readthrough (PTR) and contains both exon 8a and 8b (Eswarappa et al., 2014). Adapted from (Nowak et al., 2008, Bridgett et al., 2017, Peach et al., 2018).*

1.4.2. VEGFR receptors and their downstream mechanisms

The biological effects of VEGF-A isoforms occur after binding to tyrosine kinase receptors named VEGFR1 (Flt1 in mice) and VEGFR2 (also known as KDR in humans or Flk1 in mice). Each isoform competes when binding to the VEGF receptors at a one-to-one ratio (Varey *et al*., 2008). Each receptor has an extracellular domain which is required for VEGF-A binding, an intracellular domain which promotes phosphorylation of tyrosine residues to modulate downstream events and a transmembrane domain (Melincovici *et al*., 2018). VEGF-A isoforms have a greater binding affinity to VEGFR1 compared to VEGFR2 (Waltenberger *et al*., 1994, Peach *et al*., 2018). However, this does not induce a stronger phosphorylation of the tyrosine kinase domain downstream. In fact, it is 10-fold weaker than VEGFR2 (Shibuya, 2001, Shibuya, 2006). VEGFR1 negatively regulates angiogenesis, essentially preventing pro-angiogenic VEGF-A isoforms from binding to VEGFR2 (Shibuya, 2001, Cébe Suarez *et al*., 2006). A similar response is seen with the alternative splice variant and truncated form of

VEGFR1 known as soluble VEGFR1 (referred to as sFLT1 or sFLT-i13 in mice). This variant only has an extracellular binding domain. Therefore, it exerts an anti-angiogenic effect by binding to secreted pro-angiogenic VEGF-A in the bloodstream and sequesters its action. This prevents VEGF-A_{xxx}a from binding to VEGFR2 (Kendall and Thomas, 1993, Maynard *et al*., 2003). VEGFR2 is primarily responsible for angiogenesis with the co-receptor neuropilin 1 (NRP-1). In a similar manner to VEGFR1, VEGF-A_{165}b and VEGF-A_{165}a have similar binding to VEGFR2, but have distinct signalling outcomes (Kawamura *et al*., 2008). Kawamura *et al* confirmed that VEGF-A_{165}a efficiently binds to VEGFR2 and coreceptor NRP-1 (Kawamura *et al*., 2008). It is proposed that the cysteine and positively charged arginine residues are responsible for the binding to VEGFR2, which induces receptor dimerization and efficient auto-phosphorylation downstream (Harper and Bates, 2008, Kawamura *et al*., 2008). This is shown to modulate cell survival, proliferation, vasodilatation (through eNOS) and migration (Harper and Bates, 2008). In comparison, VEGF-A_{165}b binds to VEGFR2, but is unable to induce complex formation between VEGFR2 and NRP-1. Subsequently, this reduces the efficiency of tyrosine kinase phosphorylation which is weaker and occurs at a slower rate, perhaps due to the incomplete rotation of the kinase domain (Kawamura *et al*., 2008, Cébe Suarez *et al*., 2006).

1.4.3. VEGF-A effects in ischemic diseases

Circulating VEGF-A levels in patients with PAD are greater than healthy patients. This has been shown to positively correlate with disease severity and progression (Findley *et al*., 2008, Celletti *et al*., 2001, Kikuchi *et al*., 2014). At this point, it was unclear why VEGF-A was unable to induce collateral vessel remodelling and stimulate revascularisation. In 2014, Kikuchi *et al* identified an imbalance in ratio of VEGF-A_{165}b to VEGF-A_{165}a in the peripheral blood monocytes and serum levels of PAD patients (Kikuchi *et al*., 2014). Similarly, VEGF-A_{xxx}a was reduced in muscle biopsies (Ganta *et al*., 2017). Additionally, in CAD, VEGF-A_{165}b levels correlated with larger infarct size and resulted in the formation of fewer

vessels (Hueso *et al*., 2017). A similar response was identified in the adipose tissue of obese patients and ischemic gastrocnemius muscle of mouse models which is a major risk factor for ischemic diseases (Karki *et al*., 2017, Ngo *et al*., 2014, Kikuchi *et al*., 2014). It has been reported that the impaired revascularisation and angiogenesis is associated with the non-canonical Wnt5a signalling pathway resulting in VEGF-A_{165}b (Kikuchi *et al*., 2014, Karki *et al*., 2017). In fact, opposing effects were identified with a neutralising VEGF-A_{165}b antibody by promoting revascularisation *in vivo in* two different strains of mice indicating that the response is dependent on VEGF-A_{165}b (Ganta *et al*., 2017, Kikuchi *et al*., 2014). The progression of PAD occurs when VEGF-A isoforms bind to VEGFR receptors. Zhao *et al* reported that the impaired angiogenic response in ischemic aged mice is associated with the decoy receptor sFLT1, which subsequently suppresses VEGFR2 phosphorylation, which is the dominant receptor responsible for angiogenesis (Zhao *et al*., 2017). Ganta *et al* identified that VEGF-A_{165}b impaired VEGFR1-STAT3 and modulates impaired revascularisation in ischemic mouse models with little effect on VEGFR2 (Ganta *et al*., 2017). In contrast, Clayton *et al* identified that heterozygous VEGFR1 knockout mice had impaired blood flow recovery, collateral growth and leukocyte recruitment compared to VEGFR2 suggesting VEGFR1 is also an important receptor in collateral remodelling (Clayton *et al*., 2008). Overall, this evidence confirms that an imbalance in VEGF-A isoforms in PAD patients and ischemic mouse models is dictating downstream signalling mechanism resulting in ischemic diseases. However, the mechanism resulting in the production of VEGF-A_{165}b remains poorly understood.

1.5. SRPK1

1.5.1. SR proteins: Assembly of the spliceosome complex

A single precursor mRNA (pre-mRNA) product results in the formation of multiple mRNA products. Each one is translated into a protein with distinct structures and functions (Bowler and Oltean, 2019). Of the mRNA products produced, 20-35% contain a premature stop codon in the open reading frame, which are degraded by nonsense mediated decay to prevent the formation of a truncated protein (Yap and Makeyev, 2013). These processes are a result of alternative splicing. The spliceosome modulates the splicing reactions. It consists of 5 small ribonuclear proteins (snRNPs) including U_1, U_2, U_4, U_5, U_6 and over 200 auxiliary proteins. By recognising the 5' and 3' splice sites, the introns are removed by two transesterification reactions and selected exons are ligated. Recruitment of the spliceosome to the pre-mRNA requires the action of RNA binding proteins (RBPs), which includes serine-rich (SR) proteins (Naro and Sette, 2013). They recognise splicing regulatory elements including exon splicing enhancers to direct the spliceosome to the splice site and ensure the correct region is spliced (Wang and Burge, 2008).

Structurally, SR proteins contain one or two RNA recognition motifs (RRM) on the N terminus. This region controls the interaction of SR proteins to the exon splicing enhancers (Ghosh and Adams, 2011). The C terminus contains Arginine- Serine rich repeats (known as the RS domain). This region is divided into segments: RS1 and RS2 and is subsequently phosphorylated by Serine-arginine protein kinases (SRPKs) and Cdc-like 2 kinases (CLKs). SRPKs stimulate SRSF1 nuclear localisation by the transportin SR2 and CLKs are responsible for distribution in the nuclear speckles (Ghosh and Adams, 2011, Lai *et al*., 2001). Thus, phosphorylation of SR proteins at the RS domain are a key for spliceosome assembly, subcellular localisation and protein-protein interactions (Zhu and Krainer, 2000). The structure of SR proteins is summarised in Figure 1.3.

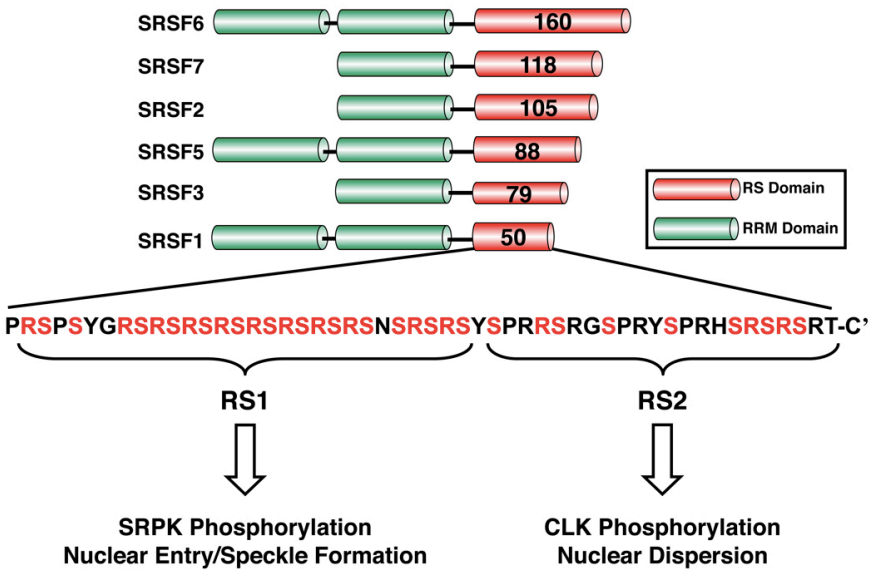


Figure 1.3. Structure of SR proteins. *SRSFs have one or two RRM domains on the N terminal and RS domains on the C terminus which is split into RS1 and RS2. Taken from (Ghosh and Adams, 2011).*

1.5.2. The role of SRPK1 in alternative splicing

The family of serine kinase enzymes that recognise and phosphorylate RS dipeptide repeats of SR proteins are known as SRPKs. There are three members: SRPK1, SRPK2 and SRPK3 (Wang *et al*., 1998, Nakagawa *et al*., 2005, Giannakouros *et al*., 2011). SRPK2 was shown to be structurally similar to SRPK1, resulting in similar kinase activity and substrate specificity. Both SRPKs are shown to be expressed in multiple tissues and cell lines (Wang *et al*., 1998). In 2005, SRPK3 was discovered. SRPK3 has high sequence similarity and kinase activity to SRPK1 and SRPK2, but differ in hinge region. SRPK3 is highly expressed in the murine heart and skeletal muscle (Nakagawa *et al*., 2005).

Structurally, SRPKs consist of two unique lobes which are connected by an insert domain. The large lobe on the C terminus is the kinase domain which is necessary for SRSF binding and phosphorylation. Whereas, the small lobe on the N terminus is the ATP binding pocket (Ghosh and Adams, 2011). SRPK1 is a constitutively active kinase and appears to be the most studied of the SRPK family member in the literature. The centre of the RS domain at the C terminus binds to the active site of SRPK1 in the cytoplasm. This results in hyperphosphorylation of the serine residues in a directional

manner from the C to N terminus on RS1 domain, which translocates to the nucleus. It is recruited to the nuclear speckles where splicing factors (including CLKs) are stored (Aubol *et al*., 2013, Ngo *et al*., 2005). The remaining serine residues are phosphorylated by CLK1 at the RS2 domain (Colwill *et al*., 1996) (indicated in Figure 1.3). Thus, the fully phosphorylated SRSF1 is released from the nuclear speckles in order to participate in splicing events by coupling to RNA polymerase II and the spliceosome (Gonçalves and Jordan, 2015, Keshwani *et al*., 2015). The control of SRPK1 is crucial for the pre-mRNA splicing events, which results in multiple protein products. Throughout this thesis, the role of SRPK1 will be explored in monocytes *in vivo.*

1.5.3. VEGF-A splice site selection in angiogenesis

The choice of proximal or distal splice site selection at the 5' end of exon 8 of the VEGF-A gene is regulated by SR proteins: SRSF1 (ASF/SF2), SRSF2 (SC35) and SRSF6 (SRp55) (Nowak *et al*., 2008, Biselli-Chicote *et al*., 2017). Phosphorylation of the splicing factor, SRSF1 has been shown to favour proximal splice site selection resulting in an upregulation of pro-angiogenic VEGF-A isoform in cancer and epithelial cells. This was enhanced with insulin-like growth factor 1 (IGF1) and TNFα (Nowak *et al*., 2008). In comparison, CLK1 and CLK4 phosphorylate SRSF6 which favours the distal splice selection on the VEGF-A. This results in an upregulation of the anti-angiogenic isoform, which is enhanced with transforming growth factor β1 (TGF-β) (Nowak *et al*., 2008, Harper and Bates, 2008). SRPK1 has a key role in phosphorylating SRSF1 supporting proximal splice site selection, however this has not been shown with SRPK2 (Nowak *et al*., 2010). Both SR protein kinase domains have 90% similarity, however SRPK1 has not been shown to interact with SRSF2. SRPK2 mediates the phosphorylation of SRSF2 (Wang *et al*., 1998). In a tumour neovascularisation model *in vivo*, the transcription factor E2F1 alters the ratio of VEGF-A isoforms favouring VEGF-A_{165}b: total VEGF due to the phosphorylation of SRSF2 (Merdzhanova *et al*., 2010). Whereas, in an *in vitro* setting in RAW264.7 macrophages, VEGF-A_{165}b was upregulated in

an SC35/SRSF2 dependent manner in the presence of Wnt5a/JNK mechanism (Kikuchi *et al*., 2014) (summarised in Figure 1.4). It appears that SRSF1 is primarily phosphorylated by SRPK1, however the involvement has not been explored in monocytes or models of ischemia. Knockdown of SRPK1 in cancer cells, was shown to switch the expression of VEGF-A isoform from VEGF-A_{165} to VEGF-A_{165}b (Mavrou *et al*., 2015). Similarly, inhibition of SRPK1 with SPHINX31 provided an effective anti-angiogenic strategy in choroidal neovascularisation in the eye (Batson *et al*., 2017). The SRPK1- SRSF1 axis is an important mechanism that has been identified and investigated in multiple cell types and diseases. It is yet to be explored in models of CVD and it could provide a potential therapeutic target, which will be investigated in this thesis.

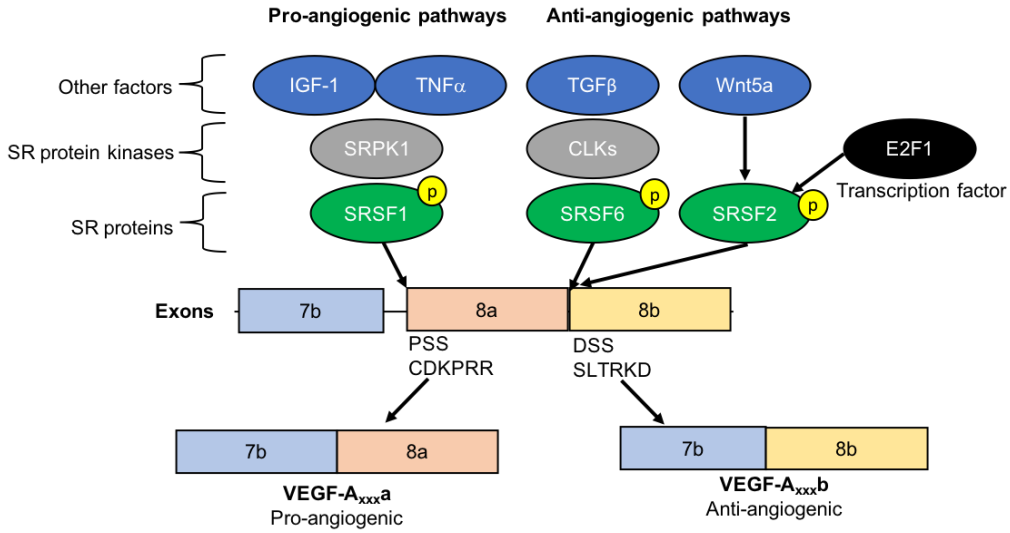


Figure 1.4. Factors that promote VEGF-A splicing. *IGF-1 and TNFα increased the expression VEGF-A_{165}a, SRPK1 phosphorylates SRSF1 to induce proximal splice site selection. Whereas TGFβ induces distal splice site selection and VEGF-A_{165}b expression due to CLKs, which phosphorylate SRSF6. SRSF2/SC35 promotes VEGF-A_{165}b expression due to an upregulation of Wnt5a or when under control of the transcription factor, E2F1 (Nowak et al., 2008, Nowak et al., 2010, Merdzhanova et al., 2010, Kikuchi et al., 2014).*

1.5.4. SPHINX31

Development of the small molecule SRPK1 inhibitors has been shown to be successful, but can be associated with other off-target effects by targeting other kinases (such as SRPK2), and therefore lack specificity and selectivity (Fukuhara *et al*., 2006). The 3-(trifluoromethyl)anilide scaffold (known as SPHINX31) is highly selective and potent for SRPK1 with an IC_{50} of 5.9nM. SPHINX31 has a 50-fold greater affinity for SRPK1 over SRPK2, the closest related kinase. This is the same as CLK1, whilst CLK4 has a 100-fold less binding affinity. The development of a type 1 kinase inhibitor (known as ATP competitive) poses particular challenges as it has to bind to a highly conserved and rigid active site region to compete with SRSF1. Therefore, it requires precise positioning in the binding pocket of SRPK1 (Müller *et al*., 2015, Bhullar *et al*., 2018). The use of an ATP assay against 50 kinases successfully confirmed that SPHINX31 inhibited 96% of the SRPK1 activity at 1μM and failed to inhibit other kinases (Batson *et al*., 2017). The compound induces its action by binding to the unique helical insert close to the hinge region of SRPK1 triggering a backbone flip. This is unique to SRPK1 highlighting its specificity (Batson *et al*., 2017). Importantly, SRPK1 inhibitors regulate the switch in alternative splicing of VEGF-A isoforms from pro-angiogenic VEGF-A_{xxx}a to anti-angiogenic VEGF-A_{xxx}b in disease models *in vitro* and *in* vivo (the mechanism is summarised in Figure 1.5). This has been shown in neovascular eye disease, age-related macular degeneration and cancer (Batson *et al*., 2017, Gammons *et al*., 2013, Mavrou *et al*., 2015). Interestingly, administration of SPHINX31 as an eyedrop in models of choroidal neovascularisation inhibited macrophage infiltration (Batson *et al*., 2017). In PAD patients and ischemic mouse models, VEGF-A isoforms have been detected and there is an imbalance (previously mentioned in Section 1.4.3.). However, it is unknown whether VEGF splicing is regulated by SRPK1 in cardiovascular disease. Thus, SPHINX31 will be used to inhibit the SRPK1 kinase activity to understand its effect, if any, in ischemic mouse models and in *in vitro* human monocytic cell lines.

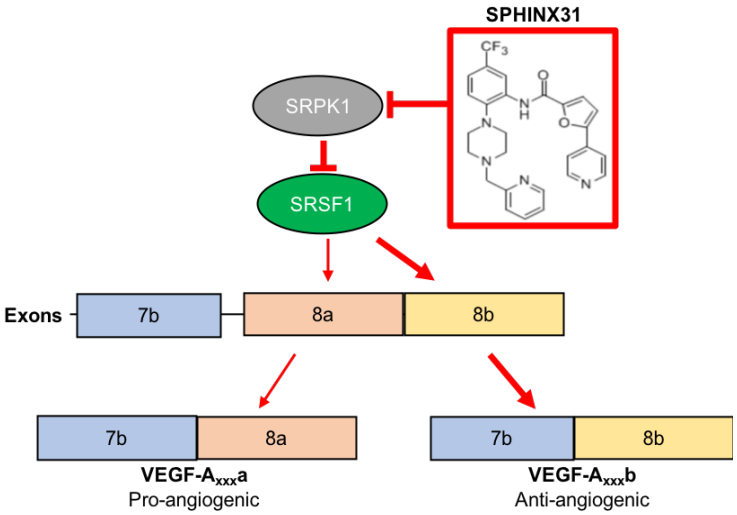


Figure 1.5. The mechanism of action of SPHINX31. *The activity of SRPK1 and phosphorylation of SRSF is inhibited with SPHINX31. This results in an increase in the anti-angiogenic VEGF-A$_{xxx}$b compared to pro-angiogenic VEGF-A$_{xxx}$a (indicated by arrow thickness). Adapted from (Batson et al., 2017).*

1.6. Hypothesis and Aims

It is clear that ischemia in the lower limb results in the recruitment of pro-inflammatory monocytes in patients with PAD and ischemic mouse models. In response the circulating monocytes have increased Wnt5a activity and over express anti-angiogenic VEGF-A_{165}b. However, the potential mechanism involved in the vascular response needs to be explored further. Understanding the mechanism of VEGF-A splicing control could result in a new therapeutic strategy to improve collateral formation and treat PAD. Therefore, I set out to test the hypothesis that revascularisation is further impaired by inhibiting or blocking the activity of the SRPK1. To address this hypothesis, I designed experiments to:

I. Confirm whether Wnt5a hyperactivity in monocytes *in vivo* results in impaired blood flow recovery and determine if this affects the angiogenic and arteriogenic capability in the gastrocnemius muscle.

II. Assess whether administration of an SRPK1 inhibitor, SPHINX31, in LysM-Wnt5a^{GOF} hind limb ischemia mouse model will induce changes in the blood flow recovery, arteriogenesis and angiogenesis. If so, evaluate the effects on VEGF-A isoform expression at a protein level, if any.

III. Develop and validate a monocyte specific SRPK1 knockout mouse model and determine the effects on blood flow recovery after induction of ischemia in the left hind limb.

IV. Determine whether impaired revascularisation in LysM-Wnt5a^{GOF} is a consequence of monocytic specific SRPK1 by using a novel transgenic SRPK1 conditional knockout mouse model. Assess the changes in vessel formation in the gastrocnemius muscle post-ischemia.

V. Establish whether human (THP-1 and U937) and mouse (RAW264.7) monocytic cell lines can be used as a suitable model

for identifying the mechanism of Wnt5a mediated upregulation of VEGF-A_{165}b *in vitro*.

Chapter 2

Materials and Methods

2.1. Cell culture

THP-1, U937 and RAW264.7 cells were purchased from ATCC. All cell lines were incubated at 37^{o}C in humidified 5% CO_2 atmosphere, unless stated otherwise.

2.1.1. Suspension cell lines

THP-1 and U937 cells are a human leukemic derived monocytic cell line. Cells were cultured in RPMI-1640 medium (Sigma-Aldrich) supplemented with 10% (for U937) or 20% (for THP-1) foetal bovine serum (FBS; Sigma-Aldrich) and 2mM L-glutamine (Thermofisher).

2.1.2. Adherent cell line

RAW264.7 cells are a mouse macrophage cell line. Cells were cultured in Dulbecco's Modified Eagle's Medium (DMEM; Sigma-Aldrich) supplemented with 10% FBS and 2mM L-glutamine (Sigma-Aldrich).

2.1.3. Sub-culture and routine passage

THP-1 and U937 cells were centrifuged at 10,000 rpm for 5 minutes to create a cell pellet and waste media was discarded. The remaining cell pellet was washed in 10ml sterile phosphate buffered saline (PBS; Sigma-Aldrich). After centrifugation, pelleted cells were re-suspended in 10ml pre-warmed fresh media and seeded to the recommended cell density 2-5 x10^5 cells/ml (recommended by ATCC) for general cell culture or stock expansion.

For RAW264.7 cells, waste media was discarded and cells were washed with PBS. Cells were detached with 3ml 1x EDTA-trypsin (Sigma) and incubated for approximately 5 minutes. Cell culture flasks were gently tapped to allow for complete detachment of cells. The trypsin was neutralised with 7ml pre-warmed fresh media and seeded in 1:3 or 1:5 manner when 80% confluent.

2.1.4. Cell counting

The number of cells in a flask were quantified using a haemocytometer by attaching a glass coverslip to the chamber. Detached adherent or suspension cells were centrifuged at 10,000 rpm for 5 minutes to create a cell pellet. The waste media was discarded and the pellet was re-suspended in 1ml of media. 10µl re-suspended cell solution was loaded onto the chamber of the haemocytometer (below the coverslip). The average number of cells were calculated per ml using the following equation:

$$Cells\ per\ ml = \frac{Average\ number\ of\ cells\ counted\ x\ Dilution\ factor}{0.0001}$$

2.1.5. Cryopreservation of cells

For cell storage and optimal rate of preservation, cells were cooled to sub-zero temperatures in freezing medium containing dimethyl sulfoxide (DMSO). Cells were centrifuged at 10,000 rpm for 5 minutes. The pellet of RAW264.7 and U937 cells were re-suspended in 90% FBS and 10% DMSO or 50% complete medium, 40% FBS and 10% DMSO for THP-1 cells. The solution was aliquoted into cryovials, placed in a Mr Frosty and frozen overnight at -80^{o}C. The following day, frozen cryovials were transferred to a -150^{o}C freezer for long-term storage.

2.1.6. Reviving cryopreserved cells

All cells were revived by pre-warming the vial to 37^{o}C, then added drop-wise to a falcon tube containing 10ml fresh media. Cells were centrifuged at 10,000 rpm for 5 minutes to remove any traces of DMSO. The supernatant was discarded and the cell pellet was re-suspended in 10ml of fresh media and transferred to a T75 flask. Cells were incubated at 37^{o}C in 5% CO_2 until confluent.

2.2. Cell treatments

2.2.1. Wnt5a

Twenty-four hours prior to treatment, monocytic cell lines were cultured in complete medium containing 0.5% FBS. The following day, cells were treated with 100 and 500ng/ml recombinant human/mouse Wnt5a protein (R&D systems). Protein was extracted for further analysis.

2.2.2. SRPK1 inhibitor: SPHINX31

Pharmacological inhibitor SPHINX31 was kindly provided by Jonathan Morris, University of New South Wales (UNSW). Twenty-four hours prior to treatment, cell culture medium was replaced with complete medium containing 0.5% FBS. Then, cells were treated with 10μM SPHINX31 for twenty-four hours and protein was extracted.

2.2.3. Hypoxia

Monocytic cell lines were cultured in complete medium contained 0.5% or 10% FBS for twenty-four hours before being exposed to 1% oxygen in a sealed hypoxia chamber. At the end of the 24-hour time point, protein was extracted for further analysis.

2.3.4. Hyperglycaemia

THP-1 and U937 cells were exposed to 11, 20, 30 and 40mM glucose for twenty-four hours. Then protein was extracted for analysis.

2.3. Isolation of primary cells

2.3.1. Splenocytes

The spleen was removed from 4-6 mice and mashed in ice cold PBS (1ml/ spleen). Cells were flushed through a 1ml syringe with a 23G needle, layered onto an equal volume of Histopaque 1083 (Sigma) and centrifuged at 400 x g (acceleration 9; brake 0) for 30 minutes at room temperature. The splenocytes were removed from interface layer, washed in PBS and

centrifuged at 250 x g for 10 minutes (acceleration 9; brake 9). The cell pellet was resuspended in 1ml of filter sterilised (0.2µm filter) ice-cold red blood cell (RBC) lysis buffer (155mM ammonium chloride, 10mM potassium bicarbonate and 0.1mM EDTA) for 1 minute to lyse remnant RBC. The cell suspension was diluted in 9ml PBS and immediately centrifuged at 250 x g for 10 minutes. Viable cells were counted using trypan blue for CD11b cell selection or unselected white blood cells were used for RNA extraction.

2.3.2. Bone marrow immune cells

The femur bone marrow was dissected from 4-6 mice as illustrated by (Liu and Quan, 2015). The bone marrow was flushed with sterile PBS three times and the cell suspension was centrifuged at 250 x g for 8 minutes. The remaining pellet was resuspended in 1ml ice-cold RBC lysis buffer for 1 minute, then diluted in 9ml PBS. The cell suspension was centrifuged at 250 x g for 10 minutes and viable bone marrow immune cells were counted for CD11b cell selection or unselected white blood cells were used for RNA extraction.

2.4. CD11b selection

The pellet from splenocytes and bone marrow immune cells was re-suspended in 90µl PBS and 10µl CD11b Microbeads (Miltenyi Biotec) per 10^7 cells and incubated at 4^{o}C for 15 minutes. The mixed population of cells were washed with 1ml of PBS per 10^7 cells and centrifuged at 300 x g for 10 minutes. The supernatant was discarded and the pellet was re-suspended in 500µl PBS. LS columns (Miltenyi Biotec) were placed on the MACS separator (Miltenyi Biotec), washed with 3ml PBS before the cell suspension was added to the column. The column reservoir was washed three times to collect unlabelled cells and placed on a 15ml falcon tube. All labelled $CD11b^+$ cells were collected by adding 5ml PBS and forcing the plunger through the column reservoir. The cell suspension was centrifuged at 300 x g for 10 minutes to create a cell pellet and the RNA was extracted for further analysis.

2.5. RNA extraction

RNA from snap frozen tissue was crushed with a mortar and pestle, transferred to a fresh Eppendorf tube with 1ml TRI Reagent (Sigma) and further homogenised using a vortex. For cells, 500µl of TRI reagent was added to the cells and the lysate was triturated rapidly 10-15 times, transferred to a fresh Eppendorf and left to stand for 5 minutes. To the homogenised tissue or lysed cells, 400µl of chloroform was added per 500µl of TRI Reagent and the mixture was shaken vigorously by hand for 3 minutes before incubating at room temperature for 10 minutes. The samples were centrifuged at 12,000 x g for 15 minutes at 4^{o}C resulting in the mixture separating into three layers: lower red phenol-chloroform phase (containing protein), interphase (containing DNA) and a colourless upper aqueous phase (containing RNA). The aqueous phase was transferred to a fresh Eppendorf tube and the RNA was precipitated overnight with equal volumes of ice-cold isopropanol at -20^{o}C. The next day, the RNA was pelleted by centrifugation at 13,000 x g for 25 minutes at 4^{o}C and the supernatant was discarded. The RNA pellet was washed twice with 1ml 75% ethanol, vortexed and centrifuged at 13,000 x g for 25 mins at 4^{o}C. After discarding the supernatant, the pellet was air-dried at room temperature for 10 minutes and dissolved in 10 to 15µl RNase/DNase free water on ice. RNA concentration was measured in the Nanodrop (A260/280 >1.7 and A260/230 >1.7) and stored at -80^{o}C.

2.6. cDNA synthesis

cDNA was generated using the Takara Primescript RT kit. 1µg of RNA was added to each reaction. For each sample, a 20µl reaction volume was prepared with 4µl of 5x primescript buffer, 1µl of 50µM oligo dT and 4µl of 100µM random 6mers. Samples were heated to 65^{o}C for 10 minutes to denature the secondary structures and prevent primer dimers. At this point, the samples were held at 4^{o}C for 5 minutes while 1µl of primescript RT enzyme was added. All samples were placed in the thermocycler and incubated at 25^{o}C for 10 minutes. This was followed by an extension step

at 37ºC for 60 minutes and a final enzyme inactivation step at 85ºC for 1 minute. cDNA was stored at -20ºC until required.

2.7. PCR

Each PCR reaction was made using Promega GoTaq G2 Master Mix (Promega, M7822). For each sample, a 15µl PCR reaction volume was prepared with 7.5µl 2x green flexi buffer, 0.6µl of 10µM forward and reverse primer (final concentration of 0.4µM) and 1µl cDNA. The samples were denatured at 95ºC for 3 minutes, followed by a 35 cycle PCR reaction which included denaturation at 95ºC for 30 seconds, annealing 56-66ºC (annealing temperature for each primer set is stated in Table 1, below) for 30 seconds and extension at 72ºC for 1 minute. A final extension at 72ºC for 5 minutes ensured full extension. Samples were held at 4ºC until gel electrophoresis. PCR products were run on a 2% agarose gel in 1x TAE (0.04M Tris-Acetate and 0.001M EDTA) with 25ng/ml ethidium bromide for 1 hour 30 minutes at 90V. The agarose gel was visualised on a UV Transilluminator GelDocEZ system. A sample with no reverse transcriptase was also run as a negative control (-RT). *Gapdh* was used as the housekeeping gene and a control of equal cDNA synthesis.

Table 1. PCR primer sequences, annealing temperatures and product size.

PCR	Forward (F)/ Reverse (R) primer sequence	Annealing temp (°C)	Product size (mouse, bp)
Wnt5a (1)	F: GAATCCCATTTGCAACCCCTCACC R: GCTCCTCGTGTACATTTTCTGCCC	60	205
Wnt5a (2)	F: CAGGTCAACAGCCGCTTCAAC R: ACAATCTCCGTGCACTTCTTGC	58	266
Flt1 (*Vegfr1*)	F: GTCACAGATGTGCCGAATGG R: TGAGCGTGATCAGCTCCAGG	60	634
sFlt1	F: GTCACAGATGTGCCGAATGG R: TGACTTTGTGTGGTACAATC	58	398
Srpk1 (ex1-ex3)	F: TCTCGCCATGGAGCGGAAAG R: GGGTCTTCCTGCTCGTCATC	62	183
Srpk1 (ex1-ex7/8)	F: TCTCGCCATGGAGCGGAAAG R: TCCAGGCCCTGTAGCACTTG	62	609
Gapdh	F: CCATCTTCCAGGAGCGAGAC R: GCCCTTCCACAATGCCAAAG	58	297

2.8. Protein extraction

2.8.1. Cell lysis

To extract proteins, treated suspension cells were transferred to a 15ml falcon tube on ice and centrifuged at 10,000 RPM at 4^{o}C for 5 minutes. The media was discarded and cell pellet was washed in ice cold PBS. After centrifugation, the cell pellet was re-suspended in 50-100µl ice cold NP40 lysis (150mM sodium chloride, 1% triton X-100 and 50mM tris (pH 8.0)) buffer supplemented with 1mM phenylmethylsulfonyl fluoride (PMSF), 1mM sodium orthovanadate (Na_3VO_4), 50mM sodium fluoride (NaF) and protease inhibitor (Sigma), then transferred to a 1.5ml Eppendorf tube.

Similarly, treated adherent RAW264.7 cells were washed in ice cold PBS three times. 50-100µl ice-cold NP40 lysis buffer (supplemented with 1mM PMSF, 1mM Na_3VO_4, 50mM NaF and protease inhibitor) were added to each well, the cells were scraped and transferred to a 1.5ml Eppendorf tube.

All samples were kept on ice for a further 10 minutes, vortexed and centrifuged at 10,000 RPM at 4^{o}C for 15 minutes to pellet the cell debris. The supernatant containing the protein was transferred to a fresh 1.5ml Eppendorf tube and stored at -80^{o}C until required.

2.8.2. Tissue lysis

Snap frozen gastrocnemius tissue was homogenised in 500µl ice-cold NP40 supplemented with 1mM PMSF, 1mM Na_3VO_4, 50mM NaF and protease inhibitor (Sigma) using a beadbug homogeniser (Benchmark Scientific) in pre-filled beadbug tube (Sigma) to mechanically homogenise tissue for 5 minutes at a speed of 400. The homogenised solution was transferred to a 1.5ml Eppendorf tube, vortexed and centrifuged at 27,000 x g for 20 minutes. The supernatant was transferred to a fresh 1.5ml Eppendorf tube and stored at -80^{o}C.

2.8.3. Protein quantification

Total protein in each sample was quantified using a Bradford protein quantification assay (Bio-Rad). Bovine serum albumin (BSA) serial dilutions were used to obtain a range of standards ranging from 4000-0µg/ml in PBS. Protein samples were diluted 1:10 and 1:50 in PBS. BSA standards and protein samples were loaded in triplicate in 96-well plates (10µl/well). Protein assay dye reagent concentrate (Bio-Rad) was diluted 1:5 in distilled water and added to 96-well plates (200µl/well). The colorimetric reaction was measured using the microplate reader at 620nm (Infinite F50, Tecan UK) after the plate was agitated for 10 seconds. All absorbance reading were corrected by subtracting from the blank and protein concentrations were calculated using the BSA standard curve on Microsoft Excel™.

2.9. Western blot

2.9.1. Sodium dodecyl sulfate-polyacryamide gel electrophoresis (SDS-PAGE)

50-100µg of protein samples were mixed with 10µl 4x laemelli buffer (BioRad), denatured for 5 minutes at 95°C and centrifuged briefly. Samples were loaded on a 10% mini-protean pre-cast gel (BioRad) with 4µl precision plus protein dual standards (BioRad) submerged in running buffer (25nM tris-base, 190nM glycine and 0.1% SDS). Samples were subjected to electrophoresis at 90V for 40 minutes followed by 120V at room temperature. The separated proteins were transferred to a methanol-activated polyvinylidene difluoride (PVDF) membrane using a trans-blot turbo transfer system (BioRad) for 10 minutes.

The membrane was blocked in 5% BSA- tris buffered saline with 0.05% tween-20 (TBS-T) for 1.5 hours at room temperature on the shaker. The blocking solution was replaced with primary antibodies diluted in 5% BSA/TBS-T (dilutions for each antibody stated in Table 2) overnight at 4°C on the shaker.

Table 2. List of primary antibodies.

Primary Antibody	Dilution
Rabbit polyclonal anti pan-VEGF (A20; Santa Cruz, sc-47778)	1:200
Mouse monoclonal anti-VEGF-A_{165}b (in- house)	1:500
Rabbit anti-SAPK/JNK (Cell signalling 9252)	1:1000
Rabbit anti- phosphor-SAPK/JNK Thr183/Tyr185 (Cell signalling, 9251)	1:1000
Anti-beta-actin (C4; Santa Cruz, sc-47778)	1:1000
Rabbit monoclonal anti – α -Tubulin (Cell Signalling, 2125S)	1:1000

Membranes were then washed three time for 5 minutes in TBS-T and incubated for one hour with Licor IgG secondary antibodies (as shown in Table 3, diluted in 5% BSA/ TBS-T) in the dark at room temperature on the shaker. The wash steps were repeated and the membrane was visualised using the Licor Odyseey imaging system.

Table 3. List of secondary antibodies.

Secondary Antibody	Dilution
IRDye 800 donkey anti-mouse (Licor, 926-32212)	1:5000
IRDye 800 donkey anti-rabbit (Licor, 926-32213)	1:5000
IRDye 680 donkey anti-mouse (Licor, 926-68072)	1:5000
IRDye 680 donkey anti-rabbit (Licor, 926-68073)	1:5000

Probed PVDF membrane were stripped with fluorescent stripping buffer (Thermofisher Scientific) for 15 minutes, washed in TBS-T three times for 5 minutes and blocked with 5% BSA/TBS-T for one hour. Then, the membranes were re-probed with desired primary antibody (Table 2) overnight as described above.

2.10. Enzyme linked immunosorbent assay (ELISA)

2.10.1. Pan-VEGF and $VEGF_{165}b$

To quantitatively detect VEGF isoforms in protein extracts from tissue (as per section 2.8.2), an ELISA was performed using the human VEGF (R&D systems, DY293B) or $VEGF_{165}b$ DuoSet (R&D systems, DY3045) ELISA kit on the plate shaker (unless stated otherwise).

High binding 96-well plates were coated with 1µg/ml pan-VEGF and 2µg/ml $VEGF_{165}b$ capture antibody overnight at room temperature on the shaker. The plates were washed three times with wash buffer (0.05% Tween-20/PBS, T-PBS) and blocked with 200µl/well of 1% BSA/PBS at room temperature for 2 hours. Serial dilutions were prepared with rhVEGF and $rhVEGF_{165}b$ diluted in NP40 (ranging from 1.95 to 500pg/ml and a blank) were added in duplicate (100µl/well). 150µg of protein tissue was added in duplicate to each well. The 96-well plates were incubated for two hours at room temperature on the shaker. Then the 96-well plates were washed

three times and incubated with 100µl/well of human VEGF (100ng/ml) or $VEGF_{165}b$ (250ng/ml) detection antibody diluted in 1% BSA/PBS for two hours. After a further wash step, 100µl/well of horseradish peroxidase (HRP)- conjugated streptavidin (diluted 1:200 in PBS) was added and the plate was left in the dark for 30 minutes. After a final wash step, 100µl/well of the substrate solution (R&D system) was incubated for an hour at room temperature in the dark. The reaction was stopped by the addition of 50µl/well 1M hydrochloric acid. The colorimetric reaction was measured using the microplate reader at 450nm (Infinite F50, Tecan UK). The protein concentration in each sample was calculated by subtracting absorbance values from the blank and the standard curves was used to calculate protein content in each sample.

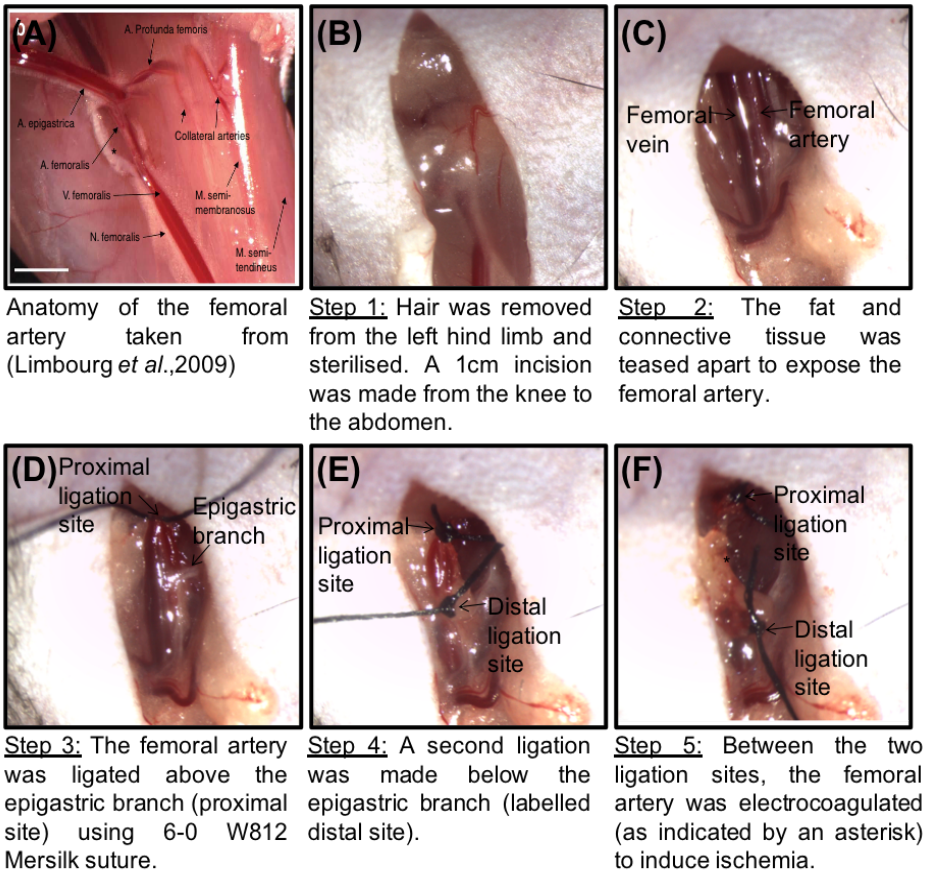
2.11. Hind limb ischemia model

All animal experiments were conducted in accordance with the Animal (Scientific Procedures) Act of 1986 (ASPA) at the University of Nottingham under the authority of the Home Office. All experiments were performed under UK Home Office licence (PPL PE6932817F) held by Professor David O Bates. Transgenic mice were bred and maintained in-house. All animals were genotyped by Transnetyx Inc. All *in vivo* experiments were performed on mixed gender mice.

2.11.1. Surgery

At the age of 10-12 weeks old (unless stated otherwise), transgenic C57BLJ mice were anaesthetised with 2% isoflurane (100% w/w, IsoFlo ®) in 100% oxygen at a flow rate of 2L/minute. Withdrawal reflexes were confirmed with toe pinching to ensure there was no movement before the mouse was moved to the imaging or surgical platform on the heat pad (Harvard Apparatus). Body temperature was controlled throughout the surgery and imaging with a rectal probe (Harvard Apparatus). Upon stable anaesthesia, the hind paws were imaged using the laser speckle imaging system (FLPI-2, Moors Instruments) to confirm blood flow to both paws. Mice were injected with pre-operative analgesic (0.05mg/kg buprenorphine,

Animalcare Group) diluted in sterile saline (0.9% NaCl) via a subcutaneous route (s.c.). Hair removal cream (Nair) was applied to the left hind limb where the surgery was to be performed and the area was sterilised with a hydrex derma spray (Scientific Laboratory Supplies). Then, the mouse was transferred to the surgical platform where the left paw was extended, taped down and covered with a sterile surgical drape (only the surgical area was exposed). Using a dissection microscope (Leica), a 1cm incision was made from the knee to the abdomen (Figure 2.1). The fat was separated from the connective tissue to expose the femoral artery from the vein and nerve. A piece of 6-0 W812 Mersilk suture (Ethicon) was passed underneath the femoral artery and the vessel was tied off above the superficial epigastric artery. A second suture was passed lower down the knee near the sapheno-popliteal bifurcation. The vessel was electro-coagulated between the two sutures using a cauterizer (Wuhan Spring Scenery Medical Instrument Co Ltd, Evergreen) at 18V. The incision was closed using surgical clay Adams clips (Scientific-Labs) and a topical tissue adhesive, GLUture (Zoetitis). After the surgery was performed, the mouse was placed on the imaging platform, where hind paws were imaged to confirm successful surgery and ischemia. A summary of the procedure is shown in Figure 2.1.



Anatomy of the femoral artery taken from (Limbourg *et al.*,2009)

Step 1: Hair was removed from the left hind limb and sterilised. A 1cm incision was made from the knee to the abdomen.

Step 2: The fat and connective tissue was teased apart to expose the femoral artery.

Step 3: The femoral artery was ligated above the epigastric branch (proximal site) using 6-0 W812 Mersilk suture.

Step 4: A second ligation was made below the epigastric branch (labelled distal site).

Step 5: Between the two ligation sites, the femoral artery was electrocoagulated (as indicated by an asterisk) to induce ischemia.

Figure 2.1. Step by step guide to induce hind limb ischemia in mice (A-F). Panel A taken from (Limbourg et al., 2009).

The animal was given time to recover in the post-operative room in a warmed, clean cage with mash. The mouse was monitored for a few hours to ensure there were no signs of pain, or suffering after surgery. The wound, paws and weights of each animal was monitored twice a day for the first seven days and then weekly thereafter. The blood flow to the paws were imaged on post-operative days 1, 2 and 3 or 3, 7, 14 and 21 and/or 28.

2.11.2. SPHINX31 Treatments

The day after surgeries, body condition and weight was checked and recorded for each mouse. One group was treated with intraperitoneal injection (i.p.) of 0.8mg/kg SPHINX31 (diluted in 0.9% NaCl), twice per week. The other group was treated with i.p. injection of 0.32% DMSO (diluted in 0.9% NaCl), twice per week. For the day 21 HLI study, both mouse groups were administered the treatment on post-operative day 1 and bi-weekly thereafter.

For the day 3 HLI study, animals were treated with a single dose of 0.8mg/kg SPHINX31 (diluted in 0.9% NaCl via an i.p.) immediately after surgery. Remaining transgenic mice were not administered any further treatment unless specifically stated.

2.11.3. HF/HS Diet

For the HF/HS diet (S1850, BioServ) induced obesity, 4-week-old mice were maintained on a HF/HS diet for the 8 weeks prior to surgery. The composition of the HF/HS diet was 36.0% fat, 36.2% carbohydrates and 20.5% protein. At the age of 12-weeks-old all mice underwent the HLI procedure on the left femoral artery (as previously described in 2.11.1) and blood flow was monitored to the paws. Mice were maintained on a HF/HS diet for the remaining 28 days.

2.11.4. Measurement of blood flow recovery *in vivo*

Prior to imaging, mice were anaesthetised with 2-3% isoflurane in 100% oxygen at a rate of 2L/minute. When anaesthetised and withdrawal reflexes confirmed no movement, the mouse was transferred to the imaging platform. Laser speckle images were taken using the Moor FLPI-2 full field laser perfusion imager, which relies on an infrared laser beam directed towards the paw. The backscattered light from the moving red blood cells is detected as coloured speckles which indicates the level on the spectrum as shown in Figure 2.2A. Speckle intensity was measured in the region of interest (ROI). Therefore, the blood flow recovery can be calculated by using the ratio of the ischemic vs contralateral speckle intensity Figure 2.2B. It is important to note that the speckle pattern of the hind paws correlates with the velocity/speed of the moving red blood cells in the ROI. This is associated with a flux value, which is calculated by the Moors Instrument analysis software. In fact, a high velocity results in a low contrast in the ROI. This technique does not provide data on the area of the vessels or the volume of blood flowing through the vessels. However, blood velocity is directly proportional to the flow. Therefore, it is considered to be representative of blood flow as referred to in this thesis.

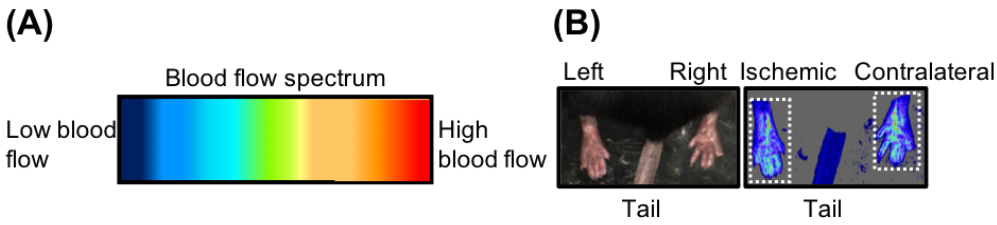


Figure 2.2. Measuring the speckle intensity using the Laser Speckle Imaging System. (A) *The blood flow spectrum highlights the levels of blood flow.* ***(B)*** *Example of the paws and laser speckle image highlighting the left (ischemic) and right (contralateral) paw and the tail. The white box around the paw indicates region of interest (ROI) used to calculate the speckle intensity.*

All mice were culled on day 3 or day 21 by an approved schedule 1 method. Mice were culled by cervical dislocation for cell isolations (method described in section 2.3). For protein and RNA work, mice were culled by an overdose of CO_2 and tissue was snap-frozen in liquid nitrogen. For immunofluorescence, mice were administered an i.p. injection of 1mg/kg medetomidine (Sedastart, Animalcare Group) and 75mg/kg ketamine (Ketaset, Zoetis). Once withdrawal reflexes confirmed no movement, cardiac perfusion was performed on the animals with 25 ml of PBS followed by 25 ml of 4% paraformaldehyde (PFA)/PBS. Gastrocnemius muscle was either snap-frozen or post-fixed in 4% PFA overnight. If post-fixed, the following day, the tissue was washed in PBS, cryo-protected in 30% sucrose and embedded in optimal cutting temperature compound (OCT, Labtech) then stored at -80^{o}C.

2.11.5. Adverse effects

Of the 150+ transgenic mice that underwent the hind limb ischemia procedure of the left femoral artery, a small number of mice experienced unexpected adverse effects due to an incorrect ligation at the proximal site (shown in Figure 2.3). All mice acquired a pale paw immediately after surgery indicating reduced blood flow. Between day 1 to 3 post-surgery, 2 mice developed a swollen foot, 4 mice developed necrotic toes and 12 mice experienced tail de-gloving (early signs of tail necrosis). After seeking advice from the Named Veterinary Surgeon (NVS), Named Animal Care

and Welfare Officer (NACWO) and Home Officer Inspector the mice were culled before the of the study to prevent pain, distress and suffering

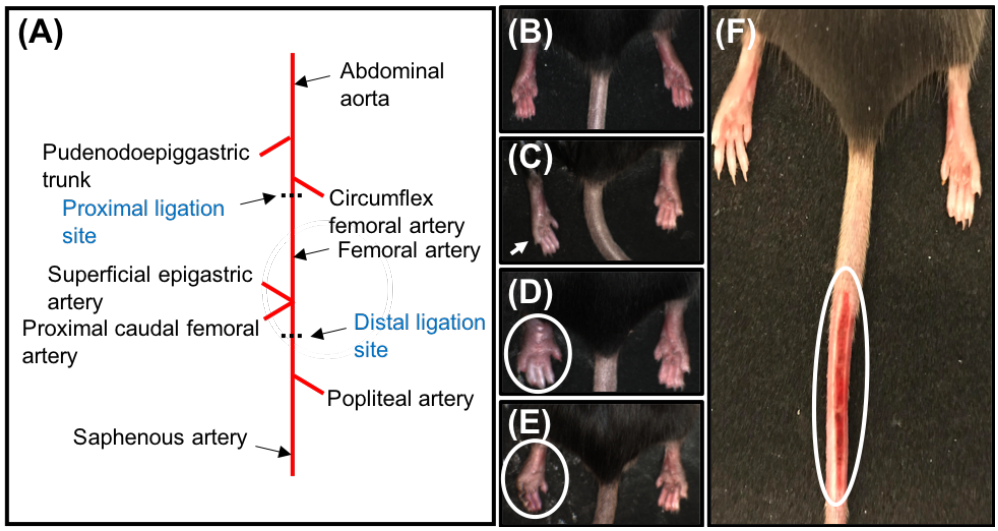


Figure 2.3. Adverse effects that occurred due to incorrect ligation of the left femoral artery. ***(A)*** *Anatomy of the left femoral artery highlighting the incorrect ligation site as shown black dotted line. The representative images highlight* ***(B)*** *Pre-op day 0: healthy paws and* ***(C)*** *Post-operative: day 0 discoloured pale left paw (white arrow). The ischemic damage (highlighted by a white circle) developed within 3 days after the ligation:* ***(D)*** *Swollen paw* ***(E)*** *Necrotic toes and* ***(F)*** *Tail de-gloving (early sign of tail necrosis).*

2.12. Immunofluorescence on gastrocnemius muscle

Gastrocnemius muscle was embedded in OCT in cryomolds ensuring muscle fibres were orientated transversely in the chamber of the cryostat. Multiple 5µm sections were cut at different points using a cryostat and mounted on superfrost plus glass slides (Thermo Scientific). All staining steps were carried out in a dark humidified StainTray slide staining system, unless stated otherwise. Sections were fixed in acetone for 5 minutes at -20^{o}C and left to dry at room temperature for 10 minutes. A PAP pen (Scientific Laboratory Supplies) was used to draw a hydrophobic circle around each muscle section, and were subsequently washed in PBS three times for 5 minutes. Sections were permeabilised in 0.1% triton-X with PBS for 5 minutes. After the wash steps were repeated, 1% BSA/PBS (blocking solution) was added for one hour at room temperature. The sections were

incubated in primary antibody (1:150, IB_4) and/or α-smooth muscle actin-cy3 (1:300, Sigma-Aldrich) diluted in blocking solution overnight at 4°C. A non-primary antibody slide was used as a negative control for the staining. The next day, sections were washed 3 times in PBS and incubated with Alexa Fluor streptavidin 488 (1:500, if co-stained) or Alexa Fluor streptavidin 555 (1:500, if IB_4 was independently stained) in 1%BSA/PBS and co-stained with DAPI (1:1,000) for one hour at room temperature. After a final wash step, cover slips were mounted with ProLong Gold Anti-Fade Reagent (Cell Signalling) and sealed with clear nail varnish the following day.

Images were taken at 10x magnification with a Leica Confocal Microscope or the Leica Kubler Codix Fluorescence Microscope. For each gastrocnemius muscle (contralateral and ischemic), 4 sections were taken and 2 fields of view per section. For quantification, capillaries and arterioles were counted using FIJI and averaged per mm^2.

2.13. Statistical analysis

All data was analysed using Microsoft Excel and GraphPad Prism, in conjunction with manufacturers software's where applicable. Specific software's included Moors Instruments, Licor Image Studio Software (lite) and FIJI for image analysis. Power calculations were performed on G*Power to determine the number of animals required to give an acceptable power of 0.80 standard and a significance of p=0.05. This is between 7-9 animals per group. Statistical tests performed were two-way analysis of variance (ANOVA) with post-hoc Bonferroni test when comparing blood flow recovery of transgenic mouse models after induction of ischemia by group over time. Vessel densities and expression levels between the ischemic and contralateral gastrocnemius muscle of mouse groups were also analysed by a two-way analysis of variance (ANOVA) with a post-hoc Bonferroni's test. For comparisons of three independent groups, a one-way analysis of variance (ANOVA) with post-hoc Bonferroni's test were used. For comparisons of two independent groups, an unpaired t-tests was used. All

data is shown as the mean ± standard error of the mean (SEM), unless stated otherwise. All results were considered statistically significant at the following thresholds if $p \leq 0.05$ (*), $p \leq 0.01$ (**), $p \leq 0.001$ (***) and $p \leq 0.0001$ (****). If this is not stated, the data is considered non-statistically significant (ns, $p > 0.05$). N values are indicated in each figure legend, where appropriate.

Chapter 3

Monocyte specific Wnt5a over expression impairs revascularisation in mice

3.1. Introduction

PAD is caused by an obstruction of the arteries, which can be circumvented by the development of collateral vessels in response to ischemia. This is driven by the resulting hypoxia. Circulating monocytes infiltrate towards the ischemic region and generate VEGF-A driving the angiogenic process in the ischemic tissue (Wu *et al*., 2010, Greve *et al*., 2008). However, PAD patients have impaired capillary density, reduced blood flow and oxygen levels in the skeletal muscle (Duscha *et al*., 2011). Inhibition of VEGF-A results in reduced angiogenesis and impaired collateral formation (Greve *et al*., 2008). Patients with PAD are unable to stimulate the known angiogenic actions of VEGF-A despite having raised circulating levels resulting in PAD and can further progress to CLI (Kikuchi *et al*., 2014, Findley *et al*., 2008, Makin *et al*., 2003). The molecular mechanism behind this is not fully known.

In 2010 it was established that the pro-inflammatory molecule Wnt5a is overexpressed in monocytes/macrophages of obese and type 2 diabetic mouse models. This over expression results in downstream activation of pJNK pathway, which in turn indicates that the non-canonical signalling pathway is involved in the process (Ouchi *et al*., 2010). Wnt signalling has also been associated with a greater infiltration of macrophages to the ischemic region in transgenic mouse models. Genetic ablation of Sfrp5, which usually acts to attenuate Wnt signalling by binding and sequestering its action, results in enhanced macrophage infiltration in ischemic tissues (Kikuchi *et al*., 2014, Ouchi *et al*., 2010). Conversely, silencing of Wnt5a *in-vivo* downregulates inflammatory mediators and reduces the pathogenesis and progression of atherosclerosis (Yang *et al*., 2014). In a clinical setting, PBMCs and monocytes of PAD patients displayed an increase in Wnt5a which positively correlated with advanced human atherosclerotic lesions and disease severity (Kikuchi *et al*., 2014, Malgor *et al*., 2014).

The link between Wnt5a and angiogenesis was first identified in retinal myeloid cells, whereby a mutation of Wnt5a was associated with an

increase in the angiogenic capability through a Flt1/sFLT1 mechanism (Stefater *et al*., 2011). However, more recent evidence suggested that hyperactivity of monocytic Wnt5a impaired limb revascularisation after HLI, as shown by a dramatic reduction in the capillary density (Kikuchi *et al*., 2014). This was shown to be associated with an increase in VEGF-A_{165}b in the ischemic gastrocnemius at an RNA and protein level (Kikuchi *et al*., 2014). Interestingly, administration of an isoform specific anti-angiogenic neutralising VEGF-A_{165}b antibody reversed and improved the blood flow recovery (Kikuchi *et al*., 2014). The molecular mechanism was further elucidated in a macrophage cell line displaying a dose dependent increase of the anti-angiogenic VEGF-A isoform with Wnt5a treatment through pJNK/SC35 (Kikuchi *et al*., 2014).

There is mounting evidence to suggest that monocytic Wnt5a has a significant role in the progression of PAD through VEGF-A_{165}b resulting in impaired revascularisation. Therefore, the purpose of this study was first to confirm whether monocytic Wnt5a hyperactivity in transgenic mouse models *in vivo* results in impaired blood flow recovery after induction of ischemia, as previously published in the literature by Kikuchi *et al*. After assessing the capillary and arteriolar density in response to ischemia in the gastrocnemius muscle, this would provide the basis for me to explore the mechanisms through which pro- and anti-angiogenic VEGF-A isoforms could be regulated in this model.

3.2. Methodology

Adult transgenic LysM-Wnt5a^{GOF} mice (C57Bl/J) were bred in-house and genotyped by Transnetyx Inc. At the age of 10-12 weeks, a total of 55 mixed gender mice were subjected to a hind limb ischemia (HLI) model of PAD. Mice were anaesthetised with 2-3% isoflurane in 100% oxygen and administered a pre-operative analgesic (0.05mg/kg buprenorphine, s.c.) diluted in sterile saline (0.9% NaCl, s.c.). Between post-operative days 0-3, a total of 18 mice experienced adverse effects including necrotic toes (n=4), swollen paw (n=2) and tail de-gloving (n=12) and were culled before the end of the study (as shown previously in Chapter 2, Figure 2.3). Remaining mice (7 STOP-Wnt5a, 15 WT and 15 LysM-Wnt5a^{GOF}; refer to Table 4 for the nomenclature for each respective mouse) were imaged on pre-operative day 0 and post-operative days. Analysis was performed using the FLPI-2 (Moors Instruments) software by taking the ratio of the ischemic vs contralateral speckle intensity at each time point. Further analysis was performed on the data by normalising to the pre-operative speckle intensity of each respective mouse.

RT-PCR was performed on the RNA extracted from splenocytes to assess the *Wnt5a* levels. On day 3, animals were culled and gastrocnemius muscle was snap-frozen in liquid nitrogen to assess the protein level of VEGF-A isoforms by western blot and ELISA. On day 21 animals were culled by cardiac perfusion and gastrocnemius muscle was dissected for histological analysis by staining with isolectin-B4 (IB_4) for capillaries and alpha-smooth muscle actin (αSMA) for arterioles. Using the FIJI image analysis software, the capillary and arteriolar density was calculated. All methods are described in detail in Chapter 2.

Table 4. Simplified mouse names used and respective nomenclature

Simplified name for transgenic mouse model	Nomenclature for mouse strains
STOP-Wnt5a	*Rosa26^{Wnt5aStopLoxP}*
LysM-Wnt5a^{GOF}	*Rosa26$^{LysM\text{-}Cre/Wnt5a}$*

3.2.1. Statistical analysis

Statistical tests performed were a two-way ANOVA with post-hoc Bonferroni's test when comparing the blood flow recovery after induction of ischemia between mouse group on post-operative days. The analysis of vessel densities or expression levels of VEGF-A isoforms between the gastrocnemius muscle of mouse groups was performed using a two-way ANOVA with post-hoc Bonferroni's test. For comparisons of two independent mouse groups (e.g. WT vs LysM-Wnt5a^{GOF}), unpaired t-tests were used.

3.3. Results

3.3.1. The LysM-Wnt5a^{GOF} mouse model

To confirm that previously identified monocytic Wnt5a is responsible for ischemia induced impaired revascularisation in PAD, a mouse model overexpressing Wnt5a in the monocytes was constructed in the same manner as Kikuchi and colleagues (Kikuchi *et al*., 2014). The transgenic mouse model was generated by breeding a knock-in mouse carrying a stop codon downstream of a strong CAG promoter (CMV enhancer, chicken beta-Actin promoter and rabbit beta-Globin splice acceptor site) followed by a cre-inducible *Wnt5a* transgene (*Rosa26*^{Wnt5aStopLoxP}; hereafter referred to as STOP-Wnt5a) flanked by two LoxP sites on the *Rosa26* locus followed by an IRES (internal ribosomal entry site) GFP Nuc (nuclear GFP) sequence with a LysozymeM-Cre (LysM-Cre) mouse (Figure 3.1A). The LysM promoter is driven in monocytes and myeloid cells allowing for cre-mediated excision of the stop codon by Cre mediated recombination at the LoxP sites. This results in Wnt5a gain of function (GOF) by its over expression in LysM expressing monocytes (*Rosa26*$^{LysM\text{-}Cre/Wnt5a}$; hereafter referred to as LysM-Wnt5a^{GOF}) as shown in Figure 3.1B.

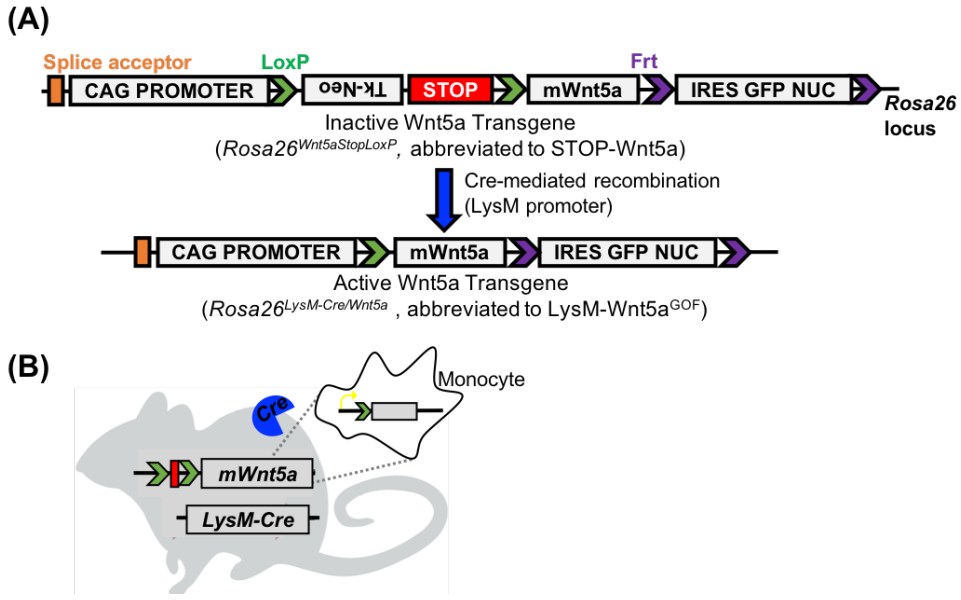


Figure 3.1. Developing mice with monocyte specific Wnt5a overexpression by Cre/LoxP strategy. (A) *The Wnt5a gene is inserted into the Rosa26 locus. By Cre/LoxP strategy, the stop codon is removed resulting in an active Wnt5a transgene in monocytes driven by the LysM promoter. Taken and adapted from (Kikuchi et al., 2014).* ***(B)*** *Heterozygous LysM-Wnt5a^{GOF} mice have cell specific Wnt5a overexpression in the monocytes.*

The pups generated from breeding in Figure 3.1A were ear notched for genotyping which was performed by Transnetyx Inc using qPCR. To genotype WT mice, primer sets were designed to flank exon 1 and 2 of the *Rosa26* locus on chromosome 6. The insertion of the inactive *Wnt5a* cassette between exon 1 and 2 of the *Rosa26* locus was confirmed by a second primer set designed to span the SV40-tag based on the plasmid 15912 (AddGene; Figure 3.2A). A final primer set spanning the *LysM-Cre* allele was necessary to confirm the recombination of the inserted inactive *Wnt5a* transgene (Figure 3.2 A and B). An example of the qPCR curves for all primer sets are shown in Figure 3.2C displaying a positive result for all primer sets if the cycle threshold (C_t) was between 23-26 confirming the mouse was heterozygote for the wildtype (WT) allele and active *Wnt5a* transgene. By calculating the delta C_t (ΔC_t) value from the C_t value for control gene (*Gapdh*) to each probe, all 23 mice had the *Rosa26*-WT locus present. Of these mice, 10 were wildtype with Cre present (red; known as WT). The remaining 13 mice were heterozygote for wildtype allele and the Wnt5a transgene, however Cre was present in 10 (green; known as LysM-Wnt5a^{GOF}) and absent in 3 (blue, known as STOP-Wnt5a) (Figure 3.2D).

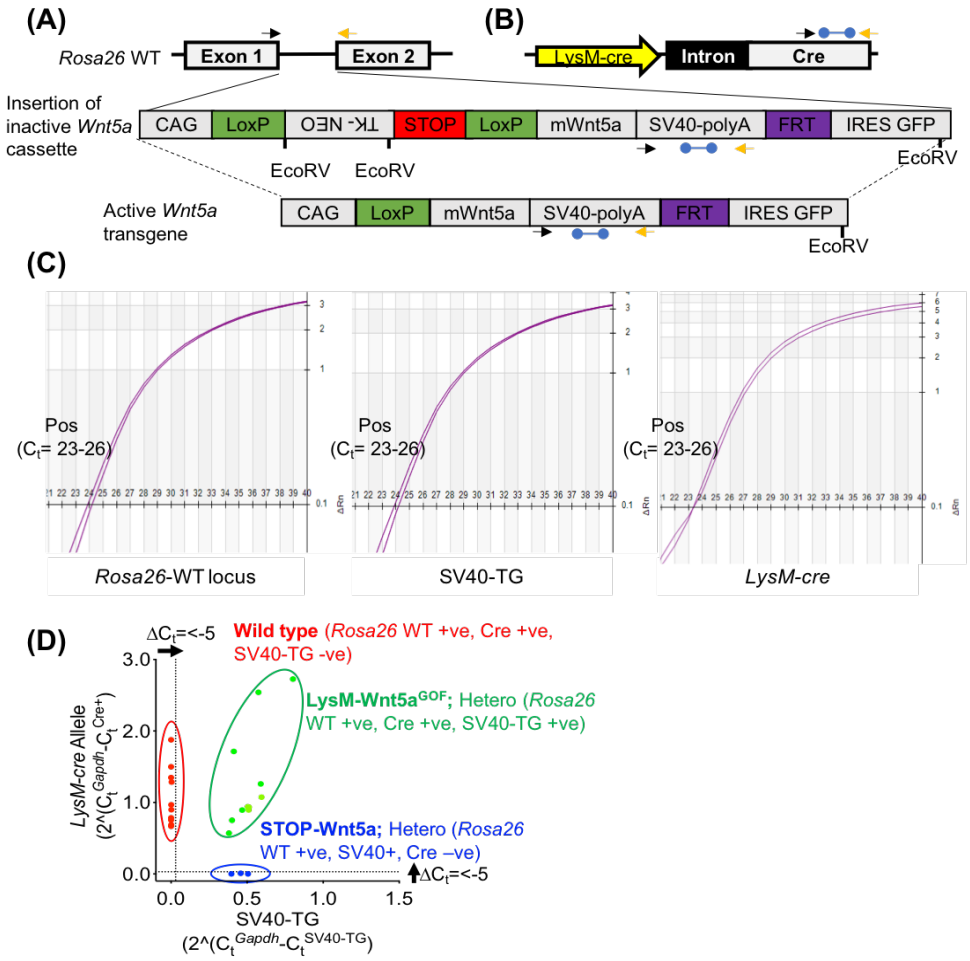


Figure 3.2. Genotyping the LysM-Wnt5a^{GOF} transgenic mice. ***(A)*** *To genotype WT mice, the primers were used on either side of exon 1 (black arrow) and 2 (orange arrow) on the Rosa26 WT locus. The inactive Wnt5a cassette was inserted between exon 1 and exon 2 in the Rosa26 WT locus. Another primer set was used to span the SV40 polyadenylation site (black and yellow arrow) with a Taqman probe (blue dumbbell) to determine the presence of an active and inactive Wnt5a transgene. This was based on Plasmid 15912 (AddGene).* ***(B)*** *To screen for the LysM-cre allele, primers were used upstream (black) and downstream (orange) of Cre, along with Taqman probe (blue dumbbell).* ***(C)*** *qPCR curves of DNA extracted from ear notches (in duplicate) using the ROSA26 WT (left), SV40-TG (middle) and Cre (right) primers.* ***(D)*** *The C_t difference between control (Gapdh) and test genes were calculated and plotted raised to the power of two. Thus, presence of the allele gives a C_t value close to or greater than the Gapdh C_t value, and so a ΔC_t value of -1 to above zero ($2^{\wedge}\Delta C_t$ of 0.5 to >1). Absence of the transgene would mean a ΔC_t less than -5 ($2^{\wedge}\Delta C_t$ of 0.03) lying outside the dotted lines. All animals have the insertion in the Rosa26 locus. WT mice have a positive LysM-cre value, and low (<0.03) SV40-TG value (red), and a LysM-Wnt5a^{GOF} mice are positive for both alleles (green). The STOP-Wnt5a showed a positive SV40-TG signal and low (<0.03) LysM-cre signal (blue).*

To confirm an overexpression of *Wnt5a*, RNA was extracted from pooled WT and LysM-Wnt5a^{GOF} splenocytes, synthesised into cDNA and RT-PCR performed. Two different primer sets spanning exon 5 of the *Wnt5a* gene along with a sample containing no reverse transcriptase (-RT, negative control) were run on an agarose gel. To optimise the annealing temperature, a gradient was performed between 52-62^{o}C on WT and LysM-Wnt5a^{GOF} splenocytes. As expected, *Wnt5a* was not detected in WT splenocytes at any annealing temperature. At 52, 54, 60 and 62^{o}C a band was present for *Wnt5a* at 205bp for LysM-Wnt5a^{GOF} (Figure 3.3A). The PCR was re-run at 60^{o}C, which confirmed the presence of *Wnt5a* in LysM-Wnt5a^{GOF} splenocytes, whilst remaining absent in WT mice (Figure 3.3B). Similar expression levels were observed using a second set of primers spanning exon 5 at 266bp (Figure 3.3C). The results were consistent with our hypothesis that the LysM-Wnt5a^{GOF} mice had an overexpression of *Wnt5a* mRNA in monocytes and validated the transgenic mouse model (Figure 3.1).

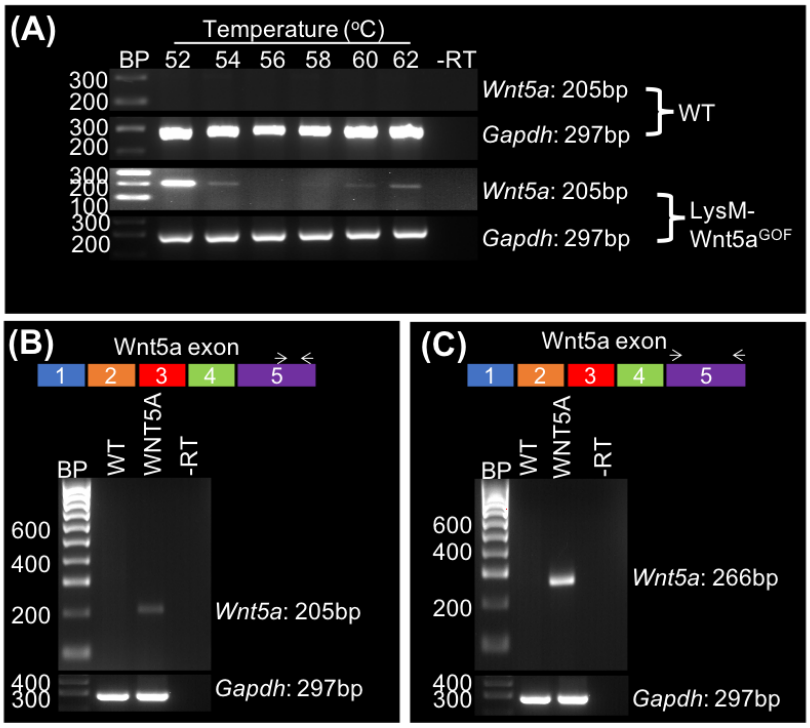


Figure 3.3. Validating the expression of Wnt5a in splenocytes of WT and LysM-Wnt5a^{GOF} mice. *RNA was extracted from the splenocytes and RT-PCR was performed to measure the Wnt5a expression levels.* ***(A)*** *Optimisation of the annealing temperature (52-62^{o}C) of Wnt5a primers spanning exon 5 (205bp).* ***(B)*** ***(C)*** *The expression levels were compared using two different set of primers at annealing temperatures of* ***(B)*** *60^{o}C and* ***(C)*** *58^{o}C annealing temperature.*

3.3.2. LysM-Wnt5a^{GOF} have impaired blood flow recovery

To check that uninduced Wnt5a mice had normal collateral formation and recovery in blood flow, parent strains (WT (N=6) and STOP-Wnt5a (N=7)) littermate mice were subjected to HLI. The representative laser speckle images (LSI) from examples of these mice are shown in Figure 3.4A. The speckle intensity correlates with the blood flow to the hind paw, where red represents high blood flow and blue represents low blood flow (Figure 3.4A). Quantification of the ischemic to contralateral blood flow ratio showed that both strains of mice recovered blood flow equally and completely within the duration of the 21-day study ($p>0.05$, Figure 3.4B). A similar trend was displayed when the data was further normalised to the pre-operative day 0 ratio of each respective mouse ($p>0.05$, Figure 3.4C).

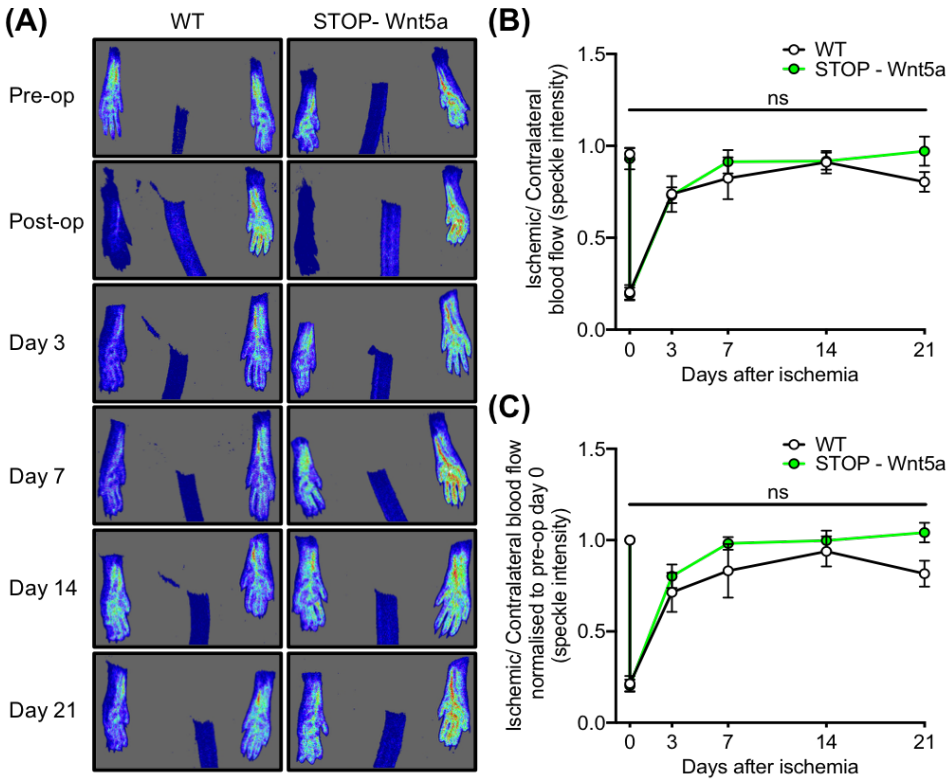


Figure 3.4. No significant difference in blood flow recovery in WT and STOP-Wnt5a mice. (A) *WT and STOP-Wnt5a mice underwent left femoral artery ligation and the blood flow to the paw was measured using the laser speckle imaging system as shown in the representative images.* ***(B)(C)*** *Quantitative analysis of the ratio of the ischemic vs non-ischemic speckle intensity was observed through to post-operative day 21.* ***(C)*** *Data was further normalised to pre-operative day 0 ratio of each respective mouse. Results indicate the mean ± SEM. All data was analysed via a two-way ANOVA (****(B)*** *Main effects: Post-operative day: $p<0.0001$;*

Genotype (mouse group): p=0.45; Interaction effect: p=0.25. ***(C)*** *Main effects: Post-operative day: p<0.0001; Genotype (mouse group): p=0.12; Interaction effect: p=0.29)) with Bonferroni post hoc test. N: WT, N=6 and STOP-Wnt5a, N=7. (ns= non-significant, p>0.05).*

Using the transgenic LysM-Wnt5a^{GOF} mouse model (Figure 3.1), we investigated the effect of monocytic Wnt5a gain of function on revascularisation of blood flow after ischemic injury. The laser speckle images from WT and LysM-Wnt5a^{GOF} mice showed a substantial difference where the ischemic paw of transgenic Wnt5a^{GOF} mice remained blue until day 7 (Figure 3.5A). This is indicative of a low blood flow, compared to the ischemic hind paws from WT mice which appeared to have completely recovered by day 7 and 14. In line with this, quantitative analysis of the speckle intensity of the ischemic to contralateral paw blood flow ratio revealed the blood flow recovery in LysM-Wnt5a^{GOF} mice was significantly lower than WT mice. After 3 days, the blood flow recovery of the ischemic to contralateral ratio had only increased to 0.19 ± 0.03 for LysM-Wnt5a^{GOF} mice compared to litter mate WT mice (0.74 ± 0.10, p<0.0001). The reduced blood flow recovery continued on day 7 (0.40 ± 0.03 compared to 0.82 ± 0.11, p<0.0001) and day 14 (0.59 ± 0.08 compared to 0.91 ± 0.06, p=0.0003). By day 21, both mouse groups had a similar level of blood flow recovery (Figure 3.5B).

Similarly, the ratio of the ischemic to contralateral speckle intensity from Figure 3.5B was normalised to the pre-operative day 0 ratio of each respective mouse, which revealed that the blood flow recovery in LysM-Wnt5a^{GOF} was significantly lower than WT mice. After 3 days, the blood flow ratio had only increased from 0.12 ± 0.01 immediately following surgery to 0.23 ± 0.04 for LysM-Wnt5a^{GOF}, which was significantly lower than the littermate WT controls (0.78 ± 0.10, p<0.0001). This trend of reduced blood flow continued on day 7 (0.47 ± 0.05 compared with 0.88 ± 0.11, p<0.0001) and day 14 (0.67 ± 0.09 compared with 0.96 ± 0.07, p=0.0046). By day 21, LysM-Wnt5a^{GOF} blood flow has recovered to a similar level as WT mice (Figure 3.5C). This supports previously published data demonstrating that

monocytic Wnt5a is responsible for impaired revascularisation (Kikuchi *et al.*, 2014).

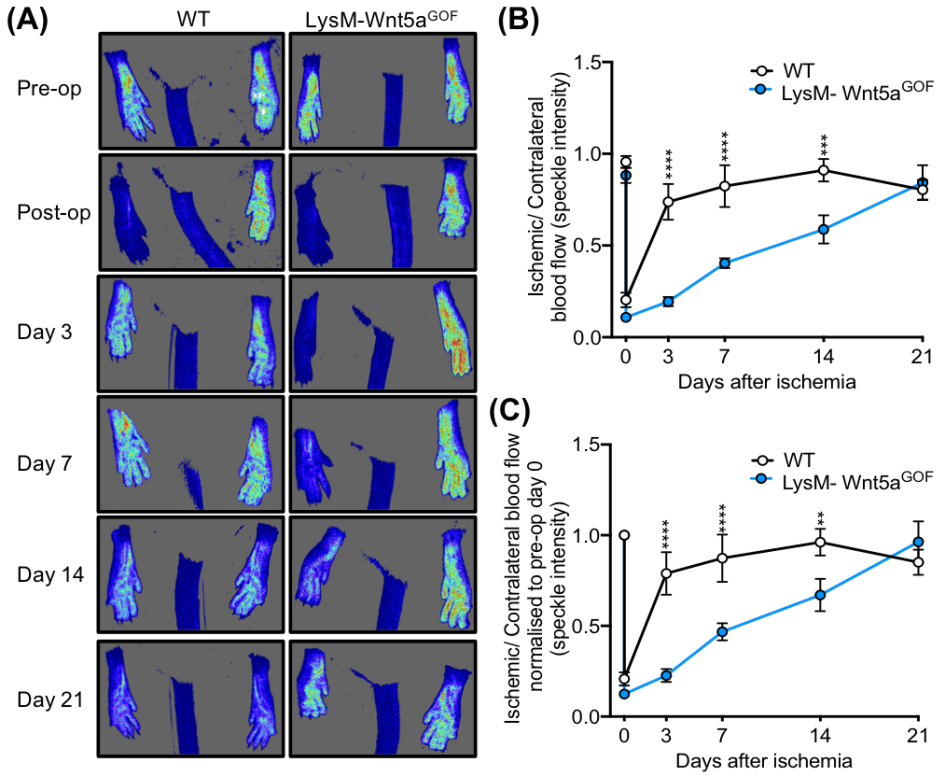


Figure 3.5. LysM-Wnt5a^{GOF} have significantly impaired recovery of blood flow compared to WT mice. (A) *WT and LysM-Wnt5a^{GOF} mice underwent left femoral artery ligation and the blood flow to the paw was measured using the laser speckle imaging system as shown in the representative images.* ***(B)(C)*** *Quantitative analysis of the ischemic vs non-ischemic speckle intensity calculated as a ratio through to post-operative day 21.* ***(C)*** *Data was further normalised to pre-operative day 0 ratio of each respective mouse. Results indicate the mean ± SEM. All data was analysed via a two-way ANOVA (**(B)** Main effects: Post-operative day: p<0.0001; Genotype (mouse group): p=0.009; Interaction effect: p<0.0001.* ***(C)*** *Main effects: Post-operative day: p<0.0001; Genotype (mouse group): p=0.027; Interaction effect: p<0.0001)) with Bonferroni post hoc test. N=7. (**=p<0.01, ***=p<0.001 and ****=p<0.0001).*

3.3.3. Capillary and arteriolar density

To explore the angiogenic effect of Wnt5a hyperactivity on blood vessel formation, fixed gastrocnemius muscle collected at post-operative day 21 was cryo-sectioned into 5µm sections, stained for isolectin-B_4 (IB_4) and imaged by confocal microscopy. WT capillaries were organised in a puncta pattern showing little difference in the capillary number. Whereas, LysM-Wnt5a^{GOF} capillaries appeared disorganised and elongated (Figure 3.6A).

Quantitative analysis was performed to determine the capillary density per mm^2, which revealed that the ischemic LysM-Wnt5a^{GOF} gastrocnemius muscle formed significantly fewer capillaries, 331.0 ± 18.64/mm^2 compared to 490.6 ± 55.49/mm^2 (p=0.032) in WT mice (Figure 3.6B). However, no differences were seen when the ischemic capillary density was calculated relative to the contralateral non-ischemic gastrocnemius muscle of each respective mouse (p=0.22, Figure 3.6C).

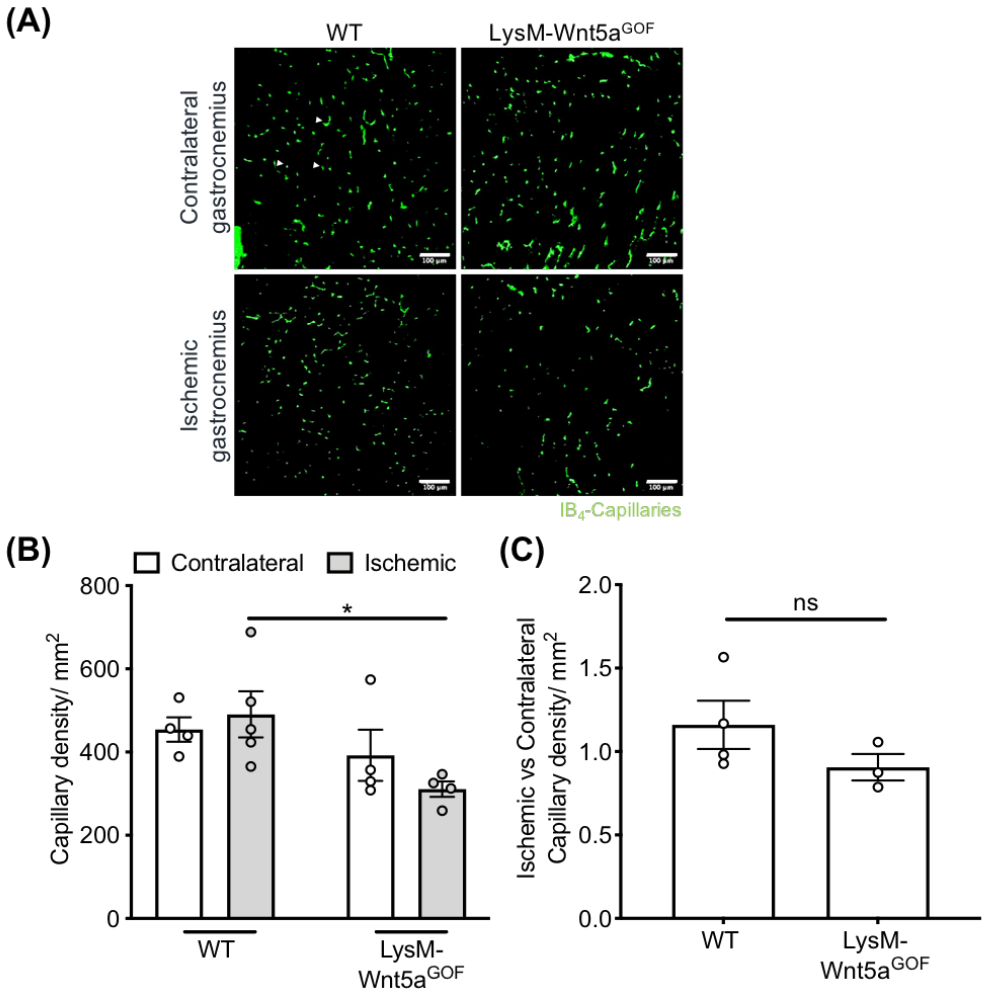


Figure 3.6. LysM-Wnt5a^{GOF} mice have impaired angiogenesis compared to WT mice on post-operative day 21. (A) *Representative immunofluorescence images of the contralateral (top) and ischemic (bottom) gastrocnemius muscle of WT and LysM-Wnt5a^{GOF} stained for capillaries with isolectin (IB$_4$). All images were taken at 10x magnification. Scale bars represent 100μm.* ***(B)(C)*** *Capillaries were counted (indicated with a white arrow head) in the contralateral and ischemic gastrocnemius muscle.* ***(B)*** *Averaged per mm^2* ***(C)*** *Further expressed as a ratio of the ischemic vs contralateral capillary density of each mouse group. All data was plotted as the mean ± SEM.* ***(B)*** *Data was analysed using a two-way ANOVA (Main effects: Genotype (mouse group): p=0.02; Gastrocnemius muscle (contralateral/ischemic): p=0.64; interaction effect: p=0.23) with post-hoc*

Bonferroni test. WT ischemic gastrocnemius: N=5 and all other groups: N=4. ***(C)*** *Data was analysed using an unpaired t-test. WT: N=4 and LysM-Wnt5a^{GOF}: N=3. (*p=<0.05 and ns=p>0.05).*

In a similar manner, the degree of arteriogenesis was analysed by immunofluorescence to assess αSMA positive vessels on post-operative day 21. Figure 3.7A shows the representative examples of the staining in the gastrocnemius muscle of WT and Wnt5a transgenic mice. Histological analysis revealed that ischemia induced a significant impairment in arteriole formation in the gastrocnemius of LysM-Wnt5a^{GOF} mice (4.32 ± 0.55/mm^2) compared to WT mice (19.21 ± 2.03/mm^2, p=0.0002). Interestingly, this trend was observed in the contralateral gastrocnemius of Wnt5a mice indicating a significant reduction in arteriolar density (10.30 ± 2.68/mm^2) compared to the WT mice (20.46 ± 1.65/mm^2, p=0.0045) (Figure 3.7B). Next, the arteriolar density data was calculated as a ratio of the ischemic to contralateral gastrocnemius muscle of each respective mouse group which confirmed a significant reduction in arteriolar density in the of LysM-Wnt5a^{GOF} mice (0.50 ± 0.11/mm^2) compared to the WT gastrocnemius muscle (0.97 ± 0.15/mm^2, p=0.04) (Figure 3.7C). Collectively, these results show that Wnt5a overexpression in the monocytes impairs blood vessel formation, arteriogenesis and angiogenesis in response to ischemia.

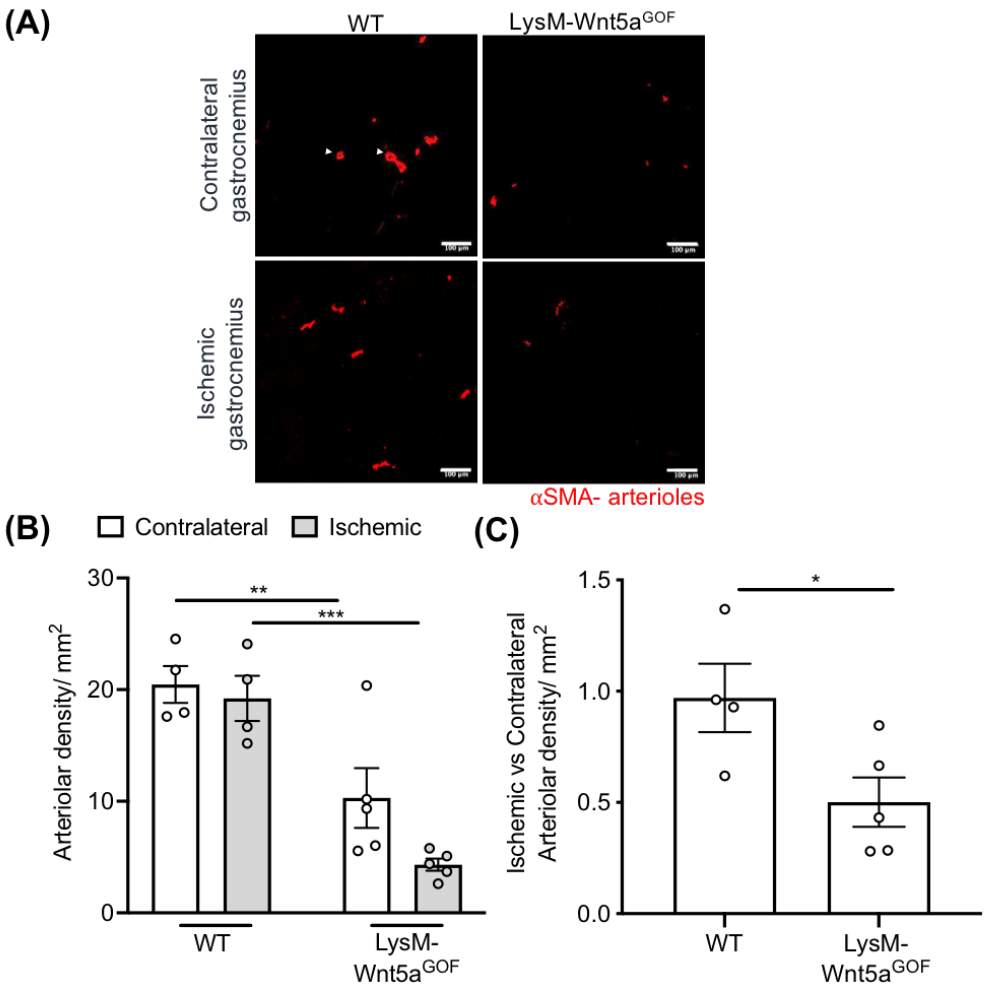


Figure 3.7. LysM-Wnt5a^{GOF} mice have impaired arteriogenesis compared to WT mice on post-operative day 21. (A) *Representative immunofluorescence images of the contralateral (top) and ischemic (bottom) gastrocnemius muscle of WT and LysM-Wnt5a^{GOF} stained for arterioles with α-smooth muscle actin (αSMA). All images were taken at 10x magnification. Scale bars represent 100μm.* ***(B)(C)*** *Arterioles were counted (indicated with a white arrow head) in the contralateral and ischemic gastrocnemius muscle.* ***(B)*** *Averaged per mm^2.* ***(C)*** *Further expressed as a ratio of the ischemic vs contralateral arteriolar density of each respective mouse group. All data was plotted as the mean ± SEM.* ***(B)*** *Data was analysed using a two-way ANOVA (Main effects: Genotype (mouse group): p<0.0001; Gastrocnemius muscle (contralateral/ischemic): p=0.08; Interaction effect: p=0.24) with post-hoc Bonferroni test.* ***(C)*** *Data was analysed using an unpaired t-test. N: WT= 4; LysM-Wnt5a^{GOF}=5. (***=p<0.001, **=p<0.01 and *=p<0.05).*

3.3.4. Expression of VEGF-A isoforms in the gastrocnemius muscle

A study conducted by Kikuchi *et al* demonstrated that anti-angiogenic $VEGF_{165}b$ impaired perfusion recovery in the ischemic muscle of LysM-$Wnt5a^{GOF}$ mice (Kikuchi *et al*., 2014). To examine this, protein was extracted and assessed from contralateral and ischemic muscle of WT and LysM-$Wnt5a^{GOF}$ at day 3 post HLI. One band was observed at 23kDa corresponding to a VEGF-$A_{165}b$ monomer, but no bands were observed for pan-VEGF. Recombinant human proteins (rhVEGF-A_{165} and rhVEGF-$A_{165}b$) were used as a control for both antibodies. Then, the membrane was stripped and re-probed for α-tubulin (52kDa) and β-actin (42kDa) as a loading control (Figure 3.8A). Densitometry analysis was performed on the VEGF-$A_{165}b$ relative to β-actin and confirmed there was no difference in the expression (n=5, p>0.05; Figure 3.8B).

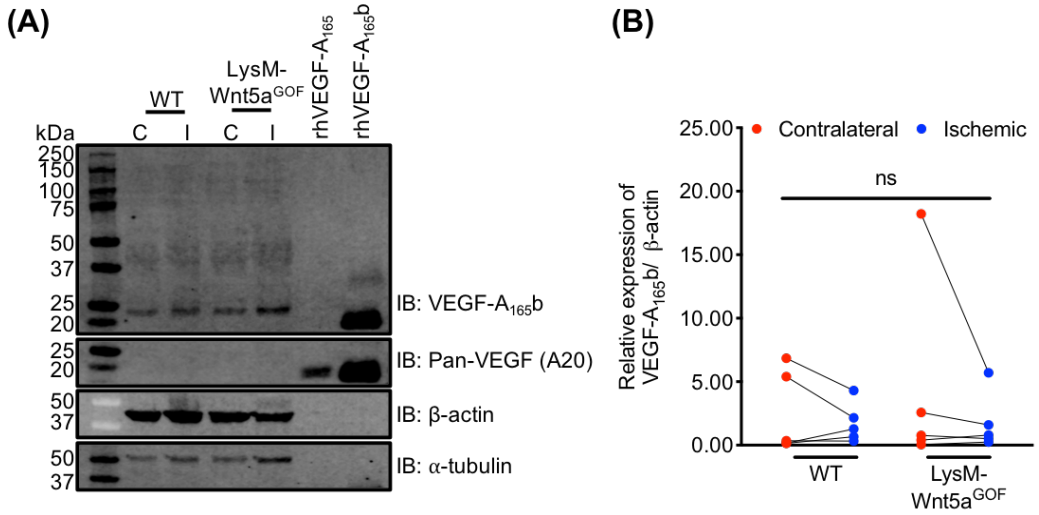


Figure 3.8. WT and LysM-$Wnt5a^{GOF}$ mice did not alter the VEGF isoform expression in the gastrocnemius muscle after HLI was induced on post-operative day 3. (A) *The left femoral artery was ligated of five WT and LysM-$Wnt5a^{GOF}$ mice and culled on day 3. Snap-frozen gastrocnemius muscle was homogenised in lysis buffer to extract the protein. Western blots were performed for pan-VEGF and VEGF-$A_{165}b$ (C=Contralateral and I=Ischemic) PVDF membranes were stripped and re-probed for α-tubulin and β-actin to confirm equal loading.* ***(B)*** *Quantitative densitometry analysis was performed by taking the ratio of VEGF-$A_{165}b$ to β-actin. Each dot and line represent each individual animal, where a red dot represents the contralateral gastrocnemius muscle and blue dot represents the ischemic gastrocnemius muscle. Data was analysed using a two-way ANOVA (Main effects and interaction effects: p>0.05) with post-hoc Bonferroni test. N=5. (ns= p>0.05).*

To quantitatively determine the VEGF content at a protein level, I analysed the gastrocnemius muscle by a colorimetric pan-VEGF and $VEGF_{165}b$ ELISA. Both total VEGF and $VEGF_{165}b$ were detectable in 150μg of protein. The ischemic and contralateral gastrocnemius of WT and LysM-$Wnt5a^{GOF}$ appeared to express a similar level of pan-VEGF and VEGF-$A_{165}b$ displaying no difference (n=8, p>0.05; Figure 3.9A-B). It was not possible to assess the pro-angiogenic VEGF levels, as there is no commercially available ELISA kit available for mouse $VEGF_{164}a$. However, Varey *et al* has previously assessed the binding affinity of $VEGF_{164}a$ and $VEGF_{165}b$ recombinant proteins to the pan-VEGF antibody using surface plasmon resonance, confirming the R&D pan-VEGF ELISA has a 42% reduced affinity to $VEGF_{165}b$ (Varey *et al*., 2008). Therefore, I calculated the concentration of $VEGF_{164}a$, which only showed a marginal difference in the gastrocnemius of WT and LysM-$Wnt5a^{GOF}$ mice, which was not statistically significant overall (n=8, p>0.05; Figure 3.9C). Next, the data was assessed as a ratio of VEGF-$A_{165}b$/pan-VEGF expression which displayed no significant difference (n=8, p>0.05; Figure 3.9D). When calculated relative to the contralateral limb, there was a 1.5-fold increase in LysM-$Wnt5a^{GOF}$ compared to WT gastrocnemius, although it was not statistically significant (n=8, p=0.26; Figure 3.9E).

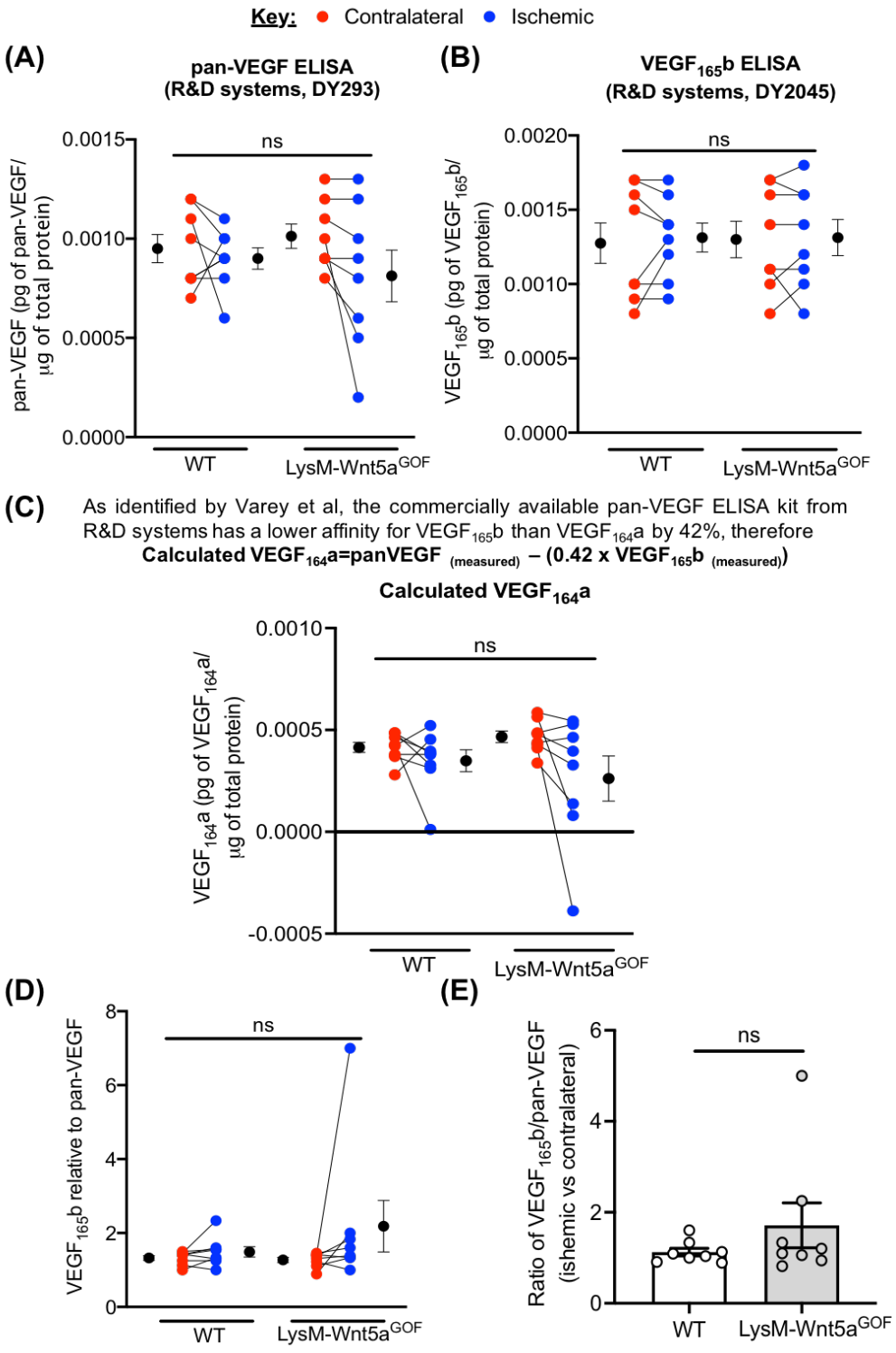


Figure 3.9. WT and LysM-Wnt5a^{GOF} mice did not alter the VEGF isoform expression at a protein level in the gastrocnemius muscle after HLI was induced for 3 days as determined by an ELISA. (A) (B) *The left femoral artery was ligated of 8 WT and LysM-Wnt5a^{GOF} mice and culled on day 3. Gastrocnemius muscle from the contralateral and ischemic hind limb was homogenised, protein was extracted and run in triplicate on a* ***(A)*** *pan-VEGF and* ***(B)*** *VEGF$_{165}$b specific ELISAs. The overall effect on VEGF levels in 150µg protein was not significant between all mouse groups.* ***(C)*** *The level of VEGF$_{164}$a was calculated based on the equation provided by Varey et al (Varey et al., 2008).* ***(D)(E)*** *The data was*

analysed as a ratio of VEGF-A_{165}b to pan-VEGF expression and ***(E)*** *Further normalised to the contralateral limb which did not show a significant change.* ***(A-D)*** *Each dot and line represent each individual mouse, where a red dot represents the contralateral gastrocnemius muscle and blue dot represents the ischemic gastrocnemius muscle. Black dots represent the mean ± SEM. Data was analysed using a two-way ANOVA (Main effects and interaction effects: p>0.05) with post hoc Bonferroni test* ***(E)*** *Results are shown as the mean ± SEM. Data was analysed using an unpaired t-test. N=8. (ns= p>0.05).*

3.4. Discussion

3.4.1. Generating the LysM-Wnt5a^{GOF} mouse model

A study in 2014 initially developed a mouse model with Wnt5a hyperactivity in myeloid cells (abbreviated to LysM-Wnt5a^{GOF}) by utilising the Cre/LoxP system (Kikuchi *et al*., 2014). In a similar manner, I developed this transgenic mouse model using a well-established ROSA26 knock-in locus which is commonly used for the integration of transgenes and is present in all cell types during all developmental stages of mice. This was controlled by a strong and ubiquitously expressed CAG promoter (Zambrowicz *et al*., 1997, Chu *et al*., 2016). However, the presence of a stop codon terminates translation thereby halting the protein synthesis (Figure 3.1). By crossing with a Cre-expressing mouse model which is under the control of a LysM promoter, this allowed for the permanent deletion of the floxed stop codon in monocytes through cre-mediated recombination that all same cell types will undergo throughout the lifetime of the mouse due to a genomic change (Cox *et al*., 2012) (Figure 3.1). These monocytes are initially produced in the bone marrow, but circulate towards the spleen where they reside upon ischemic injury. Importantly, monocytes are shown to account for a large proportion of the cell population in the spleen and is higher than those found in circulation (Swirski *et al*., 2009).

To further validate the mouse model, pups were genotyped using transgene specific probes (Figure 3.2) and the expression of *Wnt5a* was confirmed at an RNA level in splenocytes in the LysM-Wnt5a^{GOF} mouse model (Figure 3.3). Whilst this data is promising using the well-established Cre/LoxP genetic manipulation strategy, the LysM promoter has shown to be inconsistent with cell-specific stop codon deletions in neutrophils (as well as monocytes and macrophages) questioning the specificity and efficiency of the promoter itself (McCubbrey *et al*., 2017, Abram *et al*., 2014). In fact, the LysM-promoter has shown to drive the expression of transgenes in granulocytes, CD11c^{+} dendritic cells and non-haemopoietic cells (Faust *et al*., 2000, Clausen *et al*., 1999). Such literature implies the LysM-Cre strain may not be specific for monocytes/macrophage, therefore an important

follow up study would be crucial to determine the off- targets effects in different cell types in the LysM-Wnt5a^{GOF} mouse model compared to the WT which will allow us to determine the true efficiency of the LysM-Cre strain in this case, whilst further validating the monocyte specificity in this transgenic mouse model. An alternative and perhaps more reliable method to valid the LysM-Wnt5a^{GOF} mouse could be by co-staining for monocytes and GFP. The IRES-GFP-Nuc sequence should be present in all LysM-Cre expressing Wnt5a^{GOF} mice. In fact, Li *et al* used the same conditional transgene with a different Cre expressing promoter to show this in embryos (Li *et al*., 2016).

3.4.2. Wnt5a hyperactivity in monocytes impairs blood flow recovery following ischemic injury

The HLI *in vivo* mouse model is a commonly used model of PAD by ligation of the femoral artery at the age of 10-12 weeks old. This results in the development and growth of collateral vessels as a result of an angiogenic response (Aref *et al*., 2019, Limbourg *et al*., 2009). In this chapter I wanted to assess if monocytic Wnt5a would impair the blood flow recovery *in vivo.* It is known that patients with PAD and ischemic mouse models have increased Wnt5a activity and expression in the plasma and monocytes. This may be linked to impaired collateralisation and a reduction in blood flow to the lower limb. As expected, I have shown that there was no difference in the blood flow recovery in WT and STOP-Wnt5a mouse groups (Figure 3.4). Both transgenic mouse models have different transgenes containing Cre recombinase with and without LoxP floxed sites. Cre can damage the DNA in the absence of any floxed LoxP sites, therefore the data was promising as both models were essentially control groups (Janbandhu *et al*., 2014). Hyperactivity of monocytic Wnt5a *in vivo* subsequently impaired blood flow recovery when compared to the WT mouse groups (Figure 3.5). This data was consistent with previously published data by Kikuchi and colleagues which strongly supports the idea that monocytic Wnt5a is responsible for the impaired collateral formation in response tissue ischemia (Kikuchi *et al*., 2014). It also complements results from other cell types such as retinal

myeloid cells, where Stefater *et al* showed that a mutation in Wnt5a signalling increased the deep vessel branches, suggesting the response is modulated by Wnt5a (Stefater *et al*., 2011).

The impairment that was presented in Figure 3.5 could be associated with a deficiency of Sfrp5 which is upstream and usually acts by sequestering Wnt5a to prevent binding to the receptor triggering downstream events (Ouchi *et al*., 2010, Kikuchi *et al*., 2014). An increase in the ratio of Wnt5a to Sfrp5 promotes binding to the Ror2/Fzd receptor protein on the cell surface. In turn, this promotes inflammation in the ischemic hind limb region which is likely to be associated with a greater infiltration and accumulation of activated macrophage (Kikuchi *et al*., 2014) resulting in the activation of JNK (downstream of the non-canonical signalling pathway) as shown rodent models of obesity (Ouchi *et al*., 2010). The data presented is encouraging as it supports the hypothesis that Wnt5a signalling in monocytes is responsible for ischemic vascular disease.

A limitation associated with the *in vivo* studies in this chapter is that they were not blinded. The genotyping results provided by Transnetyx were interpreted and revealed prior to the study. This was to ensure that only the mice of the correct genotype, which were required for the experiment underwent the HLI procedure. This may indicate a level of bias, which could have been eliminated if independent researchers were involved at each stage of experiment including interpretation of the genotyping results, laser speckle imaging on post-operative days and analysis of the data. Although, the quantitative data linked to the speckle intensity analysis of the hind paws is automated using the Moors Instruments analysis software.

3.4.3. Monocytic Wnt5a decreases the capillary and arteriolar density in the gastrocnemius muscle

By the end of the 21-day HLI *in vivo* study, WT and LysM-Wnt5a^{GOF} mice had completely restored blood flow to the ischemic limb (Figure 3.5). Despite this, it was interesting to identify differences in the capillary (Figure

3.6) and arteriolar (Figure 3.7) density in the ischemic and non-ischemic gastrocnemius suggesting that the functionality of blood vessel is not always associated with the quantity of blood vessels present. It is interesting to note that Kikuchi and colleagues used Wnt5a hyperactive mice that did not have complete blood flow recovery at the end of the 21-day study. This correlated with a decrease in the capillary density in the ischemic gastrocnemius (Kikuchi *et al*., 2014). Similar to other cell types, the presence of the non-canonical signalling Wnt5a pathway has been shown to suppress the angiogenic response in retinal myeloid cells (Stefater *et al*., 2011).

The inability of LysM-Wnt5a^{GOF} mice to form a vascular network in the ischemic gastrocnemius could be partially be explained by their ability to regulate the expression of anti-angiogenic VEGF-A_{165}b as previously shown in a mouse macrophage cell line, RAW264.7 *in vitro* (Kikuchi *et al*., 2014). Similarly, treatment of adipose tissue with Wnt5a negatively modulated capillary spouting (Karki *et al*., 2017). It is possible to speculate that HIF-1 could be directly or indirectly associated with the impaired collateralisation seen in the gastrocnemius. In the absence of Wnt5a, it is well established that hypoxia mediated changes results in the upregulation of VEGF-A. Where, HIF-1 activation in monocytes has been critical in promoting angiogenesis *in vivo* (Ahn *et al*., 2014). *In vitro* experiments on monocytic THP-1 cells under hypoxic conditions (1% oxygen) have resulted Wnt5a activation (Kim *et al*., 2012). Together, this could explain impair the vascular network that was identified in this chapter, although it is a broad assumption given the lack of evidence. Contradictory to this, a study on pulmonary hypertension demonstrated that hypoxia inhibits the Wnt5a pathway in the arterial smooth muscle cells (Yu *et al*., 2013). It is important to note that there was no statistical significance in the capillary density of the WT and LysM-Wnt5a^{GOF} mice when expressed as a ratio of the contralateral limb (Figure 3.6C). There was a lack of paired data in each group, however the trend was approaching significance at a p value of 0.22. Had I increased the n number, this data may have achieved statistical significance.

A possible explanation for the complete blood flow recovery (Figure 3.5) and impaired collateral vessel growth might be due to a vasodilatatory response of the few arterioles present in the gastrocnemius muscle of the transgenic Wnt5a^{GOF} animals (Figure 3.7). This means that an increase in diameter would provide a sufficient blood flow to the ischemic region that would otherwise be supplied if there were more arterioles present. For the duration of the 21-study, all mice appeared to have a similar level of activity, therefore it could be possible that monocytic nitric oxide could be mediating the response (Schirmer *et al*., 2015). Contradictory to this, patients with lifelong diabetes (Breton-Romero *et al*., 2016) or severe obesity (Farb *et al*., 2016) were prone to endothelial dysfunction due to reduced nitric oxide production, which was reversed with Wnt5a inhibition. Although no visible differences were seen in the diameter of the arterioles by immunofluorescence, this is not conclusive proof that it was not occurring. To confirm this assumption, it would be important to investigate the flow-mediated vasodilation after ischemia is induced in LysM-Wnt5a^{GOF} mice and measure the nitric oxide levels from the monocytes isolated.

It remains unexplained why the arteriolar density is significantly impaired in the contralateral hind limb of LysM-Wnt5a^{GOF} mice, as fewer monocytes would migrate towards this region due to lack of inflammation (Capoccia *et al*., 2008). It could imply LysM-Wnt5a^{GOF} mice have an impaired vascular network during the early stages of development resulting in poor revascularisation prior to the study. It would be worthwhile to quantify the vascular density in a sham control Wnt5a^{GOF} mouse to confirm this. Finally, a monoclonal αSMA antibody was used to visualise the arterioles in the gastrocnemius muscle. This experiment lacked the optimal non-immune control slide, which would confirm the specificity of the antibody.

3.4.4. The effect of VEGF-A protein in the gastrocnemius muscle of LysM-Wnt5a^{GOF} mice post-ischemia

VEGF-A is a key player in angiogenesis and vascular remodelling in many different diseases and cell types, the mechanism in hind limb ischemia mouse models is yet to be determined and fully understood. The two known mechanisms connecting Wnt5a to suppressed angiogenesis. This has been identified in myeloid cells via sFlt-1 (Stefater *et al*., 2011) and JNK-SC35-VEGF-A$_{165}$b (Kikuchi *et al*., 2014). To explore the involvement of VEGF-A splice variants (Figure 3.6 and 3.7), the expression at protein level was quantified on post-operative day 3 gastrocnemius muscle using antibodies previously published as reactive with rodent samples. Initially western blots were used to quantify total VEGF-A and VEGF-A$_{165}$b levels (Figure 3.8). It was surprising that no bands were detected with the pan-VEGF antibody, as it detects total VEGF by binding which binds to receptor binding domain located in exon 3-4. It has previously been shown to be reactive with similar tissue as shown by Kikuchi and colleagues (Kikuchi *et al*., 2014). Despite this, VEGF-A$_{165}$b was detected across all samples but no trend was seen overall. Other studies have confirmed that VEGF regulates the capillary number and vascular structure in the skeletal muscle (Olfert *et al*., 2009, Delavar *et al*., 2014). It importantly raises questions as to what was the sensitivity of the VEGF-A$_{165}$b antibody for the protein extracted from the tissue as compared with the recombinant protein as the antibody easily detected VEGF-A$_{165}$b in the gastrocnemius muscle and highlights the difficulties in detecting low levels of total VEGF-A. The recombinant proteins were used as a positive control for the antibodies, but were not mouse specific suggesting an issue with the samples rather than the assay itself.

A single band was observed for VEGF-A$_{165}$b at the correct molecular weight (23kDa) for all mouse samples (Figure 3.8). Therefore, the corresponding analysis suggests that the anti-angiogenic VEGF-A isoform is not associated with an impaired capillary density in the ischemic gastrocnemius muscle of the Wnt5a^{GOF} mice (Figure 3.6). It is possible that VEGF-A$_{165}$b are cell specific changes occurring in the monocytes/macrophages, which

was not assessed in this thesis and may have been detected if monocytes were isolated from the gastrocnemius muscle. In fact, a previous study has assessed the ischemic limb of Wnt5a^{GOF} mice on post-operative day 3 and showed a significant upregulation of the macrophage marker (Mac2) compared to WT mice (Kikuchi *et al*., 2014). It is clear that the data presented in this chapter is in contrast with published data from Kikuchi and colleagues displaying a clear increase in the content of pan-VEGF and mVEGF-A$_{165}$b in the ischemic gastrocnemius of LysM-Wnt5a^{GOF} mice on day 7 post-surgery (Kikuchi *et al*., 2014). This could be due to the mouse housing, strain differences, feed, the ischemia model or other environmental or genetic differences. It is interesting that there is also differences in the two studies on the rate of recovery, with the blood flow recovery being complete within 21 days (Figure 3.5), whereas Kikuchi *et al* did not see recovery within the 28 days, indicating that this is a more rapid resolution of the ischemia than the HLI model used in Kikuchi *et al*'s paper (Kikuchi *et al*., 2014).

An alternative approach to quantifying protein levels was by using a commercially available ELISA designed to capture absolute levels of total VEGF and VEGF$_{165}$b, however extremely low levels were detected (close to the limit of detection), but again there was no difference in either overall (Figure 3.9). With this data and the literature presented on commercially available VEGF antibodies by using surface plasmon resonance predictions could be made to approximately calculate the amount of VEGF$_{164}$a in the gastrocnemius muscle post-ischemia showing little difference (Varey *et al*., 2008). This data together with the western blot does not suggest that VEGF-A is necessarily driving the difference in the impaired blood flow recovery and angiogenesis previously shown in LysM-Wnt5a^{GOF} mice. This lack of evidence does not support our original hypothesis on the effect of VEGF-A isoforms at a protein level. Under the given conditions, sufficient detection of both isoforms was not achieved using two protein assays. This is not proof that VEGF-A is not playing a significant role, but detection was not achieved under the given conditions, as studies have detected VEGF-A at a protein level (Kikuchi *et al*., 2014, Hazarika *et al*., 2007). In addition, there

is evidence supporting the requirement of VEGF-A for muscle regeneration following after ischemic injury (Arsic *et al*., 2004). Calculations performed on G* Power using the VEGF ELISA data in a two tailed analysis indicate to achieve the accepted 0.8 standard and a significance value of p=0.05, we would require a total sample size of 82 per group (Figure 3.9A-B). Whereas, Figure 3.9E would require a total sample size of 253 for an unpaired t-test. This was not possible in this study. With the current data, it is questionable whether the low levels of expression detected for pan-VEGF and VEGF-A_{165}b is a true value in this case.

3.5. Concluding remarks

The data presented in this chapter demonstrates that hyperactivity of monocytic Wnt5a impairs the blood flow recovery after ischemic injury is induced in the left femoral artery. This can be partially explained due to reduced angiogenic and arteriogenic capability, however the involvement of VEGF-A was not confirmed at a protein level. It is not yet clear which downstream effectors and mechanistic signalling pathways are involved and to what extent. Further work is needed to better understand the role of the non-canonical Wnt5a signalling pathway in monocytes which is responsible for the impaired revascularisation and collateralisation seen *in vivo.*

Chapter 4

SRPK1 as a potential regulator of Wnt5a impaired collateralisation *in vivo*

4.1. Introduction

The angiogenic signalling of VEGF-A occurs by binding to its downstream receptors, VEGFR1 (Flt1 in mouse) and VEGFR2 (Flk1 in mouse) (Simons *et al*., 2016). VEGFR1 acts as a decoy receptor due to its high binding affinity and reduced kinase activity, negatively regulating angiogenesis by preventing 'free' VEGF-A from binding and phosphorylating VEGFR2 (Kendall *et al*., 1996). The activation of VEGFR2 is modulated by the pro- and anti-angiogenic VEGF-A isoforms. Both isoforms have similar binding affinities, but result in different downstream signalling outcomes (Kawamura *et al*., 2008). VEGF-A_{165}a binds to VEGFR2 and co-receptor neuropilin-1 (NRP-1) to form a receptor complex. This induces conformational change, dimerization and autophosphorylation of the intracellular tyrosine kinase domains resulting in pro-angiogenic properties (Harper and Bates, 2008, Kawamura *et al*., 2008). In comparison, VEGF-A_{165}b does not bind to co-receptor, NRP-1 (Kawamura *et al*., 2008, Cébe Suarez *et al*., 2006). Binding to VEGFR2 alone only partially phosphorylates the kinase domain. This negatively regulates angiogenesis resulting in anti-angiogenic properties (Kawamura *et al*., 2008, Harper and Bates, 2008).

The two distinct isoforms of VEGF-A exist through a series of events that result in alternative splicing regulated by the phosphorylation of SRSF1 by the kinase SRPK1 at the 12 serine residues in the RS domain of SRSF1 (Nowak *et al*., 2008, Aubol *et al*., 2013). Following phosphorylation, the complex is translocated to the nucleus, where SRSF1 remains in the nuclear speckles to regulate splicing events through the phosphorylation of remaining serine residues by CLK-1 (Naro and Sette, 2013, Colwill *et al*., 1996). In epithelial cells, the phosphorylation of SRSF1 by SRPK1 promotes pre-mRNA proximal splice site selection of VEGF-A at exon 8a resulting in the upregulation of the pro-angiogenic VEGF-A_{xxx}a and a decrease in the anti-angiogenic splice variant, VEGF-A_{xxx}b expression (Nowak *et al*., 2010). In the presence of an SRPK1 inhibitor, SPHINX31, this is reversed. SPHINX31 occupies the binding pocket of SRPK1 by inducing backbone flip in the hinge region and preventing the

phosphorylation of SRSF1. This has been shown to generate the anti-angiogenic VEGF splice variant VEGF-A_{165}b in ocular diseases and reducing disease progression (Batson *et al*., 2017). It is clear that SRPK1 inhibition offers an effective anti-angiogenic strategy in a VEGF-A dependent manner. However, the mechanism of alternative splicing of VEGF-A in monocytes is not clear.

The stimulation of Wnt5a in macrophages has been shown to favour the expression of VEGF-A_{165}b through the splicing factor, SC35/SRSF2 (Kikuchi *et al*., 2014) and sFlt1 in adipose tissue (Karki *et al*., 2017). The involvement of SRPK1 in the control of VEGF splicing through Wnt5a in monocytes in models of cardiovascular disease has not been explored *in vivo.* It has been shown to increase VEGF-A_{165}a expression *in vivo* and *in vitro* and Wnt5a is associated with enhanced VEGF-A_{165}b levels, I therefore hypothesised that SRPK1 inhibition would further impair revascularisation.

In this chapter, I wanted to test the hypothesis that impaired collateralisation in transgenic LysM-Wnt5a^{GOF} mice (as previously shown in Chapter 3) is further impaired by inhibiting the protein kinase, SRPK1, that controls VEGF production in a similar manner to other cell types. I would do this by giving an intraperitoneal injection of a SRPK1 inhibitor, SPHINX31 over the course of the study to inhibit the kinase activity of SRPK1. This would allow me to pinpoint the mechanism that is responsible and could potentially offer a novel therapeutic that would stimulate SRPK1 and hence induce revascularisation. Thus, I aimed to measure the blood flow recovery after ischemia was induced in the left femoral artery. I also aimed to measure the angiogenic and arteriogenic capability in the gastrocnemius muscle post-ischemia. Finally, I would deduce how administration of SPHINX31 influences VEGF-A isoforms and to explore the mechanisms that could be regulated in this model (either directly or indirectly).

4.2. Methodology

Adult transgenic LysM-Wnt5a^{GOF} mice (C57BlJ) were bred in-house and genotyped by Transnetyx. At the age of 10-12 weeks old, a total of 53 (15 WT and 38 LysM-Wnt5a^{GOF}) mixed gender mice were subjected to HLI. Mice were anaesthetised with 2-3% isoflurane in 100% oxygen and administered pre-operative analgesic (0.05mg/kg buprenorphine, s.c) diluted in sterile saline (0.9% NaCl via a s.c injection). For the 3-day HLI study, a total of 8 LysM-Wnt5a^{GOF} mice were treated with a 0.8mg/kg dose SPHINX31 (i.p) immediately after surgery on post-operative day 0. The blood flow to paws were imaged on day 0 (pre- and post-operative), 1, 2 and 3. For the 21-day HLI study, a total of 9 LysM-Wnt5a^{GOF} mice were treated with 0.8mg/kg SPHINX31 (i.p, bi-weekly) and 4 were treated with 0.32% DMSO (i.p, bi-weekly) on day 1 post-surgery. The dose of SPHINX31 administered in the mice was based on a previous pharmacokinetics study, which assessed the circulating concentration of SPHINX31 after a single dose at 0.8mg/kg. After 24 hours, the concentration in the plasma was 0.225 ± 0.036 μM. This is greater than the IC_{50} in *in vitro* cell treatment. This is also the limit of SPHINX31 solubility and the optimal dose (Tzelepis *et al*., 2018, Batson *et al*., 2017). The blood flow to the paws were imaged on day 0 (pre- and post-operative) and days 3, 7, 14 and 21. Quantitative analysis was performed using the FLPI-2 software (Moors Instruments) by taking the ratio of the ischemic vs contralateral speckle intensity at each time point. The data was further normalised to the pre-operative speckle intensity of each respective mouse.

On day 3, animals were culled and gastrocnemius muscle was snap frozen for RNA (for RT-PCR) or protein (for western blotting or ELISA's) assays. On day 21, animals were culled by cardiac perfusion with PFA and gastrocnemius muscle was dissected for histological analysis by staining with IB_4 for capillaries and αSMA for arterioles. Using the FIJI image analysis software, the capillary and arteriolar density were calculated. All methods are described in detail in Chapter 2.

4.2.1. Statistical analysis

Statistical tests performed were a two-way ANOVA with post-hoc Bonferroni's test when comparing the blood flow recovery after induction of ischemia between mouse group on post-operative days. The vessel density and expression level analysis between the gastrocnemius muscle of mouse groups was performed using a two-way ANOVA with post-hoc Bonferroni's test. For comparisons of three independent groups (e.g. WT, LysM-Wnt5a^{GOF} and LysM-Wnt5a^{GOF} + SPHINX31), a one-way ANOVA with post-hoc Bonferroni's test were used.

4.3. Results

4.3.1. Impaired blood flow recovery in LysM-Wnt5a^{GOF} mice is reversed with SPHINX31

Existing literature confirms that SRPK1 inhibition switches the alternative splicing of VEGF-A isoforms towards the anti-angiogenic splice variant. Thus, it was hypothesised that SPHINX31 administration post-ischemia (after inducing HLI) would further impair the reduced blood flow recovery in transgenic LysM-Wnt5a^{GOF} mice (as shown in Chapter 3, Figure 3.1). The LSI images shown in Figure 4.1 are representative images from each group showing the blood flow recovery before surgery, immediately after surgery and on post-operative days 3, 7, 14 and 21. All animals showed a reduction in blood flow immediately after ligation of the left femoral artery (ischemic to contralateral speckle intensity ratio post-surgery was <0.20) indicating the procedure was successful, as shown by a dark blue left paw compared to pre-operative day 0. On day 1 (bi-weekly, thereafter), LysM-Wnt5a^{GOF} mice were treated with SPHINX31 (0.8mg/kg, i.p.) and surprisingly showed 70% recovery by day 3 (similar to WT) compared to 20% in untreated littermate LysM-Wnt5a^{GOF} mice (Figure 4.1A). Quantitative speckle intensity analysis of the ischemic to contralateral blood flow ratio showed that that revascularisation in LysM-Wnt5a^{GOF} was significantly slower than WT litter mice on day 3 (0.19 ± 0.03 vs 0.72 ± 0.09, p<0.0001), day 7 (0.40 ± 0.03 vs 0.82 ± 0.10, p=0.0002) and day 14 (0.58 ± 0.08 vs 0.92 ± 0.06, p=0.0039). This was rescued by SPHINX31 treatment on day 3 (0.65 ± 0.12, p <0.0001) and day 7 (0.71 ± 0.11, p=0.0072). On day 21 all mice had recovered to >0.75 of blood flow (Figure 4.1B).

Similarly, when the data from Figure 4.1B was normalised to pre-operative day 0 of each respective mouse, it was shown that revascularisation in LysM-Wnt5a^{GOF} was significantly slower than littermate WT mice on day 3 (0.23 ± 0.04 vs 0.77 ± 0.10, p<0.0001), day 7 (0.47 ± 0.05 vs 0.88 ± 0.11, p=0.0009), and day 14 (0.67 ± 0.10 vs 0.99 ± 0.07, p=0.0146). This was rescued by SPHINX31 on day 3 (0.74 ± 0.13, p<0.0001), day 7 (0.80 ± 0.12, p=0.0065) and day 14 (0.93 ± 0.08, p=0.046). The blood flow recovered up

to >0.90 on day-21 post-surgery ratio in all mouse groups (Figure 4.1C). Together, this contradicted our original hypothesis suggesting the recovery may be SRPK1 dependent as blood flow recovery is reversed with the administration of SPHINX31 and matches the WT mice.

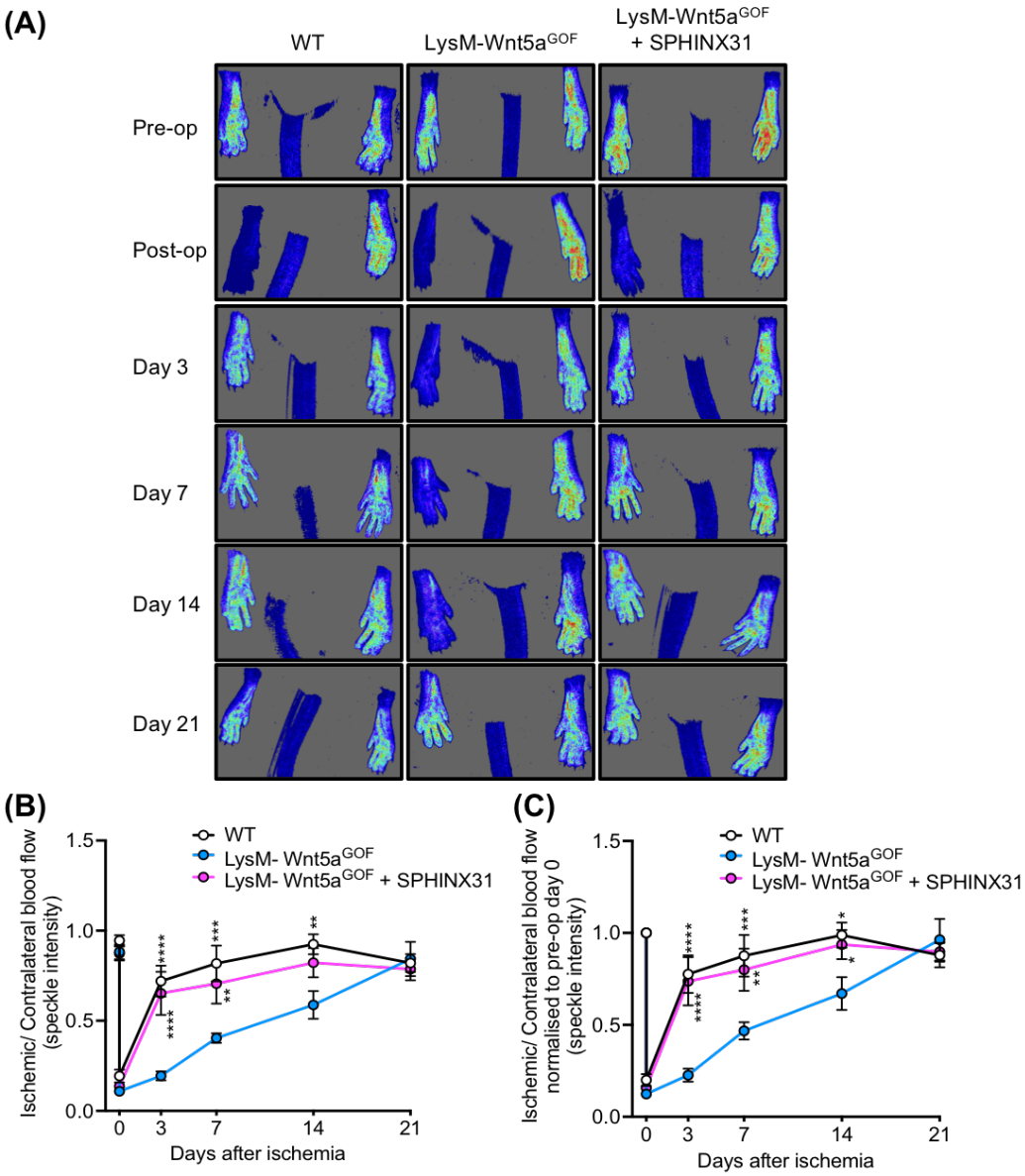


Figure 4.1. Impaired blood flow recovery in LysM-Wnt5a^{GOF} mice is reversed with SPHINX31. (A) *LysM-Wnt5a^{GOF} mice underwent left femoral artery ligation followed by treatment with SRPK1 inhibitor (SPHINX31, 0.8mg/kg, i.p, biweekly). Blood flow to the paw was measured using the laser speckle imaging system as shown in the representative images.* ***(B)(C)*** *Laser speckle contrast imager was used to quantitatively analyse ischemic vs non-ischemic blood flow recovery in WT, LyM-Wnt5a^{GOF} and LysM-Wnt5a^{GOF} + SPHINX31.* ***(C)*** *Data was further normalised to pre-operative day 0 of each respective mouse. Results are shown as mean ± SEM. Data was analysed via a two-way ANOVA (**(B)** Main effects: Post-operative day: p<0.0001, Mouse group: p=0.016; Interaction effect: p<0.0001.* ***(C)*** *Main effects: Post-operative day: p<0.0001, Mouse group: p=0.029; Interaction effect: p<0.0001)) with post-hoc Bonferroni's test. N= WT: 8, LysM-Wnt5a^{GOF}: 7*

*and LysM-Wnt5a^{GOF} + SPHINX31: 9 (****=p<0.0001, ***=p<0.001, **=p<0.01 and *=p<0.05 compared with LysM-Wnt5a^{GOF}).*

SPHINX31 was initially dissolved in DMSO and further diluted in saline for administration of a dose of 0.8mg/kg, so to ensure that effect seen in Figure 4.1 was due to SPHINX31 alone, 4 LysM-Wnt5a^{GOF} were treated with 0.32% DMSO as an additional control group. The representative LSI show the blood flow recovery of LysM-Wnt5a^{GOF} treated with and without DMSO (0.32%) for the duration of the 21-day HLI study (Figure 4.2A). Quantitative speckle analysis after ligation of the left femoral confirmed there was no statistical difference in the blood flow recovery between the two groups (p>0.05, Figure 4.2B) and when normalised to pre-operative day 0 of each respective mouse (p>0.05, Figure 4.2C).

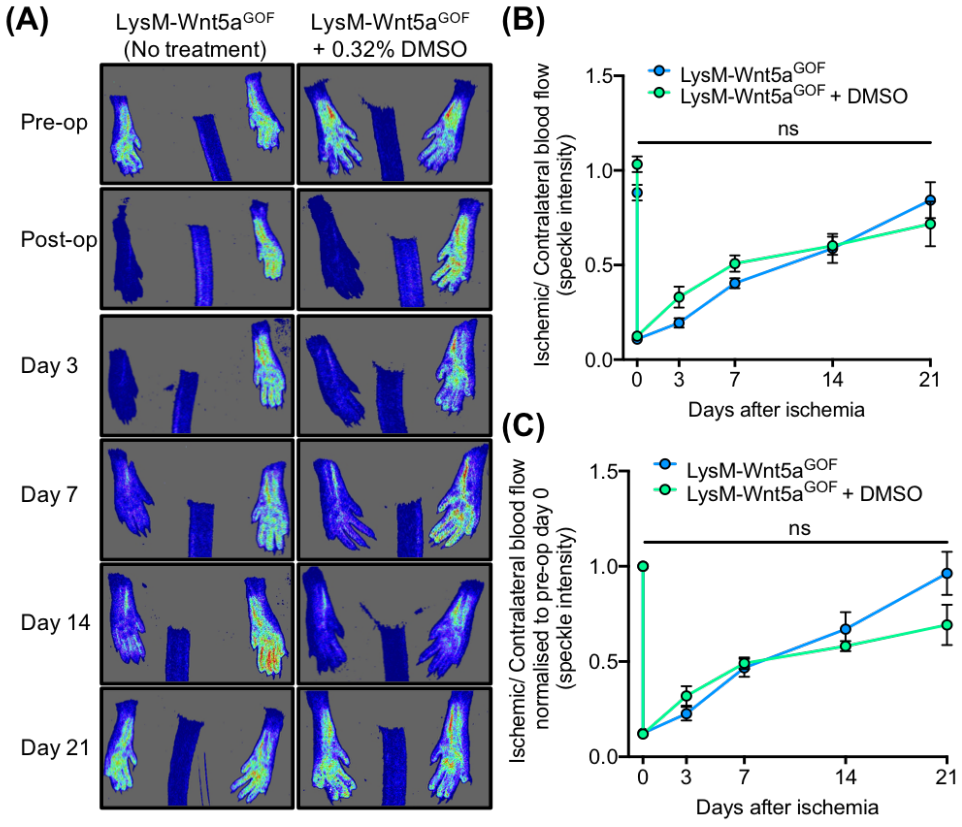


Figure 4.2. No difference in impaired revascularisation in LysM-Wnt5a^{GOF} mice treated with or without DMSO. (A) *LysM-Wnt5a^{GOF} mice received no treatment or 0.32% DMSO biweekly. The representative laser speckle images display the blood flow recovery.* ***(B)(C)*** *Quantitative analysis of the ischemic vs non-ischemic speckle intensity ratio was observed through to post-operative day 21.* ***(C)*** *Data was further normalised to pre-operative day 0. Results indicate the mean ± SEM. Data was analysed using a two-way ANOVA (****(B)*** *Main effects: Post-operative day: p<0.0001; Mouse group: p=0.52; Interaction effect: p=0.08.* ***(C)***

Main effects: Post-operative day: p<0.0001; Mouse group: p=0.64; Interaction effect: p=0.07)) with post-hoc Bonferroni's test. N= LysM-Wnt5a^{GOF}: 7 and LysM-Wnt5a^{GOF}+ DMSO: 4. (ns=p>0.05).

4.3.2. Capillary and arteriolar density

After the experimental end point at day 21, mice were culled by cardiac perfusion. The gastrocnemius muscle was dissected and cryo-sectioned for histological analysis of the vascular network. Representative IB_4 positive vessel staining for capillaries in the gastrocnemius of WT and Wnt5a transgenic mice treated with and without SPHINX31 is shown in Figure 4.3A. Quantitative analysis was performed to determine the capillary density per mm^2, which revealed that the ischemic LysM-Wnt5a^{GOF} formed significantly fewer capillaries, 331.0 ± 18.64/mm^2 in comparison to 516.3 ± 42.01/mm^2 with SPHINX31 treatment (p=0.012), which was similar to WT mice (490.6 ± 55.49/mm^2, p=0.022, Figure 4.3B). The data was also expressed as ratio of the ischemic to the contralateral tissue of each group which revealed no difference in the capillary density between all mouse groups (p>0.05, Figure 4.3C).

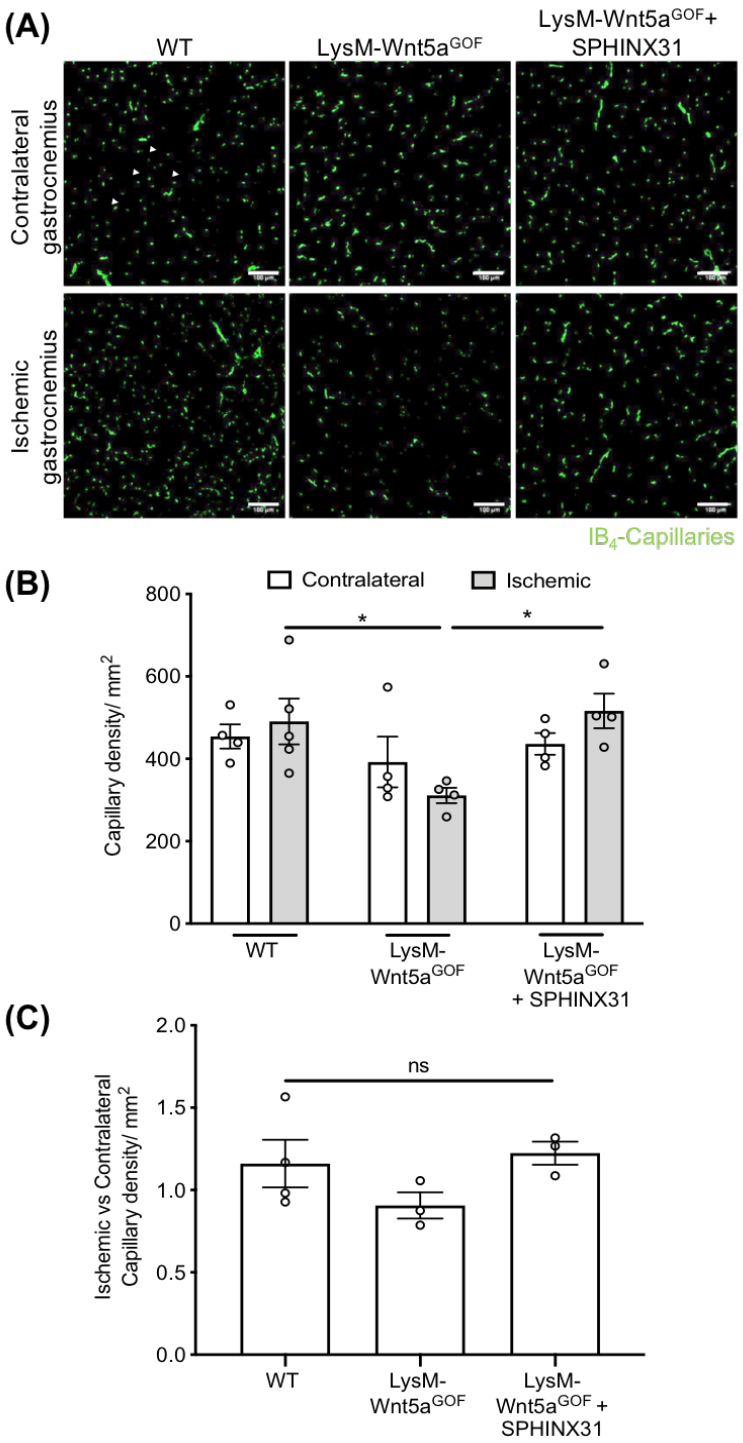


Figure 4.3. Impaired angiogenesis in LysM-Wnt5a^{GOF} mice is reversed with SPHINX31 on post-operative day 21. (A) *Representative immunofluorescent images of the contralateral (top row) and ischemic (bottom row) gastrocnemius muscle of WT, LysM-Wnt5a^{GOF} and LysM-Wnt5a^{GOF} mice treated with SPHINX31 stained for capillaries with isolectin (IB$_4$). All images were taken at 10x magnification. Scale bars represent 100μm.* ***(B)(C)*** *Capillaries were counted (indicated with a white arrow head) in the contralateral and ischemic gastrocnemius muscle.* ***(B)*** *Averaged per mm^2.* ***(C)*** *Further expressed as ratio of the ischemic vs contralateral capillary density of each mouse group. All data was plotted as the mean ± SEM.* ***(B)*** *Data was analysed using a two-way ANOVA (Main effects: Mouse group: p=0.016; Limb (contralateral/ischemic): p=0.74; Interaction*

effect: p=0.20) with post-hoc Bonferroni test. WT ischemic gastrocnemius: N=5; all other groups: N=4. ***(C)*** *Data was analysed using a one-way ANOVA with post-hoc Bonferroni test. WT: N=4; LysM-Wnt5a^{GOF} and LysM-Wnt5a^{GOF} + SPHINX31: N=3. (*=p<0.05 and ns=p>0.05).*

To determine the effect on arteriogenesis in the gastrocnemius muscle post-HLI day 21 mice, positive αSMA vessel staining was assessed by immunofluorescence and imaged by confocal microscopy as shown in Figure 4.4A. Upon quantification of the images, it was revealed that the ischemic hind limb of untreated Wnt5a transgenic mice (4.32 ± 0.55/mm^2) formed significantly fewer arterioles compared to SPHINX31 treatment (20.45 ± 4.22/mm^2, p=0.0002), which was comparable to WT (19.22 ± 2.03/mm^2, p=0.0004). Interestingly, the impairment of arteriole formation in the contralateral limb of Wnt5a mice (10.30 ± 2.68/mm^2) was significantly less than contralateral limb of littermates treated with SPHINX31 (20.19 ± 0.76/mm^2, p=0.0168) and WT (20.46 ± 1.65/mm^2, p=0.0138) mice (Figure 4.4B). The arteriolar density was calculated as a ratio of the ischemic vs contralateral gastrocnemius muscle of each mouse group, which revealed that the Wnt5a transgenic mice only produced 0.50 ± 0.11/mm^2, which is less than litter mates treated with SPHINX31 (1.03 ± 0.23/mm^2, p=0.09) and WT (0.97 ± 0.15/mm^2, p=0.14; Figure 4.4C).

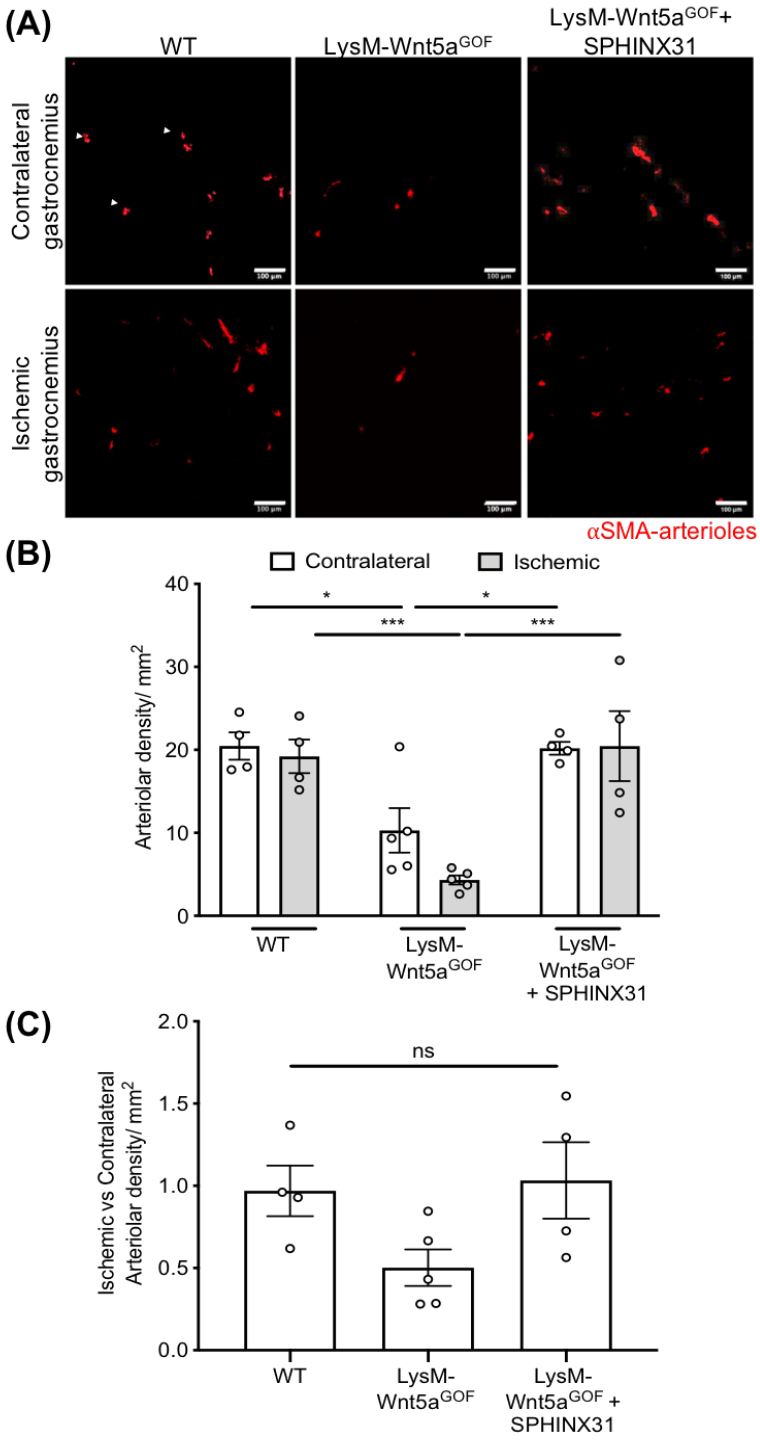


Figure 4.4. Impaired arteriogenesis in LysM-Wnt5a^{GOF} mice is reversed with SPHINX31 on post-operative day 21. (A) *Representative immunofluorescent images of the contralateral (top row) and ischemic (bottom row) gastrocnemius muscle of WT, LysM-Wnt5a^{GOF} and LysM-Wnt5a^{GOF} mice treated with SPHINX31 stained for capillaries with α-smooth muscle actin (αSMA). All images were taken at 10x magnification. Scale bars represent 100μm.* ***(B)(C)*** *Arterioles were counted (indicated with a white arrow head) in the contralateral and ischemic gastrocnemius* ***(B)*** *Averaged per mm^2* ***(C)*** *Further expressed as a ratio of the ischemic vs contralateral arteriolar density of each mouse group. All data was plotted as the mean ± SEM.* ***(B)*** *Data was analysed using a two-way ANOVA (Main effects: Mouse group: p<0.0001; gastrocnemius muscle (contralateral/ischemic):*

p=0.23; interaction effect: p=0.36) with post-hoc Bonferroni test. ***(C)*** *Data was analysed using a one-way ANOVA with post-hoc Bonferroni test. N: WT and LysM-Wnt5a^{GOF}+ SPHINX31= 4 and LysM-Wnt5a^{GOF}= 5. (***=p<0.001, *=p<0.05 and ns=p>0.05).*

4.3.3. 3-day HLI study showed no difference in blood flow recovery

Given that administration of SPHINX31 in LysM-Wnt5a^{GOF} mice rescued the impaired blood flow by >70% by post-operative day 3 (Figure 4.1 and 4.2), I wanted to investigate if the response was an immediate effect for instance suggesting an effect on vasodilatation rather than vascular remodelling, which might be expected to take a few days to become apparent. To do this, WT and LysM-Wnt5a^{GOF} mice were subjected to HLI and blood flow recovery to the paw was monitored on pre-operative day 0 and post-operative day 0, 1, 2 and 3 using the LSI system (Figure 4.5A). On post-operative day 0, animals were administered a single dose of SPHINX31 (0.8mg/kg, i.p) for the duration of the study (Figure 4.5A). Quantitative analysis of the speckle intensity as a ratio of the ischemic to contralateral paw showed that the blood flow recovery was similar in all mouse groups for the duration of the 3-day study (p>0.05, Figure 4.5B-C).

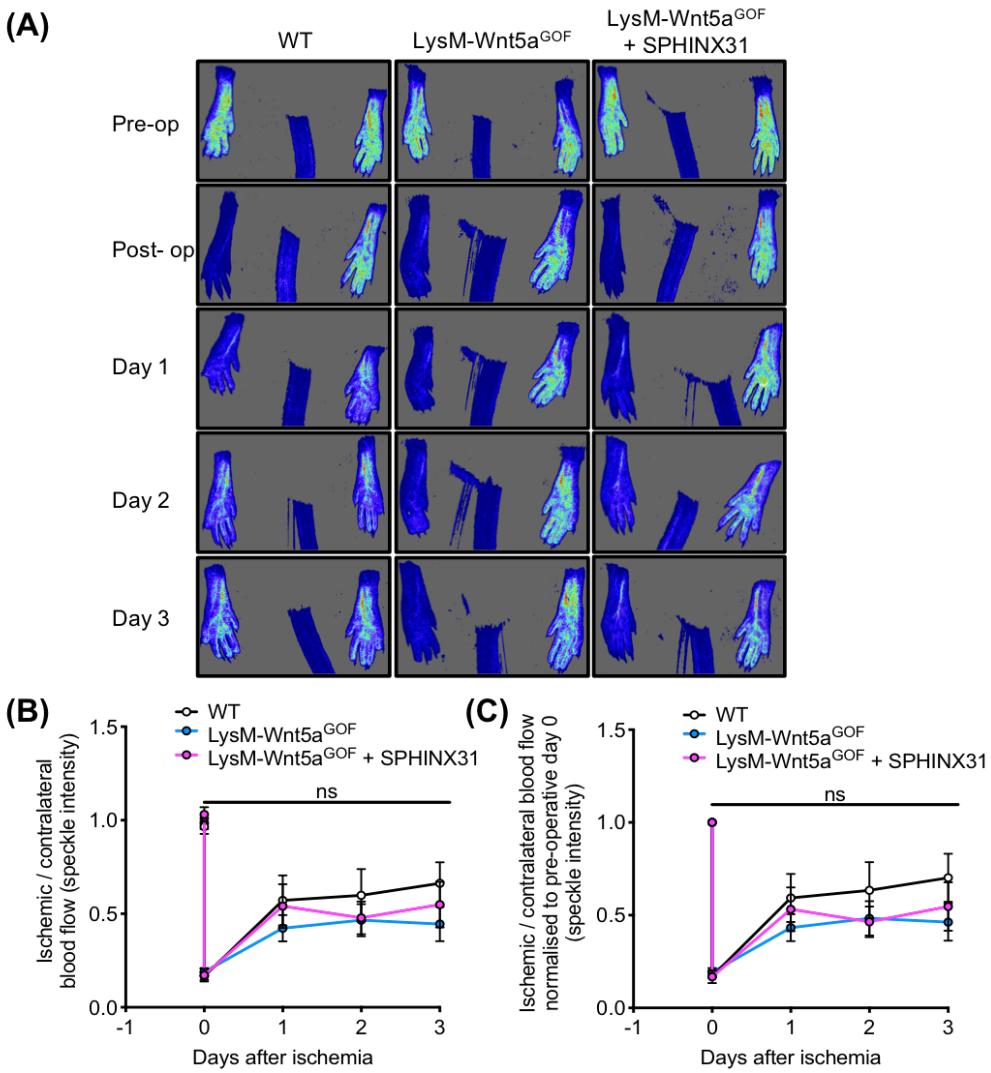


Figure 4.5. Investigating a possible early effect of SPHINX31 in LysM-Wnt5a^{GOF} mice. (A) *LysM-Wnt5a^{GOF} mice underwent left femoral artery ligation followed by treatment with SRPK1 inhibitor (SPHINX31, 0.8mg/kg, i.p, biweekly). The blood flow to the paw was measured using the laser speckle imaging system as shown in the representative images.* ***(B)(C)*** *Laser speckle contrast imager was used to quantitatively analysed as a ratio of the ischemic/non-ischemic blood flow recovery in wild-type (WT), LysM-Wnt5a^{GOF} and LysM-Wnt5a^{GOF} + SPHINX31 on post-operative days 1, 2 and 3.* ***(C)*** *Data was further normalised to pre-operative day 0 of each respective mouse. Results are shown as mean ± SEM. Data was analysed via a two-way ANOVA (****(B)*** *Main effects: Post-operative day: p<0.0001; Mouse group: p=0.58; Interaction effect: p=0.55.* ***(C)*** *Main effects: Post-operative day: p<0.0001; Mouse group: p=0.52; Interaction effect: p=0.50)) with Bonferroni post hoc test. N= WT: 7; LysM-Wnt5a^{GOF}: 10 and LysM-Wnt5a^{GOF} + SPHINX31: 8. (ns= non-significant, p>0.05).*

4.3.4. Expression of VEGF-A isoforms in the gastrocnemius at a protein level

The SRPK1 inhibitor, SPHINX31, regulates the alternative splicing of VEGF-A by preventing the phosphorylation of SRSF1. In retinal epithelial cells this has been shown to result in a switch in the ratio of two distinct VEGF-A isoforms with opposing functions: VEGF-A_{xxx}a (pro-angiogenic) and VEGF-A_{xxx}b (anti-angiogenic) (Batson *et al.*, 2017). To analyse the VEGF-A levels, protein was extracted from day 3 post HLI gastrocnemius of WT and LysM-Wnt5a^{GOF} mice treated with or without SPHINX31. One band was detected at 23kDa for VEGF-A_{165}b as a monomer, however no bands were observed when probed with a pan-VEGF (A20) antibody. The membrane was stripped and re-probed with two different loading control antibodies: α-tubulin (52kDa) and β-actin (42kDa) plus ponceau red stain (prior to the blocking of the membrane) (Figure 4.6).

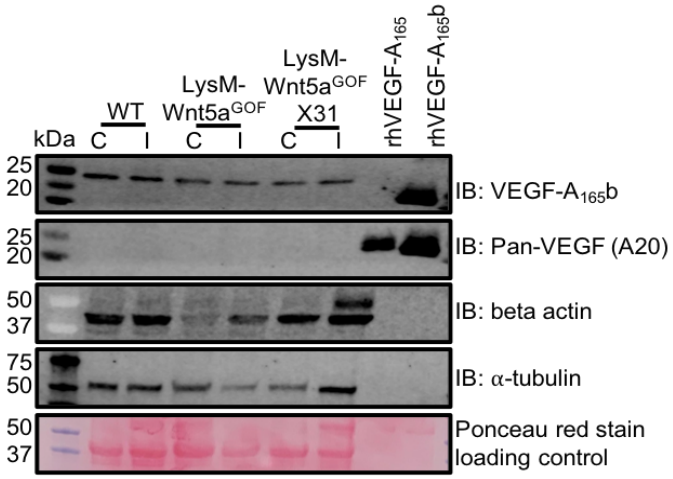


Figure 4.6. WT and LysM-Wnt5a^{GOF} mice treated with and without SPHINX31 did not alter the VEGF isoform expression in the gastrocnemius muscle after HLI was induced on post-operative day 3. *The left femoral artery was ligated of five WT and LysM-Wnt5a^{GOF} mice treated with SPHINX31 immediately after surgery and culled on day 3. Gastrocnemius muscle was homogenised in NP40 lysis buffer and protein was extracted. Western blots were performed stained with ponceau red stain, then were probed for pan-VEGF (23kDa) and VEGF-A_{165}b (23kDa). PVDF membranes were stripped and re-probed for α-tubulin (52kDa) and β-actin (42kDa) to ensure equal loading. Key: C=Contralateral and I=Ischemic. (n=5/group).*

To quantitatively determine the VEGF-A content in the gastrocnemius muscle day 3 post HLI, a colorimetric pan-VEGF and VEGF-A_{165}b ELISA was performed on 150μg of protein. All mouse groups expressed a similar level of pan-VEGF and VEGF-A_{165}b displaying no difference overall (n=8, p>0.05; Figure 4.7A-B). Based on the analysis performed by Varey *et al* using the surface plasmon resonance, the concentration of $VEGF_{164}$ in the gastrocnemius post-ischemia was approximately calculated. The gastrocnemius muscle of LysM-Wnt5a^{GOF} mice treated with SPHINX31 showed a significant decrease in VEGF-A_{164}a in the ischemic limb (0.02 ± 0.01%, p=0.0058) compared to the contralateral limb (0.06 ± 0.01%) (Figure 4.7C) (Varey *et al*., 2008). Next, I calculated the data as a ratio of VEGF-A_{165}b/pan-VEGF expression and further normalised to the contralateral limb of each respective mouse, however both were not statistically significant overall (n=8, p>0.05, Figure 4.7D-E).

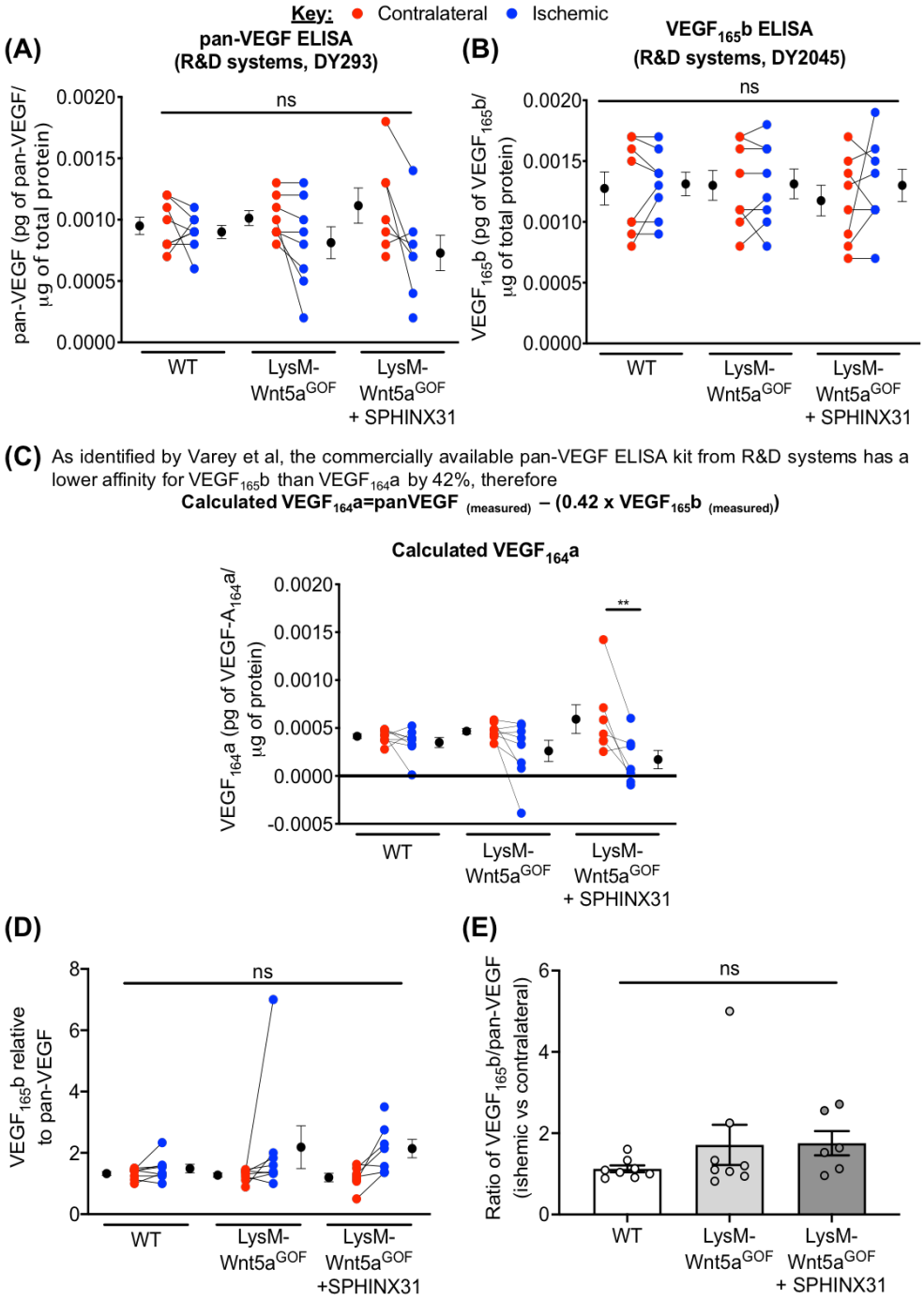


Figure 4.7. WT and LysM-Wnt5a^{GOF} mice treated with and without SPHINX31 did not alter the VEGF isoform expression in the gastrocnemius muscle on post-operative day 3. (A)(B) *The left femoral artery was ligated of eight WT and LysM-Wnt5a^{GOF} mice treated with and without SPHINX31 and culled on day 3. Gastrocnemius muscle was homogenised in NP40 lysis buffer, protein was extracted and run in triplicate on a VEGF$_{165}$b and pan-VEGF specific ELISAs. Quantitative analysis was performed per 150µg protein loaded in each well.* ***(C)*** *The level of VEGF$_{164}$a was calculated based on the equation provided by Varey et al (Varey et al., 2008).* ***(D)(E)*** *The data was analysed as a ratio of VEGF-A$_{165}$b to pan-VEGF expression and* ***(E)*** *Further normalised to the contralateral limb which did not show a significant change.* ***(A-D)*** *Each dot and line represent each mouse, where a red dot represents the contralateral and blue dot represents the ischemic gastrocnemius. Black dots represent the mean ± SEM.* ***(E)*** *Results are shown as*

*the mean ± SEM. All data was analysed using a one or two-way ANOVA with Bonferroni's post hoc test. N=8. (**= p<0.01 and ns= p>0.05).*

4.3.5. Expression of *Flt1 (VEGFR1)* and *sFlt1* in the gastrocnemius muscle

There are multiple possible reasons why SPHINX31 treatment could result in improved revascularisation and collateral formation. One is that it changes alternative splicing of other non-VEGF mRNAs from anti-to pro-angiogenic forms. Stefater and colleagues suggested that non-canonical Wnt5a signalling negatively regulates angiogenesis by a splice isoform of VEGFR1 (also known as Flt1), known as soluble fms-like tyrosine kinase-1 (sFlt1) at an RNA level, which was shown to be upregulated in Wnt5a treated RAW264.7 cells (Stefater *et al*., 2011). Later, it was identified that aged HLI mice had impaired blood flow recovery and vascular regenerative capacity in the ischemic limb. Analysis of the gastrocnemius muscle revealed it was due to an increase in sFlt1, Wnt5a and SC35/SRSF2 (Zhao *et al*., 2017). Together, this suggested a potential link between Wnt5a-Flt1/sFlt1. To explore the involvement of *Flt1*, RNA was extracted from day 3 post-HLI gastrocnemius of WT and LysM-Wnt5a^{GOF} mice (treated with or without SPHINX31). The RNA was synthesised into cDNA and RT-PCR performed to determine the expression of *Flt1*. Primers were designed to flank exon 12 (forward primer) and 16 (reverse primer), along with a -RT negative control (Figure 4.8A). To optimise the annealing temperature, a gradient was performed between 50-60ºC. A single band was observed at 634bp corresponding to *Flt1* at annealing temperatures above 52ºC (Figure 4.8A). The PCR was re-run at 60ºC on contralateral and ischemic gastrocnemius of all mouse groups. The expression of *Flt1* band at 634bp remained unchanged in the muscle of all mouse groups (Figure 4.8B). This was consistent with the quantitative densitometry analysis of bands relative *Gapdh* which revealed no significant change in the *Flt1* levels (n=5, p>0.05, Figure 4.8C).

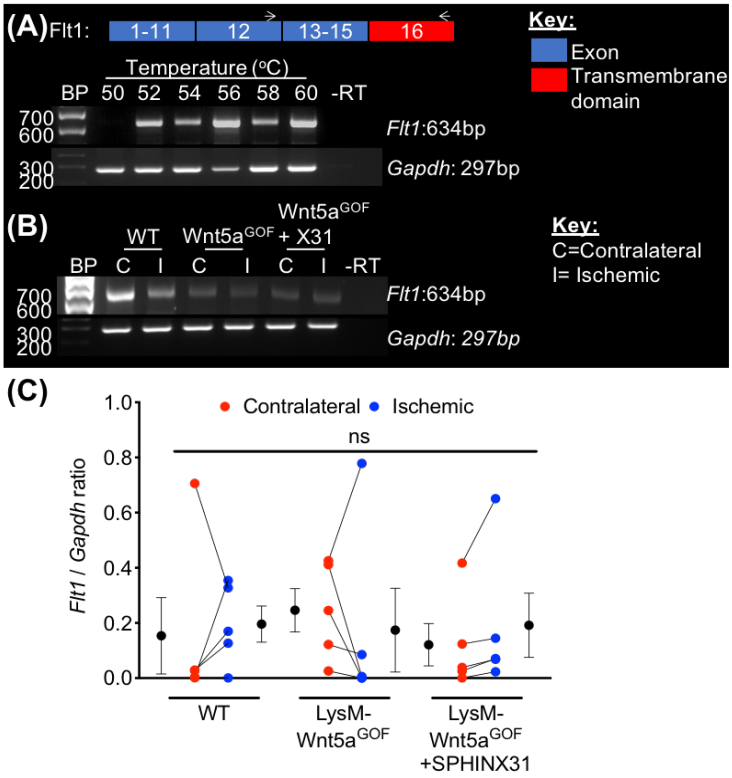


Figure 4.8. The effect of Flt1 expression in the gastrocnemius muscle. *RNA was extracted from homogenised gastrocnemius muscle from day 3 HLI mice and RT-PCR was performed to measure the Flt1 expression.* ***(A)*** *Optimisation of the annealing temperature (50-60°C) of Flt1 primers spanning exon 12 and the transmembrane domain (634bp).* ***(B)*** *The expression levels of Flt1 in the gastrocnemius of WT, LysM-Wnt5a^{GOF} and LysM-Wnt5a^{GOF} treated with SPHINX31.* ***(C)*** *Flt1 expression calculated by normalising to Gapdh (297bp). Data represents the ratio of Flt1/Gapdh of each respective mouse, where a red dot represents the contralateral and blue dot represents the ischemic limb. Black dots present the mean and error bars represent the SEM. Data was analysed using a two-way ANOVA (Main effects and interaction effects: p>0.05) with Bonferroni post hoc test. N= 5/group. (ns= p>0.05).*

Similarly, the potential involvement of a splice variant of Flt1 known as sFlt1 (or sFlt1-i13) was assessed. This isoform does not contain a transmembrane or intracellular domain; therefore, primers were designed to flank exon 12 (forward primer) and intron retention sequence after exon 13 (reverse primer), known as i13 (Figure 4.9A). To optimise the annealing temperature, a gradient was performed between 50-60°C. A single band was detected for *sFlt1* at 398bp at all temperatures, therefore 58°C was selected as the optimal annealing temperature (Figure 4.9A). The PCR was re-run on the cDNA of contralateral and ischemic gastrocnemius of all mouse groups. The *sFlt1* band remained consistent in all groups at 398bp (Figure 4.9B). Quantitative densitometry analysis of bands relative *Gapdh*

(297bp) revealed no change in the *sFlt1* levels overall (n=5, p>0.05, Figure 4.9C).

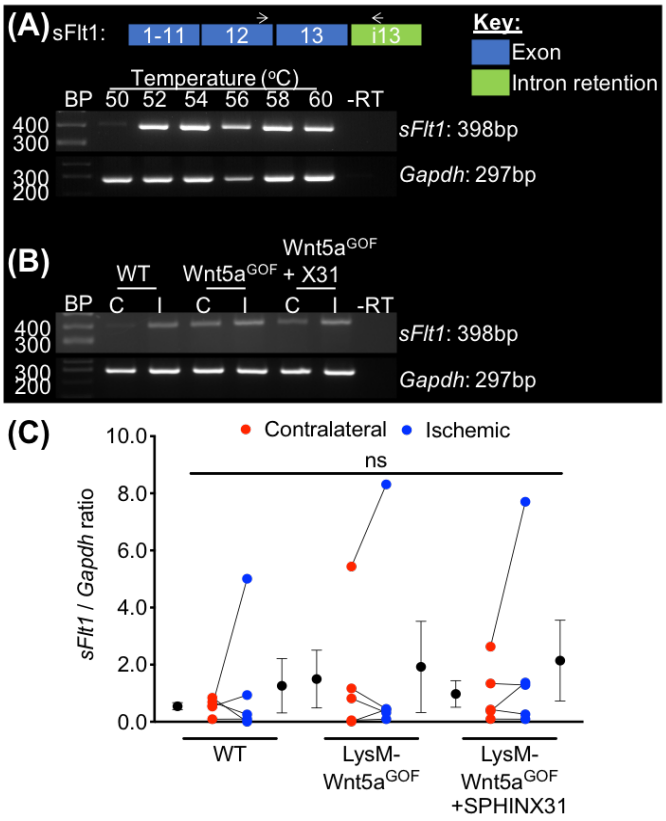


Figure 4.9. The effect of sFlt1 expression in the gastrocnemius muscle. *RNA was extracted from homogenised gastrocnemius muscle from day 3 HLI mice and RT-PCR was performed to measure the sFlt1 expression.* ***(A)*** *Optimisation of the annealing temperature (50-60°C) of sFlt1 primers spanning exon 12 and the intron retention named i13 at 398bp.* ***(B)*** *The expression levels of sFlt1 in the gastrocnemius of WT, LysM-Wnt5a^{GOF} and LysM-Wnt5a^{GOF} treated with SPHINX31.* ***(C)*** *Expression levels of sFlt1 were normalised to Gapdh as a ratio. The graph represents the ratio of contralateral (red dot) and ischemic (blue dot) gastrocnemius of each respective mouse. Black dots represent the mean and error bars represent the SEM. Data was analysed using a two-way ANOVA (Main effects and interaction effects: p>0.05) with Bonferroni post hoc test. N= 5/group. (ns=p>0.05).*

4.4. Discussion

4.4.1. SRPK1 inhibition reverses the impaired blood recovery in LysM-Wnt5a^{GOF} mice

Consistent with work from this chapter (Figure 4.1), Chapter 3 (Figure 3.5) and published literature, monocytic-Wnt5a is the key driver contributing to impaired blood flow recovery seen in PAD (Kikuchi *et al*., 2014). This has previously been shown to be due to the resulting anti-angiogenic splice variant VEGF-A$_{165}$b (Kikuchi *et al*., 2014). Use of an SRPK1 inhibitor such as SPHINX31 have been shown to increase the expression of anti-angiogenic isoforms, and reduce the expression of pro-angiogenic isoform in diseases to reduce disease progression (Batson *et al*., 2017, Gammons *et al*., 2013). However, we do not know its effect in ischemic diseases. For the first time, I have found that administration of SPHINX31 recovers the impaired blood flow recovery in LysM-Wnt5a^{GOF} mice (Figure 4.1 and 4.2). This was a surprising finding as inhibition of SRPK1 has been shown to promote VEGF-A distal splice site selection in epithelial (Gammons *et al*., 2013) and cancer cells (Gammons *et al*., 2014). This suggests that the splicing mechanism in this transgenic mouse model could be acting in a different manner to other cell types, which appears to be dependent on SRPK1.

The assumption made here is that SPHINX31 is acting directly on monocytes itself. In this study, animals were administered with SPHINX31 via an intraperitoneal route (in the peritoneal cavity) which allowed for fast absorption into the body. Primary absorption occurs through the portal circulation before circulating around the body and reaching other organs, rather than acting on a specific cell (Lukas *et al*., 1971, Turner *et al*., 2011). It is therefore possible that the SPHINX31 is acting indirectly, either through other cell types or other splicing mechanisms (or even through other kinases).

SPHINX31 has been shown to successfully inhibit SRPK1 with a high affinity and specificity. In comparison to the binding affinity of SRPK1 to

SPHINX31, the interaction to SRPK2 and CLK-1 was shown be to 50-fold less (Batson *et al*., 2017). SRPK1 has not been shown to interact with SRSF2, however SRPK2 has the ability to phosphorylate SC35/SRSF2 (Wang *et al*., 1998). Treatment of SPHINX31 on THP-1 and MOLM-13 leukemic cell lines *in vitro* has shown a decrease in pSRSF1/SRSF2 (Tzelepis *et al*., 2018). SC35/SRSF2 has a role in regulating the expression of VEGF-A_{165}b through Wnt5a in macrophages (Kikuchi *et al*., 2014). Likewise, CLK-1 has the ability to phosphorylate SRSF6 and promote VEGF-A_{165}b expression. Although this is shown in retinal pigmented epithelial cells (Nowak *et al*., 2008). Collectively with this evidence, perhaps it is possible that the partial inhibition of SRPK2 and CLK-1 could reduce the phosphorylation of SRSF2 and SRSF6 and alter the ratio of the VEGF-A isoforms. Together, this could explain the complete blood flow recovery seen in LysM-Wnt5a^{GOF} mice treated with SPHINX31.

In addition to this, it was interesting to see a rapid blood flow recovery 3 days after ischemia had been induced in the left femoral artery of LysM-Wnt5a^{GOF} mice treated with SPHINX31(Figure 4.1). At this point, mice had only been given a single dose of SPHINX31 with a half-life of 96 minutes, which is a key consideration for therapeutics (Batson *et al*., 2017). In fact, this suggests it was rapidly cleared throughout the bloodstream before the second dose was given and reduces any potential off-target effects (Batson *et al*., 2017). Therefore, it may be possible that the immediate effect could have been due to vasodilatation to allow the vessels to cope with an increase in flow rather than splicing of VEGF-A isoforms. However, no difference was seen when this study was repeated over three days with a single dose of SPHINX31 (Figure 4.5). This is not conclusive evidence that vasodilatation is not occurring. In fact, short-term treatment with Wnt5a alone has led to vasoconstriction due to impaired eNOS phosphorylation (Cho *et al*., 2018). To further confirm the effect on the vascular function, it would be interesting to perform a myography experiment to assess and measure the changes in vascular activity on the femoral artery and collateral vessels in greater depth. Overall, the data presented opposes our initial hypothesis but suggests that SRPK1 may be key in pinpointing the

mechanism responsible for the impaired blood flow recovery in ischemic diseases. Also, it is worth noting that the *in vivo* studies were not blinded (similar to Chapter 3). The allocation of the LysM-Wnt5a^{GOF} mice receiving the SPHINX31 treatment was randomly assigned to each mouse of the correct genotype prior to the surgery. On post-operative day 0, all mice did have a similar level of ischemia induced in the left femoral artery (Figure 4.1 and 4.2). However, the preparation and administration of SPHINX31 treatment was not carried out by an independent researcher throughout the *in vivo* studies. This may indicate a level of bias, which could have been eliminated if independent researchers were involved throughout the duration of the *in vivo* studies. To standardise the conditions on the laser speckle imaging days, each animal was placed on a heat pad and body temperature was maintained at ~37^{o}C. Also, the quantitative data linked to the speckle intensity in the ROI is automated using the Moors Instruments analysis software.

4.4.2. SPHINX31 improves the capillary and arteriolar density in the gastrocnemius of LysM-Wnt5a^{GOF} mice post-ischemia

At the end of the 21-day HLI study, all animals had completed restored their blood flow to the ischemic paw (Figure 4.1), however it was interesting to identify a similar capillary and arteriolar density in WT and LysM-Wnt5a^{GOF} mice treated with SPHINX31 compared with LysM-Wnt5a^{GOF} alone (Figure 4.3 and 4.4). Similar to chapter 3, the quantity of the blood vessels does not correlate with the functionality. It was surprising that SPHINX31 treatment resulted in the formation of a collateral network, as a selective SRPK1 inhibitor it has been shown to favour the anti-angiogenic VEGF splice variant in ocular diseases due to a reduction in SRSF1 phosphorylation (Batson *et al*., 2017). However, treatment of SPHINX31 on leukemic cells displayed a reduction of both SRSF1 and SRSF2 phosphorylation (Tzelepis *et al*., 2018). This implies that SPHINX31 could be affecting the phosphorylation of SRSF2 resulting in a switch to the pro-angiogenic VEGF isoform. There is currently evidence supporting a vascular response in

macrophages through a Wnt5a-SC35 (SRSF2) mechanism (Kikuchi *et al*., 2014). Similarly, epithelial cells control their VEGF splicing through various SR proteins (Nowak *et al*., 2008, Nowak *et al*., 2010). It would therefore be critical to explore the involvement of splicing factor proteins that are phosphorylated in response to SRPK1 inhibition to confirm this assumption.

Importantly, the capillary density was expressed as a ratio relative to the contralateral limb which was not statistically significant (Figure 4.3C). This was due to a lack of paired data in each group, and does not rule out the angiogenic effect identified the raw data in Figure 4.3B. Had I increased the N number; perhaps this data could have achieved significance.

It was surprising to identify a difference in the arteriolar density in the contralateral hind limb of Wnt5a^{GOF} treated with SPHINX31 compared to the contralateral hind limb of the untreated Wnt5a^{GOF} group and matched the WT mouse group. In fact, a similar trend was displayed in the ischemic gastrocnemius muscle of the respective mouse groups (Figure 4.4B). Although both groups had an overexpression of monocytic Wnt5a, the contralateral and ischemic hind limbs are likely to have different levels of inflammation in the limb. It is possible to assume that the contralateral limb has fewer monocytes migrating towards this region compared to the ischemic limb (Capoccia *et al*., 2008, Rauner *et al*., 2012). In fact, Batson *et al* has shown that SPHINX31 affects the migration of macrophages after laser CNV induction (Batson *et al*., 2017). It is possible that the intraperitoneal dose of SPHINX31 that circulates systemically and reduces the migration of infiltrating proinflammatory monocytes. Thus, resulting in reduced VEGF-A$_{165}$b expression that would be overexpressed in LysM-Wnt5a^{GOF} mice and resulting in a difference in the arteriolar density in both limbs (Kikuchi *et al*., 2014). The overexpression of Wnt5a in monocytes occurs due to genomic change following Cre-LoxP recombination (Figure 3.1), which is likely to occur from birth. The results in Figure 4.4B therefore suggest that impaired arteriole formation occurs during development and this could account for the changes seen. It would be beneficial to confirm this assumption using a sham control to assess the arteriolar density.

Interestingly, the arteriolar density was not statistically different amongst all mouse groups when expressed as a ratio relative to the contralateral limb (Figure 4.4C). This may have achieved statistical significance with an increase in N number and does not eliminate the arteriogenic effect identified in the raw data in Figure 4.4B.

It is also worth noting that that all mouse groups had complete blood flow recovery on day 21 (Figure 4.1), but displayed a difference in arteriolar density (Figure 4.4). If SPHINX31 is acting in a different manner to other cell types resulting in an upregulation of pro-angiogenic VEGF-A_{xxx}a and downstream activation of VEGFR2, which increases the expression of eNOS (resulting in the production of nitric oxide) (Harper and Bates, 2008). In addition, eNOS is shown to be a crucial component in generating new arterioles (Benest *et al*., 2008). The presence of more arterioles in the SPHINX31 treated compared to the LysM-Wnt5a^{GOF} mice suggests that the blood flow in each arteriole is lower due to the presence of more arterioles, resulting in a complete blood flow recovery. This suggests an increase in vascular reserve compared to the untreated Wnt5a^{GOF}. This assumption would need to be confirmed by assessing the endothelial function and eNOS levels. Also, a non-primary control slide was used for the immunofluorescence staining of the vessels, which is a suboptimal control. This does not assess and validate the specificity of the monoclonal αSMA antibody in the gastrocnemius muscle. Therefore, this experiment lacked a non-immune antibody of the same isotype (in this case, IgG2A), which would be the optimal control slide.

4.4.3. The effect of VEGF-A isoforms at a protein level in the gastrocnemius post-ischemia

Kinase inhibition of SRPK1 with SPHINX31 is known to switch the splicing of VEGF-A in neovascular eye diseases, this is yet to be explored in this ischemic mouse model (Batson *et al*., 2017). Therefore, the involvement of VEGF-A isoforms was explored at a protein level on post-operative day 3 in gastrocnemius muscle. As seen with WT and LysM-Wnt5a^{GOF} in Chapter

3, pan-VEGF was not detected and VEGF-A_{165}b displayed no significant difference across all samples (Figure 3.6). This remained consistent with LysM-Wnt5a^{GOF} treated with SPHINX31 gastrocnemius samples (Figure 4.6). Kikuchi and colleagues had previously used the pan-VEGF (A20) antibody which is shown to be reactive with mouse samples (Kikuchi *et al*., 2014). The detection of no protein bands for the mouse samples, compared to the human recombinant protein suggests there might be an issue with the sensitivity of the samples used. To confirm equal loading, β-tubulin, α-tubulin and ponceau red stain were used (Figure 4.6). The band intensities were different in each sample and were not considered accurate or reliable. Due to this, it was not possible to perform any quantifications. This allowed me to eliminate the use of western blotting for this experiment and no firm conclusions were drawn based on this data alone.

Absolute levels of total VEGF and $VEGF_{165}$b were quantified using the commercially available ELISA kits, which displayed no differences between the mouse groups. However, further calculations to predict the changes in VEGF-A_{164} expression which displayed a significant decrease in the ischemic limb of animals treated with SPHINX31 compared to the contralateral limb with no difference amongst the other mouse groups (Figure 4.7C). It is important to note that there was a trend of increased VEGF-A_{165}b and decreased VEGF-A_{164}a, however this did not achieve significance (Figure 4.7). In all the VEGF-A experiments, low levels were detected and quantified. As a human ELISA kit was used for mouse samples, it is questionable whether it is an accurate value of the VEGF content. Perhaps, SPHINX31 is not having an effect on VEGF-A splicing in the gastrocnemius muscle. However, it would be worthwhile to assess the VEGF-A levels in isolated monocytes and macrophages to confirm if there is a cell specific change that was not detected.

An alternative explanation of the blood flow recovery with SRPK1 inhibition could be explained by a concept known as vascular normalisation initially identified in solid tumours (Jain, 2001). It is feasible that treatment of

SPHINX31 reverts the imbalance of VEGF-A isoforms in LysM-Wnt5a^{GOF} towards an equilibrium during the first few days after the treatment was administered which is when the gastrocnemius muscle tissue was collected (Goel *et al*., 2012, Kikuchi *et al*., 2014). The vessels are likely to present a normalised phenotype during this 'normalisation window' and would also explain the lack of effect on VEGF-A splice variants in the gastrocnemius muscle. To confirm this, histological analysis of the arterioles and capillaries in the gastrocnemius on day 3 would be needed to identify if there are abnormalities and could support this assumption. It is possible that the normalised vessels are likely to be maintained for the duration of the 21-day HLI study due to biweekly treatments. Thereby, promoting remaining vasculature towards a structurally and functionally 'normal' state resulting in complete blood flow recovery (Figure 4.1) and an increase in the vascular density (Goel *et al*., 2012) (Figure 4.3 and 4.4). Despite no detectable changes in pan-VEGF and VEGF-A_{165}b in the gastrocnemius muscle, SRPK1 inhibition could be a viable therapeutic option.

4.4.4. The effect of Flt1/sFlt1 at an RNA level

VEGFR1 (Flt1) was shown to play a key role in modulating blood flow recovery and inducing muscle recovery compared to VEGFR2 (Flk1) (Amano *et al*., 2015). Interestingly, it was the lack of VEGFR1 tyrosine kinase domains (also known as a soluble form of VEGFR1, sFlt1) that was impairing the angiogenic response (Amano *et al*., 2015, Kendall and Thomas, 1993). This remained consistent in animals treated with a sFlt1 adenovirus gene transfer which resulted in impaired collateral growth in the ischemic limb (Jacobi *et al*., 2004), together suggesting sFlt-1 has a clear role as a VEGF-A antagonist.

The connection between Wnt5a and sFlt1 resulting in impaired regenerative angiogenesis was initially identified retinal myeloid cells (Stefater *et al*., 2011). Further studies have supported this observation in wound repair (Stefater *et al*., 2013), adipose tissue (Karki *et al*., 2017), and peripheral arterial disease of aged mice (Zhao *et al*., 2017). Independent studies have shown Wnt5a negatively regulates ischemia induced angiogenesis in

mouse models of obesity (Kikuchi *et al*., 2014, Ouchi *et al*., 2010). Whilst, Hazarika *et al* showed that sFlt1 and Flt1 were responsible for impaired vascular growth in the skeletal muscle of type 2 diabetic mouse models post ischemia (Hazarika *et al*., 2007). However, while there is currently no evidence to support the role of SRPK1 inhibition in Flt1 splicing, there is no published evidence against it either. SPHINX31 has been shown to reduce the phosphorylation of SRSF2 in leukemic cells, which has a role in regulating an increase in VEGF-A_{165}b and sFLT1 in a Wnt5a dependent manner in monocytes/macrophages (Kikuchi *et al*., 2014, Tzelepis *et al*., 2018, Zhao *et al*., 2017). Together these suggest that Flt1 and sFlt1 could be a molecular pathway linking Wnt5a and SRPK1 with SPHINX31. There is also contradictory evidence in carcinoma cells confirming that anti-angiogenic therapies control the splicing of Flt1 to sFlt1 (sFlt1-i13) through SC35/SRSF2 (Abou Faycal *et al*., 2019). Nevertheless, the involvement of *Flt1* (Figure 4.8) and *sFlt1* (Figure 4.9) were assessed at an RNA level using post-operative day 3 gastrocnemius muscle samples previously used in 4.4.3. The data was skewed by a single mouse in each sample. Despite this, there was little difference across all the samples overall.

The infiltration of proinflammatory monocytes towards the ischemic region play a crucial role in the angiogenic process. The rate of monocyte migration increases in the ischemic limb of older mice. Importantly this correlated with an increase in anti-angiogenic effects resulting in the production of Wnt5a, SC35 (SRSF2) and sFlt1 when compared to young mice (Zhao *et al*., 2017). All mice used in this study were 10-12 weeks old, which are relatively young compared to the 18-month-old mice used by Zhao *et al*. It is possible that the age of mice could possibly explain the lack of effect seen in the gastrocnemius muscle.

It is also important to consider the severity of PAD model used for this study compared to those published. Risk factors such as diabetes and obesity have resulted in an increase in Flt1 and sFlt1 expression (Karki *et al*., 2017, Hazarika *et al*., 2007). In addition to this, strain differences are likely to affect isoform levels. BALB/c is a model of severe PAD compared to C57/BLJ,

resulting in a difference in revascularisation rate (Chalothorn *et al*., 2007, Helisch *et al*., 2006). Thus, the model is likely to contribute to minimal differences identified.

An adequate amount of *sFlt1* and *Flt1* was detected across all samples, which is promising as they are necessary to balance, maintain and limit vascular growth to a small extent. However, this mechanism is shown not to be responsible for the complete blood flow recovery (Figure 4.1-4.3) and collateral growth seen in the gastrocnemius muscle with SRPK1 inhibition (Figure 4.3 and 4.4). SRPK1 inhibition is clearly a viable strategy that could be used for ischemic diseases. It would be worthwhile to assess the sFlt1 and Flt1 expression at a protein and RNA level in diabetic or obese LysM-Wnt5a^{GOF} treated with SPHINX31. More importantly, assessment of SR proteins which are phosphorylated/unphosphorylated with SPHINX31 in this transgenic mouse model will be key in understanding the molecular mechanism. SPHINX31 has the ability to inhibit SRPK1, and SRPK2 and CLK1 to a less extent (Batson *et al*., 2017). There are potential off-target effects, confirming the lack of selectivity. The systemic SPHINX31 administration means it is unlikely to be acting solely on monocytes and could be acting on other cell types.

4.5. Concluding remarks

The data in this chapter demonstrates that slower blood flow recovery due to impaired collateralisation, angiogenesis and arteriogenesis in mice with monocytes overexpressing Wnt5a (as previously shown in Chapter 3) was reversed, not further impaired by SRPK1 inhibition with SPHINX31. Impaired revascularisation in PAD may be dependent on SRPK1 in the monocytes but could equally be an effect on other tissues or cell types in the effected tissues. The involvement of VEGF-A and *sFlt1*/ *Flt1* were assessed, however it was not possible to detect any conclusive change under the given conditions. The data in this chapter confirms SRPK1 could be an important target. However, it was not possible to confirm how SPHINX31 is acting given the route of administration. Therefore, a monocyte specific SRPK1 knockout mouse model was generated to allow me to answer this question.

Chapter 5

The effect of revascularisation on a transgenic mouse model with Wnt5a hyperactivity and SRPK1 knockout in monocytes

5.1. Introduction

SRPK1 inhibitors modulate the switch in VEGF-A splicing resulting in the anti-angiogenic isoform, VEGF-A_{xxx}b (Gammons *et al*., 2013, Mavrou *et al*., 2015, Amin *et al*., 2011, Hatcher *et al*., 2018). In ischemic diseases, targeting SRPK1 by using an inhibitor as a pharmacological tool could be a promising treatment strategy as shown in Chapter 4. However, the intraperitoneal route of administration means that the drug rapidly absorbed into the systemic circulation (Al Shoyaib *et al*., 2019). This makes it difficult to pinpoint the mechanism of action and does not definitively show that monocytic SRPK1 is responsible for the impaired revascularisation.

A promising approach which serves as a critical tool for studying gene and cell specific functions is through the use of transgenic mouse models. The site-specific enzyme, Cre recombinase (also known as Cre) recognises DNA segments of a specific gene that are flanked by 34 bp LoxP sites resulting in a deletion of the floxed region (Sauer and Henderson, 1988, Rajewsky *et al*., 1996). This can be limited and selective for specific cell types when Cre is under the control of a chosen promoter. This is known as a 'conditional transgene'. The murine M lysozyme promoter under the control of Cre (known as LysM-Cre) has shown to be highly specific and efficient in deletions of LoxP flanked regions in monocytes (inflammatory and resident) and macrophages and to a reduced extent in granulocytes resulting in permanent inactivation of genes (Clausen *et al*., 1999, Shi *et al*., 2018, Abram *et al*., 2014). Other myeloid Cre driven promoter strains (including CD11b-cre and CD11c-cre) are inconsistent in cell specific deletions and show significant amount of unexpected deletions in dendritic cells (Abram *et al*., 2014). The Cre-mediated deletions are dependent on the selection of the cell specific promoter. During the course of this study, the LysM-Cre transgenic mouse will be used to generate a monocyte specific SRPK1 mouse strain

Previous work in this thesis has established that an overexpression of Wnt5a in monocytes results in impaired blood flow recovery (Chapter 3),

which is reversed with SRPK1 inhibition with SPHINX31 (Chapter 4) in LysM-Wnt5a^{GOF} mice. In addition to this, Wnt5a-postive macrophages are shown to accumulate in the ischemic gastrocnemius of diet-induced obese mice (Kikuchi *et al*., 2014). Therefore, I now hypothesised that monocytic SRPK1 is responsible for the impaired blood flow recovery in a Wnt5a dependent manner and in obese mice. To investigate and understand this further, in this chapter I will firstly confirm if monocytic SRPK1 is responsible for the impaired blood flow recovery by using the transgenic SRPK1^{LoxP} mouse strain developed in collaboration between Professor David Bates and Dr Lydia Teboul at MRC Harwell, Oxfordshire. Following confirmation of SRPK1 knockout in monocytes to confirm specificity of the LysM-Cre promoter, animals were bred with LysM-Wnt5a^{GOF} (Chapter 3.1) mice to develop a novel transgenic mouse model with Wnt5a hyperactivity and SRPK1 knockout in the monocytes (abbreviated to LysM-Wnt5a^{GOF}: SRPK1^{MoKO}). I will determine if induction of ischemia affects the blood flow recovery. Thus, I will analyse the changes in arteriogenesis and angiogenesis in the gastrocnemius muscle on day 21 post-ischemia. Finally, a model of obesity will be induced in the monocyte specific SRPK1 knockout mouse model and the blood flow recovery will be assessed after HLI.

5.2. Methodology

Adult transgenic mice (C57BlJ) mice were bred in-house. All genotyping on ear notches was performed by Transnetyx. At the age of 10-12 weeks, a total of 80 mixed gender mice were subjected to the hind limb ischemia (HLI) model of PAD as described in Chapter 2. I used 12 WT, 17 SRPK1^{LoxP}, 21 SRPK1^{MoKO}, 8 STOP-Wnt5a: SRPK1^{LoxP}, 8 LysM-Wnt5a^{GOF} and 14 LysM-Wnt5a^{GOF}: SRPK1^{MoKO} mice (refer to Table 5 for the nomenclature for each respective mouse group). This included a total of 20 mice, which were placed on a high fat, high sucrose (HF/HS) diet to for 12 weeks before and then during the 28-day HLI study to induce obesity. Analysis was performed using the FLPI-2 software (Moors Instruments) by calculating the ratio of the ischemic vs contralateral speckle intensity at each time point.

RT-PCR was performed on the RNA extracted from pooled splenocytes and bone marrow immune cells, as well as selected and non-selected CD11^{+} monocytes to assess the *Srpk1* expression in ischemic and non-ischemic mice. On day 3, animals were culled and bone marrow immune cells or splenocytes were extracted for RNA (for RT-PCR). On day 21, animals were culled by cardiac perfusion and gastrocnemius muscle was dissected for histological analysis by staining for capillaries with IB_4 and arterioles with αSMA. Using the FIJI image analysis software, capillary and arteriolar density was calculated. All methods are described in detail in Chapter 2.

Table 5. Simplified mouse names used and respective nomenclature

Simplified name for transgenic mouse model	**Nomenclature for mouse strains**
STOP-Wnt5a	*Rosa26^{Wnt5aStopLoxP}*
LysM-Wnt5a^{GOF}	*Rosa26$^{LysM\text{-}Cre/Wnt5a}$*
SRPK1^{LoxP}	*Srpk1^{tm1c}* • Homozygous: *Srpk1$^{tm1c\ (-/-)}$* • Heterozygous: *Srpk1$^{tm1c\ (-/+)}$*
SRPK1^{MoKO}	*Srpk1$^{tm1d/LysM\text{-}Cre}$*
STOP-Wnt5a: SRPK1^{LoxP}	*Rosa26^{Wnt5aStopLoxP}; Srpk1$^{tm1c\ (-/-)}$*
LysM-Wnt5a^{GOF}: SRPK1^{MoKO}	*Rosa26$^{LysM\text{-}Cre/Wnt5a}$; Srpk1^{tm1d}*

5.2.1. Statistical analysis

Statistical tests performed were a two-way ANOVA with post-hoc Bonferroni's test when comparing blood flow recovery after the induction of ischemia between mouse groups on post-operative days. The analysis of vessel densities between the contralateral/ischemic gastrocnemius between mouse groups was performed using a two-way ANOVA with post-hoc Bonferroni's test. For comparisons of three independent mouse groups (e.g. WT, LysM-Wnt5a^{GOF} and LysM-Wnt5a^{GOF}: SRPK1^{MoKO}), a one-way ANOVA with post-hoc Bonferroni's test were used. For two independent mouse groups (e.g. WT vs SRPK1^{MoKO}), unpaired t-tests were used.

5.3. Results

5.3.1. Developing the SRPK1^{LoxP} transgenic mice

The SRPK1^{LoxP} mice were generated at MRC Harwell in Abingdon, Oxfordshire under a collaboration agreement with Professor Bates' laboratory. To screen for WT or *Srpk1^{tm1c}* allele (mouse referred to as SRPK1^{LoxP}), animals were ear notched for genotyping which was performed by Transnetyx Inc using qPCR. To identify WT mice, primer sets were designed upstream and downstream of the insertion site (Figure 5.1A). By CRISPR/CAS9 recombination, two LoxP sites were inserted on both sides of exon 7 to generate a SRPK1^{LoxP} mouse. These mice were genotyped by using primers that are upstream of the FRT site and downstream of the LoxP site (Figure 5.1B). An example of the qPCR curves of the DNA from the 11 ear notches are shown in Figure 5.1C displays the difference between the C_t value for the test and *Gapdh* control. The ΔC_t value was calculated from the difference between the C_t value for *Gapdh* and the *Srpk1*-WT or *Srpk1^{tm1c}* primer sets confirming that a low ΔC_t value (i.e. the test product is roughly equivalent to *Gapdh*) is inversely proportional to whether the allele is present (as shown in Figure 5.1D). The ΔC_t value was raised to the power of two to detect the fold increase of the target probe with each PCR cycle (Figure 5.1E). It can be seen that for the litters shown below, four mice were WT due to the presence of the *Srpk1*-WT allele (red, Figure 5.1E). Of the remaining 7 ear notches, 4 were heterozygote for the *Srpk1*-WT and *Srpk1^{tm1c}* allele (green, Figure 5.1E) and 3 were homozygote for the *Srpk1^{tm1c}* allele (blue, Figure 5.1E).

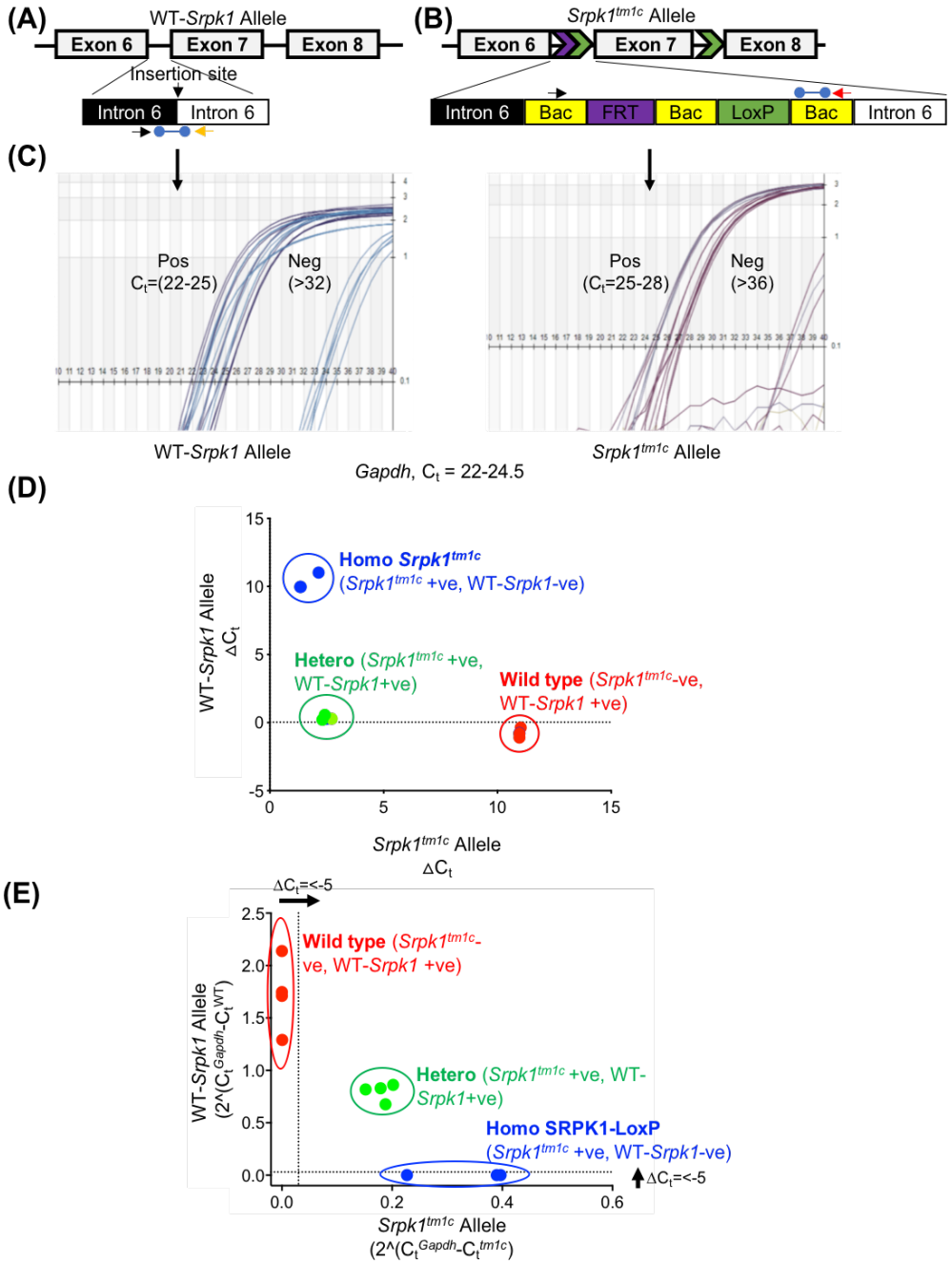


Figure 5.1. Development and genotyping of the SRPK1^{LoxP} transgenic mouse performed by Transnetyx Inc. (A) *To screen wild type alleles, Srpk1 primers were used upstream (black) and downstream (orange) of the putative insertion site and a probe used that spanned the insertion site (blue dumbbell).* ***(B)*** *LoxP sites were inserted either side of exon 7 using CRISPR-Cas9 recombination. To genotype the mice, primers were used in the insert upstream of the FRT recombination site (black arrow) and downstream of the LoxP site (red arrow) but still in the insert. A Taqman probe was used in the insert (blue dumbbell).* ***(C)*** *qPCR of DNA extracted from ear punches from 11 mice (in duplicate) using WT-Srpk1 primers (left) or Srpk1^{tm1c} primers (right).* ***(D)*** *The C_t difference between control (Gapdh) and test gene was calculated (-ΔC_t), where a low value (Gapdh≅test) is inversely proportional to the amount of target gene present, where red is wildtype, green is heterozygous and blue is homozygous.* ***(E)*** *The ΔC_t value for each test gene was raised to the power of two and plotted. Thus, presence of the wildtype*

allele gives a positive value (2^{-5}=0.03) and the presence of the Srpk1^{tm1c} sites giving a positive value (>2^{-5}) with a C_t value of Gapdh closer than 5 cycles to the test cycle threshold (i.e. $2^{\Delta Ct}$ of >0.03) lying outside the dotted lines. Thus, a wild type animal has a positive WT value, and low (<0.03) Srpk1^{tm1c} value (red), and a heterozygous animal is positive for both alleles (green). Homozygotes showed no WT-Srpk1 signal, but a positive Srpk1^{tm1c} signal (blue).

5.3.2. The SRPK1 knockout mouse model

To determine whether SRPK1 in monocytes contributes to collateral vessel development, a novel mouse model was developed with SRPK1 knockout in the monocytes (abbreviated to SRPK1^{MoKO}). This was generated by breeding a homozygote SRPK1^{LoxP} mouse, which carries a *Srpk1$^{tm1c\ (-/-)}$* allele with the critical exon (exon 7) flanked by two LoxP sites (essentially a WT mouse, which is a control group (Figure 5.2A)) with a LysM-Cre mouse. The LysM promoter (driven in monocytes) allows for cre-mediated excision of the critical exon by Cre/LoxP recombination. This results in a monocyte specific SRPK1 knockout mouse model, which is homozygous for the *Srpk1^{tm1d}* allele and heterozygous for the LysM-Cre allele, shown in Figure 5.2B (hereafter referred to as SRPK1^{MoKO}).

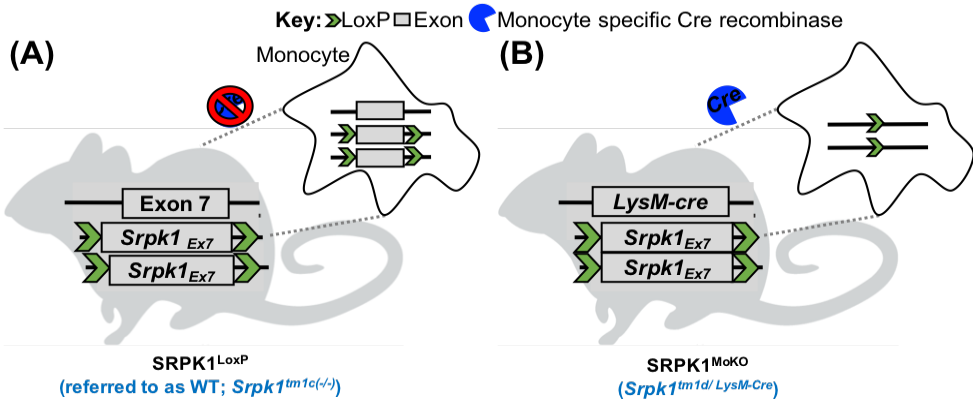


Figure 5.2. Schematic diagram displaying the homozygous SRPK1^{LoxP} mouse model without (essentially WT) and with Cre present (SRPK1^{MoKO}). (A) *The Srpk1 gene is flanked by two LoxP sites at exon 7 (also known as the critical exon) and is not targeting for excision due to the absence of Cre-recombinase. This mouse is functionally a WT.* ***(B)*** *The Srpk1 gene is flanked by two LoxP sites at exon 7 and is heterozygous for the LysM-Cre allele. Thus, cre recombinase target the two LoxP sites removing exon 7 of the Srpk1 gene in the monocytes resulting in degradation of the remaining Srpk1 transcript. This mouse is a monocyte specific SRPK1 knockout (referred to as SRPK1^{MoKO}).*

The annealing temperature was optimised by performing a PCR temperature gradient on RNA extracted and cDNA synthesised from bone marrow immune cells of WT mice. The density of the *Srpk1* band detected on the agarose gel increased with temperature between 54-62^{o}C at 183bp (Figure 5.3A). The PCR was re-run on selected CD11b^{+} and non-selected CD11b^{-} cells from a mixed population of bone marrow immune cells and from splenocytes in WT and SRPK1^{MoKO} mice. The agarose gel confirmed that *Srpk1* was detected at extremely low levels in CD11b^{+} and CD11b^{-} cells from the bone marrow of SRPK1^{MoKO} mice compared to WT mice. Similarly, in the spleen a *Srpk1* band was weakly expressed at 183bp in selected CD11b^{+} monocytes of SRPK1^{MoKO} mice compared to the non-selected CD11b^{-} cells and WT mice. *Gapdh* primers (297bp) were used to confirm equal loading of cDNA in each sample (Figure 5.3B).

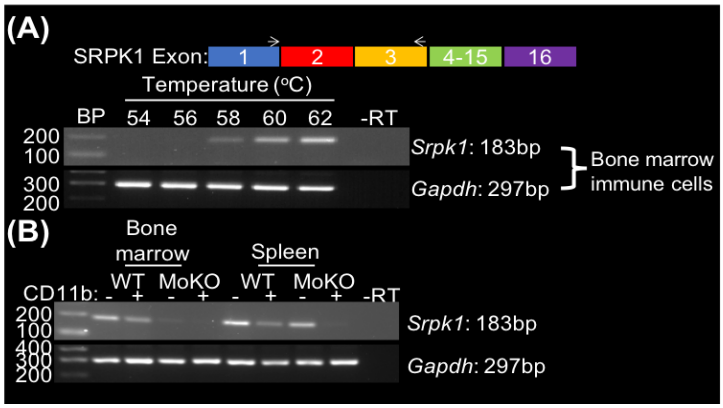


Figure 5.3. Determining the expression of Srpk1 in selected CD11b^{+} monocytes of WT and SRPK1^{MoKO} mice using primers that span exon 1 and 3. *RNA was extracted from bone marrow immune cells, selected and non-selected CD11b^{+} cells from WT and SRPK1^{MoKO} mice. RT-PCR was performed to measure the Srpk1 expression levels (183bp).* ***(A)*** *Optimisation of the annealing temperature (54-62^{o}C) of the primer set on a mixed population of bone marrow immune cells. Srpk1 (183bp) and Gapdh (297bp) was detected at the expected height.* ***(B)*** *The Srpk1 expression in CD11b^{-} and CD11b^{+} cells from WT and SRPK1^{MoKO} mice at 62^{o}C annealing temperature. (MoKO= SRPK1^{MoKO}).*

To assess *Srpk1* knockout directly at an RNA level, primers were designed to span exon 1 and exon 7/8. RT-PCR was performed on cDNA synthesised and previously used in Figure 5.3 at an annealing temperature of 62^{o}C (Figure 5.3). The agarose gel confirmed that *Srpk1* is present at 609bp in non-selected and selected WT bone marrow immune cells and splenocytes.

In SRPK1^{MoKO} mice, expression levels were extremely low in the bone marrow immune cells and CD11b^{+} splenocytes. *Srpk1* was detected in the CD11b^{-} in the splenocytes of SRPK1^{MoKO} mice. *Gapdh* (297bp) was used to confirm equal loading of all samples (Figure 5.4).

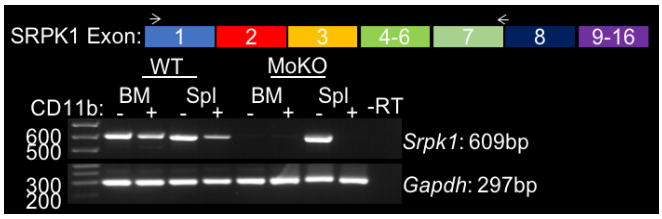


Figure 5.4. Determining the expression of Srpk1 in selected CD11b^{+} monocytes of WT and SRPK1^{MoKO} mice using primers that span exon 1 and exon 7/8. *RNA was extracted from bone marrow immune cells, selected and non-selected CD11b^{+} cells from WT and SRPK1^{MoKO} mice. RT-PCR was performed to measure the Srpk1 expression levels (609bp). The Srpk1 expression in CD11b^{-} and CD11b^{+} cells from WT and SRPK1^{MoKO} mice at 62^{o}C annealing temperature (BM=Bone marrow; Spl= Spleen; MoKO= SRPK1^{MoKO}).*

5.3.3. Effects of SRPK1 knockout on hindlimb ischemia

To determine whether the excision of SRPK1 in the monocytes altered the blood flow recovery after ischemia, littermate WT and SRPK1^{MoKO} mice (shown in the schematic diagram in Figure 5.2) were subjected to HLI of the left femoral artery. The representative speckle images from both mouse strains is shown in Figure 5.5A. Quantitative analysis of the ischemic vs contralateral speckle intensity ratio to calculate blood flow recovery showed that all mice recovered blood flow equally for the duration of the study. The blood flow recovery plateaus after day 7 and at day 21 the blood flow had not completely recovered in both mouse groups (WT: 0.74 ± 0.07 and SRPK1^{MoKO} normal chow: 0.64 ± 0.07, p>0.05; Figure 5.5B). Interestingly, the severity of ischemia induced on post-operative day 0 was greater in SRPK1^{MoKO} (0.12 ± 0.02) compared to WT (0.18 ± 0.01, p=0.05; Figure 5.5C). Therefore, the data was further normalised to post-operative day 0 of each respective mouse, which confirmed that the blood flow recovery was quicker in SRPK1^{MoKO} compared to the WT mice on day 7 (5.29 ± 1.00 vs 3.52 ± 0.14, p=0.65), 14 (5.86 ± 1.06 vs 3.64 ± 0.35, p=0.47) and 21 (6.16 ± 1.20 vs 4.22 ± 0.43, p=0.64; Figure 5.5D).

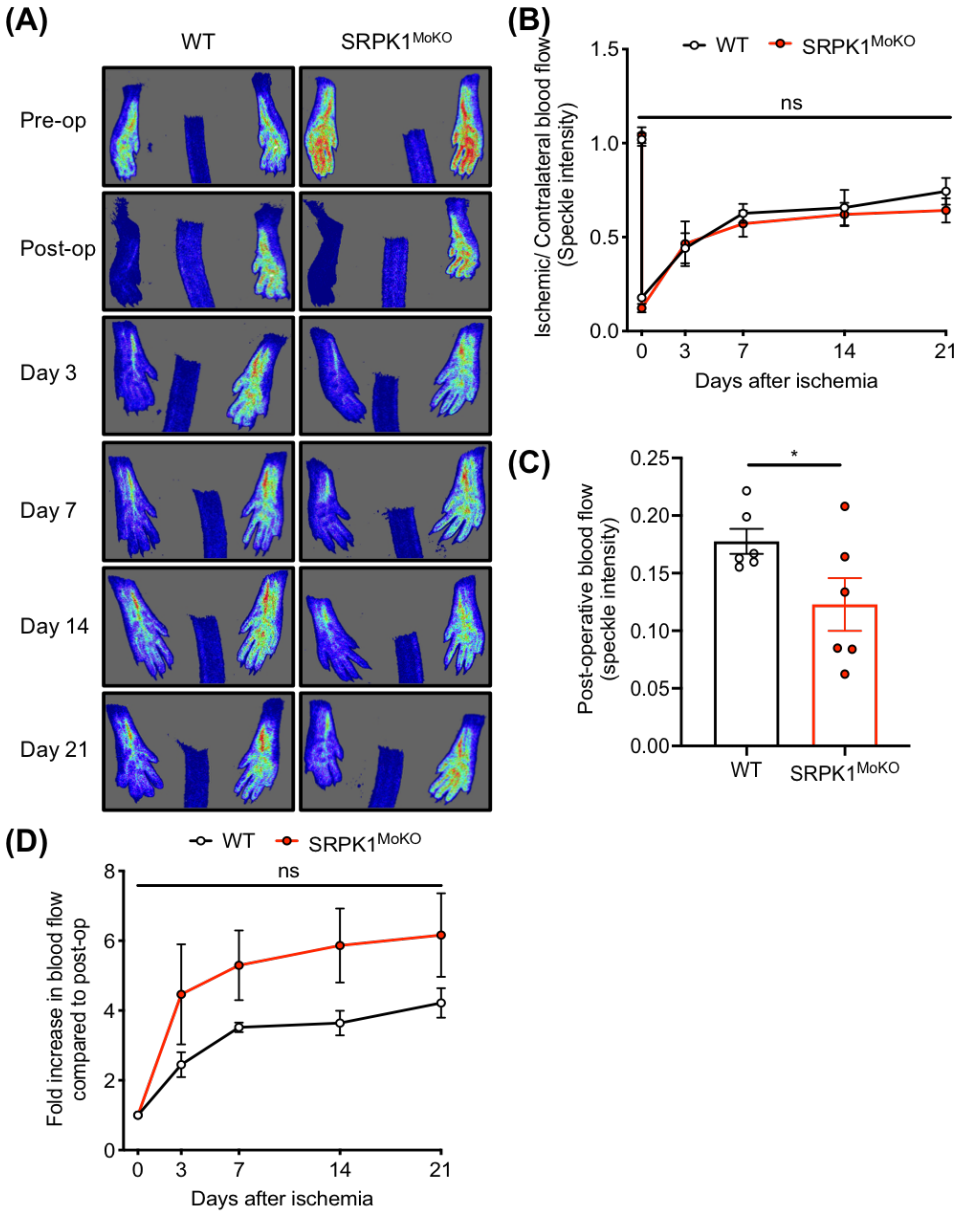


Figure 5.5. No difference in blood flow recovery in WT and SRPK1^{MoKO} mice after inducing ischemia in the left femoral artery (A) *WT and SRPK1^{MoKO} mice underwent left femoral artery ligation and the blood flow to the paw was measured using the laser speckle imaging system as shown in the representative images.* ***(B)*** *Quantitative analysis of the ischemic vs non-ischemic speckle intensity was observed through to post-operative day 21.* ***(C)*** *The level of ischemia induced on post-operative day 0 in WT and SRPK1^{MoKO}.* ***(D)*** *The data was further normalised to post-operative day 0 of each respective mouse.* ***(B)(D)*** *Results indicate the mean ± SEM. Data was analysed using a two-way ANOVA (****(B)*** *Main effects: Post-operative day: p<0.0001, Genotype (mouse group): p=0.68; Interaction effect: p=0.82.* ***(D)*** *Main effects: Post-operative day: p=0.0003, Genotype (mouse group): p=0.12; Interaction effect: p=0.24)) with Bonferroni post hoc test.* ***(C)*** *Error bars are shown as the mean ± SEM. Data was analysed using an unpaired t-test. N=6/group. (*=p<0.05 and ns= non-significant, p>0.05).*

5.3.4. Generating a transgenic mouse model with monocyte specific Wnt5a hyperactive and SRPK1 knockout

To generate a transgenic mouse model with monocyte specific Wnt5a overexpression with SRPK1 knockout, heterozygous LysM-Wnt5a^{GOF} mice (Figure 3.1) were crossed with heterozygous SRPK1^{LoxP} mice. The offspring from this breeding pair inherit an active LysM-Wnt5a^{GOF} and SRPK1^{LoxP}, therefore are heterozygote for both alleles (*Rosa26$^{LysM\text{-}Cre/Wnt5a}$; Srpk1$^{tm1c(-/+)}$, also* referred to as LysM-Wnt5a^{GOF}:SRPK1^{LoxP}). Finally, the resultant mice were further crossed with homozygous SRPK1^{LoxP} mice (Figure 5.2). The litters from this breeding cross allows LysM-Cre recombinase to target the loxP site on all alleles in the monocytes. Therefore, the stop codon is removed from the inactive Wnt5a transgene and exon 7 is removed from the *Srpk1* allele resulting in an active Wnt5a transgene and degradation of the *Srpk1* gene transcript. Together, this results in a monocyte specific SRPK1 knockout with Wnt5a overexpression mouse model (*Rosa26$^{LysM\text{-}Cre/Wnt5a}$; Srpk1^{tm1d},* hereafter referred to LysM-Wnt5a^{GOF}: SRPK1^{MoKO}). A WT littermate is also produced, which does not carry LysM-Cre recombinase, therefore LoxP sites are not targeted for recombination (*Rosa26^{Wnt5aStopLoxP}; Srpk1$^{tm1c\ (-/-)}$*). A summary of the breeding is shown in Figure 5.6.

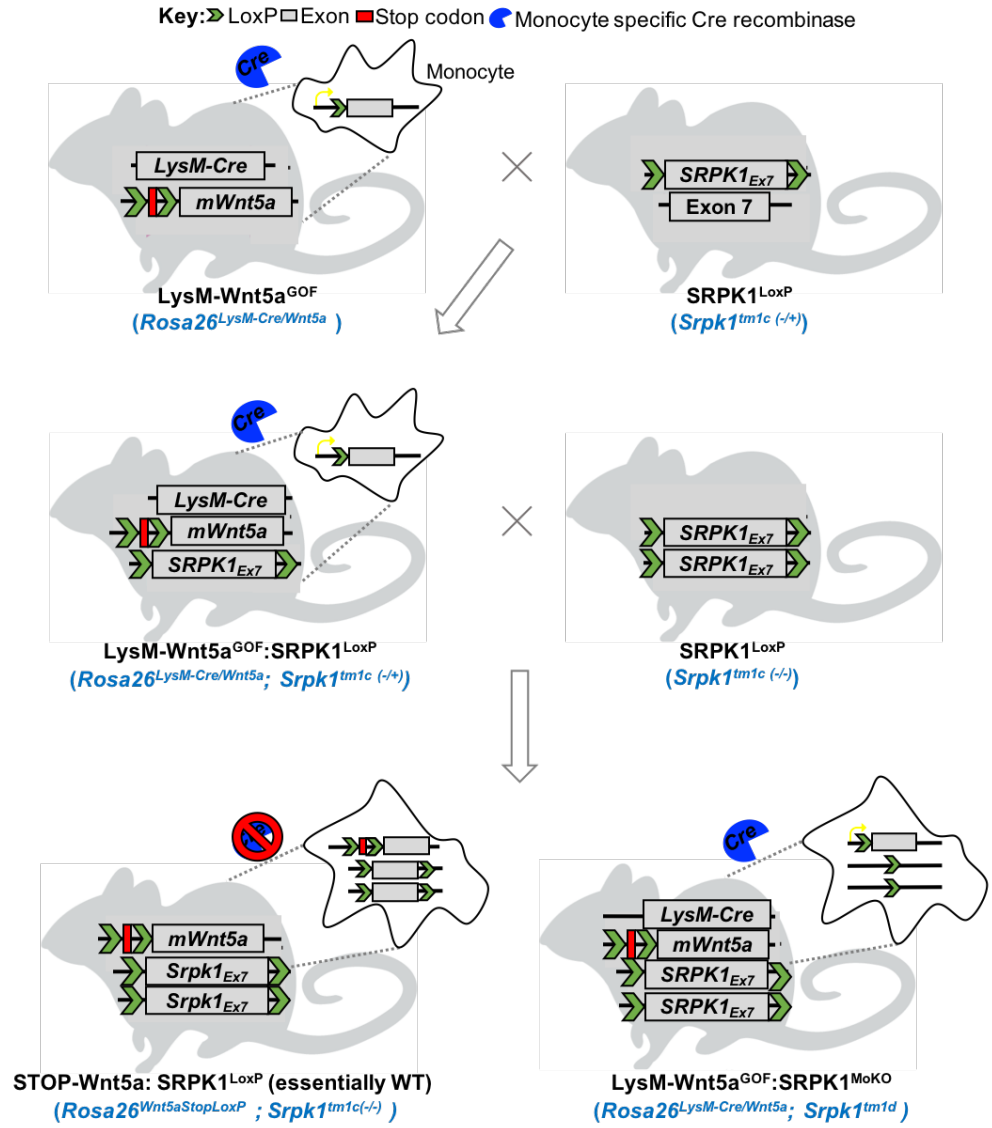


Figure 5.6. Generating the monocytic specific Wnt5a overexpression and SRPK1 knockout mouse model. *Heterozygous LysM-Wnt5a^{GOF} were bred with heterozygous SRPK1^{LoxP}. The litters were further bred with homozygous SRPK1^{LoxP} mice resulting in the STOP-Wnt5a: SRPK1^{LoxP} control group (WT) and experimental transgenic mice, LysM-Wnt5a^{GOF}: SRPK1^{MoKO}.*

5.3.5. SRPK1 knockout in monocytes reverses impaired blood flow recovery in LysM-Wnt5a^{GOF} mice

Previous data in Chapter 4 confirmed that inhibition of SRPK1 activity with SPHINX31 reverses the impaired blood flow recovery in LysM-Wnt5a^{GOF} mice (Figure 4.1). Therefore, I investigated the role of monocytic SRPK1 after ischemia in a transgenic Wnt5a hyperactive mouse model. This study required four groups of experimental mice as shown in Figure 5.7. The first mouse group is heterozygous for the STOP-Wnt5a transgene and

homozygous for the SRPK1^{LoxP} allele (*Rosa26^{Wnt5aStopLoxP}; Srpk1$^{tm1c\ (-/-)}$*). This is essentially a WT mouse and serves as a control line for this experiment (also STOP-Wnt5a: SRPK1^{LoxP}; hereafter referred to as WT-littermate). The absence of Cre-recombinase does not allow LoxP sites to be targeted for recombination or excision (Figure 5.7A). Similarly, the second mouse group has Cre present and serves as an additional control group for this experiment (Figure 5.7B). The third mouse group are the heterozygous LysM-Wnt5a^{GOF} with LysM-Cre present (*Rosa26$^{LysM\text{-}Cre/Wnt5a}$*). This allows Cre mediated excision of the stop codon only in monocytes and myeloid cells resulting in Wnt5a overexpression (hereafter referred to as LysM-Wnt5a^{GOF}; Figure 5.7C). The final group carry all these alleles, so the presence of LysM-Cre allows for cell-specific deletion of exon 7 in the homozygous SRPK1 allele and removal of the stop codon in the STOP-Wnt5a transgene, thereby resulting in the novel transgenic mouse model *Rosa26$^{LysM\text{-}Cre/Wnt5a}$: Srpk1^{tm1d}* (named LysM-Wnt5a^{GOF}:SRPK1^{MoKO}, Figure 5.7C).

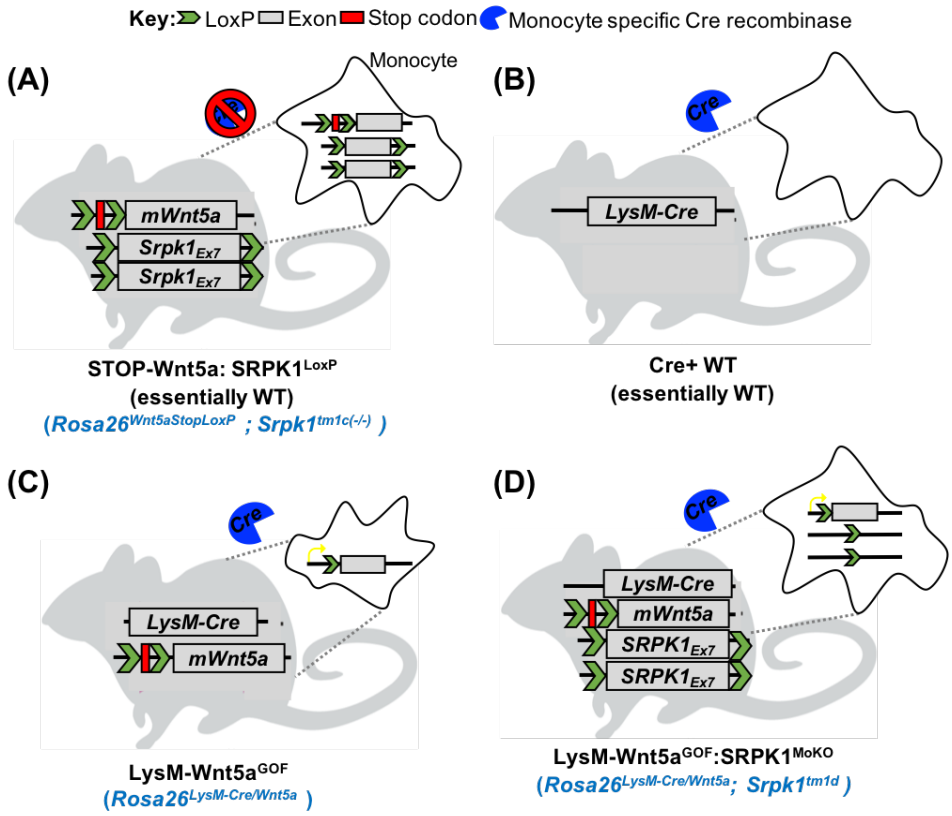


Figure 5.7. Schematic diagram displaying the three transgenic mouse groups included in the 21-day HLI study. (A) *Homozygous for the SRPK1^{LoxP} allele and heterozygous for the STOP-Wnt5a transgene – essentially a WT mouse.*

(B) *Cre+ WT mouse group- essentially WT.* ***(C)*** *LysM-Wnt5a^{GOF} mouse.* ***(D)*** *Cre-mediated excision exon 7 from the Srpk1 allele and removal the stop codon in the STOP-Wnt5a transgene in monocytes and myeloid cells only (referred to as LysM-Wnt5a^{GOF}:SRPK1^{MoKO}).*

Subsequently, all mouse groups (shown in Figure 5.7) were subjected to HLI of the left femoral artery. The representative speckle images shown in Figure 5.8A are from each group showing the blood flow seen before surgery, immediately after and on post-operative days 3, 7, 14 and 21. As expected all animals showed a marked reduction in blood flow immediately after surgery (post-op), as shown by a dark blue paw compared to pre-operative day 0, thereby indicated a successful surgery. By post-operative day 7, the ischemic hind limb of LysM-Wnt5a^{GOF} had a high blue coverage of the paw indicating an ischemic paw compared to WT and LysM-Wnt5a^{GOF}:SRPK1^{MoKO} which showed an increase in blood flow (Figure 5.8A). Analysis of the LSI images demonstrated that the blood flow recovery (ratio of ischemic vs contralateral speckle intensity) in LysM-Wnt5a^{GOF}: SRPK1^{MoKO} occurred at a similar rate to WT. In the LysM-Wnt5a^{GOF} group, the blood flow was significantly slower on day 3 (0.21 ± 0.03 compared to 0.48 ± 0.07 for WT, p=0.003) and day 7 (0.43 ± 0.03 compared to 0.68 ± 0.08 for WT, p=0.005 and 0.65 ± 0.08 for LysM-Wnt5a^{GOF}: SRPK1^{MoKO}, p=0.043). After day 7, all mouse groups had a similar recovery rate and at day 21 recovered by >0.70 (Figure 5.8B).

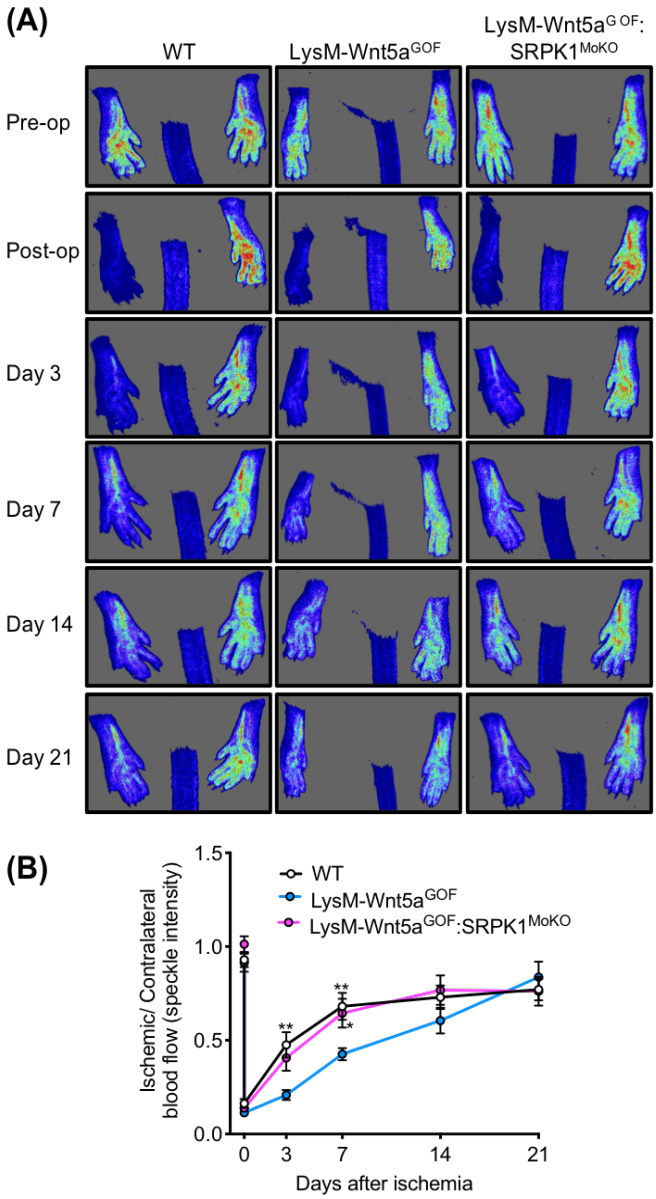


Figure 5.8. LysM-Wnt5a^{GOF} induced impairment of revascularisation is controlled by monocytic specific SPRK1 activity in vivo. (A) *WT, LysM-Wnt5a^{GOF} and LysM-Wnt5a^{GOF}:SRPK1^{MoKO} mice underwent left femoral artery. The blood flow to the paw was monitored using the laser speckle imaging system as shown in the representative images.* ***(B)*** *Quantitative analysis of the ischemic/ non-ischemic speckle intensity was calculated to post-operative day 21. Data was analysed via a two-way ANOVA (Main effects: Post-operative day: p<0.0001, Genotype (mouse group): p=0.12; Interaction effect: p=0.031) with Bonferroni's post hoc test. Results are shown as the mean ± SEM. N: WT- 14 (included 6 Cre+ WT and 8 STOP-Wnt5a: SRPK1^{LoxP}), LysM-Wnt5a^{GOF}- 8 and LysM-Wnt5a^{GOF}: SRPK1^{MoKO} - 8. group (**= p<0.01 and *=p<0.05).*

5.3.6. Capillary and arteriolar density

On day 21, all mice were culled by cardiac perfusion. The gastrocnemius muscle was dissected, cryoprotected and cryo-sectioned for histological analysis of the vascular network. Representative IB_4 positive vessel staining for capillaries in the gastrocnemius muscle of WT, LysM-Wnt5a^{GOF} and LysM-Wnt5a^{GOF}: SRPK1^{MoKO} is shown in Figure 5.9A. Quantitative analysis was performed to determine the capillary density per mm^2, which revealed that there was no significant difference between the capillary densities in the ischemic LysM-Wnt5a^{GOF}: SRPK1^{MoKO} (375.40 ± 49.63/mm^2), LysM-Wnt5a^{GOF} (311.00 ± 18.64/mm^2) and WT (425.00 ± 52.83/mm^2) ($p>0.05$, Figure 5.9B). Next, the data was calculated as a ratio of the ischemic vs contralateral capillary density of each respective mouse which showed no difference amongst all mouse groups ($p>0.05$, Figure 5.9C).

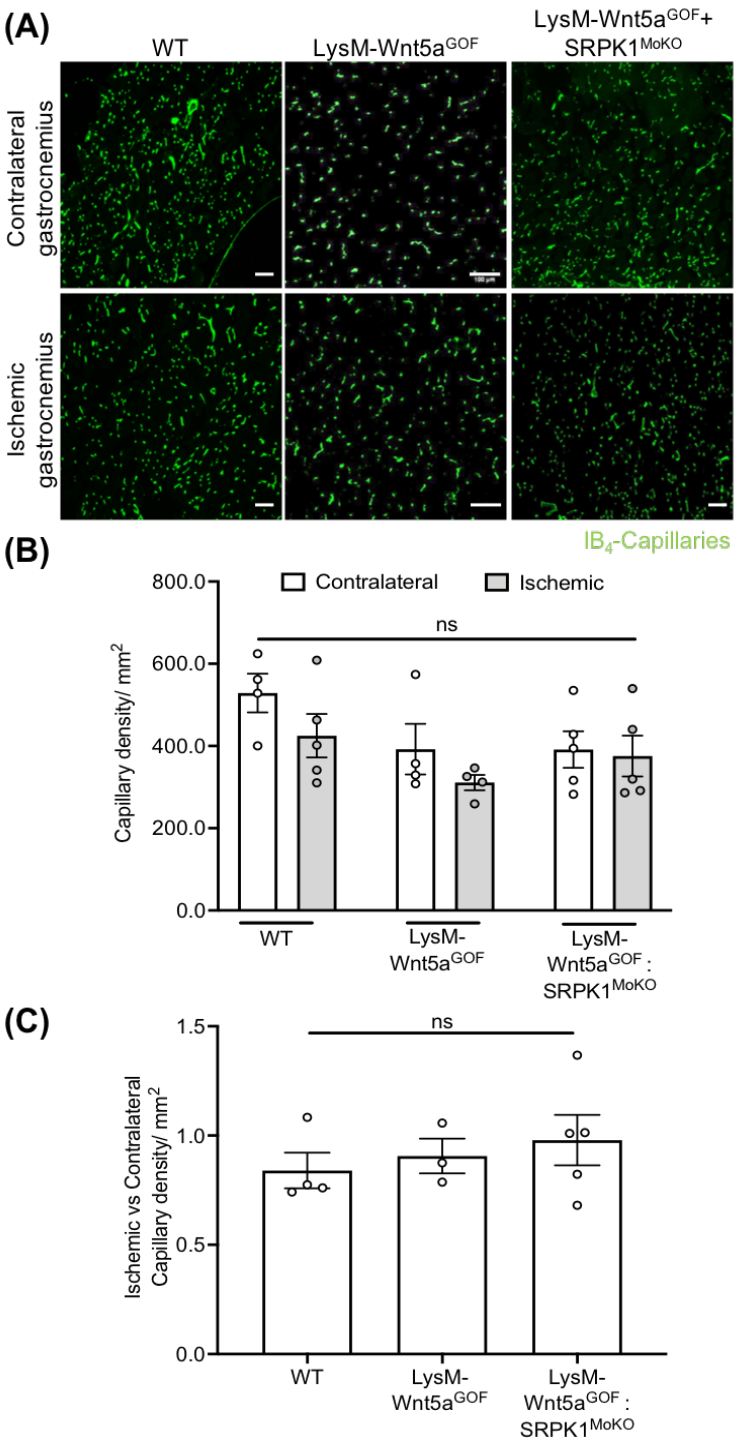


Figure 5.9. LysM-Wnt5a^{GOF}: SRPK1^{MoKO} mice have an unaltered capillary density on post-operative day 21. (A) *Representative immunofluorescent images of the contralateral (top) and ischemic (bottom) gastrocnemius muscle of WT, LysM-Wnt5a^{GOF} and LysM-Wnt5a^{GOF}:SRPK1^{MoKO} stained for capillaries with isolectin (IB$_4$). All images were taken at 10x magnification. Scale bars represent 100µm.* ***(B)(C)*** *Capillaries were counted in the contralateral and ischemic gastrocnemius* ***(B)*** *Averaged per mm^2* ***(C)*** *Further expressed as a ratio of the ischemic vs contralateral capillary density of each mouse group. All data was plotted as the mean ± SEM.* ***(B)*** *Data was analysed using a two-way ANOVA (Main effects: Genotype (mouse group): p=0.22; Gastrocnemius muscle (contralateral/ischemic): p=0.07; Interaction effect: p=0.50) with post-hoc*

Bonferroni test. WT ischemic and LysM-Wnt5a^{GOF}:SRPK1^{MoKO} (contralateral and ischemic gastrocnemius): N=5; all other groups: N=4. ***(C)*** *Data was analysed using a one-way ANOVA with post-hoc Bonferroni's test. WT: N=4; LysM-Wnt5a^{GOF}: N=3 and LysM-Wnt5a^{GOF}: SRPK1^{MoKO}: N=5. (ns=p>0.05).*

To determine the effects on arteriogenesis in the gastrocnemius post HLI day 21 mice, positive αSMA vessel staining was assessed by immunofluorescence and imaged by confocal microscopy as shown in Figure 5.10A. Upon quantification of the images, it was revealed that the ischemic hind limb of LysM-Wnt5a^{GOF} formed significantly fewer arterioles (4.32 ± 0.55/mm^2) compared with the LysM-Wnt5a^{GOF}: SRPK1^{MoKO} (13.15 ± 2.48/mm^2, p=0.005), which was comparable to the WT mice (12.75 ± 1.60/mm^2, p=0.008) (Figure 5.10B). The arteriolar density was also calculated as a ratio of the ischemic vs contralateral limb of each respective group. The LysM-Wnt5a^{GOF} only produced 0.50 ± 0.11/mm^2, which was significantly less than LysM-Wnt5a^{GOF}: SRPK1^{MoKO} (1.32 ± 0.14/mm^2, p=0.049) and WT (1.34 ± 0.34/mm^2, p=0.044) as shown in Figure 5.10C.

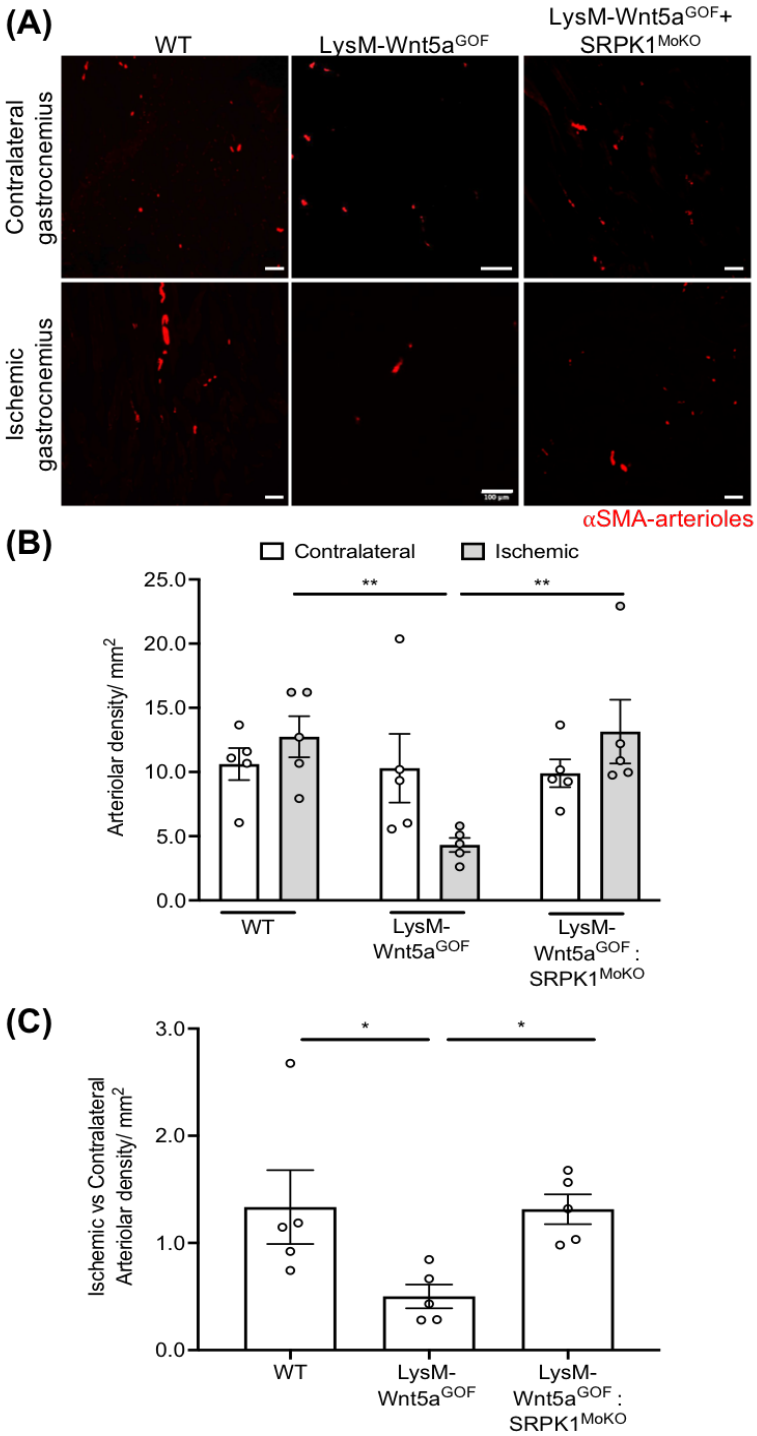


Figure 5.10. LysM-Wnt5a^{GOF} mice have impaired arteriogenesis, which is reversed in LysM-Wnt5a^{GOF}: SRPK1^{MoKO} mice on post-operative day 21. (A) *Representative immunofluorescent images of the contralateral (top) and ischemic (bottom) gastrocnemius muscle of WT, LysM-Wnt5a^{GOF} and LysM-Wnt5a^{GOF}: SRPK1^{MoKO} stained for arterioles with α-smooth muscle actin (αSMA). All images were taken at 10x magnification. Scale bars represent 100μm.* ***(B)(C)*** *Arterioles were counted in the contralateral and ischemic gastrocnemius muscle.* ***(B)*** *Averaged per mm^2.* ***(C)*** *Further expressed as a ratio of the ischemic vs contralateral arteriolar density. All data was plotted as the mean ± SEM.* ***(B)*** *Data was analysed using a two-way ANOVA with post-hoc Bonferroni test (Main effects: Genotype (mouse group): p=0.08; Gastrocnemius muscle*

(contralateral/ischemic): p=0.87; Interaction effect: p=0.02) with post-hoc Bonferroni test. ***(C)*** *Data was analysed using a one-way ANOVA with post-hoc Bonferroni's test. N=5/group. (**=p<0.01 and *=p<0.05).*

To determine the *Srpk1* expression of bone marrow resident monocytes of WT, SRPK1^{MoKO} and LysM-Wnt5a^{GOF}: SRPK1^{MoKO} mice on day 3 post-HLI, RNA was extracted and cDNA was synthesised from cells isolated from the bone marrow (following RBC lysis), but not selected for monocytes. The PCR was run at 62ºC using *Srpk1* primers previously optimised in Figure 5.3. A single *Srpk1* band was observed at 183bp in all samples, which remained unchanged (Figure 5.11A). Quantitative densitometry analysis of *Srpk1* bands relative to *Gapdh* (297bp) revealed no significant change overall (n=6, p>0.05, Figure 5.11B).

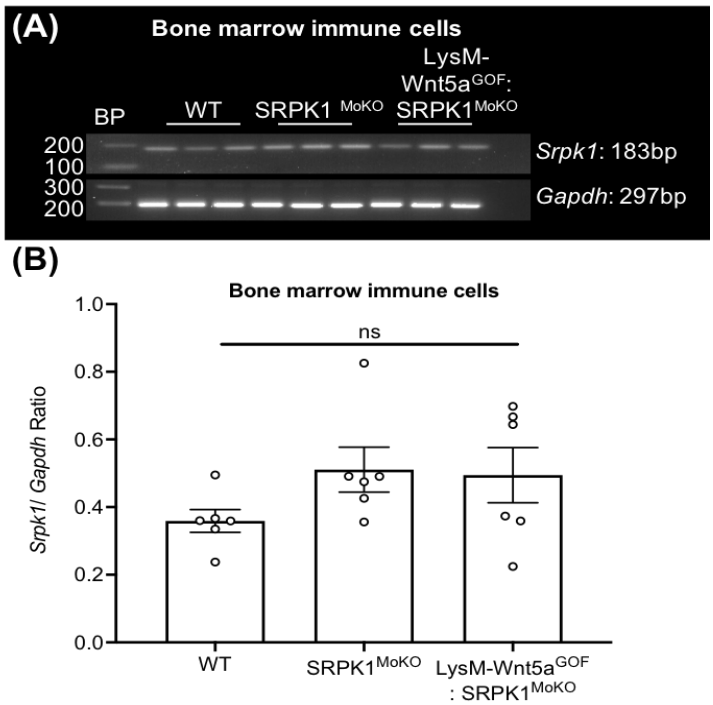


Figure 5.11. The Srpk1 expression in bone marrow immune cells on day 3 post-ischemia. *RNA was extracted from bone marrow immune cells and RT-PCR was performed to measure the Srpk1 expression using previously optimised primers in Figure 5.3 (spanning exon 1 and 3 of the Srpk1 gene).* ***(A)*** *The expression levels of Srpk1 (183bp) and Gapdh (297bp) in bone marrow immune cells of WT, SRPK1^{MoKO} and LysM-Wnt5a^{GOF}:SRPK1^{MoKO}.* ***(B)*** *Quantitative analysis was performing by normalising the band intensity of Srpk1 to Gapdh as a ratio. Error bars represent the mean ± SEM. Data was analysed using a one-way ANOVA with Bonferroni's post hoc test. N=6/group. (ns=p>0.05).*

5.3.7. SRPK1 knockout reverses the impaired blood flow due to obesity

A previous study has confirmed that mice fed on a HF/HS diet have Wnt5a overexpression in macrophages and myeloid cells in the ischemic gastrocnemius muscle in comparison to a normal chow diet, which resulted in impaired blood flow recovery and is dependent on VEGF-A_{165}b. This impairment was reversed with a VEGF-A_{165}b neutralising antibody (Kikuchi *et al*., 2014). Thus, it was hypothesised that HF/HS mice would have impaired blood flow recovery, which would be reversed with $SRPK1^{MoKO}$. At the age of 4-weeks, WT and $SRPK1^{MoKO}$ mice (as shown in the schematic in Figure 5.2) were maintained on a HF/HS diet for the duration of the study. After 8 weeks, all diet-induced obese mice were subjected to HLI of the left femoral artery. The representative speckle images are shown in Figure 5.12A. Quantitative analysis of the ischemic to contralateral blood flow recovery ratio showed that all mice recovered blood flow equally for the duration of the 28-day study (WT: 0.73 ± 0.05 vs $SRPK1^{MoKO}$: 0.75 ± 0.03; $p>0.05$ Figure 5.12B). Interestingly, the severity of ischemia induced in the $SRPK1^{MoKO}$ mice was greater than the WT mice (0.12 ± 0.01 vs 0.22 ± 0.03; $p=0.017$, Figure 5.12C). Thus, the data was further normalised to post-operative day 0 which confirmed that revascularisation was quicker in HF/HS $SRPK1^{MoKO}$ mice compared to WT mice on day 14 (5.21 ± 0.41 vs 3.23 ± 0.41, $p=0.0023$), 21 (5.40 ± 0.40 vs 3.55 ± 0.41, $p=0.0034$) and 28 (6.29 ± 0.51 vs 3.73 ± 0.46, $p<0.0001$) (Figure 5.12D). Dr. Mussarat Wahid conducted the HF/HS study, performed surgeries and speckle imaging for the duration of the 28-day study.

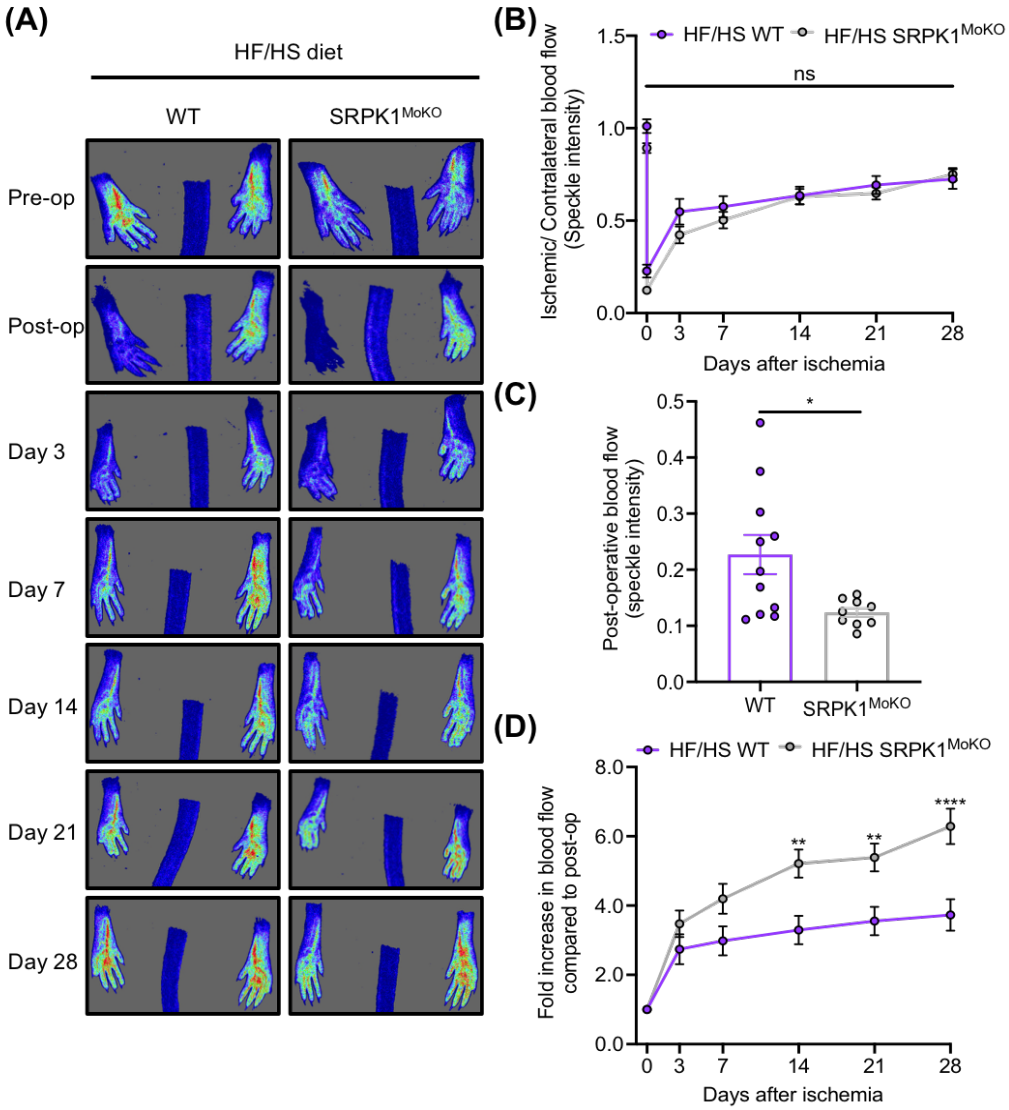


Figure 5.12. Blood flow recovery is reversed in SRPK1^{MoKO} mice fed on a HF/HS diet. ***(A)*** *WT and SRPK1^{MoKO} mice were fed on a HF/HS diet and underwent left femoral artery ligation. Blood flow to the paw was measured using the laser speckle imaging system as shown in the representative images.* ***(B)*** *Quantitative analysis of the ischemic vs non-ischemic speckle intensity was observed through to post-operative day 28.* ***(C)*** *The level of ischemia induced on post-operative day 0 of each respective mouse.* ***(D)*** *Data was further normalised to post-operative day 0 of each respective mouse.* ***(B)(D)*** *Results indicate the mean ± SEM. Data was analysed using a two-way ANOVA (****(B)*** *Main effects: Post-operative day: p<0.0001, Genotype (mouse group): p=0.056; Interaction effect: p=0.12.* ***(D)*** *Main effects: Post-operative day: p<0.0001, Genotype (mouse group): p=0.006; Interaction effect: p<0.0001)) with Bonferroni post hoc test.* ***(C)*** *Results are shown as the mean ± SEM. Data was analysed using an unpaired t-test. N= WT: 11 and SRPK1^{MoKO}: 9. (****= p<0.0001, **= p<0.01, *=p<0.05 and ns=p>0.05). Data courtesy of Dr. Mussarat Wahid.*

5.4. Discussion

5.4.1. Generating and validating the SRPK1 knockout mouse model

The development of the *Srpk1* conditional allele was initially produced in collaboration with Dr Lydia Teboul. The allele was produced by inserting a LacZ and neomycin-resistance cassette between exon 6 and 7 of the *Srpk1* gene. This region is flanked by FLP recombinase target sites (known as *FRT* sites, 34bp), which disrupts the function of the gene. The protein Flppase recombinase (known as FLP, derived from *Saccharomyces cerevisiae*) targets the *FRT* sites resulting in recombination and removal of this region. Thus, exon 7 of the *Srpk1* gene is flanked by two LoxP sites and is a functional wild type allele (Coleman *et al*., 2015). To confirm this, pups were genotyped using transgene specific probes (Figure 5.1). By further crossing homozygous $SRPK1^{LoxP}$ with LysM-Cre mice, and utilising the Cre/LoxP strategy, the LoxP sites flanking exon 7 in myeloid cells are targeted and removed (Figure 5.2). The gene expression of *Srpk1* in monocytes was assessed by using primers designed to span exon 1 and 3, which is upstream of the critical exon. To select for monocytes and macrophages from a mixed population of bone marrow immune cells and splenocytes, CD11b microbeads were used. The CD11b antigen surface marker is strongly expressed in monocytes/macrophages and is weakly expression on other cell types including granulocytes, NK and dendritic cells. The LysM-Cre promoter is also shown to target these cell types (Abram *et al*., 2014). However, Pelletier *et al* confirmed the specificity and purity of the CD11b microbeads for myeloid cells using FACS (Pelletier and Girard, 2006). As expected *Srpk1* mRNA encoded by this region was very weakly expressed in the positively and negatively selected CD11b cells in the bone marrow. Similarly, the *Srpk1* gene was very weakly expressed in the $CD11b^{+}$ population of splenocytes (Figure 5.3). The difference between the spleen and bone marrow is that circulating monocytes reside in the spleen and account for a large proportion of the total cell population (Swirski *et al*., 2009). Other cell types include B and T cells are not targeted by LysM-Cre and are likely to result in a *Srpk1* band in the $CD11b^{-}$ cell population in

the spleen (Swirski *et al*., 2009, Abram *et al*., 2014). In a recent study, LysM-Cre was used to target lung macrophages, which were successfully targeted. However, the reporter was also expressed in a quarter of the epithelial cells which were targeted along with dendritic cells (McCubbrey *et al*., 2017). Therefore, it would be important to assess other cell types to confirm the specificity of LysM-Cre in the SRPK1^{MoKO} mouse model.

The use of CD11b microbeads were to target CD11b^{+} monocytes in the bone marrow and account for over 90% of the total cell population that was selected. The few non-selected CD11b^{-} cells account for the faint *Srpk1* band detected (Oliva-Martin *et al*., 2015). The data confirms genomic deletion of the *Srpk1* gene between exon 1 and 3. A final reverse primer was designed to span exon 7/8 (Figure 5.4) and therefore target the knockout exon. This matched the trend from Figure 5.3. The reverse primer did not fully anneal or amplify in the SRPK1^{MoKO} as this is the site that is excised. Therefore, this could explain why a very faint *Srpk1* band was detected in Figure 5.4.

On NCBI and *Ensembl*, exon 7 is made up of 107 base pairs. It is likely that the deletion of this region yields an out of frame mutation resulting in degradation of the remaining transcript. Alternatively, it is possible that deletion of exon 7 results in exon skipping on exon 8 which results in a 273-nucleotide deletion and an in-frame protein product. Therefore, the removal of exon 7 disrupts the transcription of the remaining exons. Thus, a shift in the open reading frame results in a different amino acid sequence. This is likely to result in the remaining transcript being degraded by nonsense mediated decay (NMD) before translation is initiated (Hug *et al*., 2016, Nickless *et al*., 2017). NMD acts a quality control mechanism, thus preventing the formation of a short, truncated and non-functional SRPK1 protein (Hug *et al*., 2016). To confirm this assumption, it would be necessary to assess the SRPK1 expression at a protein level in monocytes. If SRPK1 is present, it would be important to assess the structure of the protein as it is likely to be altered.

Alternative methods to validate the SRPK1^{MoKO} using flow cytometry and immunofluorescence (by co-staining with LysM and SRPK1 antibodies) were considered. Flow cytometry would require intracellular staining and a fixation/permeabilisation step. However, there were only two compatible mouse SRPK1 antibodies for this method and were unconjugated. It would be necessary to conjugate the antibody and a significant amount of optimisation would be required to check compatibility on cell lines before using precious isolated mouse samples. *In vitro* monocytic cell lines (human and mouse) are not a suitable model as will be addressed in Chapter 6.

5.4.2. Monocytic SRPK1 knockout alone did not significantly impair blood flow recovery

Existing literature confirms that non-canonical Wnt5a signalling is mediated in mice fed on a high fat, high sucrose diet, but not a normal chow diet (Fuster *et al*., 2015, Kikuchi *et al*., 2014, Ouchi *et al*., 2010). In a HF/HS diet there is likely to be a decrease in the ratio of Sfrp5 to Wnt5a inducing activation and phosphorylation of JNK downstream (Ouchi *et al*., 2010). This enhances the infiltration of macrophages (Han *et al*., 2013) . However, ischemic injury in the left femoral artery in mice fed on a normal chow diet still results in tissue inflammation and induces the expression of inflammatory meditators such a liposaccharide, IL-1β, MCP-1 and TNFα. This has shown to increase the expression of Wnt5a in the ischemic myocardium and gastrocnemius muscle (Rauner *et al*., 2012, Nakamura *et al*., 2016). Surprisingly in the myocardium, this was shown to be colocalised to the macrophage cell population and resulted in downstream phosphorylation of JNK (Nakamura *et al*., 2016). It is therefore possible that this could elevate the expression of VEGF-A$_{165}$b as seen in the LysM-Wnt5a^{GOF} mice (Kikuchi *et al*., 2014). The data from previous chapters (Figure 4.1) suggests that SRPK1 is acting in alternative mechanism to epithelial (Gammons *et al*., 2013) and cancer cells (Gammons *et al*., 2014). Thus, it was hypothesised that blood flow recovery in SRPK1^{MoKO} would be quicker in comparison to WT mice. The data supports this hypothesis however it did not reach statistically significance when normalised to post-

operative day 0 (Figure 5.5). This does not eliminate the role of SRPK1 in monocytes. Kikuchi *et al* did not identify VEGF-A_{165}b in the ischemic gastrocnemius muscle of lean mice (Kikuchi *et al*., 2014). However, this could be explained by differences in the level of ischemia induced in the mouse models. This was an unblinded *in vivo* study where six mice were used per group in this study, which was not sufficient to achieve significance in this case. Calculations performed on G* power using an ANOVA indicate that an n of 9 would be necessary to achieve an acceptable power of 0.8 standard and a significance of p=0.05. Assessment of the Wnt5a and VEGF-A levels in the ischemic and non-ischemic muscle would have pinpointed the mechanism that could activated after ligation of the femoral artery.

5.4.3. SRPK1 knockout in Wnt5a hyperactive mouse models reverses the impaired blood flow recovery in LysM-Wnt5a^{GOF} mice

In line with the data in previous chapters (Figure 3.5 and Figure 4.1), it is clear that monocytic-Wnt5a overexpression is responsible for impaired blood flow recovery in ischemic mouse models (Figure 5.8). Consistent with Kikuchi and colleagues it is likely that this response is due to the production of anti-angiogenic VEGF-A_{165}b in a JNK-SC35 (SRSF2) dependent manner in monocytes (Kikuchi *et al*., 2014). However, the role of monocytic-SRPK1 has not been explored in this mechanism. For the first time, my data from Chapter 4 confirmed that inhibition of SRPK1 with SPHINX31 reverses the impaired the blood flow recovery in LysM-Wnt5a^{GOF} mice and induced arteriogenesis and angiogenesis. This led me to hypothesise that impaired blood flow recovery in LysM-Wnt5a^{GOF} mice is dependent on SRPK1 in the monocytes, thus blood flow recovery would be quicker in the absence of monocytic SRPK1. A complex breeding plan was appropriately devised to generate a novel double transgenic mouse model termed LysM-Wnt5a^{GOF}: SRPK1^{MoKO}. This was to ensure the pups generated could be maximised in use for the maintenance of breeding colonies and *in vivo* experiments. This was in-line with the NC3Rs guidelines, whilst ensuring that the scientific

aims of the *in vivo* study were achieved (schematic diagrams are shown in Figure 5.6 and 5.7). After all the mice had undergone the HLI procedure (Figure 5.7), for the first time I have found that SRPK1 knockout in the monocytes recovers the impaired blood flow recovery in LysM-Wnt5a^{GOF} mice (Figure 5.8). The supports the data in Chapter 4 and the hypothesis that SRPK1 regulates VEGF expression in monocytes differently from that in epithelial cells. It is clear that SRPK1 in the monocytes is acting in a different manner to other cell types. In epithelial cells, SRPK1 is shown to promote the phosphorylation of SRSF1, thereby increasing the ratio of pro-angiogenic VEGF-A$_{xxx}$a compared to VEGF-A$_{xxx}$b (Nowak *et al*., 2010). Therefore, absence of SRPK1 should revert this process, which was not seen here. It is unlikely that the absence of SRPK1 alters non-canonical Wnt5a signalling by pJNK. Previous studies have shown that SRPK1 knockout in fibroblasts (by Cre/LoxP) and carcinoma cells (using siRNA) either had no effect or increased the phosphorylation of JNK (Ren *et al*., 2015, Wang *et al*., 2014). It is likely that Wnt5a is phosphorylating JNK in the monocytes and SRPK1 is affecting the non-canonical Wnt5a signalling mechanism downstream. Although this was not assessed in the monocytes, it could have been confirmed by isolating the CD11b+ monocytes and assessing the JNK/pJNK expression at a protein level using western blotting.

The blood flow recovery seen with monocyte specific SRPK1 knockout in Figure 5.8 could be linked to SRSF2/SC35 phosphorylation which has shown to overexpress VEGF-A$_{165}$b in a Wnt5a dependent manner as previously mentioned (Kikuchi *et al*., 2014). SRPK1 has not been directly shown to have an interaction with SRSF2/ SC35, however SRSF2 is phosphorylated by SRPK2 (Wang *et al*., 1998).Conditional knockout of SRPK1 in mouse embryonic fibroblasts have shown a moderate increase in SRPK2, which has resulted in a decrease in phosphorylation of SR proteins (particularly SRSF2 and SRSF6) (Wang *et al*., 2014). Importantly, both these splicing factors are involved in promoting VEGF-A distal splice selection and VEGF-A$_{165}$b expression (Kikuchi *et al*., 2014, Nowak *et al*., 2008). In addition to this, SRPK2 has the ability to weakly phosphorylate

SRSF1 (Wang *et al*., 1998, Long *et al*., 2019). In retinal pigmented epithelial cells, SRSF1 phosphorylation resulted in proximal splice site selection, thus increasing the expression of the pro-angiogenic VEGF-A isoform (Nowak *et al*., 2008). Together, it is possible that knockout of SRPK1 in monocytes could overexpress the pro-angiogenic VEGF-A splice variant, resulting in a complete blood flow recovery and could explain the findings. This assumption could have been assessed by co-staining the contralateral and ischemic gastrocnemius muscle with VEGF-A isoform specific antibodies with a monocyte specific antibody using immunofluorescence.

Alternatively, the splicing of sFlt-1 negatively regulates angiogenesis in Wnt5a manner and is shown to act via SC35 (SRSF2) in macrophages of aged mice (Zhao *et al*., 2017). The mice in this study are in the young category compared to aged mice used by Zhao *et al* (Zhao *et al*., 2017). Perhaps this mechanism is occurring in LysM-Wnt5a^{GOF} and LysM-Wnt5a^{GOF}: SRPK1^{MoKO} mice. It is possible that the phosphorylation of SC35 (SRSF2) is reduced in the LysM-Wnt5a^{GOF}: SRPK1^{MoKO} mice. In turn, sFlt1 expression is reduced, which usually acts by binding to VEGF and sequestering it action, thereby negatively regulating angiogenesis (Kendall *et al*., 1996). Roberts *et al* has shown that VEGFR1/Flt1 can affect the signalling of VEGFR2/Flk1 on endothelial cells to rescue to blood vessel growth (Roberts *et al*., 2004). In line with the phosphorylation of VEGFR2/Flk1 was significantly upregulated in the ischemic limb of 8-week-old mice (Zhao *et al*., 2017). However, it is possible that VEGFR1 also plays an important role (Ganta *et al*., 2017). Thus, the VEGF-A secreted from monocytes could bind and phosphorylate VEGFR2/Flk1 on endothelial cells and promotes angiogenesis. This could potentially explain the reversal in blood flow recovery seen in the LysM-Wnt5a^{GOF}: SRPK1^{MoKO} mice.

Also, it is worth noting that the *in vivo* studies were not blinded. The genotyping results of each mouse was revealed prior to the study to ensure only mice of the correct genotype underwent the procedure and additional mice could be used in the complex breeding plan (Figure 5.6) as previously mentioned. The risk of bias could have been reduced if independent

researchers were involved in interpreting the genotyping results, performing laser speckle imaging on post-operative days and data analysis. Despite this, the ischemia level induced in the left femoral artery was similar in all mouse groups on post-operative day 0 and body temperature was monitored during the procedure and post-operative imaging days by placing the animal on a heat pad to standardise the conditions.

Overall, it is clear that monocytic SRPK1 is responsible for the impaired blood flow recovery in Wnt5a hyperactive mouse models. To build on this work further, it would be interesting to explore the involvement of SR proteins that could be involved and assess the SC35/SRSF2 levels. Importantly investigating the involvement of VEGF receptors that are phosphorylated on endothelial cells by immunofluorescence would better understand the mechanism that is resulting in improved blood flow recovery compared to LysM-Wnt5a^{GOF} mice.

5.4.4. Monocytic SRPK1 restores the arteriolar density, but not the capillary density of LysM-Wnt5a^{GOF} mice post-ischemia

On day 21 of the HLI study, all animals had complete blood flow recovery, which matched the contralateral paw of each respective mouse (Figure 5.8). There was a slight reduction in the capillary density of the ischemic gastrocnemius muscle of LysM-Wnt5a^{GOF} mice compared to LysM-Wnt5a^{GOF}:SRPK1^{MoKO}. However, this data set did not achieve statistical significance, perhaps due to a low n number (Figure 5.9). The LysM-Wnt5a^{GOF} mice formed fewer arterioles (Figure 5.10), which could be compensated by the formation of capillaries in a hypoxic environment. There are a greater number of capillaries compared to arterioles per mm^2 in the gastrocnemius muscle. Therefore, a small difference in capillary number is unlikely to be detectable. However, a small difference in the arteriole number would result in a more pronounced effect.

It was surprising that no differences were identified in the capillary density of LysM-Wnt5a^{GOF}: SRPK1^{MoKO} mice (Figure 5.9). Perhaps the existing capillaries were developing into arterioles and could explain why the LysM-Wnt5a: SRPK1^{MoKO} had improved arteriole formation compared to LysM-Wnt5a^{GOF}, which matched the WT mice (Figure 5.10). This supports the data in Chapter 4 (Figure 4.4). Following occlusion of the femoral artery, there is likely to be an increase in shear stress which triggers vascular remodelling and an arteriogenic response. Benest *et al* identified that the vasodilator eNOS (thus NO production), VEGF and Ang-1 have a crucial role in this process resulting in the recruitment of VSMCs (Benest *et al*., 2008, Stone *et al*., 2017). There is clear evidence throughout this chapter that confirms monocytic-SRPK1 is acting in a different manner to published literature. It is possible that there is an increase in the ratio of VEGF-A$_{xxx}$a/ VEGF-A$_{xxx}$b which initiates downstream signalling through VEGFR2 and phosphorylation of Akt (Harper and Bates, 2008, Zhao *et al*., 2017). Thus, increasing the phosphorylation of eNOS resulting in NO production. Perhaps, Ang-1 levels are also increased resulting in arteriole formation. However, there is a lack of evidence supporting the role of Ang-1 in the non-canonical Wnt5a pathway.

By the end of the 21 days, it is likely the functional arterioles in the gastrocnemius muscle of LysM-Wnt5a^{GOF}:SRPK1^{MoKO} mice have an increase in vascular reserve due to an increase in arterioles present resulting in complete blood flow recovery. Therefore, these animals display a normal response which matched the WT mice, whereas, the LysM-Wnt5a^{GOF} mice would have a larger lumen diameter due to vasodilatation resulting in a decrease in vascular reserve. This could explain why all mouse groups had complete blood flow recovery on day 21 (Figure 5.8). However, contradictory evidence in the literature shows that a combination of Sfrp5 and Wnt5a is necessary to restore the impaired actions of Wnt5a alone, inducing NO production by eNOS phosphorylation resulting in vasodilatation in rats (Cho *et al*., 2018). Similarly, in diabetic patients downstream pJNK negatively correlates with the flow mediated dilation

(Breton-Romero *et al*., 2016). In this experiment, the diameter of the lumen was not quantitatively assessed by immunofluorescence, as no visible differences were identified. However further experiments would be needed to assess the flow mediated vasodilation using ultrasound as shown by Schuler *et al* (Schuler *et al*., 2014). This would provide conclusive evidence of this assumption. In this set of experiments, a non-primary antibody slide was used to confirm non-specific binding of the streptavidin. This experiment lacked an isotype control for the αSMA antibody. This would confirm the specificity of the observed arteriole staining. However, there are no IgG2A-Cy3 conjugated antibodies available.

5.4.5. No difference in the *Srpk1* expression in bone marrow immune cells of day 3 post-ischemic mice

Haematopoietic stem cells in the bone marrow undergo a series of differentiation steps to become myeloid cells, and eventually develop into monocytes where they reside before being released into the bloodstream (Mosser and Edwards, 2008). They are known to account for the majority of cells in the bone marrow, but also consists of other immune cell types (Zhao *et al*., 2012). The data in Figure 5.3 and 5.4 confirmed *Srpk1* was weakly expressed in the selected $CD11b^{+}$ monocytes of non-ischemic $SRPK1^{MoKO}$ mice, thus I hypothesised that *Srpk1* would be absent or weakly expressed in bone marrow immune cells post-ischemia. However, no difference was seen amongst the three mouse groups (Figure 5.10). It is likely that LysM-Cre did target the floxed critical exon of the *Srpk1* gene of the monocytes (as shown in the schematic diagrams in Figure 5.2 and 5.7). However, ischemia is likely to result in mobilisation of the CD11b+ monocytes from the bone marrow leaving the other cell types present in the bone marrow including T cell ($CD4^{+}$ and $CD8^{+}$), dendritic cells, B cells, natural killer cells, neutrophils and eosinophils (Zhao *et al*., 2012, Oliva-Martin *et al*., 2015). LysM-Cre does not target B and T cells in the bone marrow (Abram *et al*., 2014). Therefore, the *Srpk1* band present is likely to account for the cells not targeted and explains why it was not possible to detect *Srpk1* knockout without monocyte isolation.

Previous optimisation of selected $CD11b^+$ on individual bone marrow immune cells followed by RNA extraction confirmed that the RNA quality (even after pooling two mice) was not sufficient for downstream experiments (data not shown). With six mice per group, an n of 3 would not have been achieved. Therefore, non-selected bone marrow immune cells (followed by lysis of red blood cells) were used for this experiment. Had I increased the n number and selected for $CD11b^+$, confirmation of *Srpk1* knockout might have been achieved in $SRPK1^{MoKO}$ and LysM-$Wnt5a^{GOF}$: $SRPK1^{MoKO}$ mice (similar to the data shown in Figure 5.3 and 5.4).

5.4.6. Impaired blood flow recovery in diet-induced obese WT is reversed with monocyte specific SRPK1 knockout

Research surrounding diet induced obese C57/BlJ mice (fed on a HF/HS diet) confirmed that Wnt5a is upregulated in the macrophages/myeloid cells (Kikuchi *et al*., 2014, Fuster *et al*., 2015) and adipose tissue (Fuster *et al*., 2015, Ouchi *et al*., 2010) when compared to lean mice (fed normal chow diet). Similarly, obese patients have high Wnt5a levels in the adipose tissue (Karki *et al*., 2017) and serum (Schulte *et al*., 2012). In fact, it was shown to positively correlate with an increase in BMI (Akoumianakis *et al*., 2019). The Wnt5a levels are shown to negatively correlate with Sfrp5, which usually acts by binding and sequestering the action of Wnt5a preventing downstream phosphorylation of JNK (Fuster *et al*., 2015, Ouchi *et al*., 2010, Kikuchi *et al*., 2014).Collectively with the data in Chapter 3 (Figure 3.5) and Chapter 4 (Figure 4.1), I hypothesised that diet-induced obese mice would have impaired blood flow recovery which is reversed with $SRPK1^{MoKO}$ (similar to Figure 5.8). The data in Figure 5.12 supports this hypothesis. Metabolic dysfunction is associated with mice fed on a HF/HS diet, as the downstream phosphorylation of JNK is upregulated (Ouchi *et al*., 2010, Fuster *et al*., 2015). If this is the case, then phosphorylation of the serine residue on the insulin receptor substrate (IRS-1) could result in insulin resistance (Ouchi *et al*., 2010). Similarly, the presence of JNK in macrophages has been shown to promote insulin resistance and impair insulin secretion in obese mice compared to JNK knockout (Han *et al*., 2013). In addition, activation of JNK results in an upregulation of pro-

inflammatory cytokines, which stimulates the activation and accumulation of macrophages in the adipose tissue (Ouchi *et al*., 2010, Fuster *et al*., 2015). Elevated Wnt5a levels positively correlate with anti-angiogenic VEGF-A_{165}b (Kikuchi *et al*., 2014, Karki *et al*., 2017), thus preventing downstream phosphorylation of VEGFR1 and VEGFR2 (Harper and Bates, 2008, Ngo *et al*., 2014, Ganta *et al*., 2017). This response subsequently reduces the phosphorylation of eNOS resulting in endothelial dysfunction and could explain the impaired blood flow recovery in obese WT mice shown in Figure 5.12 (Breton-Romero *et al*., 2016, Farb *et al*., 2016).

In fact, administration of a neutralising VEGF-A_{165}b antibody reverts this process as there is a decrease in 'free' VEGF-A_{165}b and sFLT1(Kikuchi *et al*., 2014, Karki *et al*., 2017, Ngo *et al*., 2014). Therefore, this promotes revascularisation as there is an increase in available VEGF-A_{xxx}a in the ischemic muscle, which would induce the phosphorylation of the VEGFR2 on endothelial cells (Zhao *et al*., 2017, Kikuchi *et al*., 2014). In addition, activation of VEGFR1 is shown to significant role in enhanced perfusion and angiogenesis of the ischemic muscle in the absence of VEGF-A_{165}b (Ganta *et al*., 2017).

Interestingly, diet-induced obese SRPK1^{MoKO} mice reverse the impaired blood flow recovery (Figure 5.12). Previous studies have shown that HF/HS diet decreases the level of insulin growth factor binding protein (IGFBP) compared to lean mice. However, insulin growth factor 1 (IGF-1) remained unchanged in the plasma and protein kinase C (PKC) is activated downstream (Rajwani *et al*., 2012, Huang *et al*., 2009). Stimulation of IGF-1 on cells is known to activate PKC resulting in proximal splice site selection, upregulating the expression VEGF-A_{165} (Nowak *et al*., 2010, Harper and Bates, 2008). This mechanism occurs in the presence of SRPK1, thus it is not likely to be the pathway resulting in revascularisation in the monocytes of this mouse model. In the absence of SRPK1, it is possible that SRPK2 is phosphorylating SRSF1 in the monocytes (Wang *et al*., 1998, Long *et al*., 2019), upregulating the pro-angiogenic VEGF-A isoform which is secreted in the bloodstream (Nowak *et al*., 2008). An

increase in body weight has shown to be inversely proportional to anti-angiogenic sFLT1 levels in the adipose tissue (Herse *et al*., 2011). In contrast, in RAW264.7 cells, Wnt5a stimulated an increase in sFLT-1 (Stefater *et al*., 2011) . Perhaps, obese mice have reduced sFLT1 and an increase 'free' circulating VEGF-A_{xxx}a. Thus, binding to VEGFR on endothelial cells would induce revascularisation and blood flow recovery.

In this study animals were maintained on a HF/HS diet for 12 weeks (from the age of 4 weeks), similar to Kikuchi *et al* (Kikuchi *et al*., 2014). In comparison to other studies, animals were maintained on a HF/HS diet from the age 8-10 weeks old for a duration of 12-24 weeks (Fuster *et al*., 2015, Ouchi *et al*., 2010). Older mice are shown to have a severe revascularisation and prolonged blood flow recovery compared to younger mice used in this study (Zhao *et al*., 2017). It would be interesting to assess the revascularisation of older mice. In addition to this, I would like to have assessed the Wnt5a and Sfrp5 levels in the serum and myeloid cells to confirm if a HF/HS diet induced Wnt5a expression in these animals. Overall, the data is in line with Figure 5.8 and confirms impaired revascularisation is dependent on SRPK1 in the monocytes.

5.5. Concluding remarks

Consistent with previous chapters of this thesis, monocytic Wnt5a resulted in impaired blood flow recovery. For the first time, I have generated and validated and SRPK1^{MoKO} mouse model. Obese SRPK1^{MoKO} mouse had faster blood flow recovery compared to WT mice. In addition to this, LysM-Wnt5a^{GOF}: SRPK1^{MoKO} reversed the impaired blood recovery in LysM-Wnt5a^{GOF} mice, which matched the WT mice. Thus, confirming that impaired revascularisation in ischemic mouse models are dependent on SRPK1 in the monocytes. Further work is required to understand the downstream mechanism that is occurring in monocytes and potentially resulting in splicing of VEGF-A isoforms.

Chapter 6

Monocytic cell lines are not a suitable *in vitro* model

6.1. Introduction

The non-canonical Wnt5a/Sfrp5 signalling pathway has been shown to contribute to impaired revascularisation due to a switch in VEGF-A splicing. In retinal myeloid cells, a mutation in the Wnt5a ligand was shown to increase the angiogenic branching in the deep retinal vasculature (Stefater *et al*., 2011). In rodent models of PAD infiltration of Wnt5a positive macrophages in the ischemic limb resulted in impaired blood flow recovery (Kikuchi *et al*., 2014). A similar response was shown in a myocardial reperfusion mouse model (Nakamura *et al*., 2016). In a clinical setting, monocytic- Wnt5a was shown to regulate the anti-angiogenic VEGF-A_{165}b levels, which positively correlated with disease severity in PAD patients (Kikuchi *et al*., 2014). Similarly, the angiogenic response in the adipose tissue of obese patients was impaired due to Wnt5a and VEGF-A_{165}b (Karki *et al*., 2017).

As shown throughout this thesis, monocytic-Wnt5a plays a significant role in impaired blood flow recovery and the associating impaired angiogenic response. In addition, I have demonstrated the importance of monocytic-SRPK1 in this mechanism. The majority of studies in this field focus on primary cells isolated from patients and animals or *in vivo* mouse models. In most cases, patient samples can be difficult to obtain and *in vivo* studies are expensive. At the present, only a single study has shown the signalling of VEGF-A_{165}b through a Wnt5a mediated mechanism in a cultured RAW264.7 cells (Kikuchi *et al*., 2014). However, this is representative of mouse models and not patient samples. At the earlier stages of this thesis, the ethics approval under which collection of monocytes from patients had been planned was removed and a new ethics approval was required. This meant that no primary monocytes from patients with PAD were available until the ethics approval was approved in March 2020, the week before all patient sample collection were suspended. Thus, I attempted to establish a reliable *in vitro* human monocytic cell line to assess the Wnt5a mechanism and VEGF-A alternative splicing. In this chapter, I aimed to establish an *in vitro* model of monocytes. Both human and mouse monocytic cell lines

would be exposed to a series of conditions (including hypoxia, hyperglycaemia and drug treatments) to mimic the *in vivo* conditions seen in the previous chapters and published literature. I went on to determine the impact, if any, on VEGF-A isoforms at a protein level. In addition to this, I also aimed to validate the use of *in vivo* models compared to *in vitro* cell lines.

6.2. Methodology

THP-1, U937 and RAW264.7 cell lines were cultured for a series of *in vitro* experiments. Cell viability of THP-1 and U937 cells were assessed. Further assays were performed to analyse the protein content of VEGF-A splice variants on an intracellular level (by western blot on lysed cells). Monocytic cell lines (THP-1, U937 and/or RAW264.7) were all serum starved overnight, then treated with Wnt5a or SPHINX31 for 24 hours. THP-1 and U937 cells were cultured in hyperglycaemic media for 24 hours. The glucose concentrations selected were 11mM, 20mM, 30mM and 40mM. THP-1 and U937 cells were also used in hypoxic experiments and were subjected to 1% oxygen by being placed in a sealed hypoxia chamber for 24 hours. This is a severe hypoxic condition associated with regions of an atherosclerotic plaque. In all cases, the protein expression was analysed by western blot and probed for pan-VEGF and VEGF-A_{165}b or JNK and phosphorylated JNK (pJNK) plus β-actin. All methods are described in detail in Chapter 2.

6.3. Results

6.3.1. Effect of serum starvation on cell growth and VEGF-A protein content

To assess the effect of serum starvation on cell growth, two human monocytic cell lines (THP-1 and U937) were subjected to an FBS dose escalation experiment. THP-1 and U937 cells were cultured in complete medium with 0, 0.5, 1, 2, 5 and 10% FBS for 24 hours, then viable cells were counted using trypan blue. Both cell lines showed minimal difference in cell growth when cultured with up to 5% FBS. There was a significant increase in the cell growth of U937 cells (7.06 ± 0.23x10^5 cells/ml) compared to THP-1 cells (5.23 ± 0.57x10^5 cells/ml, p=0.038) (Figure 6.1).

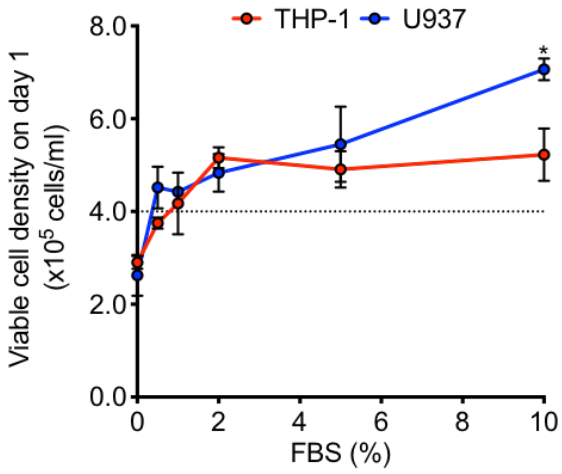


Figure 6.1. The effect of FBS concentration on cell density of THP-1 and U937 cells after 24 hours*. Cells were seeded at a cell density of 4x10^5 cells/ml (indicated by a dotted line) in 0, 0.5, 1, 2, 5 and 10% FBS in RPMI medium (supplemented with 2mM l-glutamine) for twenty-four hours. Then viable cells were counted using trypan blue to calculate the cell density with a haemocytometer. Data was analysed using a two-way ANOVA with post hoc Bonferroni test. Results are shown as the mean ± SEM. N=3/condition. (*=p<0.05).*

From the above assay, I wanted to assess the intracellular VEGF-A content. To test this, THP-1 and U937 protein lysates were probed for pan-VEGF (A20, 23kDa) and VEGF-A_{165}b (23kDa). Recombinant human proteins (rhVEGF-A_{165}a and rhVEGF-A_{165}b) were used as a positive control. In the THP-1 protein lysates, pan-VEGF and VEGF-A_{165}b monomer were detected at all FBS concentrations. Quantitative densitometry analysis relative to β-actin revealed no change across all groups ($p>0.05$, Figure 6.2A). Similarly, in U937 cells no significant difference was observed in the protein expression of pan-VEGF and VEGF-A_{165}b monomer with an increasing FBS concentrations in the cell culture medium ($p>0.05$, Figure 6.2B).

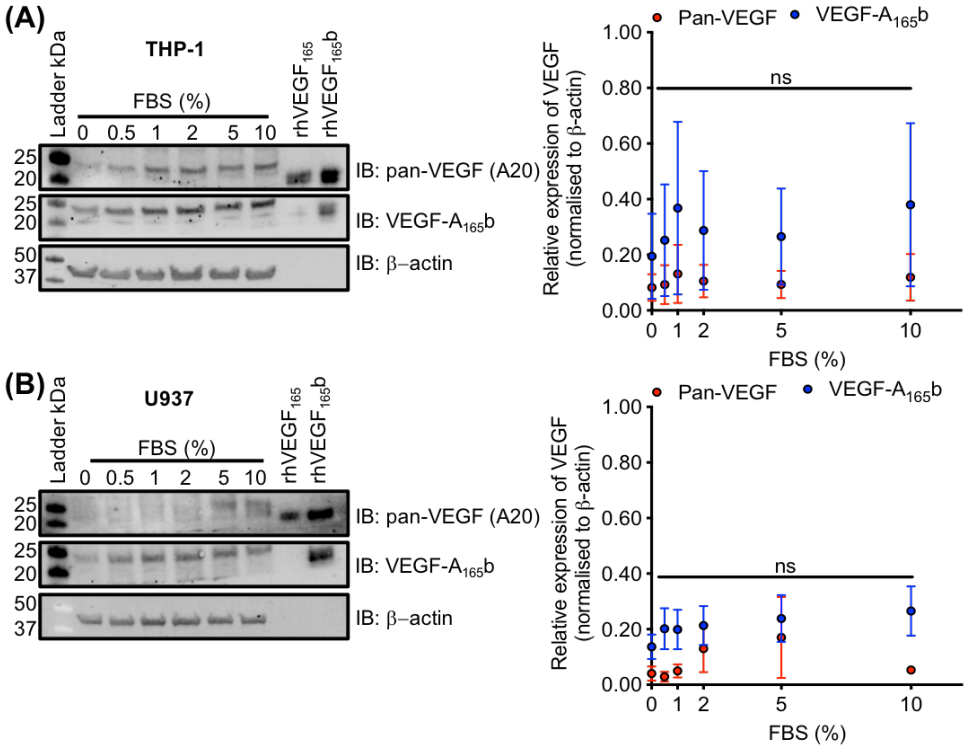


Figure 6.2. The expression of pan-VEGF and VEGF-A_{165}b in THP-1 and U937 cells in 0, 0.5, 1, 2, 5 and 10% FBS. *Cells were cultured in increasing concentrations of FBS in RPMI medium (supplemented with 2mM L-glutamine) for twenty-four hours. Western blots were performed on the protein cell lysates by probing for pan-VEGF (23kDa), VEGF-A_{165}b monomer (23kDa) and β–actin (42kDa). Quantitative densitometry analysis was performed on pan-VEGF or VEGF-A_{165}b relative to beta actin to quantify the change in expression in* ***(A)*** *THP-1* ***(B)*** *U937 cells. All results are shown as the mean ± SEM. Data was analysed using a two-way ANOVA with post hoc Bonferroni test. N=3/condition. (ns=p>0.05).*

6.3.2. Non-canonical Wnt5a signalling in monocytic cell lines

Based on previously published data, mouse models of ischemia and PAD patients have increased Wnt5a levels. As a result, pro-inflammatory monocytes are recruited to the site of inflammation and overexpress anti-angiogenic VEGF-A_{165}b (Kikuchi *et al*., 2014). Therefore, I hypothesised that treatment with Wnt5a would mediate the upregulation of VEGF-A_{165}b in monocytic cell lines. To assess this, human and mouse monocytes were treated with varying doses of Wnt5a for 24 hours. Protein lysates were assayed by western blotting for pan-VEGF and VEGF-A_{165}b expression. Membranes were stripped and re-probed for β-actin. Quantitative densitometry analysis showed no significant difference between the VEGF isoforms relative to β-actin in THP-1 ($p>0.05$, Figure 6.3A), U937 ($p>0.05$, Figure 6.3B) and RAW264.7 ($p>0.05$, Figure 6.3C) cells after an n of three for each treatment.

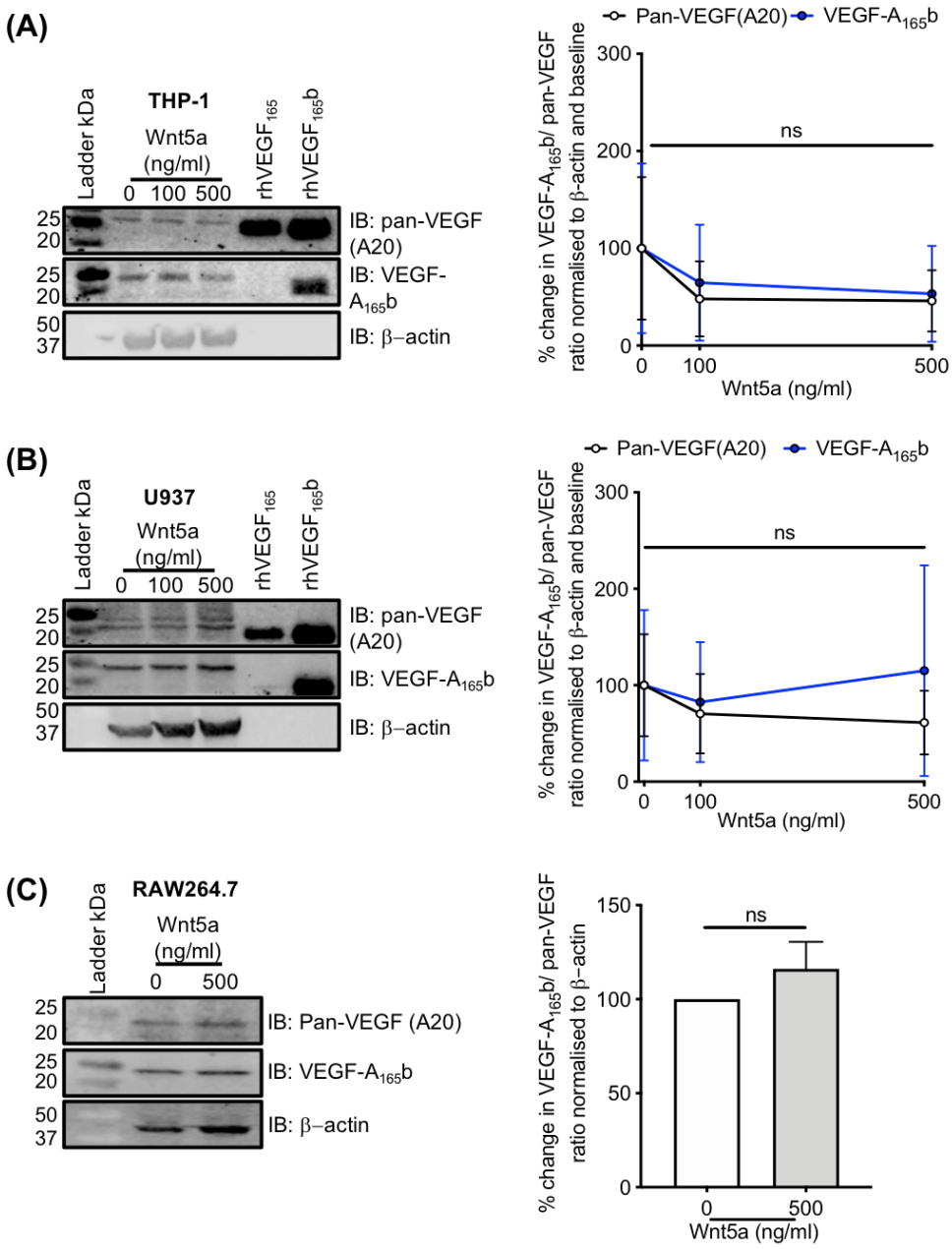


Figure 6.3. The expression of pan-VEGF and VEGF-A$_{165}$b in THP-1, U937 and RAW264.7 cells treated with Wnt5a. *Cells were serum starved for 24 hours in 0.5% FBS and then treated with 0, 100 and/or 500ng/ml Wnt5a for a further 24 hours. Extracted protein was ran on a western blot and probed pan-VEGF (23kDa), VEGF-A$_{165}$b (23kDa) and β-actin (42kDa). Quantitative densitometry analysis was performed on pan-VEGF or VEGF-A$_{165}$b relative to β-actin.* ***(A)*** *THP-1* ***(B)*** *U937 and* ***(C)*** *RAW264.7 cells.* ***(A)(B)*** *Results are shown as the mean ± SEM. Data was analysed using a two-way ANOVA with post hoc Bonferroni test.* ***(C)*** *Results are shown as the mean + SEM. Data was analysed using an unpaired t-test. N=3/group. (ns=p>0.05).*

The non-canonical Wnt5a signalling mechanism results in the downstream activation of JNK phosphorylation (abbreviated to pJNK). Similar to Kikuchi and colleagues, monocytic cell lines were untreated or pre-treated with 100 and/or 500ng/ml Wnt5a for 30 minutes (Kikuchi *et al*., 2014). Extracted protein lysates were subjected to JNK and pJNK western blotting. HEK-293 cells treated with or without UV light were used as controls for the antibodies (labelled 'positive control' on Figure 6.4). In THP-1 cells, JNK was present in untreated and treated cells, however pJNK (46 and 54kDa) was not present (Figure 6.4A). Whereas JNK was only present in the untreated cells, pJNK was not detected in all of the samples (Figure 6.4B). Interestingly, RAW264.7 cells cultured with 500ng/ml Wnt5a resulted in a significant increase of 10-fold in pJNK when the densitometry was quantitively analysed by normalising to the loading control (β-actin) and untreated sample (p=0.041, Figure 6.4C).

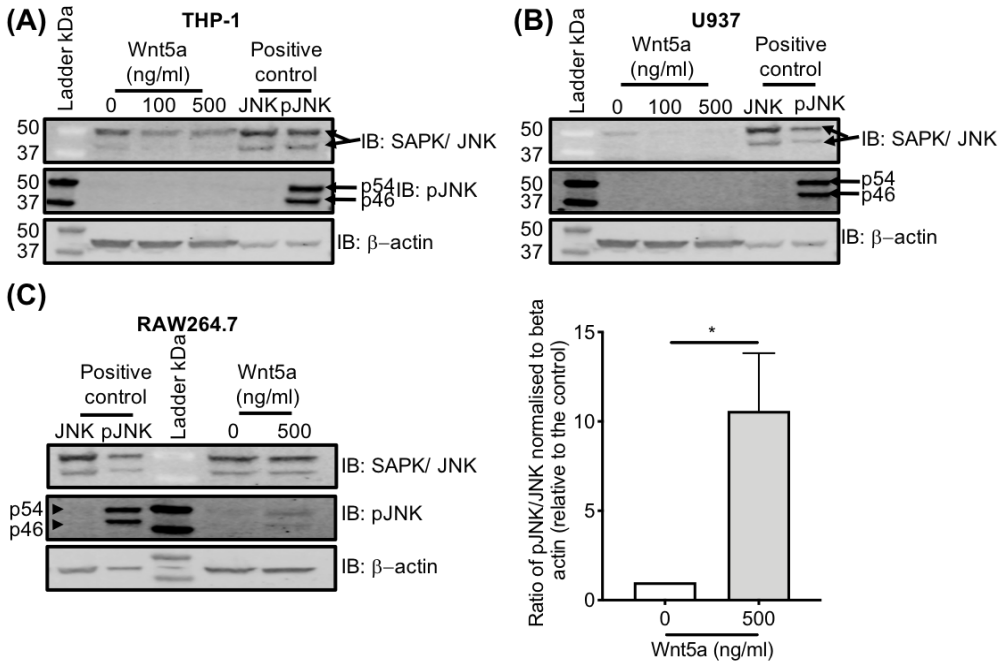


Figure 6.4. The expression of JNK and pJNK in THP-1 and U937 and RAW264.7 cells treated with Wnt5a. *Cells were serum starved for 24 hours in 0.5% FBS and then treated with 0, 100 and/or 500ng/ml Wnt5a for 30 minutes. Cells were lysed in NP40 lysis buffer, protein was extracted and a western blot was performed for SAPK/JNK, pJNK and β-actin in* ***(A)*** *THP-1* ***(B)*** *U937* ***(C)*** *RAW264.7. The pJNK/JNK was quantified relative to the untreated sample (0ng/ml Wnt5a) and β-actin. Positive controls were used for the antibodies and are HEK-293 cells treated with and without UV. All results are shown as the mean + SEM. Data was analysed by unpaired t- test. N=3/group. (*=p<0.05).*

6.3.3. Hypoxia

The transcriptional response to reduced oxygen (1% O_2) is mediated through highly conserved HIF transcription factors that promotes pro-angiogenic pathways which are mediated through VEGF-A. To explore this in monocytic cell lines, THP-1 cells were cultured in 0.5% or 10% FBS for twenty-four hours, and exposed to normoxic (Nx) or hypoxic (Hx) conditions. Proteins were extracted from treated cells and run on a western blot. Bands were observed at the expected size for pan-VEGF and VEGF-A_{165}b monomer at 23kDa (approximately) as shown in Figure 6.5A-B. The expression was quantified relative to the loading control, β-actin, showing little difference and was not statistically significant overall ($p>0.05$, Figure 6.5C-D).

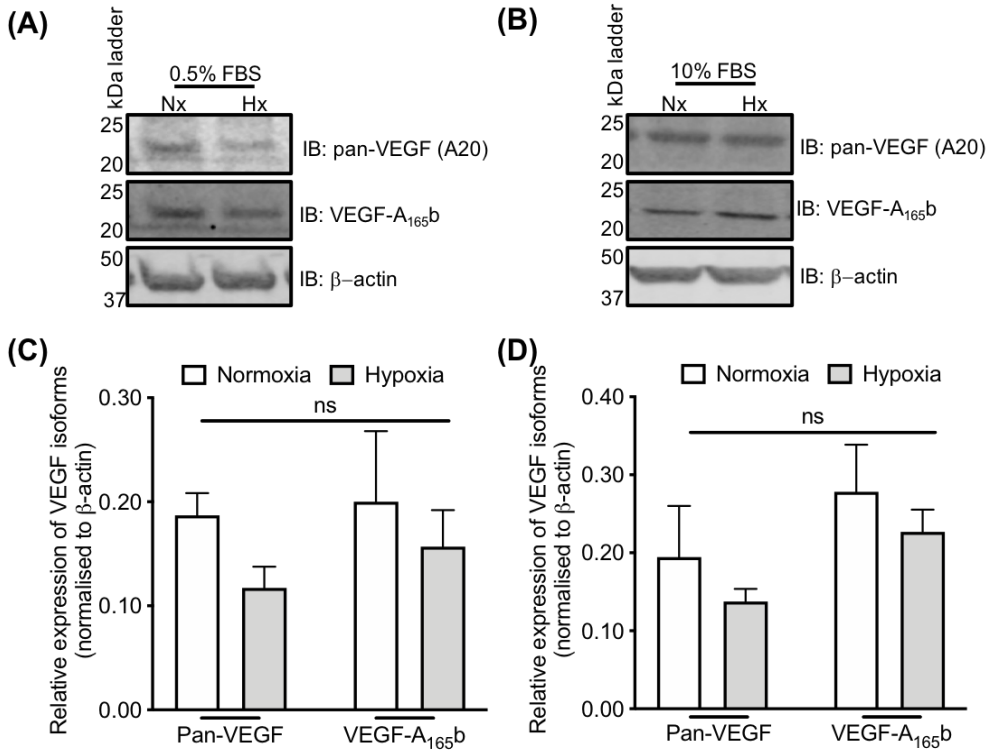


Figure 6.5. The protein expression of pan-VEGF and VEGF-A_{165}b treated with 0.5% or 10% FBS in Nx or Hx conditions in THP-1 cells. *Cells were cultured in two different concentrations of FBS (0.5% or 10%) for 24 hours and were exposed to Nx and Hx for a further 24 hours. Cells were lysed in NP40 lysis buffer to extract protein and a western blot was performed using pan-VEGF and VEGF-A_{165}b antibody on THP-1 cells treated with* ***(A)*** *0.5% FBS or* ***(B)*** *10%.* ***(C)(D)*** *Densitometry analysis was performed on pan-VEGF and VEGF-A_{165}b bands relative to β–actin. All results are shown as the mean + SEM. Data was analysed with two-way ANOVA with post-hoc Bonferroni's test. N=3/group. (ns= p>0.05).*

Similarly, U937 cells were also cultured in 0.5% or 10% FBS for a twenty-four hours before being exposed to Nx or Hx conditions. Following treatment, cells were lysed and run on a western blot. Bands were observed at 23kDa corresponding to pan-VEGF and VEGF-A_{165}b as expected (Figure 6.6A-B). Densitometry analysis was performed on the bands as a ratio relative to β-actin (42kDa), which showed no significant difference in the expression of both isoforms in Nx and Hx conditions ($p>0.05$, Figure 6.6C-D).

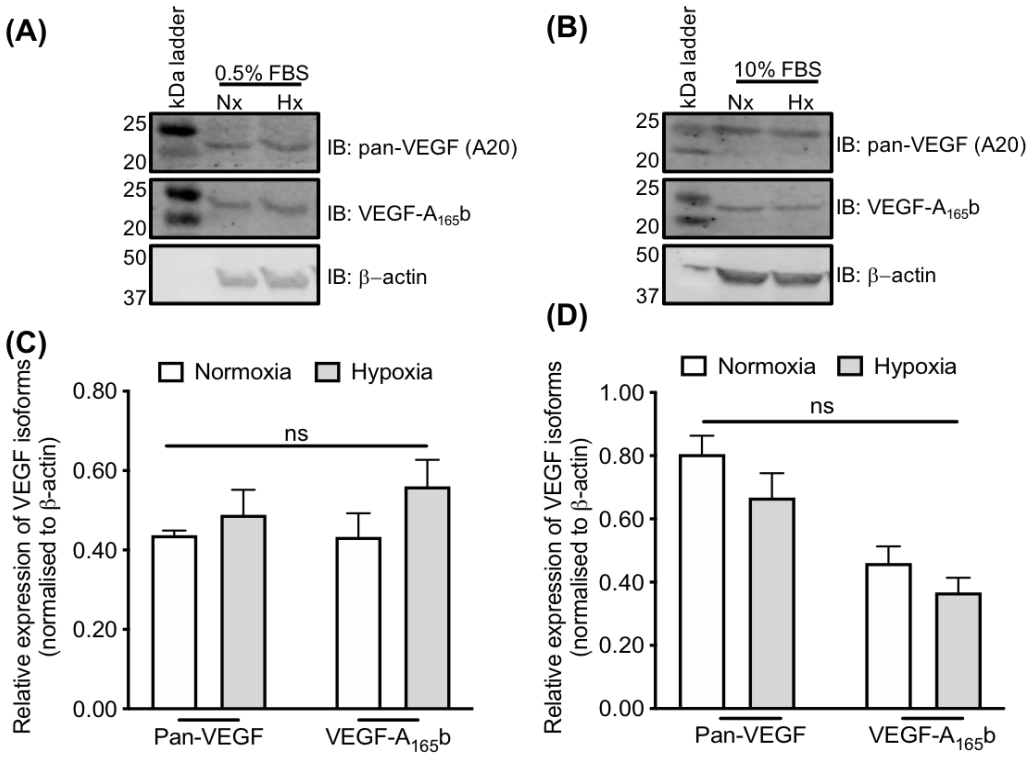


Figure 6.6. The protein expression of pan-VEGF and VEGF-A_{165}b treated with 0.5% or 10% FBS in Nx or Hx conditions in U937 cells. *Cells were cultured in two different concentrations of FBS (0.5% or 10%) for 24 hours and were exposed to Nx and Hx for a further 24 hours. Cells were lysed in NP40 lysis buffer, protein was extracted and a western blot was performed using pan-VEGF and VEGF-A_{165}b antibody on cells cultured in* ***(A)*** *0.5% FBS or* ***(B)*** *10% FBS.* ***(C) (D)*** *Densitometry analysis was performed pan-VEGF and VEGF-A_{165}b relative to β-actin. All results are shown as the mean + SEM. Data was analysed using a two-way ANOVA with post-hoc Bonferroni's test. N=3/group. (ns= $p>0.05$).*

6.3.4. Hyperglycaemia

Diabetes is characterised by hyperglycaemia which plays a critical role in vascular complications; in turn it modifies the splicing of VEGF-A isoforms in different cell and tissue types (Perrin *et al*., 2005, Oltean *et al*., 2015, Doronzo *et al*., 2012). To explore the hyperglycaemic effect in monocytic cell lines, THP-1 and U937 cells were cultured in the presence of normal (11mM) and high (20, 30 and 40mM) glucose for twenty-four hours, and protein extracts from lysed cells were ran on a western blot. Bands were observed for pan-VEGF (23kDa) and VEGF-A_{165}b (23kDa) showing little difference in the expression in THP-1 (Figure 6.7A) and U937 cells (Figure 6.7B). Membranes were stripped and re-probed for β-actin (loading control). Densitometry analysis of pan-VEGF and VEGF-A_{165}b relative to β-actin and normalised to the baseline glucose (11mM), which displayed no statistical difference in the expression at all concentrations of glucose in THP-1 ($p>0.05$, Figure 6.7C) and U937 ($p>0.05$, Figure 6.7D) cell lines.

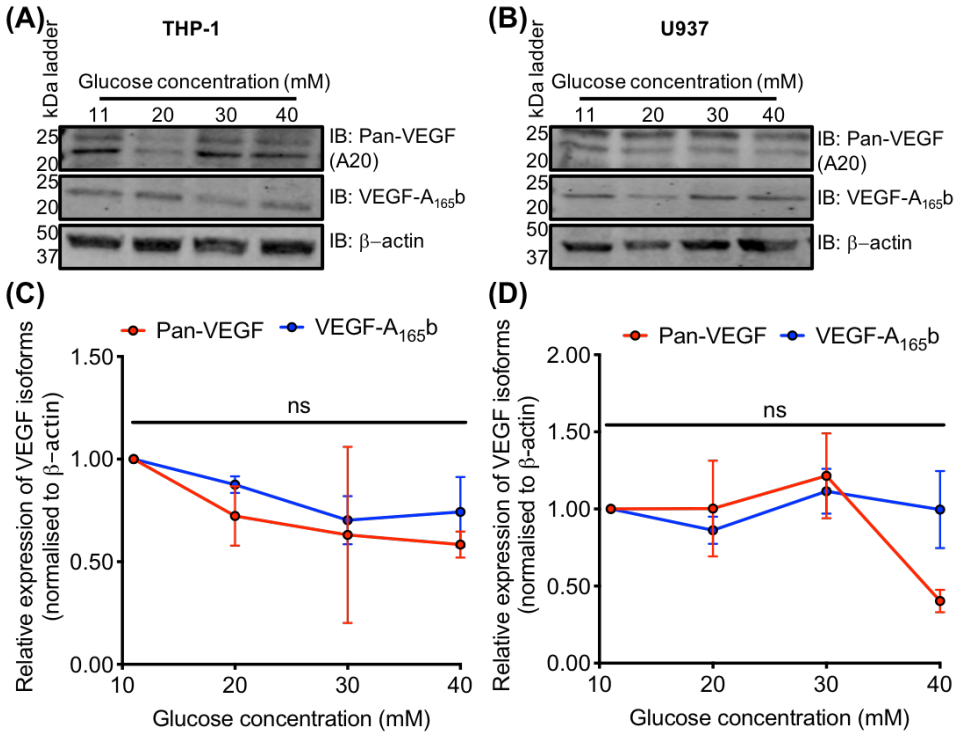


Figure 6.7. The expression of pan-VEGF and VEGF-A_{165}b in THP-1 and U937 cells cultured in 11, 20, 30 and 40mM glucose. *THP-1 and U937 cells treated with increasing concentrations of glucose for 24 hours. Protein was then extracted and western blotting was performed for pan-VEGF (23kDa), VEGF-A_{165}b (23kDa) and β-actin (42kDa) on* ***(A)*** *THP-1* ***(B)*** *U937 cells.* ***(C)*** ***(D)*** *Quantitative densitometry analysis was performed on pan-VEGF or VEGF-A_{165}b relative to β-*

actin and normalised to baseline glucose (11mM) ***(C)*** *THP-1* ***(D)*** *U937 cells. All results are shown as the mean ± SEM. Data was analysed using a two-way ANOVA with post-hoc Bonferroni test. N=3/group. (ns=p>0.05).*

6.3.5. SPHINX31

SRPK1 is known to control the splicing of VEGF-A splice variants in multiple cell types. The selective inhibition of SRPK1 with SPHINX31 in models of choroidal angiogenesis inhibits the SRPK1 activity and phosphorylation of SRSF1, resulting in a shift in the alternative splicing from a pro- to anti-angiogenic isoform (Batson *et al*., 2017). It is not known if SRPK1 regulates the VEGF-A splicing in monocytic cell lines, therefore I hypothesised that treatment with SPHINX31 would result in an upregulation of VEGF-A_{165}b in monocytic cell lines. Serum starved monocytic cell lines were treated with 10μM SPHINX31, then protein was extracted and run on western blots. In both cell lines, a band was observed at the expected size for pan-VEGF and VEGF-A_{165}b (dimer) at 46kDa in THP-1 (Figure 6.8A) and U937 (Figure 6.8B) cells. Blots were stripped and re-probed for β-actin. Densitometry analysis was performed on the bands corresponding to pan-VEGF or VEGF-A_{165}b relative to β-actin showing no statistical significance in THP-1 and U937 cells overall ($p>0.05$, Figure 6.8C-D).

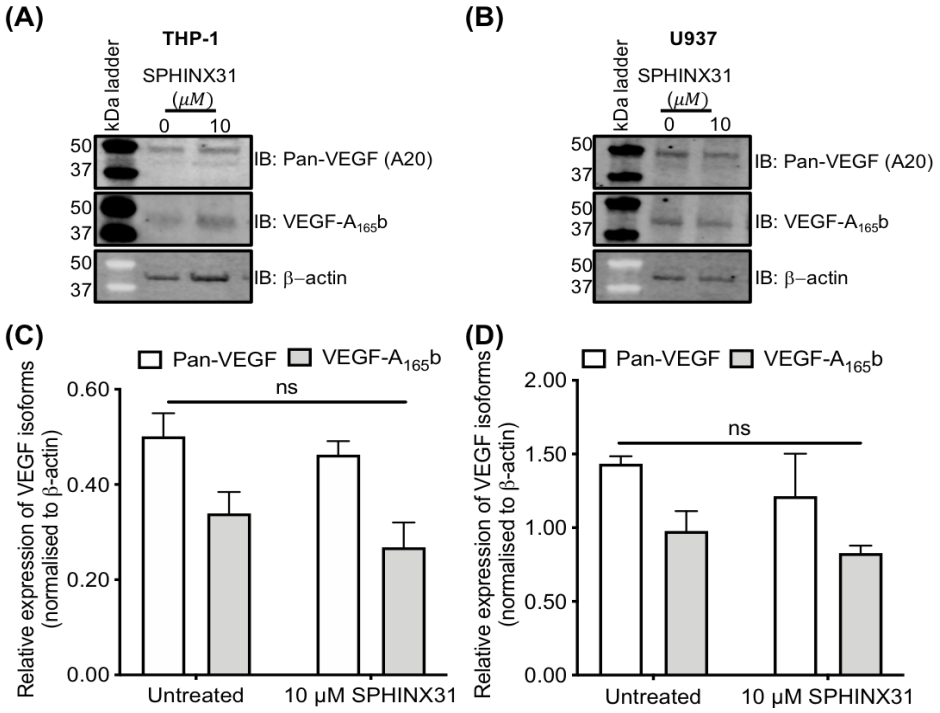


Figure 6.8. The expression of pan-VEGF and VEGF-A$_{165}$b in THP-1 and U937 cells treated with SPHINX31. *THP-1 and U937 cells were serum starved for 24 hours in 0.5% FBS and then treated with 0 and 10μM SPHINX31 for a further 24 hours. Proteins were extracted from treated cells and a western blot was performed, probing for pan-VEGF (46kDa), VEGF-A$_{165}$b (46kDa) and β-actin (42kDa) on **(A)** THP-1 and **(B)** U937 cells. Quantitative densitometry analysis was performed on pan-VEGF or VEGF-A$_{165}$b relative to β-actin on **(C)** THP-1 **(D)** U937. All results are shown as the mean + SEM. Data was analysed using a two-way ANOVA with post hoc Bonferroni test. N=3/group. (ns=p>0.05).*

6.4. Discussion

In this chapter, two human monocytic cell lines were used to establish an *in vitro* model. The THP-1 cells are derived from a 1-year-old with acute monocytic leukaemia whereas U937 cells are derived from a 39-year-old patient with histiocytic lymphoma. At the time of writing this study, only a single study has assessed the expression of VEGF-A isoform, VEGF-A_{165}a in human THP-1 cells using an SRPK1 inhibitor, which displayed a dose dependent decrease (Tzelepis *et al*., 2018). Therefore, cell lines were exposed to a series of conditions and treatments to assess the protein level of VEGF-A isoforms; however, no differences were identified. The simplistic and artificial environment is not comparable to an *in vivo* environment required for vascular remodelling. Multiple cell types (including smooth muscle cells, pericytes, fibroblasts, endothelial cells) and physiological forces (including shear stress, and oxygen tension) are necessary to induce the angiogenic process. Primary monocyte isolated from patients and rodents are exposed to this environment prior to isolation and molecular analysis in the laboratory. Therefore, it is more representative compared to cell lines.

6.4.1. No effect with serum starvation

Serum is a commonly used supplement in cell culture medium for the maintenance and growth of cell lines. It is likely to interfere with cell-based treatments. This can be eliminated by the removal of serum (known as serum starvation) from cell culture medium and is shown to induces cell cycle synchronisation. Serum starvation of primary cells (human dermal fibroblast and adipose stem cells) was shown to have little effect on cell viability and proliferation (Chen *et al*., 2012). This is likely to be cell specific. It is possible that monocytic cell lines will respond differently when serum is reduced or eliminated. Initial optimisation confirmed that the viability of THP-1 and U937 cells was not significantly altered in reduced serum or serum free medium for 24 hours (Figure 6.1). The effect of serum starvation on VEGF-A expression in monocytic cell lines has not been assessed previously. However, serum starvation in colon cancer cell lines has

induced the expression of VEGF as a result of Erk1/2 phosphorylation (Akagi *et al*., 1998, Jung *et al*., 1999). Thus, the expression of VEGF-A was assessed at a protein level in THP-1 and U937 cells and showed no difference (Figure 6.2). Given the minimal effects of serum starvation on both monocytic cell lines, I chose to use 0.5% FBS to culture THP-1 and U937 cells prior to treatment (with Wnt5a and SPHINX31) and cell culture conditions (hypoxia).

6.4.2. The non-canonical signalling pathway is not activated in monocytic cell lines

A previous study by Kikuchi identified that Wnt5a stimulation in a cultured mouse macrophage cell line (RAW264.7) promoted an increase in VEGF-A_{165}b at a protein level (Kikuchi *et al*., 2014). Similarly, I wanted to examine the Wnt5a mechanism in human monocytic cell lines (THP-1 and U937 cells) using RAW264.7 cells as a positive control. Thus, I hypothesised that treatment with Wnt5a would mediate an upregulation VEGF-A_{165}b. However, no differences were detected in VEGF-A isoforms at a protein level in all cell lines (Figure 6.3). The RAW264.7 cells were cultured and treated in a similar manner to Kikuchi and colleagues. However, the cells were not serum starved prior to treatment (Kikuchi *et al*., 2014). It is possible that the little differences seen in this experiment were due to Wnt5a alone, rather than a combination of Wnt5a and 10% serum as presented by Kikuchi and colleagues (Kikuchi *et al*., 2014). In addition, there are likely to be variations in the cell culture conditions, cell passage, growth medium constituents and batch of Wnt5a used. To confirm that Wnt5a signalling was activated in cultured cell lines, the phosphorylation of the stress kinase JNK was assessed. This mechanism has previously been identified in macrophages and adipocytes (Kikuchi *et al*., 2014, Ouchi *et al*., 2010). However, THP-1 cells did not result in JNK phosphorylation downstream (Figure 6.4A). This finding contradicts existing literature, as a previous study has confirmed that pre-treatment with Wnt5a induces JNK activation in THP-1 cells, which was blocked with a JNK inhibitor, SP000125 (Kim *et al*., 2012). Whereas, differentiated THP-1 cells treated with Wnt5a had

increased ROR2 receptor on the cell surface which dictates the downstream intracellular signalling cascade (Ackers *et al*., 2020). In comparison, JNK was not present nor phosphorylated in U937 cells (Figure 6.4B). Perhaps the co-receptor ROR2 is not expressed on the cell membrane preventing Wnt5a from sequestering the downstream pathway and could potentially explain why no differences were identified. However, there is no evidence in the literature to support assumption. As previously mentioned RAW264.7 cells were used as a positive control and were treated in a similar manner to both human monocytic cell lines and presented a 10-fold increase in pJNK (Figure 6.4C). This is in-line with the data presented in Kikuchi *et al*'s paper (Kikuchi *et al*., 2014). This confirms that there is unlikely to be an issue with the batch of recombinant Wnt5a used in this experiment. Perhaps I should have assessed and confirmed the expression of ROR2 and Fzd on the cell membrane of THP-1 and U937 cells prior to treatment with Wnt5a.

Previous human studies have shown that monocytes isolated from PAD patients overexpress Wnt5a compared to healthy patients and other cell types (Kikuchi *et al*., 2014). This is associated with an increase in circulating VEGF-A levels resulting in endothelial dysfunction and vascular impairment downstream (Kikuchi *et al*., 2014, Findley *et al*., 2008, Breton-Romero *et al*., 2016). In all these studies, patient were over the age of 50 and had other clinical disease such as diabetes and high cholesterol that have built up over an extended period of time. This is not comparable to human cell lines, perhaps due to an oversimplified cell culture environment. Riddy *et al* has shown primary $CD14^+$ monocytes are genotypically different compared to THP-1 and U937 cells, which express similar antigens on the cell surface confirming they are unable to replicate the profile of primary monocytes. Surprisingly, THP-1 cells responded to chemoattractant and induced migration, which was similar to freshly isolated $CD14^+$ monocytes. However, U937 cells failed to migrate under the same conditions (Riddy *et al*., 2018). In addition to this Aldo *et al* found that THP-1 cells were sensitive to cell density and culture conditions, which alters the expression of the monocytic $CD14^+$ marker (Aldo *et al*., 2013). It is clear that monocytic cell

lines are unable to mimic freshly isolated human monocytes. In this case, both cell lines were not considered a useful model. I would have also liked to assess the VEGF-A and Wnt5a levels in the monocytes of PAD patients. However, the ethics approval was withdrawn for reasons outside my control and new ethics approval took nearly a year to be approved and then the COVID-19 pandemic prevented me from undertaking these experiments.

6.4.3. No effect on VEGF-A splicing in hypoxic conditions

The occlusion of an artery results in tissue ischemia. As a result, the hypoxia stabilises hypoxia inducible factors (HIF) that modulate the molecular mechanism. This occurs when HIF1α and HIF2α heterodimerises with HIF1β to regulate the transcription VEGF-A. The importance of HIF1α has been shown in animal models of PAD indicating that absence of HIF1α correlated with impaired flow recovery, which was further impaired with age and reduced VEGF-A levels in the calf muscle (Bosch-Marce *et al*., 2007). Monocytes play a crucial role in this process by responding to the changes in oxygen supply and stromal derived factor-1. Thus, migrating towards the ischemic region (Hummitzsch *et al*., 2020). Findley *et al* confirmed that plasma VEGF-A levels positively correlated with the severity of PAD (Findley *et al*., 2008). Surprisingly, patients with PAD have elevated VEGF-A_{165}b levels in the plasma and PBMCs compared to healthy patients (Kikuchi *et al*., 2014). Similar effects were seen in selected $CD14^+$ patient samples when exposed to hypoxia (Ganta *et al*., 2017). Although the effect on monocytic cells has not been explored, Kim *et al* has shown that Wnt5a is activated in THP-1 cells exposed to 1% oxygen (Kim *et al*., 2012). Thus, it was hypothesised that hypoxia would alter the splicing of VEGF-A isoforms in monocytic cell lines. However, no differences were identified at a protein level (Figure 6.5 and 6.6). Previous studies have exposed primary monocytes to hypoxia for a shorter time frame which resulted in an upregulation of VEGF levels at an RNA (Schultz *et al*., 1999) and protein level (Ganta *et al*., 2017). Similarly, other studies have confirmed that THP-1 cells exposed to hypoxic conditions for 1 to 3 days had an increase in HIF1α at a protein level (Oda *et al*., 2006, Huang *et al*., 2016). It is possible

that there was an issue with the hypoxic chamber when the experiments were conducted. Therefore, the cells were not hypoxic and could explain why a difference in VEGF-A isoforms was not seen. Had I assessed the expression of a hypoxia marker such as HIF-1a and optimised the time frame to ensure the cell lines were hypoxic, I may have identified a difference.

6.4.4. No effect on VEGF-A splicing in hyperglycaemic conditions

Hyperglycaemia is the key factor which contributes to the development of diabetes and is a major risk factor of PAD. This has resulted in an increase in Wnt5a in obese patients (Fuster *et al*., 2015, Karki *et al*., 2017) and rodents (Ouchi *et al*., 2010, Kikuchi *et al*., 2014). Importantly Wnt5a has shown to positively correlate with the anti-angiogenic VEGF-A_{165}b levels in the adipose tissue (Karki *et al*., 2017) and PBMCS (Kikuchi *et al*., 2014). This has also been shown to negatively correlate with ABPI values, where a low ABPI indicates a higher severity of PAD (Kikuchi *et al*., 2014). Similarly, obese Zucker rats showed a decrease in VEGF-A_{164} in VSMCs compared to lean mice (Doronzo *et al*., 2012). However, the VEGF-A isoforms have not been assessed in monocytic cell lines exposed to hyperglycaemia in a cell culture environment. To determine the potential, THP-1 and U937 cells were exposed to moderate (11 and 20mM) to high (30mM and 40mM) glucose. However, both cell lines showed no differences in the expression of VEGF-A at a protein level (Figure 6.7). The cells were only exposed to hyperglycaemia for 24 hours, which is unlikely to mimic an *in vivo* environment. Perhaps, the cells were not hyperglycaemic in this short time frame. Previous studies have exposed THP-1 cells to hyperglycaemic conditions for 48 or 72 hours (Nandy *et al*., 2011, Shanmugam *et al*., 2003). Had I optimised the time frame of the experiment, I may have identified a change. Additionally, the monocytic cell lines were only exposed to a series of hyperglycaemic glucose concentrations and were not exposed to a normoglycemic control (such as 5mM glucose), which would reflect a non-diabetic patient in Figure 6.7. Previous *in vitro*

hyperglycaemia experiments have exposed THP-1 cells to both normal and high glucose when comparing monocyte adhesion, migration and the associating inflammatory response (Nandy *et al*., 2011, Dasu *et al*., 2007). Perhaps, this could explain why no differences were identified in the expression of VEGF-A isoforms at a protein level. Potentially a combination of hypoxia, hyperglycaemia and Wnt5a treatment would be more representative of an *in vivo* environment compared to an independent treatment of hyperglycaemia.

6.4.5. SPHINX31 did not alter the VEGF-A splicing in monocytic cell lines

SRPK1 mediates the phosphorylation of SRSF1 to regulate the expression of VEGF-A isoforms (Nowak *et al*., 2010). SPHINX31 inhibits the activity of SRPK1 and switches the splicing of VEGF-A isoforms from VEGF-A_{165}a to VEGF-A_{165}b in retinal pigmented epithelial cells (Batson *et al*., 2017). Thus, it was hypothesised that SPHINX31 would switch the splicing of VEGF-A isoforms in monocytic cell lines. However, there was no difference in the expression levels of pan-VEGF and VEGF-A_{165}b in THP-1 and U937 cells (Figure 6.8). Both human monocytic cell lines were treated with 10μM SPHINX31. Tzelepis *et al* showed a concentration dependent reduction of $VEGF_{165}$a at a protein level with SPHINX31 treatment on THP-1 cells. Thus, there was a clear reduction in VEGF-A_{165}a with 10μM SPHINX31 (Tzelepis *et al*., 2018). In comparison, Batson *et al* used a maximum of 5μM SPHINX31 which showed a dose dependent increase in VEGF-A_{165}b in retinal pigmented epithelial cells (Batson *et al*., 2017). SPHINX31 has shown to be toxic to retinal pigmented epithelial cells (<5% at 100μM SPHINX31) (Batson *et al*., 2017). Similarly, SPHINX13 is toxic in THP-1 cells, however this has not been assessed in U937 cells. SPHINX31 was diluted in DMSO at a final concentration of <1% which is unlikely to affect the cell number and viability of THP-1 and U937 cells (Hajighasemi and Tajic, 2017).

Phosphorylation of SRSF1 by SRPK1 is shown to restore cell proliferation and survival. However, the viability of THP-1 cells was maintained for 24 hours with 3μM SPHINX31 and showed a significant reduction in pSRSF1 (Tzelepis *et al*., 2018). However, kinase assays have demonstrated 96% inhibition of SRPK1 with 1μM SPHINX31 (Batson *et al*., 2017). It is possible that SRPK1 inhibition with 10μM SPHINX31 negatively affected the cells resulting in cell death or reduced the proliferation of the cells. However, no visible differences were identified after treatment. Had I performed a dose response, I may have seen a difference in VEGF-A isoforms at a protein level at a lower concentration.

6.5. Concluding remarks

Collateralisation and vascular remodelling is an *in vivo* process, which requires a complex environment and multiple cell types to understand the process. The data in this chapter confirms that an over simplified and isolated cell culture environment is not representative of an *in vivo* system and is not feasible to understand the molecular mechanism underlying the vascular remodelling in PAD. Thus, confirming the use of mouse models in the previous chapters. This further validates that *in vitro* monocytic cell lines are not suitable to understand the physiological process in great depth. Further work to assess the expression of VEGF-A isoform levels in primary monocytes isolated from mouse and patient samples would necessary to allow direct comparisons to be made to the cell lines used in this chapter.

Chapter 7

Future work and translational relevance

The risk of PAD increases in patients with obesity and/or type 2 diabetes and rodent models of ischemia due to increased Wnt5a levels. This results in an impairment in the formation of collateral vessels, which is necessary to circumvent the blood supply to the associating tissue. Consequently, patients experience symptoms including intermittent claudication, gangrene and necrosis of the lower limbs. The present thesis highlights the potential use of the SRPK1 inhibitors to prevent the progression of PAD, which could be used as a therapeutic treatment. In addition, the role of monocytic SRPK1 specifically in the monocytes was explored in a Wnt5a dependent manner and in diet-induced obese mice, which presented novel findings.

7.1. COVID-19 Impact Statement

The abrupt closure of the university in response to the COVID-19 pandemic in March to August 2020 resulted in termination of all experiments. During this period, I volunteered to work at the National Lighthouse laboratories in Cheshire which was considered my placement by the MRC IMPACT doctoral training programme. Due to the disruptions that occurred during the lockdown, an additional 16-week funded extension was granted by the University of Nottingham. However, this was not enough to compensate for some of the time lost in the lab. Since returning to the lab, there has been increased difficulty with receiving ordered goods and no access to the wards to retrieve patient blood samples since approval of our ethics in March 2020. There have been two further national lockdown where the lab has remained open. However, the ability to access patient samples has been extremely challenging during this period. Here I will briefly discuss the data, future research directions, clinical implications and address the limitations of the hind limb ischemia mouse model.

7.2. The Wnt5a-SRPK1 mechanism of action in ischemic mouse models

The current literature surrounding monocytic Wnt5a in ischemic mouse models and PAD patients is limited. However, it is known that overexpression of Wnt5a results in impaired blood flow recovery and angiogenesis in animal models of PAD. Similar findings were presented in diet-induced obese mice fed on a HF/HS diet. In addition, a global knockout of Sfrp5 in a transgenic mouse model resulted in an upregulation of Wnt5a in the macrophages of the ischemic limb and subsequently impaired the revascularisation after HLI was induced (Kikuchi *et al*., 2014). In obese mice, Wnt5a was upregulated in the adipose tissue resulting in metabolic dysfunction and an accumulation of macrophages (Ouchi *et al*., 2010, Fuster *et al*., 2015). Thus, mediating the downstream activation of the stress kinase JNK which is phosphorylated (Kikuchi *et al*., 2014). Similar findings were presented endothelial cells isolated from diabetic patients (Breton-Romero *et al*., 2016) and adipose tissue of obese patients (Farb *et al*., 2016). The present work in this thesis (Chapter 3, 4 and 5) highlights that Wnt5a hyperactivity in the monocytes modulates the impaired blood flow recovery in models of PAD and is consistent with the literature. This is in line with other cell types such as retinal myeloid cells, where angiogenesis was induced by a mutation in Wnt5a (Stefater *et al*., 2011). This indicates the importance of monocytic Wnt5a in revascularisation. It is likely that the circulating levels of Sfrp5 are reduced to induce the non-canonical Wnt5a signalling pathway (Ouchi *et al*., 2010).

At the time of writing this thesis, only a single study has identified the role of anti-angiogenic VEGF-A_{165}b in a Wnt5a-dependent manner in PAD. It has been shown to occur via pJNK-SC35 in RAW264.7 cells *in vitro* (Kikuchi *et al*., 2014). However, in retinopathy the activation of JNK induces VEGF-A expression at a protein level, which results in an angiogenic response (Guma *et al*., 2009). There is no evidence in the literature to directly supporting the role of SRPK1 in this signalling mechanism or in ischemic mouse models. Existing literature confirms that SRPK1 phosphorylates

SRSF1 favouring proximal splice site selection resulting in an upregulation of pro-angiogenic VEGF-A_{xxx}a (Nowak *et al*., 2010) (summarised in Figure 7.1A). Thus, SRPK1 inhibition with SPHINX31 is an effective anti-angiogenic strategy in models of ocular neovascularisation (Batson *et al*., 2017). Similar findings were presented with other SRPK1 inhibitors in melanoma growth, podocytes, prostate cancer and aged related macular degeneration (Amin *et al*., 2011, Gammons *et al*., 2014, Hatcher *et al*., 2018, Mavrou *et al*., 2015). More recent literature presented by Li *et al* identified that an alternative novel SRPK1 inhibitor, which binds to the docking groove. This novel peptide presented similar findings to other SRPK1 inhibitors previously mentioned and reduced the revascularisation in chick embryos (Li *et al*., 2021). Collectively, this led to the hypothesis that administration of SPHINX31 would impair the blood flow recovery in LysM-Wnt5a^{GOF} mice after HLI. However, this was proven to be wrong in Chapter 4, which indicated that SPHINX31 improves (and does not further impair) the blood flow recovery and matched the WT mice. It indicated that this mechanism could be dependent on SRPK1. I believe this is the first time this finding has been presented in this cell type or disease model, suggesting that SRPK1 acts in a different manner in monocytes. Of the published SRPK1 inhibitors, SPHINX31 has the highest specificity. However, it has the potential to bind to SRPK2 and CLK-1 at a reduced affinity compared to SRPK1 (Batson *et al*., 2017). Both these kinases promote distal splice site selection to induce the expression of VEGF-A_{xxx}b through independent pathways. SRPK2 phosphorylates SRSF2 and CLK-1 phosphorylates SRSF6 to modulate the expression of the anti-angiogenic VEGF isoform (Wang *et al*., 1998, Kikuchi *et al*., 2014, Nowak *et al*., 2008). Therefore, partial inhibition would increase the ratio of pro-angiogenic VEGF-A_{xxx}a. This mechanism could potentially explain how SPHINX31 is acting *in vivo* to induce revascularisation in Chapter 4. Based on this, I would hypothesise that phosphorylation of SRSF2 and SRSF6 would be downregulated in the monocytes (summarised in Figure 7.1B).

However, the use of the novel transgenic mouse models in Chapter 5 (SRPK1^{MoKO} and LysM-Wnt5a^{GOF}: SRPK1^{MoKO}) validates the data from

Chapter 4 confirming that it is monocytic SRPK1 that is primarily responsible for the impaired blood flow recovery in the LysM-Wnt5a^{GOF} mice, not an off-target effect on SRPK2 or CLKs. In Chapter 5, I only assessed the expression of *Srpk1* to confirm knockout in monocytes and post-ischemia in leukocytes. SRPK1 knockout in embryonic fibroblasts was shown to have no effect on SRPK2 (Wang *et al*., 2014). Therefore, it is possible that the phosphorylation of SRSFs are affected directly or indirectly due to the presence of other SRPKs. In fact, Wang *et al* specifically showed that the phosphorylation level of SRSFs decreased from WT and conditional SRPK1 knockouts in embryonic fibroblasts (from heterozygotes to homozygotes) (Wang *et al*., 2014). Although it is likely to be cell specific. This was not assessed in the monocytes post-ischemia; however, it could be acting in a similar manner to SPHINX31 as previously mentioned above (summarised in Figure 7.1B). SRPK2 has been shown to efficiently phosphorylate multiple SR proteins (Wang *et al*., 1998). Therefore, I believe that the expression of SR could have been explored at a protein level using immunoprecipitation on monocytes with a phosphor-SR antibody and probing using a specific SRSF specific antibody. Alternatively, this could be tested using western blotting and probing with SRSF specific antibodies. This would identify the SR proteins that were phosphorylated and pinpoint the mechanism that is occurring in this thesis. Given the novel findings it would be necessary to perform RNA sequencing on isolated monocytes post-ischemia. This would provide the basis for identifying multiple other novel targets that are involved in this signalling pathway. Perhaps, if SRPK2 is shown to be a critical component in this mechanism, it would be necessary to generate a monocyte cell-specific double SRPK1 and SRPK2 knockout mouse model and assess the blood flow recovery after induction of ischemia. I would hypothesise that these mice would have an impaired blood flow recovery compared to the WT mice and would match the LysM-Wnt5a^{GOF} mice as shown in the throughout this thesis.

A previous study by Mavrou *et al* found that knockout of SRPK1 decreased the prostate tumour growth in a manner which was dependent on VEGF splice variants. Similar effects were seen with SRPK1 inhibitors (Mavrou *et*

al., 2015). In this thesis, the involvement of VEGF-A isoforms was explored in the gastrocnemius muscle on post-operative day 3, however no detectable differences were seen across all samples (Chapter 3 and Chapter 4). The use of a pan-VEGF antibody for western blotting did not detect any bands, whereas the commercially available ELISA kit detected extremely low levels. It is important to note that these were developed to detect human VEGF and may have a lower affinity for mouse VEGF. The differences in the two techniques suggests there was an issue in the samples, reagents or the assays. It is clear that detection levels were not sufficient under the given conditions. Previous studies have detected VEGF-A in mouse samples (Kikuchi *et al*., 2014, Hazarika *et al*., 2007). Other studies have shown that a neutralising VEGF-A_{165}b antibody in ischemic mouse models increases the rate of blood flow recovery confirming that VEGF-A_{165}b is acting in anti-angiogenic manner (Kikuchi *et al*., 2014, Ganta *et al*., 2017). Therefore, I am cautious to draw any conclusions based on this data alone. I believe that the involvement of VEGF-A splice variants cannot be completely eliminated given the effects seen on the capillary and arteriolar densities in Chapter 3, 4 and 5. In this thesis, VEGFR1 and 2 receptors were not assessed. However, these receptors are a key component in dictating the downstream response of VEGF-A isoforms (Harper and Bates, 2008). I would hypothesise that VEGFR2 is upregulated in LysM-Wnt5a^{GOF} mice treated SPHINX31 treatment and LysM-Wnt5a^{GOF}: SRPK1^{MoKO} compared to LysM-Wnt5a^{GOF} mice. This could be assessed by immunofluorescence staining on the gastrocnemius muscle post-ischemia and co-staining with VEGFR2 and VEGF-A_{165}b.

In addition, the levels of *sFlt1* and *Flt1* were assessed in gastrocnemius muscle in Chapter 4, but there was a lack of effect. Previous studies have assessed sFLT1 levels, but at a protein level. In fact, these studies examined the cell culture medium, plasma or in the myeloid cells (Zhao *et al*., 2017, Karki *et al*., 2017, Stefater *et al*., 2011). As previously shown by Karki *et al*, Wnt5a levels positively correlated with VEGF-A_{165}b. This reduced capillary sprout formation and increase sFLT1 levels, which is

known to negatively regulate angiogenesis in adipose fat (Karki *et al*., 2017). Although pro-angiogenic VEGF-A_{164} levels were calculated in this study, I am cautious to draw direct conclusions from this data alone due to the extremely low levels detected. Perhaps, VEGF-A does have a role but it was not detected throughout this thesis. Zhao *et al* identified a Wnt5a/SC35-sFLT1 mechanism which resulted in impaired revascularisation in older mice (Zhao *et al*., 2017). The mice used throughout this thesis were not in the 'older' category, nor were they in the 'younger' category. Perhaps, I should have assessed the sFLT1 levels in other tissues at an RNA and protein level before eliminating the potential involvement and drawing any firm conclusions. Therefore, I propose sFLT1 levels could be downregulated and this reduces its antagonist effect on pro-angiogenic VEGF-A_{xxx}a in SPHINX31 treated and $SRPK1^{MoKO}$ mice resulting in improved revascularisation and angiogenesis (Figure 7.1B).

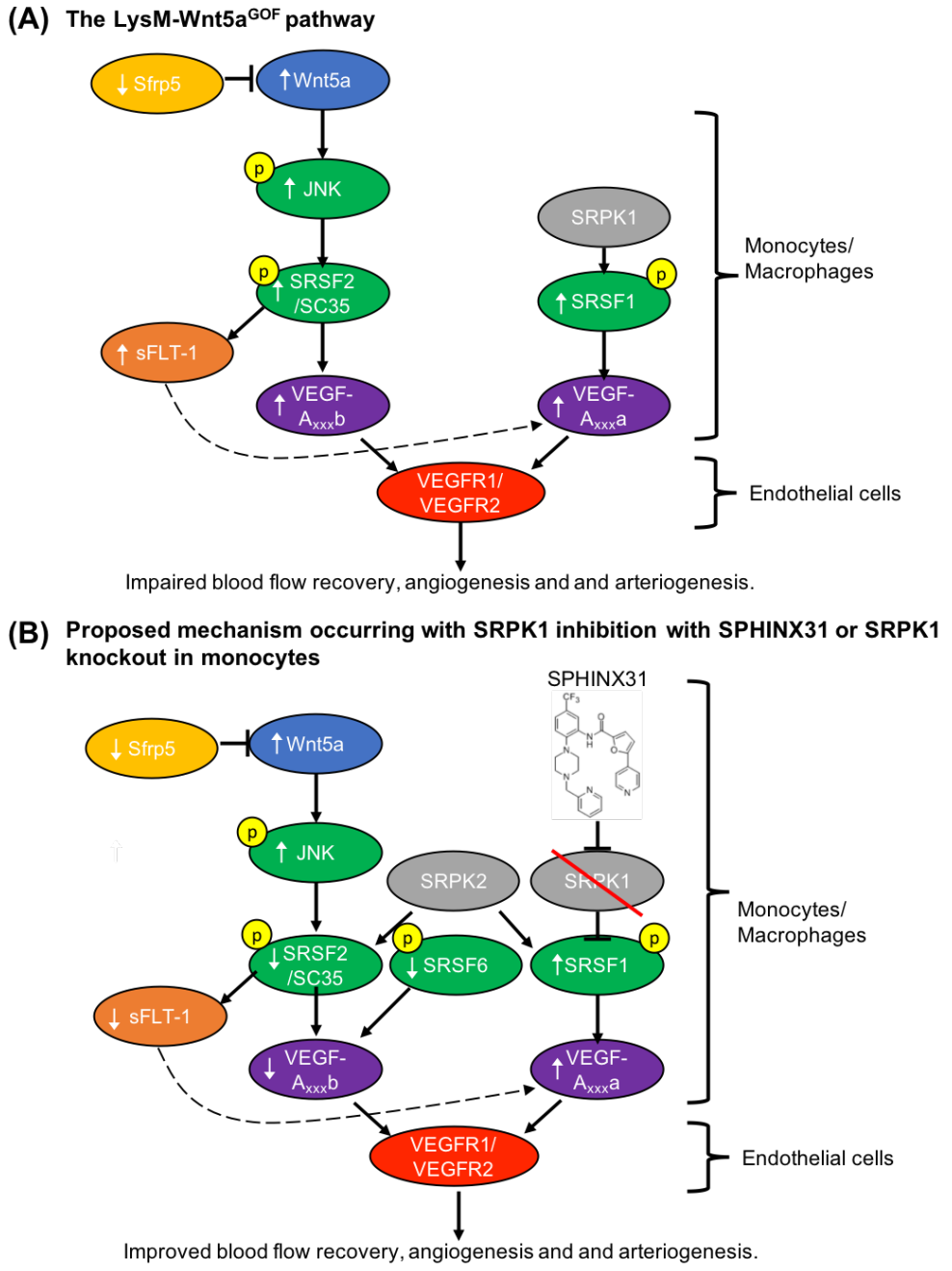


Figure 7.1. Schematic of the proposed mechanism that could be occurring in the LysM-Wnt5a^{GOF} mice and with SRPK1 inhibition or SRPK1 knockout in the monocytes. ***(A)*** *Upregulation of monocytic Wnt5a in LysM-Wnt5a^{GOF} mice decreases the ratio of Sfrp5. Wnt5a increases the phosphorylation of JNK resulting in downstream phosphorylation of SC35/SRSF2. This stimulates the expression of sFLT1 and VEGF-A$_{xxx}$b. sFLT1 acts to sequester the action of VEGF-A$_{xxx}$a produced by SRPK1-pSRSF1 reducing the binding to VEGFR1/2 on endothelial cells. Therefore, more VEGF-A$_{xxx}$b is available to bind to VEGFR1 and 2. A reduction in downstream phosphorylation of VEGF receptors results in impaired blood flow recovery, arteriogenesis and angiogenesis.* ***(B)*** *With SRPK1 inhibition or knockout (either in LysM-Wnt5a^{GOF} or diet-induced obese mice), SRPK1-pSRSF1 activity is reduced. It is possible SRPK2 induces the phosphorylation of SRSF1 resulting in an increase in the expression of VEGF-A$_{xxx}$a. However, SRPK2 could decrease the phosphorylation of SC35/SRSF2. This could potentially alter the expression of sFLT1 and VEGF-A$_{xxx}$b. Perhaps, SRSF6 could also reduce the*

expression of VEGF-A_{xxx}b in an independent pathway. Reduced sFLT1 means there is more VEGF-A_{xxx}a available to bind to VEGFR receptors inducing the downstream phosphorylation. This results in an increase in blood flow recovery, angiogenesis and arteriogenesis. Black dotted arrow= the sequestering action of sFLT1 when bound to VEGF-A_{xxx}a. Red diagonal line= SRPK1 knockout.

7.3. The HLI mouse model vs PAD: limitations

The murine hind limb ischemia procedure is a model of PAD commonly used to assess revascularisation, angiogenesis and arteriogenesis. This method was used in this thesis to induce ischemia by ligating the femoral artery followed by electrocoagulation in the different transgenic mouse models in Chapter 3, 4 and 5. There are other variations of the surgical procedure in the literature, which include single electrocoagulation or ligation of the femoral artery, single electrocoagulation of the iliac artery and double electrocoagulation of the both arteries (Aref *et al*., 2019). The differences in the acute ischemia procedure in the hind limb alter the severity of ischemia and rate of blood flow recovery. This does not mimic the progressive build-up of an atherosclerotic plaque over a long period of time resulting in a gradual occlusion in PAD and CLI patients (Aref *et al*., 2019). An alternative method using ameroid constrictors has been shown to mimic the chronic process resulting in more severe ischemia. However, this method is associated with technical challenges and requires optimisation (Au - Padgett *et al*., 2016, Aref *et al*., 2019). Krishna *et al* developed a 2 -stage ischemia model which occurred by progressive narrowing over 14 days using ameroid constrictors, which resulted in severe ischemia, reduced functional performance and activity compared to acute HLI (Krishna *et al*., 2020). Secondly, all of the *in-vivo* HLI studies in this thesis were performed on young (10-12-week-old) mice, which have been shown to have a quicker rate of blood flow recovery compared to aged mice (18-month-old) (Westvik *et al*., 2009). This is unlikely to translate to patients with PAD which are over the age of 50 (with metabolic diseases such as diabetes). Perhaps, additional studies should have been performed on older transgenic mice to allow direct comparisons to be made.

7.4. Clinical perspective: the bigger picture

The work throughout this thesis has identified that monocytic-SRPK1 is responsible for impaired revascularisation in ischemic mouse models (Chapter 5). The use of SPHINX31 showed therapeutic potential of SRPK1 inhibitors *in vivo* (Chapter 4). I believe that it can be translated to a clinical setting in the future. However, there are a couple of points to address.

Firstly, it is important to consider the screening techniques that are used to diagnose and identify patients with PAD. Currently, the main method to identify patients with PAD is by assessing the ankle brachial pressure index (ABPI), which is ratio of the systolic blood pressure in the ankle compared to the arm. An ABPI ratio of <0.9 suggests the presence of PAD due to reduced blood flow to the lower limbs. However, 90% of ABPI measurements are undertaken when patients experience physical symptoms (such as intermittent claudication) and/or visual changes in the lower limb such as discolouration, ulcers and wounds (Davies *et al*., 2014). Therefore, the ABPI levels are not always assessed in PAD patients that are asymptomatic, which explains why this group is often under diagnosed. To overcome this, a combination of factors are taken into account to diagnose PAD patients early to maximise the efficiency of treatment and to prevent progression to CLI. This includes risk factors, age and physical examination (such as the 6-minute walk test) (McDermott *et al*., 2008). Consistently, throughout this thesis, I show that Wnt5a is a crucial component in impaired revascularisation in ischemic mouse models. Although, this has not been confirmed in patients throughout this thesis, existing literature has shown that Wnt5a levels are upregulated in patients with PAD, specifically in the monocytes (Kikuchi *et al*., 2014). This has also been shown in the adipose tissue and endothelial cells of diabetic and obese patients, which are risk factors of PAD (Bretón-Romero *et al*., 2016, Ouchi *et al*., 2010). In contrast, the plasma levels of Sfrp5 are reduced in both groups of patients (Hu *et al*., 2013). Similar effects were seen in the serum of CAD patients (even with heart failure) (Tong *et al*., 2020). This leads me to speculate that Wnt5a or Sfrp5 could be a diagnostic biomarker

for PAD as well as other ischemic vascular diseases. It could be assessed by isolating the monocytes and plasma (or serum) from blood samples of healthy and PAD patients (with and without diabetes) and measuring the Sfrp5 or Wnt5a expression. Direct comparisons could be made with the ABPI levels to confirm if there is a correlation, similar to the data presented by Kikuchi and colleagues (Kikuchi *et al*., 2014). Alternatively, the intracellular expression of SRPK1 in monocytes could be assessed as it appears to be novel regulator of impaired revascularisation as shown in this thesis. In fact, there is no literature in support or against the role of SRPK1 in PAD patients or other ischemic diseases. I would hypothesise that a high SRPK1 expression would correlate with a low ABPI in PAD patients showing a negative correlation. This could be another biomarker.

Secondly, it is necessary to consider the type of drug that would be used to specifically target monocytes in clinics. As previously mentioned in the discussion of Chapter 4, administration of SPHINX31 via an intraperitoneal route means that it could have been acting on multiple cell types which poses specific risks. Tzelepis *et al* has shown that inhibition of SRPK1 resulted in cell cycle arrest, reduced proliferation and induced apoptosis in leukemic cell lines (Tzelepis *et al*., 2018). Similarly, silencing of SRPK1 inhibited cell proliferation in oesophageal cell carcinoma cells (Ren *et al*., 2015). Even in pancreatic carcinoma cells, silencing of SRPK1 induced apoptosis even in the absence of a chemotherapy drug (Hayes *et al*., 2006). Conditional knockout of SRPK1 in mouse embryonic fibroblasts reduced cell growth (Wang *et al*., 2014). This indicates that SRPK1 inhibitors need to be designed to circulate throughout the body, but only targeting and inhibiting the SRPK1 activity in monocytes to prevent adverse effects occurring by targeting other cell types in patients. Perhaps, this could be achieved using an antibody-drug conjugate, which is commonly used in oncology to target specific cell types, whilst having little/no effect on other cells. It consists of a monoclonal antibody, a small molecular weight drug and a linker. The antigens would be designed to target specific receptors on monocytes, which would be internalised by endocytosis allowing the

SRPK1 inhibitor to be released (Zhao *et al*., 2020). This would decrease the effect on other cell types and enhance the efficacy on monocytes itself.

In fact, the work presented in this thesis is not limited to PAD. It can also be translated to other ischemic vascular diseases such as CAD. A study in 2004 found that VEGF levels were upregulated in the monocytes of stable angina CAD patients (Panutsopulos *et al*., 2003). Later, Hueso *et al* assessed the VEGF-A isoform content in the serum of ST-Elevation Myocardial Infarction (STEMI) patients. There was shown to be an upregulation of VEGF-A_{165}b: VEGF-A at a protein level, which negatively correlated with the function of the left ventricle (Hueso *et al*., 2017). The angiogenic response was assessed in *vitro* using STEMI patient serum resulting in impaired tube formation, which was reversed with a neutralising VEGF-A_{165}b antibody (Hueso *et al*., 2017). With the novel findings presented throughout this thesis, perhaps SRPK1 could be modulating the response in CAD. This could be assessed *in vivo* using a myocardial ischemia and reperfusion mouse model and administering an SRPK1 inhibitor, which may result in a smaller myocardial infarct size. In fact, Wnt5a plasma levels are shown to be upregulated in CAD and obese patients (Akoumianakis *et al*., 2019). Perhaps there is a direct link with SRPK1, which is yet to be explored. This could also be investigated using an *in vivo* obese CAD mouse model.

7.4. Summary

The results from this present thesis highlight that hyperactivity of monocytic Wnt5a is responsible for impaired blood flow recovery and collateral growth in ischemic mouse models, even in obesity. Through experiments, I conclude that this mechanism is dependent on SRPK1 in monocytes. SRPK1 inhibitors such as SPHINX31 have been shown to have potential as a therapeutic candidate for PAD. Under the given conditions, it was not possible to detect changes in VEGF-A splice variants downstream. This does not eliminate the involvement of VEGF-A and further work is needed explore downstream mechanisms that are potentially involved (as summarised in Figure 7.1). The graphical abstract in Figure 7.2 summarises the key findings of this thesis.

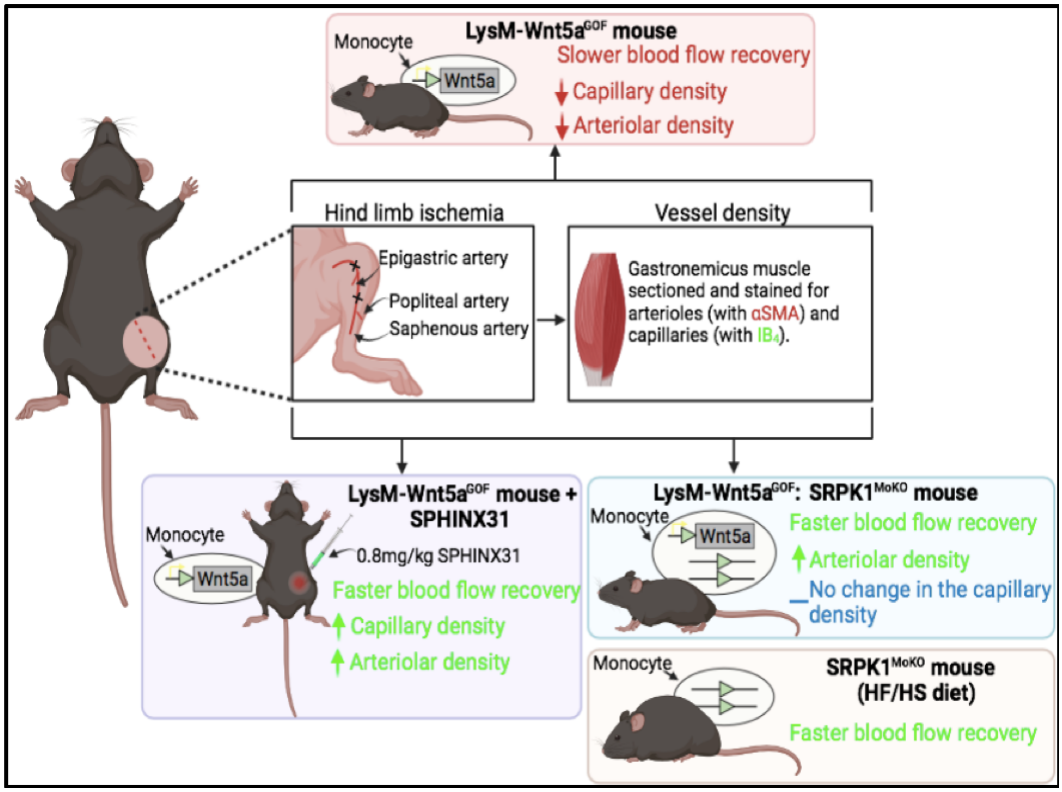


Figure 7.2. A graphical abstract summarising the key findings of this thesis. *All transgenic mouse models used in this thesis (LysM-Wnt5a^{GOF}, Chapter 3; LysM-Wnt5a^{GOF} + SRPK1 inhibitor SPHINX31, Chapter 4; LysM-Wnt5a^{GOF}: SRPK1^{MoKO} and obese-SRPK1^{MoKO}, Chapter 5) underwent the HLI procedure and the blood flow recovery was assessed. The cross in the hind limb ischemia panel indicate the ligation site. On post-operative day 21, the gastrocnemius muscle was collected and vessel densities were assessed. In summary, the data shows that SRPK1 inhibition with a pharmacological inhibitor (SPHINX31) and knockout of monocytic-SRPK1 improves the blood flow recovery and promotes revascularisation in the gastrocnemius muscle (bottom panels) compared to the LysM-Wnt5a^{GOF} mice (top panel). Similarly, obese-SRPK1^{MoKO} mice had a quicker rate of blood flow recovery. Collectively, this indicates that the impaired revascularisation is dependent on monocytic-SRPK1 and could be a new therapeutic target for PAD. The diagram was created on Biorender.com.*

REFERENCES

Abaci, A., Oguzhan, A., Kahraman, S., Eryol, N. K., Unal, S., Arinc, H. & Ergin, A. 1999. Effect of diabetes mellitus on formation of coronary collateral vessels. *Circulation,* 99**,** 2239-42.

Abou Faycal, C., Gazzeri, S. & Eymin, B. 2019. A VEGF-A/SOX2/SRSF2 network controls VEGFR1 pre-mRNA alternative splicing in lung carcinoma cells. *Sci Rep,* 9**,** 336.

Abram, C. L., Roberge, G. L., Hu, Y. & Lowell, C. A. 2014. Comparative analysis of the efficiency and specificity of myeloid-Cre deleting strains using ROSA-EYFP reporter mice. *J Immunol Methods,* 408**,** 89-100.

Ackers, I., Szymanski, C., Silver, M. J. & Malgor, R. 2020. Oxidized Low-Density Lipoprotein Induces WNT5A Signaling Activation in THP-1 Derived Macrophages and a Human Aortic Vascular Smooth Muscle Cell Line. *Front Cardiovasc Med,* 7**,** 567837.

Ahn, G. O., Seita, J., Hong, B. J., Kim, Y. E., Bok, S., Lee, C. J., Kim, K. S., Lee, J. C., Leeper, N. J., Cooke, J. P., Kim, H. J., Kim, I. H., Weissman, I. L. & Brown, J. M. 2014. Transcriptional activation of hypoxia-inducible factor-1 (HIF-1) in myeloid cells promotes angiogenesis through VEGF and S100A8. *Proc Natl Acad Sci U S A,* 111**,** 2698-703.

Akagi, Y., Liu, W., Zebrowski, B., Xie, K. & Ellis, L. M. 1998. Regulation of vascular endothelial growth factor expression in human colon cancer by insulin-like growth factor-I. *Cancer Res,* 58**,** 4008-14.

Akoumianakis, I., Sanna, F., Margaritis, M., Badi, I., Akawi, N., Herdman, L., Coutinho, P., Fagan, H., Antonopoulos, A. S., Oikonomou, E. K., Thomas, S., Chiu, A. P., Chuaiphichai, S., Kotanidis, C. P., Christodoulides, C., Petrou, M., Krasopoulos, G., Sayeed, R., Lv, L., Hale, A., Naeimi Kararoudi, M., Mcneill, E., Douglas, G., George, S., Tousoulis, D., Channon, K. M. & Antoniades, C. 2019. Adipose tissue-derived WNT5A regulates vascular redox signaling in obesity via USP17/RAC1-mediated activation of NADPH oxidases. *Sci Transl Med,* 11.

Al Shoyaib, A., Archie, S. R. & Karamyan, V. T. 2019. Intraperitoneal Route of Drug Administration: Should it Be Used in Experimental Animal Studies? *Pharm Res,* 37**,** 12.

Aldo, P. B., Craveiro, V., Guller, S. & Mor, G. 2013. Effect of culture conditions on the phenotype of THP-1 monocyte cell line. *Am J Reprod Immunol,* 70**,** 80-6.

Amano, H., Kato, S., Ito, Y., Eshima, K., Ogawa, F., Takahashi, R., Sekiguchi, K., Tamaki, H., Sakagami, H., Shibuya, M. & Majima, M. 2015. The Role of Vascular Endothelial Growth Factor Receptor-1 Signaling in the Recovery from Ischemia. *PLoS One,* 10**,** e0131445.

Amin, E. M., Oltean, S., Hua, J., Gammons, M. V., Hamdollah-Zadeh, M., Welsh, G. I., Cheung, M. K., Ni, L., Kase, S., Rennel, E. S., Symonds, K. E., Nowak, D. G., Royer-Pokora, B., Saleem, M. A., Hagiwara, M., Schumacher, V. A., Harper, S. J., Hinton, D. R., Bates, D. O. & Ladomery, M. R. 2011. WT1 mutants reveal SRPK1 to be a downstream angiogenesis target by altering VEGF splicing. *Cancer Cell,* 20**,** 768-80.

Arai, M., Misao, Y., Nagai, H., Kawasaki, M., Nagashima, K., Suzuki, K., Tsuchiya, K., Otsuka, S., Uno, Y., Takemura, G., Nishigaki, K., Minatoguchi, S. & Fujiwara, H. 2006. Granulocyte colony-stimulating factor: a noninvasive regeneration therapy for treating atherosclerotic peripheral artery disease. *Circ J,* 70**,** 1093-8.

Aref, Z., De Vries, M. R. & Quax, P. H. A. 2019. Variations in Surgical Procedures for Inducing Hind Limb Ischemia in Mice and the Impact of These Variations on Neovascularization Assessment. *Int J Mol Sci,* 20.

Arnold, W. P., Mittal, C. K., Katsuki, S. & Murad, F. 1977. Nitric oxide activates guanylate cyclase and increases guanosine 3':5'-cyclic monophosphate levels in various tissue preparations. *Proc Natl Acad Sci U S A,* 74**,** 3203-7.

Arsic, N., Zacchigna, S., Zentilin, L., Ramirez-Correa, G., Pattarini, L., Salvi, A., Sinagra, G. & Giacca, M. 2004. Vascular endothelial growth factor stimulates skeletal muscle regeneration in vivo. *Mol Ther,* 10**,** 844-54.

Asahara, T., Murohara, T., Sullivan, A., Silver, M., Van Der Zee, R., Li, T., Witzenbichler, B., Schatteman, G. & Isner, J. M. 1997. Isolation of putative progenitor endothelial cells for angiogenesis. *Science,* 275**,** 964-7.

Au - Padgett, M. E., Au - Mccord, T. J., Au - Mcclung, J. M. & Au - Kontos, C. D. 2016. Methods for Acute and Subacute Murine Hindlimb Ischemia. *JoVE*, e54166.

Aubol, B. E., Plocinik, R. M., Hagopian, J. C., Ma, C. T., Mcglone, M. L., Bandyopadhyay, R., Fu, X. D. & Adams, J. A. 2013. Partitioning RS domain phosphorylation in an SR protein through the CLK and SRPK protein kinases. *J Mol Biol,* 425, 2894-909.

Bates, D. O., Cui, T. G., Doughty, J. M., Winkler, M., Sugiono, M., Shields, J. D., Peat, D., Gillatt, D. & Harper, S. J. 2002. VEGF165b, an inhibitory splice variant of vascular endothelial growth factor, is down-regulated in renal cell carcinoma. *Cancer Res,* 62, 4123-31.

Batson, J., Toop, H. D., Redondo, C., Babaei-Jadidi, R., Chaikuad, A., Wearmouth, S. F., Gibbons, B., Allen, C., Tallant, C., Zhang, J., Du, C., Hancox, J. C., Hawtrey, T., Da Rocha, J., Griffith, R., Knapp, S., Bates, D. O. & Morris, J. C. 2017. Development of Potent, Selective SRPK1 Inhibitors as Potential Topical Therapeutics for Neovascular Eye Disease. *ACS Chem Biol,* 12, 825-832.

Baumgartner, I., Pieczek, A., Manor, O., Blair, R., Kearney, M., Walsh, K. & Isner, J. M. 1998. Constitutive expression of phVEGF165 after intramuscular gene transfer promotes collateral vessel development in patients with critical limb ischemia. *Circulation,* 97, 1114-23.

Beckman, J. A. & Creager, M. A. 2016. Vascular Complications of Diabetes. *Circ Res,* 118, 1771-85.

Beckman, J. A., Duncan, M. S., Damrauer, S. M., Wells, Q. S., Barnett, J. V., Wasserman, D. H., Bedimo, R. J., Butt, A. A., Marconi, V. C., Sico, J. J., Tindle, H. A., Bonaca, M. P., Aday, A. W. & Freiberg, M. S. 2019. Microvascular Disease, Peripheral Artery Disease, and Amputation. *Circulation,* 140, 449-458.

Behroozian, A. & Beckman, J. A. 2020. Microvascular Disease Increases Amputation in Patients With Peripheral Artery Disease. *Arterioscler Thromb Vasc Biol,* 40, 534-540.

Benest, A. V., Stone, O. A., Miller, W. H., Glover, C. P., Uney, J. B., Baker, A. H., Harper, S. J. & Bates, D. O. 2008. Arteriolar genesis and angiogenesis induced by endothelial nitric oxide synthase overexpression results in a mature vasculature. *Arterioscler Thromb Vasc Biol,* 28, 1462-8.

Bentzon, J. F., Otsuka, F., Virmani, R. & Falk, E. 2014. Mechanisms of plaque formation and rupture. *Circ Res,* 114**,** 1852-66.

Bhatnagar, P., Wickramasinghe, K., Wilkins, E. & Townsend, N. 2016. Trends in the epidemiology of cardiovascular disease in the UK. *Heart,* 102**,** 1945-1952.

Bhatt, P. M., Lewis, C. J., House, D. L., Keller, C. M., Kohn, L. D., Silver, M. J., Mccall, K. D., Goetz, D. J. & Malgor, R. 2012. Increased Wnt5a mRNA Expression in Advanced Atherosclerotic Lesions, and Oxidized LDL Treated Human Monocyte-Derived Macrophages. *Open Circ Vasc J,* 5**,** 1-7.

Bhullar, K. S., Lagarón, N. O., Mcgowan, E. M., Parmar, I., Jha, A., Hubbard, B. P. & Rupasinghe, H. P. V. 2018. Kinase-targeted cancer therapies: progress, challenges and future directions. *Mol Cancer,* 17**,** 48.

Biselli-Chicote, P. M., Biselli, J. M., Cunha, B. R., Castro, R., Maniglia, J. V., Neto, D. S., Tajara, E. H., Góis Filho, J. F., Fukuyama, E. E., Pavarino É, C. & Goloni-Bertollo, E. M. 2017. Overexpression of Antiangiogenic Vascular Endothelial Growth Factor Isoform and Splicing Regulatory Factors in Oral, Laryngeal and Pharyngeal Squamous Cell Carcinomas. *Asian Pac J Cancer Prev,* 18**,** 2171-2177.

Boring, L., Gosling, J., Cleary, M. & Charo, I. F. 1998. Decreased lesion formation in CCR2-/- mice reveals a role for chemokines in the initiation of atherosclerosis. *Nature,* 394**,** 894-7.

Bosch-Marce, M., Okuyama, H., Wesley, J. B., Sarkar, K., Kimura, H., Liu, Y. V., Zhang, H., Strazza, M., Rey, S., Savino, L., Zhou, Y. F., Mcdonald, K. R., Na, Y., Vandiver, S., Rabi, A., Shaked, Y., Kerbel, R., Lavallee, T. & Semenza, G. L. 2007. Effects of aging and hypoxia-inducible factor-1 activity on angiogenic cell mobilization and recovery of perfusion after limb ischemia. *Circ Res,* 101**,** 1310-8.

Botti, C., Maione, C., Coppola, A., Sica, V. & Cobellis, G. 2012. Autologous bone marrow cell therapy for peripheral arterial disease. *Stem cells and cloning : advances and applications,* 5**,** 5-14.

Bowler, E. & Oltean, S. 2019. Alternative Splicing in Angiogenesis. *Int J Mol Sci,* 20.

Bramante, C. T., Lee, C. J. & Gudzune, K. A. 2017. Treatment of Obesity in Patients With Diabetes. *Diabetes spectrum : a publication of the American Diabetes Association,* 30**,** 237-243.

Branco, B. C., Montero-Baker, M. F. & Mills, J. L., Sr. 2015. The pros and cons of endovascular and open surgical treatments for patients with acute limb ischemia. *J Cardiovasc Surg (Torino),* 56**,** 401-7.

Breton-Romero, R., Feng, B., Holbrook, M., Farb, M. G., Fetterman, J. L., Linder, E. A., Berk, B. D., Masaki, N., Weisbrod, R. M., Inagaki, E., Gokce, N., Fuster, J. J., Walsh, K. & Hamburg, N. M. 2016. Endothelial Dysfunction in Human Diabetes Is Mediated by Wnt5a-JNK Signaling. *Arterioscler Thromb Vasc Biol,* 36**,** 561-9.

Bretón-Romero, R., Feng, B., Holbrook, M., Farb, M. G., Fetterman, J. L., Linder, E. A., Berk, B. D., Masaki, N., Weisbrod, R. M., Inagaki, E., Gokce, N., Fuster, J. J., Walsh, K. & Hamburg, N. M. 2016. Endothelial Dysfunction in Human Diabetes Is Mediated by Wnt5a-JNK Signaling. *Arterioscler Thromb Vasc Biol,* 36**,** 561-9.

Bridgett, S., Dellett, M. & Simpson, D. A. 2017. RNA-Sequencing data supports the existence of novel VEGFA splicing events but not of VEGFA(xxx)b isoforms. *Scientific reports,* 7**,** 58-58.

Bura, A., Planat-Benard, V., Bourin, P., Silvestre, J. S., Gross, F., Grolleau, J. L., Saint-Lebese, B., Peyrafitte, J. A., Fleury, S., Gadelorge, M., Taurand, M., Dupuis-Coronas, S., Leobon, B. & Casteilla, L. 2014. Phase I trial: the use of autologous cultured adipose-derived stroma/stem cells to treat patients with non-revascularizable critical limb ischemia. *Cytotherapy,* 16**,** 245-57.

Burri, P. H. & Djonov, V. 2002. Intussusceptive angiogenesis--the alternative to capillary sprouting. *Mol Aspects Med,* 23**,** S1-27.

Capoccia, B. J., Gregory, A. D. & Link, D. C. 2008. Recruitment of the inflammatory subset of monocytes to sites of ischemia induces angiogenesis in a monocyte chemoattractant protein-1-dependent fashion. *J Leukoc Biol,* 84**,** 760-8.

Carmeliet, P., Ferreira, V., Breier, G., Pollefeyt, S., Kieckens, L., Gertsenstein, M., Fahrig, M., Vandenhoeck, A., Harpal, K., Eberhardt, C., Declercq, C., Pawling, J., Moons, L., Collen, D., Risau, W. & Nagy, A. 1996. Abnormal blood vessel development and

lethality in embryos lacking a single VEGF allele. *Nature,* 380**,** 435-9.

Cébe Suarez, S., Pieren, M., Cariolato, L., Arn, S., Hoffmann, U., Bogucki, A., Manlius, C., Wood, J. & Ballmer-Hofer, K. 2006. A VEGF-A splice variant defective for heparan sulfate and neuropilin-1 binding shows attenuated signaling through VEGFR-2. *Cell Mol Life Sci,* 63**,** 2067-77.

Celletti, F. L., Waugh, J. M., Amabile, P. G., Brendolan, A., Hilfiker, P. R. & Dake, M. D. 2001. Vascular endothelial growth factor enhances atherosclerotic plaque progression. *Nat Med,* 7**,** 425-9.

Chalothorn, D., Clayton, J. A., Zhang, H., Pomp, D. & Faber, J. E. 2007. Collateral density, remodeling, and VEGF-A expression differ widely between mouse strains. *Physiol Genomics,* 30**,** 179-91.

Chang, E.-A., Jin, S.-W., Nam, M.-H. & Kim, S.-D. 2019. Human Induced Pluripotent Stem Cells : Clinical Significance and Applications in Neurologic Diseases. *Journal of Korean Neurosurgical Society,* 62**,** 493-501.

Chen, M., Huang, J., Yang, X., Liu, B., Zhang, W., Huang, L., Deng, F., Ma, J., Bai, Y., Lu, R., Huang, B., Gao, Q., Zhuo, Y. & Ge, J. 2012. Serum starvation induced cell cycle synchronization facilitates human somatic cells reprogramming. *PLoS One,* 7**,** e28203.

Cho, Y. K., Kang, Y. M., Lee, S. E., Lee, Y., Seol, S. M., Lee, W. J., Park, J. Y. & Jung, C. H. 2018. Effect of SFRP5 (Secreted Frizzled-Related Protein 5) on the WNT5A (Wingless-Type Family Member 5A)-Induced Endothelial Dysfunction and Its Relevance With Arterial Stiffness in Human Subjects. *Arterioscler Thromb Vasc Biol,* 38**,** 1358-1367.

Chu, V. T., Weber, T., Graf, R., Sommermann, T., Petsch, K., Sack, U., Volchkov, P., Rajewsky, K. & Kühn, R. 2016. Efficient generation of Rosa26 knock-in mice using CRISPR/Cas9 in C57BL/6 zygotes. *BMC Biotechnol,* 16**,** 4.

Clausen, B. E., Burkhardt, C., Reith, W., Renkawitz, R. & Förster, I. 1999. Conditional gene targeting in macrophages and granulocytes using LysMcre mice. *Transgenic Res,* 8**,** 265-77.

Clayton, J. A., Chalothorn, D. & Faber, J. E. 2008. Vascular endothelial growth factor-A specifies formation of native collaterals and regulates collateral growth in ischemia. *Circ Res,* 103**,** 1027-36.

Coleman, J. L., Brennan, K., Ngo, T., Balaji, P., Graham, R. M. & Smith, N. J. 2015. Rapid Knockout and Reporter Mouse Line Generation and Breeding Colony Establishment Using EUCOMM Conditional-Ready Embryonic Stem Cells: A Case Study. *Front Endocrinol (Lausanne),* 6**,** 105.

Colwill, K., Pawson, T., Andrews, B., Prasad, J., Manley, J. L., Bell, J. C. & Duncan, P. I. 1996. The Clk/Sty protein kinase phosphorylates SR splicing factors and regulates their intranuclear distribution. *Embo j,* 15**,** 265-75.

Cominacini, L., Garbin, U., Pasini, A. F., Davoli, A., Campagnola, M., Rigoni, A., Tosetti, L. & Lo Cascio, V. 1999. The expression of adhesion molecules on endothelial cells is inhibited by troglitazone through its antioxidant activity. *Cell Adhes Commun,* 7**,** 223-31.

Connolly, D. T., Heuvelman, D. M., Nelson, R., Olander, J. V., Eppley, B. L., Delfino, J. J., Siegel, N. R., Leimgruber, R. M. & Feder, J. 1989. Tumor vascular permeability factor stimulates endothelial cell growth and angiogenesis. *J Clin Invest,* 84**,** 1470-8.

Cooper, J. C., Sharkey, A. M., Charnock-Jones, D. S., Palmer, C. R. & Smith, S. K. 1996. VEGF mRNA levels in placentae from pregnancies complicated by pre-eclampsia. *Br J Obstet Gynaecol,* 103**,** 1191-6.

Cooper, L. T., Jr., Hiatt, W. R., Creager, M. A., Regensteiner, J. G., Casscells, W., Isner, J. M., Cooke, J. P. & Hirsch, A. T. 2001. Proteinuria in a placebo-controlled study of basic fibroblast growth factor for intermittent claudication. *Vasc Med,* 6**,** 235-9.

Couffinhal, T., Kearney, M., Witzenbichler, B., Chen, D., Murohara, T., Losordo, D. W., Symes, J. & Isner, J. M. 1997. Vascular endothelial growth factor/vascular permeability factor (VEGF/VPF) in normal and atherosclerotic human arteries. *Am J Pathol,* 150**,** 1673-85.

Cox, B. C., Liu, Z., Lagarde, M. M. & Zuo, J. 2012. Conditional gene expression in the mouse inner ear using Cre-loxP. *J Assoc Res Otolaryngol,* 13**,** 295-322.

Creager, M. A., Olin, J. W., Belch, J. J., Moneta, G. L., Henry, T. D., Rajagopalan, S., Annex, B. H. & Hiatt, W. R. 2011. Effect of hypoxia-inducible factor-1alpha gene therapy on walking performance in patients with intermittent claudication. *Circulation,* 124**,** 1765-73.

Dai, X. & Faber, J. E. 2010. Endothelial nitric oxide synthase deficiency causes collateral vessel rarefaction and impairs activation of a cell cycle gene network during arteriogenesis. *Circ Res,* 106**,** 1870-81.

Dasu, M. R., Devaraj, S. & Jialal, I. 2007. High glucose induces IL-1beta expression in human monocytes: mechanistic insights. *Am J Physiol Endocrinol Metab,* 293**,** E337-46.

Davies, J. H., Kenkre, J. & Williams, E. M. 2014. Current utility of the ankle-brachial index (ABI) in general practice: implications for its use in cardiovascular disease screening. *BMC Fam Pract,* 15**,** 69.

Delavar, H., Nogueira, L., Wagner, P. D., Hogan, M. C., Metzger, D. & Breen, E. C. 2014. Skeletal myofiber VEGF is essential for the exercise training response in adult mice. *Am J Physiol Regul Integr Comp Physiol,* 306**,** R586-95.

Denninger, J. W. & Marletta, M. A. 1999. Guanylate cyclase and the .NO/cGMP signaling pathway. *Biochim Biophys Acta,* 1411**,** 334-50.

Dewald, O., Zymek, P., Winkelmann, K., Koerting, A., Ren, G., Abou-Khamis, T., Michael, L. H., Rollins, B. J., Entman, M. L. & Frangogiannis, N. G. 2005. CCL2/Monocyte Chemoattractant Protein-1 regulates inflammatory responses critical to healing myocardial infarcts. *Circ Res,* 96**,** 881-9.

Doronzo, G., Viretto, M., Russo, I., Mattiello, L., Anfossi, G. & Trovati, M. 2012. Effects of high glucose on vascular endothelial growth factor synthesis and secretion in aortic vascular smooth muscle cells from obese and lean Zucker rats. *Int J Mol Sci,* 13**,** 9478-88.

Dua, A. & Lee, C. J. 2016. Epidemiology of Peripheral Arterial Disease and Critical Limb Ischemia. *Tech Vasc Interv Radiol,* 19**,** 91-5.

Duscha, B. D., Robbins, J. L., Jones, W. S., Kraus, W. E., Lye, R. J., Sanders, J. M., Allen, J. D., Regensteiner, J. G., Hiatt, W. R. & Annex, B. H. 2011. Angiogenesis in skeletal muscle precede improvements in peak oxygen uptake in peripheral artery disease patients. *Arterioscler Thromb Vasc Biol,* 31**,** 2742-8.

Eitenmüller, I., Volger, O., Kluge, A., Troidl, K., Barancik, M., Cai, W. J., Heil, M., Pipp, F., Fischer, S., Horrevoets, A. J., Schmitz-Rixen, T. & Schaper, W. 2006. The range of adaptation by collateral vessels after femoral artery occlusion. *Circ Res,* 99**,** 656-62.

Eswarappa, S. M., Potdar, A. A., Koch, W. J., Fan, Y., Vasu, K., Lindner, D., Willard, B., Graham, L. M., Dicorleto, P. E. & Fox, P. L. 2014. Programmed translational readthrough generates antiangiogenic VEGF-Ax. *Cell,* 157**,** 1605-18.

Farb, M. G., Karki, S., Park, S. Y., Saggese, S. M., Carmine, B., Hess, D. T., Apovian, C., Fetterman, J. L., Bretón-Romero, R., Hamburg, N. M., Fuster, J. J., Zuriaga, M. A., Walsh, K. & Gokce, N. 2016. WNT5A-JNK regulation of vascular insulin resistance in human obesity. *Vasc Med,* 21**,** 489-496.

Faust, N., Varas, F., Kelly, L. M., Heck, S. & Graf, T. 2000. Insertion of enhanced green fluorescent protein into the lysozyme gene creates mice with green fluorescent granulocytes and macrophages. *Blood,* 96**,** 719-26.

Ferrara, N., Gerber, H. P. & Lecouter, J. 2003. The biology of VEGF and its receptors. *Nat Med,* 9**,** 669-76.

Ferrara, N. & Henzel, W. J. 1989. Pituitary follicular cells secrete a novel heparin-binding growth factor specific for vascular endothelial cells. *Biochem Biophys Res Commun,* 161**,** 851-8.

Findley, C. M., Mitchell, R. G., Duscha, B. D., Annex, B. H. & Kontos, C. D. 2008. Plasma levels of soluble Tie2 and vascular endothelial growth factor distinguish critical limb ischemia from intermittent claudication in patients with peripheral arterial disease. *J Am Coll Cardiol,* 52**,** 387-93.

Fischer, M., Schwabe, C. & Schulte, K. L. 2006. Value of the hemobahn/viabahn endoprosthesis in the treatment of long chronic lesions of the superficial femoral artery: 6 years of experience. *J Endovasc Ther,* 13**,** 281-90.

Folkman, J. & Klagsbrun, M. 1987. Angiogenic factors. *Science,* 235**,** 442-447.

Fraser, H. M., Dickson, S. E., Lunn, S. F., Wulff, C., Morris, K. D., Carroll, V. A. & Bicknell, R. 2000. Suppression of luteal angiogenesis in the

primate after neutralization of vascular endothelial growth factor. *Endocrinology,* 141**,** 995-1000.

Fukuhara, T., Hosoya, T., Shimizu, S., Sumi, K., Oshiro, T., Yoshinaka, Y., Suzuki, M., Yamamoto, N., Herzenberg, L. A., Herzenberg, L. A. & Hagiwara, M. 2006. Utilization of host SR protein kinases and RNA-splicing machinery during viral replication. *Proc Natl Acad Sci U S A,* 103**,** 11329-33.

Fuster, J. J., Zuriaga, M. A., Ngo, D. T., Farb, M. G., Aprahamian, T., Yamaguchi, T. P., Gokce, N. & Walsh, K. 2015. Noncanonical Wnt signaling promotes obesity-induced adipose tissue inflammation and metabolic dysfunction independent of adipose tissue expansion. *Diabetes,* 64**,** 1235-48.

Gammons, M. V., Fedorov, O., Ivison, D., Du, C., Clark, T., Hopkins, C., Hagiwara, M., Dick, A. D., Cox, R., Harper, S. J., Hancox, J. C., Knapp, S. & Bates, D. O. 2013. Topical antiangiogenic SRPK1 inhibitors reduce choroidal neovascularization in rodent models of exudative AMD. *Invest Ophthalmol Vis Sci,* 54**,** 6052-62.

Gammons, M. V., Lucas, R., Dean, R., Coupland, S. E., Oltean, S. & Bates, D. O. 2014. Targeting SRPK1 to control VEGF-mediated tumour angiogenesis in metastatic melanoma. *Br J Cancer,* 111**,** 477-85.

Ganta, V. C., Choi, M., Kutateladze, A. & Annex, B. H. 2017. VEGF165b Modulates Endothelial VEGFR1-STAT3 Signaling Pathway and Angiogenesis in Human and Experimental Peripheral Arterial Disease. *Circ Res,* 120**,** 282-295.

Gardner, A. W. & Afaq, A. 2008. Management of lower extremity peripheral arterial disease. *J Cardiopulm Rehabil Prev,* 28**,** 349-57.

Ghosh, G. & Adams, J. A. 2011. Phosphorylation mechanism and structure of serine-arginine protein kinases. *Febs j,* 278**,** 587-97.

Giannakouros, T., Nikolakaki, E., Mylonis, I. & Georgatsou, E. 2011. Serine-arginine protein kinases: a small protein kinase family with a large cellular presence. *Febs j,* 278**,** 570-86.

Goel, S., Wong, A. H. & Jain, R. K. 2012. Vascular normalization as a therapeutic strategy for malignant and nonmalignant disease. *Cold Spring Harb Perspect Med,* 2**,** a006486.

Gonçalves, V. & Jordan, P. 2015. Posttranscriptional Regulation of Splicing Factor SRSF1 and Its Role in Cancer Cell Biology. *Biomed Res Int,* 2015**,** 287048.

Gornik, H. L. & Beckman, J. A. 2005. Cardiology patient page. Peripheral arterial disease. *Circulation,* 111**,** e169-72.

Graz, H., D'souza, V. K., Alderson, D. E. C. & Graz, M. 2018. Diabetes-related amputations create considerable public health burden in the UK. *Diabetes Res Clin Pract,* 135**,** 158-165.

Greve, J. M., Williams, S. P., Bernstein, L. J., Goldman, H., Peale, F. V., Jr., Bunting, S. & Van Bruggen, N. 2008. Reactive hyperemia and BOLD MRI demonstrate that VEGF inhibition, age, and atherosclerosis adversely affect functional recovery in a murine model of peripheral artery disease. *J Magn Reson Imaging,* 28**,** 996-1004.

Guma, M., Rius, J., Duong-Polk, K. X., Haddad, G. G., Lindsey, J. D. & Karin, M. 2009. Genetic and pharmacological inhibition of JNK ameliorates hypoxia-induced retinopathy through interference with VEGF expression. *Proc Natl Acad Sci U S A,* 106**,** 8760-5.

Hajighasemi, F. & Tajic, S. 2017. Assessment of Cytotoxicity of Dimethyl Sulfoxide in Human Hematopoietic Tumor Cell Lines. *Iranian Journal of Blood and Cancer,* 9**,** 48-53.

Han, M. S., Jung, D. Y., Morel, C., Lakhani, S. A., Kim, J. K., Flavell, R. A. & Davis, R. J. 2013. JNK expression by macrophages promotes obesity-induced insulin resistance and inflammation. *Science,* 339**,** 218-22.

Harper, S. J. & Bates, D. O. 2008. VEGF-A splicing: the key to anti-angiogenic therapeutics? *Nat Rev Cancer,* 8**,** 880-7.

Hatcher, J. M., Wu, G., Zeng, C., Zhu, J., Meng, F., Patel, S., Wang, W., Ficarro, S. B., Leggett, A. L., Powell, C. E., Marto, J. A., Zhang, K., Ki Ngo, J. C., Fu, X. D., Zhang, T. & Gray, N. S. 2018. SRPKIN-1: A Covalent SRPK1/2 Inhibitor that Potently Converts VEGF from Pro-angiogenic to Anti-angiogenic Isoform. *Cell Chem Biol,* 25**,** 460-470.e6.

Hayes, G. M., Carrigan, P. E., Beck, A. M. & Miller, L. J. 2006. Targeting the RNA splicing machinery as a novel treatment strategy for pancreatic carcinoma. *Cancer Res,* 66**,** 3819-27.

Hazarika, S., Dokun, A. O., Li, Y., Popel, A. S., Kontos, C. D. & Annex, B. H. 2007. Impaired angiogenesis after hindlimb ischemia in type 2 diabetes mellitus: differential regulation of vascular endothelial growth factor receptor 1 and soluble vascular endothelial growth factor receptor 1. *Circ Res,* 101**,** 948-56.

Helisch, A., Wagner, S., Khan, N., Drinane, M., Wolfram, S., Heil, M., Ziegelhoeffer, T., Brandt, U., Pearlman, J. D., Swartz, H. M. & Schaper, W. 2006. Impact of mouse strain differences in innate hindlimb collateral vasculature. *Arterioscler Thromb Vasc Biol,* 26**,** 520-6.

Henry, T. D., Pepine, C. J., Lambert, C. R., Traverse, J. H., Schatz, R., Costa, M., Povsic, T. J., David Anderson, R., Willerson, J. T., Kesten, S. & Perin, E. C. 2017. The Athena trials: Autologous adipose-derived regenerative cells for refractory chronic myocardial ischemia with left ventricular dysfunction. *Catheter Cardiovasc Interv,* 89**,** 169-177.

Herse, F., Fain, J. N., Janke, J., Engeli, S., Kuhn, C., Frey, N., Weich, H. A., Bergmann, A., Kappert, K., Karumanchi, S. A., Luft, F. C., Muller, D. N., Staff, A. C. & Dechend, R. 2011. Adipose tissue-derived soluble fms-like tyrosine kinase 1 is an obesity-relevant endogenous paracrine adipokine. *Hypertension,* 58**,** 37-42.

Hood, J. D., Meininger, C. J., Ziche, M. & Granger, H. J. 1998. VEGF upregulates ecNOS message, protein, and NO production in human endothelial cells. *Am J Physiol,* 274**,** H1054-8.

Hsu, P. C., Su, H. M., Lee, H. C., Juo, S. H., Lin, T. H., Voon, W. C., Lai, W. T. & Sheu, S. H. 2014. Coronary collateral circulation in patients of coronary ectasia with significant coronary artery disease. *PLoS One,* 9**,** e87001.

Hu, W., Li, L., Yang, M., Luo, X., Ran, W., Liu, D., Xiong, Z., Liu, H. & Yang, G. 2013. Circulating Sfrp5 is a signature of obesity-related metabolic disorders and is regulated by glucose and liraglutide in humans. *J Clin Endocrinol Metab,* 98**,** 290-8.

Huang, W., Bansode, R., Mehta, M. & Mehta, K. D. 2009. Loss of protein kinase Cbeta function protects mice against diet-induced obesity and development of hepatic steatosis and insulin resistance. *Hepatology,* 49**,** 1525-36.

Huang, X., He, Z., Jiang, X., Hou, M., Tang, Z., Zhen, X., Liang, Y. & Ma, J. 2016. Folic Acid Represses Hypoxia-Induced Inflammation in THP-1 Cells through Inhibition of the PI3K/Akt/HIF-1alpha Pathway. *PLoS One,* 11**,** e0151553.

Hueso, L., Rios-Navarro, C., Ruiz-Sauri, A., Chorro, F. J., Nunez, J., Sanz, M. J., Bodi, V. & Piqueras, L. 2017. Dynamics and implications of circulating anti-angiogenic VEGF-A(165)b isoform in patients with ST-elevation myocardial infarction. *Sci Rep,* 7**,** 9962.

Hug, N., Longman, D. & Cáceres, J. F. 2016. Mechanism and regulation of the nonsense-mediated decay pathway. *Nucleic Acids Res,* 44**,** 1483-95.

Hummitzsch, L., Berndt, R., Kott, M., Rusch, R., Faendrich, F., Gruenewald, M., Steinfath, M., Albrecht, M. & Zitta, K. 2020. Hypoxia directed migration of human naïve monocytes is associated with an attenuation of cytokine release: indications for a key role of CCL26. *J Transl Med,* 18**,** 404.

Ito, W. D., Arras, M., Scholz, D., Winkler, B., Htun, P. & Schaper, W. 1997a. Angiogenesis but not collateral growth is associated with ischemia after femoral artery occlusion. *Am J Physiol,* 273**,** H1255-65.

Ito, W. D., Arras, M., Winkler, B., Scholz, D., Schaper, J. & Schaper, W. 1997b. Monocyte chemotactic protein-1 increases collateral and peripheral conductance after femoral artery occlusion. *Circ Res,* 80**,** 829-37.

Jackson, K. A., Majka, S. M., Wang, H., Pocius, J., Hartley, C. J., Majesky, M. W., Entman, M. L., Michael, L. H., Hirschi, K. K. & Goodell, M. A. 2001. Regeneration of ischemic cardiac muscle and vascular endothelium by adult stem cells. *J Clin Invest,* 107**,** 1395-402.

Jacobi, J., Tam, B. Y., Wu, G., Hoffman, J., Cooke, J. P. & Kuo, C. J. 2004. Adenoviral gene transfer with soluble vascular endothelial growth factor receptors impairs angiogenesis and perfusion in a murine model of hindlimb ischemia. *Circulation,* 110**,** 2424-9.

Jain, R. K. 2001. Normalizing tumor vasculature with anti-angiogenic therapy: a new paradigm for combination therapy. *Nat Med,* 7**,** 987-9.

Janbandhu, V. C., Moik, D. & Fässler, R. 2014. Cre recombinase induces DNA damage and tetraploidy in the absence of loxP sites. *Cell Cycle,* 13**,** 462-70.

Jazwa, A., Tomczyk, M., Taha, H. M., Hytonen, E., Stoszko, M., Zentilin, L., Giacca, M., Yla-Herttuala, S., Emanueli, C., Jozkowicz, A. & Dulak, J. 2013. Arteriogenic therapy based on simultaneous delivery of VEGF-A and FGF4 genes improves the recovery from acute limb ischemia. *Vasc Cell,* 5**,** 13.

Jung, Y. D., Nakano, K., Liu, W., Gallick, G. E. & Ellis, L. M. 1999. Extracellular signal-regulated kinase activation is required for up-regulation of vascular endothelial growth factor by serum starvation in human colon carcinoma cells. *Cancer Res,* 59**,** 4804-7.

Karakoyun, R., Köksoy, C., Şener, Z., Gündüz, U., Karakaş, B. & Karakoyun, M. 2014. Comparison of quality of life in patients with peripheral arterial disease caused by atherosclerosis obliterans or Buerger's disease. *Cardiovascular journal of Africa,* 25**,** 124-129.

Karki, S., Ngo, D. T. M., Farb, M. G., Park, S. Y., Saggese, S. M., Hamburg, N. M., Carmine, B., Hess, D. T., Walsh, K. & Gokce, N. 2017. WNT5A regulates adipose tissue angiogenesis via antiangiogenic VEGF-A165b in obese humans. *Am J Physiol Heart Circ Physiol,* 313**,** H200-h206.

Kawamura, H., Li, X., Harper, S. J., Bates, D. O. & Claesson-Welsh, L. 2008. Vascular endothelial growth factor (VEGF)-A165b is a weak in vitro agonist for VEGF receptor-2 due to lack of coreceptor binding and deficient regulation of kinase activity. *Cancer Res,* 68**,** 4683-92.

Keck, P. J., Hauser, S. D., Krivi, G., Sanzo, K., Warren, T., Feder, J. & Connolly, D. T. 1989. Vascular permeability factor, an endothelial cell mitogen related to PDGF. *Science,* 246**,** 1309-12.

Kendall, R. L. & Thomas, K. A. 1993. Inhibition of vascular endothelial cell growth factor activity by an endogenously encoded soluble receptor. *Proc Natl Acad Sci U S A,* 90**,** 10705-9.

Kendall, R. L., Wang, G. & Thomas, K. A. 1996. Identification of a natural soluble form of the vascular endothelial growth factor receptor, FLT-1, and its heterodimerization with KDR. *Biochem Biophys Res Commun,* 226**,** 324-8.

Keshwani, M. M., Aubol, B. E., Fattet, L., Ma, C. T., Qiu, J., Jennings, P. A., Fu, X. D. & Adams, J. A. 2015. Conserved proline-directed phosphorylation regulates SR protein conformation and splicing function. *Biochem J,* 466**,** 311-22.

Kikuchi, R., Nakamura, K., Maclauchlan, S., Ngo, D. T., Shimizu, I., Fuster, J. J., Katanasaka, Y., Yoshida, S., Qiu, Y., Yamaguchi, T. P., Matsushita, T., Murohara, T., Gokce, N., Bates, D. O., Hamburg, N. M. & Walsh, K. 2014. An antiangiogenic isoform of VEGF-A contributes to impaired vascularization in peripheral artery disease. *Nat Med,* 20**,** 1464-71.

Kim, H. J., Jang, S. Y., Park, J. I., Byun, J., Kim, D. I., Do, Y. S., Kim, J. M., Kim, S., Kim, B. M., Kim, W. B. & Kim, D. K. 2004. Vascular endothelial growth factor-induced angiogenic gene therapy in patients with peripheral artery disease. *Exp Mol Med,* 36**,** 336-44.

Kim, J., Chang, W., Jung, Y., Song, K. & Lee, I. 2012. Wnt5a activates THP-1 monocytic cells via a β-catenin-independent pathway involving JNK and NF-κB activation. *Cytokine,* 60**,** 242-8.

Koblizek, T. I., Weiss, C., Yancopoulos, G. D., Deutsch, U. & Risau, W. 1998. Angiopoietin-1 induces sprouting angiogenesis in vitro. *Curr Biol,* 8**,** 529-32.

Krishna, S. M., Omer, S. M., Li, J., Morton, S. K., Jose, R. J. & Golledge, J. 2020. Development of a two-stage limb ischemia model to better simulate human peripheral artery disease. *Sci Rep,* 10**,** 3449.

Kusumanto, Y. H., Van Weel, V., Mulder, N. H., Smit, A. J., Van Den Dungen, J. J., Hooymans, J. M., Sluiter, W. J., Tio, R. A., Quax, P. H., Gans, R. O., Dullaart, R. P. & Hospers, G. A. 2006. Treatment with intramuscular vascular endothelial growth factor gene compared with placebo for patients with diabetes mellitus and critical limb ischemia: a double-blind randomized trial. *Hum Gene Ther,* 17**,** 683-91.

Lai, M. C., Lin, R. I. & Tarn, W. Y. 2001. Transportin-SR2 mediates nuclear import of phosphorylated SR proteins. *Proc Natl Acad Sci U S A,* 98**,** 10154-9.

Lara-Hernandez, R., Lozano-Vilardell, P., Blanes, P., Torreguitart-Mirada, N., Galmés, A. & Besalduch, J. 2010. Safety and efficacy of therapeutic angiogenesis as a novel treatment in patients with critical limb ischemia. *Ann Vasc Surg,* 24**,** 287-94.

Lazarous, D. F., Unger, E. F., Epstein, S. E., Stine, A., Arevalo, J. L., Chew, E. Y. & Quyyumi, A. A. 2000. Basic fibroblast growth factor in patients with intermittent claudication: results of a phase I trial. *J Am Coll Cardiol,* 36**,** 1239-44.

Le Joncour, A., Soudet, S., Dupont, A., Espitia, O., Koskas, F., Cluzel, P., Hatron, P. Y., Emmerich, J., Cacoub, P., Resche-Rigon, M., Lambert, M. & Saadoun, D. 2018. Long-Term Outcome and Prognostic Factors of Complications in Thromboangiitis Obliterans (Buerger's Disease): A Multicenter Study of 224 Patients. *J Am Heart Assoc,* 7**,** e010677.

Lee, H. C., An, S. G., Lee, H. W., Park, J. S., Cha, K. S., Hong, T. J., Park, J. H., Lee, S. Y., Kim, S. P., Kim, Y. D., Chung, S. W., Bae, Y. C., Shin, Y. B., Kim, J. I. & Jung, J. S. 2012. Safety and effect of adipose tissue-derived stem cell implantation in patients with critical limb ischemia: a pilot study. *Circ J,* 76**,** 1750-60.

Leung, D. W., Cachianes, G., Kuang, W. J., Goeddel, D. V. & Ferrara, N. 1989. Vascular endothelial growth factor is a secreted angiogenic mitogen. *Science,* 246**,** 1306-9.

Leuschner, F., Dutta, P., Gorbatov, R., Novobrantseva, T. I., Donahoe, J. S., Courties, G., Lee, K. M., Kim, J. I., Markmann, J. F., Marinelli, B., Panizzi, P., Lee, W. W., Iwamoto, Y., Milstein, S., Epstein-Barash, H., Cantley, W., Wong, J., Cortez-Retamozo, V., Newton, A., Love, K., Libby, P., Pittet, M. J., Swirski, F. K., Koteliansky, V., Langer, R., Weissleder, R., Anderson, D. G. & Nahrendorf, M. 2011. Therapeutic siRNA silencing in inflammatory monocytes in mice. *Nat Biotechnol,* 29**,** 1005-10.

Levien, L. J. & Veller, M. G. 1999. Popliteal artery entrapment syndrome: more common than previously recognized. *J Vasc Surg,* 30**,** 587-98.

Li, D., Sinha, T., Ajima, R., Seo, H. S., Yamaguchi, T. P. & Wang, J. 2016. Spatial regulation of cell cohesion by Wnt5a during second heart field progenitor deployment. *Dev Biol,* 412**,** 18-31.

Li, Q., Zeng, C., Liu, H., Yung, K. W. Y., Chun, C., Xie, Q., Zhang, Y., Wan, S. W. C., Mak, B. S. W., Xia, J., Xiong, S., Ngo, J. C. & 2021. Protein–protein interaction inhibitor of SRPKs alters the splicing isoforms of VEGF and inhibits angiogenesis. *ISCIENCE*

Li, Y., Hazarika, S., Xie, D., Pippen, A. M., Kontos, C. D. & Annex, B. H. 2007. In mice with type 2 diabetes, a vascular endothelial growth factor (VEGF)-activating transcription factor modulates VEGF signaling and induces therapeutic angiogenesis after hindlimb ischemia. *Diabetes,* 56**,** 656-65.

Libby, P. 2012. Inflammation in atherosclerosis. *Arterioscler Thromb Vasc Biol,* 32**,** 2045-51.

Limbourg, A., Korff, T., Napp, L. C., Schaper, W., Drexler, H. & Limbourg, F. P. 2009. Evaluation of postnatal arteriogenesis and angiogenesis in a mouse model of hind-limb ischemia. *Nat Protoc,* 4**,** 1737-46.

Linton, M. F., Yancey, P. G., Davies, S. S., Jerome, W. G., Linton, E. F., Song, W. L., Doran, A. C. & Vickers, K. C. 2000. The Role of Lipids and Lipoproteins in Atherosclerosis. *In:* FEINGOLD, K. R., ANAWALT, B., BOYCE, A., CHROUSOS, G., DE HERDER, W. W., DUNGAN, K., GROSSMAN, A., HERSHMAN, J. M., HOFLAND, J., KALTSAS, G., KOCH, C., KOPP, P., KORBONITS, M., MCLACHLAN, R., MORLEY, J. E., NEW, M., PURNELL, J., SINGER, F., STRATAKIS, C. A., TRENCE, D. L. & WILSON, D. P. (eds.) *Endotext.* South Dartmouth (MA): MDText.com, Inc.
Copyright © 2000-2021, MDText.com, Inc.

Liu, X. & Quan, N. 2015. Immune Cell Isolation from Mouse Femur Bone Marrow. *Bio-protocol,* 5**,** e1631.

Long, Y., Sou, W. H., Yung, K. W. Y., Liu, H., Wan, S. W. C., Li, Q., Zeng, C., Law, C. O. K., Chan, G. H. C., Lau, T. C. K. & Ngo, J. C. K. 2019. Distinct mechanisms govern the phosphorylation of different SR protein splicing factors. *J Biol Chem,* 294**,** 1312-1327.

Luengo-Fernández, R., Leal, J., Gray, A., Petersen, S. & Rayner, M. 2006. Cost of cardiovascular diseases in the United Kingdom. *Heart,* 92**,** 1384-9.

Lukas, G., Brindle, S. D. & Greengard, P. 1971. The route of absorption of intraperitoneally administered compounds. *J Pharmacol Exp Ther,* 178**,** 562-4.

Makin, A. J., Chung, N. A., Silverman, S. H. & Lip, G. Y. 2003. Vascular endothelial growth factor and tissue factor in patients with established peripheral artery disease: a link between angiogenesis and thrombogenesis? *Clin Sci (Lond),* 104**,** 397-404.

Mäkinen, K., Manninen, H., Hedman, M., Matsi, P., Mussalo, H., Alhava, E. & Ylä-Herttuala, S. 2002. Increased vascularity detected by digital subtraction angiography after VEGF gene transfer to human lower limb artery: a randomized, placebo-controlled, double-blinded phase II study. *Mol Ther,* 6**,** 127-33.

Malgor, R., Bhatt, P. M., Connolly, B. A., Jacoby, D. L., Feldmann, K. J., Silver, M. J., Nakazawa, M., Mccall, K. D. & Goetz, D. J. 2014. Wnt5a, TLR2 and TLR4 are elevated in advanced human atherosclerotic lesions. *Inflamm Res,* 63**,** 277-85.

Marletta, M. A. 1994. Nitric oxide synthase: aspects concerning structure and catalysis. *Cell,* 78**,** 927-30.

Marti, H. J., Bernaudin, M., Bellail, A., Schoch, H., Euler, M., Petit, E. & Risau, W. 2000. Hypoxia-induced vascular endothelial growth factor expression precedes neovascularization after cerebral ischemia. *Am J Pathol,* 156**,** 965-76.

Mavrou, A., Brakspear, K., Hamdollah-Zadeh, M., Damodaran, G., Babaei-Jadidi, R., Oxley, J., Gillatt, D. A., Ladomery, M. R., Harper, S. J., Bates, D. O. & Oltean, S. 2015. Serine-arginine protein kinase 1 (SRPK1) inhibition as a potential novel targeted therapeutic strategy in prostate cancer. *Oncogene,* 34**,** 4311-9.

Maynard, S. E., Min, J. Y., Merchan, J., Lim, K. H., Li, J., Mondal, S., Libermann, T. A., Morgan, J. P., Sellke, F. W., Stillman, I. E., Epstein, F. H., Sukhatme, V. P. & Karumanchi, S. A. 2003. Excess placental soluble fms-like tyrosine kinase 1 (sFlt1) may contribute to endothelial dysfunction, hypertension, and proteinuria in preeclampsia. *J Clin Invest,* 111**,** 649-58.

Mccubbrey, A. L., Allison, K. C., Lee-Sherick, A. B., Jakubzick, C. V. & Janssen, W. J. 2017. Promoter Specificity and Efficacy in Conditional

and Inducible Transgenic Targeting of Lung Macrophages. *Front Immunol,* 8**,** 1618.

Mcdermott, M. M., Guralnik, J. M., Ferrucci, L., Tian, L., Liu, K., Liao, Y., Green, D., Sufit, R., Hoff, F., Nishida, T., Sharma, L., Pearce, W. H., Schneider, J. R. & Criqui, M. H. 2008. Asymptomatic peripheral arterial disease is associated with more adverse lower extremity characteristics than intermittent claudication. *Circulation,* 117**,** 2484-2491.

Melincovici, C. S., Boşca, A. B., Şuşman, S., Mărginean, M., Mihu, C., Istrate, M., Moldovan, I. M., Roman, A. L. & Mihu, C. M. 2018. Vascular endothelial growth factor (VEGF) - key factor in normal and pathological angiogenesis. *Rom J Morphol Embryol,* 59**,** 455-467.

Merdzhanova, G., Gout, S., Keramidas, M., Edmond, V., Coll, J. L., Brambilla, C., Brambilla, E., Gazzeri, S. & Eymin, B. 2010. The transcription factor E2F1 and the SR protein SC35 control the ratio of pro-angiogenic versus antiangiogenic isoforms of vascular endothelial growth factor-A to inhibit neovascularization in vivo. *Oncogene,* 29**,** 5392-403.

Mosser, D. M. & Edwards, J. P. 2008. Exploring the full spectrum of macrophage activation. *Nat Rev Immunol,* 8**,** 958-69.

Mouquet, F., Cuilleret, F., Susen, S., Sautiere, K., Marboeuf, P., Ennezat, P. V., Mcfadden, E., Pigny, P., Richard, F., Hennache, B., Vantyghem, M. C., Bertrand, M., Dallongeville, J., Jude, B. & Van Belle, E. 2009. Metabolic syndrome and collateral vessel formation in patients with documented occluded coronary arteries: association with hyperglycaemia, insulin-resistance, adiponectin and plasminogen activator inhibitor-1. *Eur Heart J,* 30**,** 840-9.

Müller, S., Chaikuad, A., Gray, N. S. & Knapp, S. 2015. The ins and outs of selective kinase inhibitor development. *Nat Chem Biol,* 11**,** 818-21.

Müller-Ehmsen, J., Krausgrill, B., Burst, V., Schenk, K., Neisen, U. C., Fries, J. W., Fleischmann, B. K., Hescheler, J. & Schwinger, R. H. 2006. Effective engraftment but poor mid-term persistence of mononuclear and mesenchymal bone marrow cells in acute and chronic rat myocardial infarction. *J Mol Cell Cardiol,* 41**,** 876-84.

Nahrendorf, M. & Swirski, F. K. 2017. Cholesterol, CCR2, and monocyte phenotypes in atherosclerosis. *Eur Heart J,* 38**,** 1594-1596.

Nakagawa, O., Arnold, M., Nakagawa, M., Hamada, H., Shelton, J. M., Kusano, H., Harris, T. M., Childs, G., Campbell, K. P., Richardson, J. A., Nishino, I. & Olson, E. N. 2005. Centronuclear myopathy in mice lacking a novel muscle-specific protein kinase transcriptionally regulated by MEF2. *Genes Dev,* 19**,** 2066-77.

Nakamura, K., Sano, S., Fuster, J. J., Kikuchi, R., Shimizu, I., Ohshima, K., Katanasaka, Y., Ouchi, N. & Walsh, K. 2016. Secreted Frizzled-related Protein 5 Diminishes Cardiac Inflammation and Protects the Heart from Ischemia/Reperfusion Injury. *J Biol Chem,* 291**,** 2566-75.

Nammian, P., Asadi-Yousefabad, S. L., Daneshi, S., Sheikhha, M. H., Tabei, S. M. B. & Razban, V. 2021. Comparative analysis of mouse bone marrow and adipose tissue mesenchymal stem cells for critical limb ischemia cell therapy. *Stem Cell Res Ther,* 12**,** 58.

Nandy, D., Janardhanan, R., Mukhopadhyay, D. & Basu, A. 2011. Effect of hyperglycemia on human monocyte activation. *J Investig Med,* 59**,** 661-7.

Naro, C. & Sette, C. 2013. Phosphorylation-mediated regulation of alternative splicing in cancer. *Int J Cell Biol,* 2013**,** 151839.

Nasseryan, J., Hajizadeh, E., Rasekhi, A. & Ahangar, H. 2016. Investigation factors affecting the first recurrence of coronary artery disease in patients undergone angioplasty using cox survival model. *Med J Islam Repub Iran,* 30**,** 441.

Ngo, D. T., Farb, M. G., Kikuchi, R., Karki, S., Tiwari, S., Bigornia, S. J., Bates, D. O., Lavalley, M. P., Hamburg, N. M., Vita, J. A., Hess, D. T., Walsh, K. & Gokce, N. 2014. Antiangiogenic actions of vascular endothelial growth factor-A165b, an inhibitory isoform of vascular endothelial growth factor-A, in human obesity. *Circulation,* 130**,** 1072-80.

Ngo, J. C., Chakrabarti, S., Ding, J. H., Velazquez-Dones, A., Nolen, B., Aubol, B. E., Adams, J. A., Fu, X. D. & Ghosh, G. 2005. Interplay between SRPK and Clk/Sty kinases in phosphorylation of the splicing factor ASF/SF2 is regulated by a docking motif in ASF/SF2. *Mol Cell,* 20**,** 77-89.

Nickless, A., Bailis, J. M. & You, Z. 2017. Control of gene expression through the nonsense-mediated RNA decay pathway. *Cell Biosci,* 7**,** 26.

Nissen, N. N., Polverini, P. J., Koch, A. E., Volin, M. V., Gamelli, R. L. & Dipietro, L. A. 1998. Vascular endothelial growth factor mediates angiogenic activity during the proliferative phase of wound healing. *Am J Pathol,* 152**,** 1445-52.

Nowak, D. G., Amin, E. M., Rennel, E. S., Hoareau-Aveilla, C., Gammons, M., Damodoran, G., Hagiwara, M., Harper, S. J., Woolard, J., Ladomery, M. R. & Bates, D. O. 2010. Regulation of vascular endothelial growth factor (VEGF) splicing from pro-angiogenic to anti-angiogenic isoforms: a novel therapeutic strategy for angiogenesis. *J Biol Chem,* 285**,** 5532-40.

Nowak, D. G., Woolard, J., Amin, E. M., Konopatskaya, O., Saleem, M. A., Churchill, A. J., Ladomery, M. R., Harper, S. J. & Bates, D. O. 2008. Expression of pro- and anti-angiogenic isoforms of VEGF is differentially regulated by splicing and growth factors. *J Cell Sci,* 121**,** 3487-95.

Oda, T., Hirota, K., Nishi, K., Takabuchi, S., Oda, S., Yamada, H., Arai, T., Fukuda, K., Kita, T., Adachi, T., Semenza, G. L. & Nohara, R. 2006. Activation of hypoxia-inducible factor 1 during macrophage differentiation. *Am J Physiol Cell Physiol,* 291**,** C104-13.

Okazaki, J., Guntani, A., Homma, K., Kyuragi, R., Kawakubo, E. & Maehara, Y. 2011. Fibromuscular dysplasia of the lower extremities. *Annals of vascular diseases,* 4**,** 143-149.

Okita, K., Ichisaka, T. & Yamanaka, S. 2007. Generation of germline-competent induced pluripotent stem cells. *Nature,* 448**,** 313-7.

Olfert, I. M., Howlett, R. A., Tang, K., Dalton, N. D., Gu, Y., Peterson, K. L., Wagner, P. D. & Breen, E. C. 2009. Muscle-specific VEGF deficiency greatly reduces exercise endurance in mice. *J Physiol,* 587**,** 1755-67.

Oliva-Martin, M. J., Sánchez-Abarca, L. I., Carrillo-Jiménez, A., Pérez-Simón, J. A. & Venero, J. L. 2015. Evaluation of a method for murine monocyte isolation by bone marrow depletion. *Anal Biochem,* 480**,** 42-8.

Oltean, S., Qiu, Y., Ferguson, J. K., Stevens, M., Neal, C., Russell, A., Kaura, A., Arkill, K. P., Harris, K., Symonds, C., Lacey, K., Wijeyaratne, L., Gammons, M., Wylie, E., Hulse, R. P., Alsop, C., Cope, G., Damodaran, G., Betteridge, K. B., Ramnath, R., Satchell,

S. C., Foster, R. R., Ballmer-Hofer, K., Donaldson, L. F., Barratt, J., Baelde, H. J., Harper, S. J., Bates, D. O. & Salmon, A. H. J. 2015. Vascular Endothelial Growth Factor-A165b Is Protective and Restores Endothelial Glycocalyx in Diabetic Nephropathy. *Journal of the American Society of Nephrology : JASN,* 26**,** 1889-1904.

Ouchi, N., Higuchi, A., Ohashi, K., Oshima, Y., Gokce, N., Shibata, R., Akasaki, Y., Shimono, A. & Walsh, K. 2010. Sfrp5 is an anti-inflammatory adipokine that modulates metabolic dysfunction in obesity. *Science,* 329**,** 454-7.

Panutsopulos, D., Zafiropoulos, A., Krambovitis, E., Kochiadakis, G. E., Igoumenidis, N. E. & Spandidos, D. A. 2003. Peripheral monocytes from diabetic patients with coronary artery disease display increased bFGF and VEGF mRNA expression. *J Transl Med,* 1**,** 6.

Park, J. J., Kwon, Y. W., Kim, J. W., Park, G. T., Yoon, J. W., Kim, Y. S., Kim, D. S., Kwon, S. M., Bae, S. S., Ko, K., Kim, C. S. & Kim, J. H. 2021. Coadministration of endothelial and smooth muscle cells derived from human induced pluripotent stem cells as a therapy for critical limb ischemia. *Stem Cells Transl Med,* 10**,** 414-426.

Peach, C. J., Mignone, V. W., Arruda, M. A., Alcobia, D. C., Hill, S. J., Kilpatrick, L. E. & Woolard, J. 2018. Molecular Pharmacology of VEGF-A Isoforms: Binding and Signalling at VEGFR2. *Int J Mol Sci,* 19.

Pelletier, M. & Girard, D. 2006. Differential effects of IL-15 and IL-21 in myeloid (CD11b+) and lymphoid (CD11b-) bone marrow cells. *J Immunol,* 177**,** 100-8.

Perrin, R. M., Konopatskaya, O., Qiu, Y., Harper, S., Bates, D. O. & Churchill, A. J. 2005. Diabetic retinopathy is associated with a switch in splicing from anti- to pro-angiogenic isoforms of vascular endothelial growth factor. *Diabetologia,* 48**,** 2422-7.

Pipp, F., Boehm, S., Cai, W. J., Adili, F., Ziegler, B., Karanovic, G., Ritter, R., Balzer, J., Scheler, C., Schaper, W. & Schmitz-Rixen, T. 2004. Elevated fluid shear stress enhances postocclusive collateral artery growth and gene expression in the pig hind limb. *Arterioscler Thromb Vasc Biol,* 24**,** 1664-8.

Pipp, F., Heil, M., Issbrücker, K., Ziegelhoeffer, T., Martin, S., Van Den Heuvel, J., Weich, H., Fernandez, B., Golomb, G., Carmeliet, P.,

Schaper, W. & Clauss, M. 2003. VEGFR-1-selective VEGF homologue PlGF is arteriogenic: evidence for a monocyte-mediated mechanism. *Circ Res,* 92**,** 378-85.

Rafieian-Kopaei, M., Setorki, M., Doudi, M., Baradaran, A. & Nasri, H. 2014. Atherosclerosis: process, indicators, risk factors and new hopes. *Int J Prev Med,* 5**,** 927-46.

Rajagopalan, S., Mohler, E. R., 3rd, Lederman, R. J., Mendelsohn, F. O., Saucedo, J. F., Goldman, C. K., Blebea, J., Macko, J., Kessler, P. D., Rasmussen, H. S. & Annex, B. H. 2003. Regional angiogenesis with vascular endothelial growth factor in peripheral arterial disease: a phase II randomized, double-blind, controlled study of adenoviral delivery of vascular endothelial growth factor 121 in patients with disabling intermittent claudication. *Circulation,* 108**,** 1933-8.

Rajewsky, K., Gu, H., Kühn, R., Betz, U. A., Müller, W., Roes, J. & Schwenk, F. 1996. Conditional gene targeting. *J Clin Invest,* 98**,** 600-3.

Rajwani, A., Ezzat, V., Smith, J., Yuldasheva, N. Y., Duncan, E. R., Gage, M., Cubbon, R. M., Kahn, M. B., Imrie, H., Abbas, A., Viswambharan, H., Aziz, A., Sukumar, P., Vidal-Puig, A., Sethi, J. K., Xuan, S., Shah, A. M., Grant, P. J., Porter, K. E., Kearney, M. T. & Wheatcroft, S. B. 2012. Increasing circulating IGFBP1 levels improves insulin sensitivity, promotes nitric oxide production, lowers blood pressure, and protects against atherosclerosis. *Diabetes,* 61**,** 915-24.

Rauner, M., Stein, N., Winzer, M., Goettsch, C., Zwerina, J., Schett, G., Distler, J. H., Albers, J., Schulze, J., Schinke, T., Bornhäuser, M., Platzbecker, U. & Hofbauer, L. C. 2012. WNT5A is induced by inflammatory mediators in bone marrow stromal cells and regulates cytokine and chemokine production. *J Bone Miner Res,* 27**,** 575-85.

Ren, G., Sheng, L., Liu, H., Sun, Y., An, Y. & Li, Y. 2015. The crucial role of SRPK1 in TGF-β-induced proliferation and apoptosis in the esophageal squamous cell carcinomas. *Med Oncol,* 32**,** 209.

Riddy, D. M., Goy, E., Delerive, P., Summers, R. J., Sexton, P. M. & Langmead, C. J. 2018. Comparative genotypic and phenotypic analysis of human peripheral blood monocytes and surrogate monocyte-like cell lines commonly used in metabolic disease research. *PLoS One,* 13**,** e0197177.

Risau, W. 1997. Mechanisms of angiogenesis. *Nature,* 386**,** 671-4.

Rivard, A., Silver, M., Chen, D., Kearney, M., Magner, M., Annex, B., Peters, K. & Isner, J. M. 1999. Rescue of diabetes-related impairment of angiogenesis by intramuscular gene therapy with adeno-VEGF. *The American journal of pathology,* 154**,** 355-363.

Roberts, D. M., Kearney, J. B., Johnson, J. H., Rosenberg, M. P., Kumar, R. & Bautch, V. L. 2004. The vascular endothelial growth factor (VEGF) receptor Flt-1 (VEGFR-1) modulates Flk-1 (VEGFR-2) signaling during blood vessel formation. *Am J Pathol,* 164**,** 1531-5.

Rufaihah, A. J., Huang, N. F., Jamé, S., Lee, J. C., Nguyen, H. N., Byers, B., De, A., Okogbaa, J., Rollins, M., Reijo-Pera, R., Gambhir, S. S. & Cooke, J. P. 2011. Endothelial cells derived from human iPSCS increase capillary density and improve perfusion in a mouse model of peripheral arterial disease. *Arteriosclerosis, thrombosis, and vascular biology,* 31**,** e72-e79.

Sanchis-Gomar, F., Perez-Quilis, C., Leischik, R. & Lucia, A. 2016. Epidemiology of coronary heart disease and acute coronary syndrome. *Ann Transl Med,* 4**,** 256.

Sasmaz, H. & Yilmaz, M. B. 2009. Coronary collaterals in obese patients: impact of metabolic syndrome. *Angiology,* 60**,** 164-8.

Sauer, B. & Henderson, N. 1988. Site-specific DNA recombination in mammalian cells by the Cre recombinase of bacteriophage P1. *Proc Natl Acad Sci U S A,* 85**,** 5166-70.

Schaper, W. & Scholz, D. 2003. Factors regulating arteriogenesis. *Arterioscler Thromb Vasc Biol,* 23**,** 1143-51.

Schierling, W., Troidl, K., Mueller, C., Troidl, C., Wustrack, H., Bachmann, G., Kasprzak, P. M., Schaper, W. & Schmitz-Rixen, T. 2009. Increased intravascular flow rate triggers cerebral arteriogenesis. *J Cereb Blood Flow Metab,* 29**,** 726-37.

Schioppa, T., Uranchimeg, B., Saccani, A., Biswas, S. K., Doni, A., Rapisarda, A., Bernasconi, S., Saccani, S., Nebuloni, M., Vago, L., Mantovani, A., Melillo, G. & Sica, A. 2003. Regulation of the chemokine receptor CXCR4 by hypoxia. *J Exp Med,* 198**,** 1391-402.

Schirmer, S. H., Millenaar, D. N., Werner, C., Schuh, L., Degen, A., Bettink, S. I., Lipp, P., Van Rooijen, N., Meyer, T., Böhm, M. & Laufs, U. 2015.

Exercise promotes collateral artery growth mediated by monocytic nitric oxide. *Arterioscler Thromb Vasc Biol,* 35**,** 1862-71.

Scholz, D., Cai, W. J. & Schaper, W. 2001. Arteriogenesis, a new concept of vascular adaptation in occlusive disease. *Angiogenesis,* 4**,** 247-57.

Schulte, D. M., Müller, N., Neumann, K., Oberhäuser, F., Faust, M., Güdelhöfer, H., Brandt, B., Krone, W. & Laudes, M. 2012. Pro-inflammatory wnt5a and anti-inflammatory sFRP5 are differentially regulated by nutritional factors in obese human subjects. *PLoS One,* 7**,** e32437.

Schultz, A., Lavie, L., Hochberg, I., Beyar, R., Stone, T., Skorecki, K., Lavie, P., Roguin, A. & Levy, A. P. 1999. Interindividual heterogeneity in the hypoxic regulation of VEGF: significance for the development of the coronary artery collateral circulation. *Circulation,* 100**,** 547-52.

Senger, D. R., Galli, S. J., Dvorak, A. M., Perruzzi, C. A., Harvey, V. S. & Dvorak, H. F. 1983. Tumor cells secrete a vascular permeability factor that promotes accumulation of ascites fluid. *Science,* 219**,** 983-5.

Shanmugam, N., Reddy, M. A., Guha, M. & Natarajan, R. 2003. High glucose-induced expression of proinflammatory cytokine and chemokine genes in monocytic cells. *Diabetes,* 52**,** 1256-64.

Sharma, A. M., Norton, P. T. & Zhu, D. 2014. Conditions presenting with symptoms of peripheral arterial disease. *Seminars in interventional radiology,* 31**,** 281-291.

Shi, J., Hua, L., Harmer, D., Li, P. & Ren, G. 2018. Cre Driver Mice Targeting Macrophages. *Methods Mol Biol,* 1784**,** 263-275.

Shibuya, M. 2001. Structure and function of VEGF/VEGF-receptor system involved in angiogenesis. *Cell Struct Funct,* 26**,** 25-35.

Shibuya, M. 2006. Vascular endothelial growth factor receptor-1 (VEGFR-1/Flt-1): a dual regulator for angiogenesis. *Angiogenesis,* 9**,** 225-30; discussion 231.

Simons, M., Gordon, E. & Claesson-Welsh, L. 2016. Mechanisms and regulation of endothelial VEGF receptor signalling. *Nat Rev Mol Cell Biol,* 17**,** 611-25.

Slovut, D. P. & Lipsitz, E. C. 2012. Surgical technique and peripheral artery disease. *Circulation,* 126**,** 1127-38.

Stefater, J. A., 3rd, Lewkowich, I., Rao, S., Mariggi, G., Carpenter, A. C., Burr, A. R., Fan, J., Ajima, R., Molkentin, J. D., Williams, B. O., Wills-Karp, M., Pollard, J. W., Yamaguchi, T., Ferrara, N., Gerhardt, H. & Lang, R. A. 2011. Regulation of angiogenesis by a non-canonical Wnt-Flt1 pathway in myeloid cells. *Nature,* 474**,** 511-5.

Stefater, J. A., 3rd, Rao, S., Bezold, K., Aplin, A. C., Nicosia, R. F., Pollard, J. W., Ferrara, N. & Lang, R. A. 2013. Macrophage Wnt-Calcineurin-Flt1 signaling regulates mouse wound angiogenesis and repair. *Blood,* 121**,** 2574-8.

Steinl, D. C. & Kaufmann, B. A. 2015. Ultrasound imaging for risk assessment in atherosclerosis. *Int J Mol Sci,* 16**,** 9749-69.

Stone, O. A., Carter, J. G., Lin, P. C., Paleolog, E., Machado, M. J. & Bates, D. O. 2017. Differential regulation of blood flow-induced neovascularization and mural cell recruitment by vascular endothelial growth factor and angiopoietin signalling. *J Physiol,* 595**,** 1575-1591.

Strehl, C., Fangradt, M., Fearon, U., Gaber, T., Buttgereit, F. & Veale, D. J. 2014. Hypoxia: how does the monocyte-macrophage system respond to changes in oxygen availability? *J Leukoc Biol,* 95**,** 233-41.

Swirski, F. K., Nahrendorf, M., Etzrodt, M., Wildgruber, M., Cortez-Retamozo, V., Panizzi, P., Figueiredo, J. L., Kohler, R. H., Chudnovskiy, A., Waterman, P., Aikawa, E., Mempel, T. R., Libby, P., Weissleder, R. & Pittet, M. J. 2009. Identification of splenic reservoir monocytes and their deployment to inflammatory sites. *Science,* 325**,** 612-6.

Takeshita, S., Isshiki, T., Mori, H., Tanaka, E., Tanaka, A., Umetani, K., Eto, K., Miyazawa, Y., Ochiai, M. & Sato, T. 1997. Microangiographic assessment of collateral vessel formation following direct gene transfer of vascular endothelial growth factor in rats. *Cardiovasc Res,* 35**,** 547-52.

Tanaka, R., Masuda, H., Kato, S., Imagawa, K., Kanabuchi, K., Nakashioya, C., Yoshiba, F., Fukui, T., Ito, R., Kobori, M., Wada, M., Asahara, T. & Miyasaka, M. 2014. Autologous G-CSF-mobilized peripheral blood

CD34+ cell therapy for diabetic patients with chronic nonhealing ulcer. *Cell Transplant,* 23**,** 167-79.

Thukkani, A. K. & Kinlay, S. 2015. Endovascular intervention for peripheral artery disease. *Circ Res,* 116**,** 1599-613.

Tong, S., Du, Y., Ji, Q., Dong, R., Cao, J., Wang, Z., Li, W., Zeng, M., Chen, H., Zhu, X. & Zhou, Y. 2020. Expression of Sfrp5/Wnt5a in human epicardial adipose tissue and their relationship with coronary artery disease. *Life Sci,* 245**,** 117338.

Turner, P. V., Brabb, T., Pekow, C. & Vasbinder, M. A. 2011. Administration of substances to laboratory animals: routes of administration and factors to consider. *J Am Assoc Lab Anim Sci,* 50**,** 600-13.

Tuttle, J. L., Nachreiner, R. D., Bhuller, A. S., Condict, K. W., Connors, B. A., Herring, B. P., Dalsing, M. C. & Unthank, J. L. 2001. Shear level influences resistance artery remodeling: wall dimensions, cell density, and eNOS expression. *Am J Physiol Heart Circ Physiol,* 281**,** H1380-9.

Tzelepis, K., De Braekeleer, E., Aspris, D., Barbieri, I., Vijayabaskar, M. S., Liu, W. H., Gozdecka, M., Metzakopian, E., Toop, H. D., Dudek, M., Robson, S. C., Hermida-Prado, F., Yang, Y. H., Babaei-Jadidi, R., Garyfallos, D. A., Ponstingl, H., Dias, J. M. L., Gallipoli, P., Seiler, M., Buonamici, S., Vick, B., Bannister, A. J., Rad, R., Prinjha, R. K., Marioni, J. C., Huntly, B., Batson, J., Morris, J. C., Pina, C., Bradley, A., Jeremias, I., Bates, D. O., Yusa, K., Kouzarides, T. & Vassiliou, G. S. 2018. SRPK1 maintains acute myeloid leukemia through effects on isoform usage of epigenetic regulators including BRD4. *Nat Commun,* 9**,** 5378.

Varey, A. H., Rennel, E. S., Qiu, Y., Bevan, H. S., Perrin, R. M., Raffy, S., Dixon, A. R., Paraskeva, C., Zaccheo, O., Hassan, A. B., Harper, S. J. & Bates, D. O. 2008. VEGF 165 b, an antiangiogenic VEGF-A isoform, binds and inhibits bevacizumab treatment in experimental colorectal carcinoma: balance of pro- and antiangiogenic VEGF-A isoforms has implications for therapy. *Br J Cancer,* 98**,** 1366-79.

Waltenberger, J., Claesson-Welsh, L., Siegbahn, A., Shibuya, M. & Heldin, C. H. 1994. Different signal transduction properties of KDR and Flt1, two receptors for vascular endothelial growth factor. *J Biol Chem,* 269**,** 26988-95.

Waltenberger, J., Lange, J. & Kranz, A. 2000. Vascular endothelial growth factor-A-induced chemotaxis of monocytes is attenuated in patients with diabetes mellitus: A potential predictor for the individual capacity to develop collaterals. *Circulation,* 102**,** 185-90.

Wang, H. Y., Lin, W., Dyck, J. A., Yeakley, J. M., Songyang, Z., Cantley, L. C. & Fu, X. D. 1998. SRPK2: a differentially expressed SR protein-specific kinase involved in mediating the interaction and localization of pre-mRNA splicing factors in mammalian cells. *J Cell Biol,* 140**,** 737-50.

Wang, P., Zhou, Z., Hu, A., Ponte De Albuquerque, C., Zhou, Y., Hong, L., Sierecki, E., Ajiro, M., Kruhlak, M., Harris, C., Guan, K. L., Zheng, Z. M., Newton, A. C., Sun, P., Zhou, H. & Fu, X. D. 2014. Both decreased and increased SRPK1 levels promote cancer by interfering with PHLPP-mediated dephosphorylation of Akt. *Mol Cell,* 54**,** 378-91.

Wang, Z. & Burge, C. B. 2008. Splicing regulation: from a parts list of regulatory elements to an integrated splicing code. *Rna,* 14**,** 802-13.

Wei, D., Wang, G., Tang, C., Qiu, J., Zhao, J., Gregersen, H. & Deng, L. 2012. Upregulation of SDF-1 is associated with atherosclerosis lesions induced by LDL concentration polarization. *Ann Biomed Eng,* 40**,** 1018-27.

Weinberg, I. & Jaff, M. R. 2012. Nonatherosclerotic arterial disorders of the lower extremities. *Circulation,* 126**,** 213-22.

Westvik, T. S., Fitzgerald, T. N., Muto, A., Maloney, S. P., Pimiento, J. M., Fancher, T. T., Magri, D., Westvik, H. H., Nishibe, T., Velazquez, O. C. & Dardik, A. 2009. Limb ischemia after iliac ligation in aged mice stimulates angiogenesis without arteriogenesis. *J Vasc Surg,* 49**,** 464-73.

White, C. J. & Gray, W. A. 2007. Endovascular therapies for peripheral arterial disease: an evidence-based review. *Circulation,* 116**,** 2203-15.

Wong, N. D. 2014. Epidemiological studies of CHD and the evolution of preventive cardiology. *Nat Rev Cardiol,* 11**,** 276-89.

Woolard, J., Wang, W. Y., Bevan, H. S., Qiu, Y., Morbidelli, L., Pritchard-Jones, R. O., Cui, T. G., Sugiono, M., Waine, E., Perrin, R., Foster,

R., Digby-Bell, J., Shields, J. D., Whittles, C. E., Mushens, R. E., Gillatt, D. A., Ziche, M., Harper, S. J. & Bates, D. O. 2004. VEGF165b, an inhibitory vascular endothelial growth factor splice variant: mechanism of action, in vivo effect on angiogenesis and endogenous protein expression. *Cancer Res,* 64**,** 7822-35.

Wu, W. K., Llewellyn, O. P., Bates, D. O., Nicholson, L. B. & Dick, A. D. 2010. IL-10 regulation of macrophage VEGF production is dependent on macrophage polarisation and hypoxia. *Immunobiology,* 215**,** 796-803.

Yang, L., Chu, Y., Wang, Y., Zhao, X., Xu, W., Zhang, P., Liu, X., Dong, S., He, W. & Gao, C. 2014. siRNA-mediated silencing of Wnt5a regulates inflammatory responses in atherosclerosis through the MAPK/NF-κB pathways. *Int J Mol Med,* 34**,** 1147-52.

Yap, K. & Makeyev, E. V. 2013. Regulation of gene expression in mammalian nervous system through alternative pre-mRNA splicing coupled with RNA quality control mechanisms. *Mol Cell Neurosci,* 56**,** 420-8.

Yilmaz, M. B., Biyikoglu, S. F., Akin, Y., Guray, U., Kisacik, H. L. & Korkmaz, S. 2003. Obesity is associated with impaired coronary collateral vessel development. *Int J Obes Relat Metab Disord,* 27**,** 1541-5.

Yu, J., Demuinck, E. D., Zhuang, Z., Drinane, M., Kauser, K., Rubanyi, G. M., Qian, H. S., Murata, T., Escalante, B. & Sessa, W. C. 2005. Endothelial nitric oxide synthase is critical for ischemic remodeling, mural cell recruitment, and blood flow reserve. *Proc Natl Acad Sci U S A,* 102**,** 10999-1004.

Yu, X. M., Wang, L., Li, J. F., Liu, J., Li, J., Wang, W., Wang, J. & Wang, C. 2013. Wnt5a inhibits hypoxia-induced pulmonary arterial smooth muscle cell proliferation by downregulation of β-catenin. *Am J Physiol Lung Cell Mol Physiol,* 304**,** L103-11.

Zambrowicz, B. P., Imamoto, A., Fiering, S., Herzenberg, L. A., Kerr, W. G. & Soriano, P. 1997. Disruption of overlapping transcripts in the ROSA beta geo 26 gene trap strain leads to widespread expression of beta-galactosidase in mouse embryos and hematopoietic cells. *Proc Natl Acad Sci U S A,* 94**,** 3789-94.

Zhao, E., Xu, H., Wang, L., Kryczek, I., Wu, K., Hu, Y., Wang, G. & Zou, W. 2012. Bone marrow and the control of immunity. *Cell Mol Immunol,* 9**,** 11-9.

Zhao, G., Cheng, X. W., Piao, L., Hu, L., Lei, Y., Yang, G., Inoue, A., Ogasawara, S., Wu, H., Hao, C. N., Okumura, K. & Kuzuya, M. 2017. The Soluble VEGF Receptor sFlt-1 Contributes to Impaired Neovascularization in Aged Mice. *Aging Dis,* 8**,** 287-300.

Zhao, H., Zhao, X., Liu, X., Cao, Y., Hippe, D. S., Sun, J., Li, F., Xu, J. & Yuan, C. 2013. Association of carotid atherosclerotic plaque features with acute ischemic stroke: a magnetic resonance imaging study. *Eur J Radiol,* 82**,** e465-70.

Zhao, P., Zhang, Y., Li, W., Jeanty, C., Xiang, G. & Dong, Y. 2020. Recent advances of antibody drug conjugates for clinical applications. *Acta Pharm Sin B,* 10**,** 1589-1600.

Zhu, J. & Krainer, A. R. 2000. Pre-mRNA splicing in the absence of an SR protein RS domain. *Genes & development,* 14**,** 3166-3178.